Three-body physics of ultracold gases: theory of weakly bound quantum states in strongly interacting systems

by

Jacek Gębala

Record book number: 385636

The thesis written under the supervision of
Prof. dr hab. Michał Tomza
University of Warsaw
Prof. dr José P. D'Incao
University of Massachusetts Boston

Warsaw, June 2026

Summary

This thesis investigates few-body quantum physics in ultracold atomic gases and atom–ion mixtures, with a particular focus on the role of finite-range interactions and the breakdown of universal Efimov physics in the presence of realistic interparticle potentials.

The first part of this thesis comprises four chapters that introduce the few-body physics of ultracold gases. The first chapter reviews significant experimental and theoretical developments in ultracold physics over the past 25 years. The second chapter examines the emergence of ultracold three-body systems as a fundamental platform for addressing a wide range of physical problems. Chapter three presents a theoretical overview of the quantum three-body problem. The fourth chapter expands upon this discussion by emphasizing universal behavior in quantum phenomena, such as the Efimov effect and the universal properties of three-body observables.

The second part of the thesis, in the fifth chapter, describes ion-atom systems near Feshbach resonances. By calculating the bound and scattering properties of a three-body system, the thesis shows that long-range atom–ion interactions cause strong deviations from universal predictions based on short-range or van der Waals models. In these ionic systems, inelastic decay channels are suppressed, which leads to lower recombination rates and longer lifetimes of Efimov states than in neutral systems. The results also reveal a dense spectrum of long-lived triatomic molecular ion states, showing that atom–ion mixtures are a promising platform for studying non-universal few-body physics driven by long-range forces.

The third part of the thesis, in the sixth chapter, examines neutral three-body systems near Feshbach resonances with varying widths. By studying homonuclear bosonic systems, it is shown that the Efimov spectrum exhibits non-universal behavior for narrow resonances ($s_{\mathrm{res}} < 1$). This happens because an effective repulsive interaction appears in the atom–dimer channel, changing both the ground and excited Efimov states. The results highlight that short-range physics, exchange interactions, and van der Waals forces all play important roles in whether universal Efimov scaling applies. As an example, ^{7}Li in the $|F = 1, m_F = 0\rangle$ state is studied, showing how a smaller resonance width increases non-universal effects.

The seventh chapter describes in detail the constraints on numerical calculations of three-body observables. Some of these limitations can be attributed to two-body physics, while others stem from intrinsic numerical effects, which influence the convergence of three-body potentials. The final chapter presents a summary of the results along with an outlook for future research.

In summary, this thesis demonstrates that deviations from universality in Efimov physics occur naturally in real systems due to finite interaction ranges and resonance properties. Both ion-atom and narrow-resonance atomic systems provide distinct opportunities to investigate the boundaries of universal three-body theory, revealing a more intricate structure of few-body quantum states than predicted by idealized models.

Key words

few-body physics, three-body problem, bound states, hyperspherical coordinates, three-body recombination, Efimov physics, three-body universality

The title of thesis in Polish language

Fizyka trójciałowa w ultrazimnych gazach: teoria słabo związanych stanów kwantowych w układach silnie oddziałujących

Acknowledgements

I would like to thank my supervisors, Prof. Michał Tomza and Prof. José P. D'Incao, both of whom have been mentors throughout my scientific career. I am deeply grateful for the support, guidance, and dedication they have generously offered over the years.

I am also grateful to my family and friends, many of whom have understood the challenges of pursuing a doctoral degree and have continuously provided encouragement and support.

Finally, I would like to express my special thanks to the community of the Faculty of Physics at the University of Warsaw, which fosters a stimulating and collaborative environment for scientific research and fruitful interactions. In this context, I would especially like to acknowledge the excellent collaborators of the Quantum Molecular Systems Group who deserve special recognition.

I would like to gratefully acknowledge the National Science Centre Poland (grants No. 2020/38/E/ST2/00564 and 2023/49/N/ST2/03439) for the financial support and the Poland's high-performance computing infrastructure PLGrid (HPC Centers: ACK Cyfronet AGH) for providing computer facilities and technical support (computational grants No. PLG/2023/016115, PLG/2024/017527, and PLG/2025/018938).

The syntax corrections to the text were partially supported by the GPT-4o and o-series OpenAI models, and the Grammarly tool.

Contents

1. Ultracold physics . . . 6
1.1. Scattering of ultracold atoms . . . 7
1.2. Experimental methods for the cooling and trapping of ultracold samples . . . 9
1.3. Ion-atom systems . . . 11

2. Three-body physics . . . 13
2.1. Experimental results . . . 13
2.2. Efimov effect . . . 15
2.3. Universality of the Efimov effect . . . 18

3. Three-body theory . . . 20
3.1. The Jacobi coordinates for N particles . . . 21
3.2. The hyperspherical coordinates for N particles . . . 23
3.2.1. The Laplacian in canonical hyperspherical coordinates . . . 25
3.2.2. The operator Λ^2 in canonical hyperspherical coordinates . . . 26
3.2.3. The clustering method . . . 31
3.3. The adiabatic approach for N particles . . . 38
3.4. The Johnson coordinates in the body-fixed frame . . . 41
3.4.1. Rotation of the lab-fixed frame . . . 42
3.4.2. Parametrization of the Jacobi vectors in the body-fixed frame . . . 45
3.4.3. The operator Λ^2 in Johnson coordinates . . . 47
3.4.4. The quasi-coordinates and the Euler angles . . . 53
3.4.5. The expansion of the wavefunction . . . 56

4. Universality . . . 59
4.1. The Efimov effect . . . 59
4.1.1. The Faddeev expansion of the wavefunction . . . 61
4.1.2. The eigenvalue problem for Λ^2 . . . 62
4.1.3. The Bethe-Peierls boundary condition . . . 66
4.1.4. Explicit formula of the solution of the eigenvalue problem for Λ^2 . . . 68
4.2. The three-body recombination . . . 79
4.3. The effective range theory . . . 83

5. Weakly bound three-body states in ion-atom-atom systems . . . 89
5.1. Ion-atom-atom dynamics . . . 90
5.2. Efimov physics in ion-atom-atom systems . . . 94
5.3. The three-body recombination . . . 96
5.4. Mechanism of universality in ion-atom-atom systems . . . 98
5.5. Summary . . . 105

6. Universality near narrow Feshbach resonances 106
6.1. The interaction model 107
6.2. The tuning of the s_{res} parameter 109
6.3. The Efimov spectrum 111

7. Strategies for computational accuracy 116
7.1. The eigenvalue problem for the adiabatic hamiltonian $\hat{H}_{\mathrm{ad}}$ 116
7.2. The slow-variable discretization method 118
7.3. The convergence of the three-body recombination rate 120

8. Conclusion & Outlook 124

9. Bibliography 126

Chapter 1

Ultracold physics

Ultracold atomic and molecular quantum gases have become a well-established and highly engaging field of scientific research in atomic physics over the past 25 years. Because external fields can control the strength of interatomic interactions, ultracold systems are ideal for investigating fundamentals of quantum physics and chemistry, as well as for understanding atomic and molecular dynamics. Similarly, the theoretical study of few-body interactions is paramount for analyzing experimental stability and for gaining a deep understanding of the underlying quantum physics of ultracold gases, with temperatures in the μK–nK range.

The scattering of particles at sufficiently low collision energy is determined by their s-wave *scattering length*, usually denoted by a. The term *ultracold* refers to temperature ranges, where the collision energy is low enough for the average interparticle distance $\sqrt[3]{1/n}$, where n is the atomic density, to become large and comparable to a. A few-body system has properties determined mainly by a and λ if the density of the system is low enough to create conditions where the atom separations are large compared to the range of interactions. In the other case, many-body effects dominate the dynamics of an ultracold system.

The general experimental mechanisms for preparing ultracold gases involve laser cooling [1, 2] and evaporative cooling [3, 4]. The progress in these experimental techniques allowed the preparation of dilute, ultracold samples at temperatures as low as nK and atomic densities in the range of $10^{12} - 10^{15}$ cm^{-3}. These developments were recognized by the 1997 Nobel Prize in Physics [5–7]. In 1995, researchers achieved a new state of matter – the Bose-Einstein condensate (BEC) in a dilute gas of alkali atoms, which resulted in another Nobel prize in physics – in 2001 [8, 9].

During the early experimental development of cold and ultracold physics, two breakthroughs significantly improved the degree to which ultracold systems could be studied and controlled. The first is the ability to tune the scattering length in cold gases through Feshbach resonances [10–14]. The second is the use of optical potentials, specifically strong, periodic potentials for controlling, trapping, and changing the dimensionality of cold gases [15]. These developments enabled the achievement of experimental conditions where classical and semi-classical theories fail to describe atomic interactions. Even in dilute samples, the physics of cold and ultracold gases becomes strongly correlated, and quantum effects dominate their dynamics.

Reaching the strong-coupling regime experimentally was first described in Ref. [16]. This study demonstrated Bose-Einstein condensation in a magnetically trapped sample of ^{85}Rb atoms via Feshbach resonances. Due to three-body losses, whose rate scales as a^4 [17], the sample lifetime decreased drastically. Approaches to circumvent this difficulty included loading a Bose-Einstein condensate into a three-dimensional optical lattice potential and per-

forming a quantum transition from the superfluid into the Mott insulator [18]. It was the first observed quantum phase transition and enabled the realization of the strong-correlation regime in an ultracold gas using a novel approach. Other developments in research on Bose gases in reduced dimensionality settings included the first realization of a hard-core Bose gas in one dimension [19, 20] and realizing a crossover between a normal phase and a phase with quasi-long range order in two dimensions [21].

Recent research on Bose-Einstein condensates (BECs) with strong dipolar interactions has expanded significantly since their first realization using chromium atoms [22], with further developments reported in [23]. The experimental team achieved forced evaporative cooling of ^{52}Cr atoms in a crossed optical dipole trap. At a critical temperature of approximately $T_c \approx 700\,\mathrm{nK}$, they observed the formation of a Bose–Einstein condensate, indicated by the emergence of a two-component velocity distribution. Under these conditions, the team produced nearly pure condensates containing more than 5×10^4 atoms, showing unparalleled control over the strongly interacting quantum system.

The Pauli principle suppresses the three-body losses in ultracold Fermi gases. The strong-coupling regime could therefore be reached through Feshbach resonances [24, 25]. Crucially, the BEC-BCS crossover has been extensively studied, demonstrating that fermions are experimentally stable and easy to control [26]. One of the studies showed collective excitation modes of a fermionic gas of ^{6}Li in the BEC-BCS crossover regime [27]. Deviations from BEC-BCS theory were also studied for the same system [28]. Radio-frequency spectroscopy has also allowed researchers to study the process of Cooper pair formation due to many-body effects [29].

Recent breakthroughs in the study of ultracold Fermi gases include the research on pairing fluctuations and whether they could produce a pseudogap in unitary Fermi gases [30]. This work sheds light on understanding the pseudogap in high-temperature superconducting materials. Other work on the pseudogap has examined nonlocal pairing in a Hubbard lattice gas, providing real-space evidence of paired fermions in the lattice [31]. Furthermore, atom-resolved detection of bosonic and fermionic quantum gases enabled the direct measurement of two-particle correlations [32]. In an interesting theoretical article, the authors proposed a platform based on ultracold fermionic molecules trapped in optical lattices to address dynamics beyond standard approximations that arise in specific molecular dynamical problems [33].

In summary, the field of ultracold physics is rapidly developing, and we could introduce many other important subjects in these first paragraphs. These topics include the Bose–Fermi mixtures [34–36], spinor gases [37], and quantum spin systems in optical lattices [38]. Further rapidly advancing directions encompass dipolar quantum gases [39], Rydberg-dressed interactions [40], non-equilibrium dynamics and thermalization [41], synthetic gauge fields [42] and topological quantum matter [43], as well as the development of quantum gas microscopy techniques that enable single-atom-resolved measurements [44]. Researchers have shown increasing interest not only in the strongly coupled regime of interactions, but also in the use of cold atoms in optical lattices for quantum information processing, as discussed in Ref. [45].

1.1. Scattering of ultracold atoms

The control of ultracold atoms and molecules is generally achieved using laboratory fields, utilizing Feshbach resonances. Typically, this effect is studied by detecting a substantial loss of atoms due to enhanced three-body recombination. The first research on this quantum phenomenon has been concluded and came from the background of both the nuclear physics [46, 47] and the atomic physics [48, 49] – giving a complete theoretical description of

the coupling of a discrete state to the continuum. An important example of the first observation of a Feshbach resonance was given in Ref. [50], where a photodetachment of an electron from the H^- system – into $H+e^-$ was quantitatively analyzed. The Feshbach resonance came from a temporary trapping of the outgoing electron in a doubly excited hydrogen state.

For quantum gases, Feshbach resonances were first theoretically studied in a system of hydrogen and deuterium (H+D and D+D) [51]. Firstly, they were considered to be an effect disrupting the preparation of a stable spin-polarized gas. Further research led to the first proposal to use Feshbach resonances to control the sign and strength of the interaction between ultracold atoms [52]. Another early observation of the Feshbach resonance has been reported in an optically trapped BEC of Na atoms [11]. The experiment demonstrated unprecedented control over the interaction's strength. The authors confirmed that near a Feshbach resonance, the scattering length can be tuned and the atom-loss rate could be modified by orders of magnitude. The latter can be attributed to strongly enhanced three-body recombination and molecule formation. Generally, three-body recombination and the atom-molecule relaxation leading to recombination are the major processes that lead to atomic losses in ultracold systems [53].

Subsequent work on Feshbach resonances showed promise for further control and the creation of deeply bound molecular states. A landmark achievement was the creation of ultracold KRb molecules in their rovibrational ground state via stimulated Raman adiabatic passage (STIRAP) from Feshbach molecules, which opened the field of ultracold dipolar molecular gases [54]. Similar work has been carried out to demonstrate hyperfine-resolved two-photon transfer into the singlet ground state of the NaK molecule [55]. More recent advances in the studies on Feshbach resonances include the state-of-the-art coupled-channel and ab-initio scattering calculations showing specific mechanisms (spin-exchange, spin-rotation, anisotropy) that can mediate resonances in atom–molecule systems and predict both broad and very narrow resonances – giving targets for experiments [56].

A Feshbach resonance occurs due to coupling between a bound molecular state in a closed channel and the scattering in an open channel. The energy of either state can be tuned to the other, leading to mixing between them. The energy difference can be tuned through various physical processes, including: Zeeman shifts of open and closed channels (magnetically tuned Fechbach resonance) [57], near-resonant laser coupling between an open-channel atom pair to an excited molecular bound state (optical Feshbach resonance) [58], electric field shifting the molecular energy levels (Electric-field induced Feshbach resonance) [59], confinement-induced resonances in low-dimensional systems [60], and direct control over the collision energy [50], where the system forms a temporary excited state. The most commonly used and studied type is the magnetically tuned resonance, for which the low-energy scattering behavior can be described by the dependence of the s-wave scattering length on the magnetic field B, given by

$$a(B) = a_{\mathrm{bg}}\left(1 - \frac{\Delta}{B - B_0}\right) , \tag{1.1}$$

which was introduced in Ref. [61], and where B_0 is the resonance position, a_{bg} represents the background scattering length, and Δ is the resonance *width* defined as the distance between the resonance's position B_0 and the zero crossing at $B_0 + \Delta$. For s-wave scattering, let us consider the scattering amplitude

$$f(k) = \frac{1}{k\cot\delta_0(k) - ik} , \tag{1.2}$$

where k is the relative wavenumber related to the collision energy of two particles E_{col} by

$k = \sqrt{2\mu E_{\rm coll}/\hbar^2}$, μ being their reduced mass, and where $\delta_0(k)$ is the scattering phase shift for the s-wave collision.

We will consider a condition for the pole of the scattering amplitude, i.e., $k \cot \delta_0 = ik$, which is true at the Feshbach resonance. A second condition is given by $k = i\kappa$, which is related to the appearance of a bound state with energy $E_{\rm b} = -\hbar^2\kappa^2/(2\mu)$. Near the resonance, such a bound state describing the Feshbach molecule emerges just below threshold. The effective range expansion for the scattering phase shift states that

$$k \cot \delta_0 = -\frac{1}{a} + \frac{1}{2} r_{\rm eff} k^2 + \mathcal{O}(k^4) \ , \tag{1.3}$$

where $r_{\rm eff}$ is the *effective range* for scattering (for a more detailed discussion about the effective range theory, see Section 4.3). The effective-range expansion is valid for both scattering and bound states near the threshold. Combining the mentioned conditions and the effective range expansion, we obtain

$$-\kappa = i\kappa \cot \delta_0 = -\frac{1}{a} - \frac{1}{2} r_{\rm eff} \kappa^2 \ . \tag{1.4}$$

We can rewrite the second part of the equation

$$\frac{1}{2} r_{\rm eff} \kappa^2 - \kappa + \frac{1}{a} = 0 \ , \tag{1.5}$$

which leads us to quadratic solutions for the binding energy E_b of the shallow dimer

$$\kappa = \frac{1 - \sqrt{1 + 2r_{\rm eff}/a}}{r_{\rm eff}} \ , \tag{1.6}$$

where we pick one of the solutions to the quadratic equation, which tends to zero for $a \to \infty$. Finally, we obtain the expression for the binding energy $|E_b|$ of the Feshbach molecule related to the effective range of interaction and the scattering length, which is true for large, positive scattering lengths

$$|E_b| = \frac{\hbar^2\kappa^2}{2\mu} = \frac{\hbar^2}{2\mu r_{\rm eff}^2} \left(1 - \sqrt{1 - \frac{2r_{\rm eff}}{a}}\right)^2 \ . \tag{1.7}$$

In the universal range ($a \gg r_{\rm eff}$), this relation reduces to the simple expression $|E_b| = \hbar^2/(2\mu a^2)$. The presented reasoning allowed us to briefly introduce the concepts of universality, resonance *width*, and the effective range. One of the objectives of this thesis is the characterization of the universal and non-universal properties of Feshbach resonances classified as *narrow* or *wide* resonances (or closed- and open-channel dominated resonances, respectively) in the context of three-body physics and the formation and properties of Efimov states. The full discussion on the two-coupled-channel model for scattering is presented in Ref. [62–64].

1.2. Experimental methods for the cooling and trapping of ultracold samples

We offer a brief overview of the principal methods for preparing ultracold samples and discuss notable recent experimental progress. As mentioned before in this Chapter, the development of Doppler laser cooling stimulated a rapid progress of ultracold research [5, 65, 66]. The technique takes advantage of two counter-propagating laser beams of equal intensity, tuned slightly below an electronic transition. An atom or molecule moving toward one beam perceives a

higher Doppler-shifted frequency and is more likely to absorb a photon from that direction. The spontaneous emission occurs isotropically and yields no net momentum change. However, each absorption event imparts momentum opposite to the particle's motion, producing a net cooling force. Three pairs of counter-propagating laser beams create a damping force in all directions, and the system is often referred to as optical molasses. The recoil temperature of particles sets the limit of this method as their motion fluctuates due to spontaneously emitted photons – called the recoil limit.

To achieve atomic densities far higher than those obtainable with magnetic fields alone, magneto-optical traps (MOTs), which combine laser cooling with magnetic field gradients, are used. MOTs are the most widely employed trapping technique in ultracold experiments. They combine Doppler cooling with a spatially varying magnetic field. Circularly polarized light provides the cooling force, while a quadrupole magnetic field shifts atoms that drift away from the trap center into resonance with the appropriate laser beam, producing a restoring force. The 3-D generalization of an MOT uses an anti-Helmholtz coil and three orthogonal σ_+ and σ_- standing waves. The first realizations of MOT required a previously cooled sample [67–69]. However, it soon became routine to load atoms directly into a magneto-optical trap from an uncooled vapor [70].

Recent work has demonstrated significant experimental progress in cooling and trapping techniques. For example, researchers at the Fritz Haber Institute achieved the first magneto-optical trap (MOT) of a stable, chemically inert closed-shell molecule, aluminum monofluoride (AlF) [71]. Optical molasses has also been realized for several laser-coolable molecules—primarily diatomics with highly diagonal Franck–Condon factors (FCFs). For most molecules, however, optical molasses remains impractical due to extensive ro-vibrational branching arising from non-diagonal FCFs.

An optical method for stabilizing ultracold molecules using non-diagonal FCFs is the Stimulated Raman Adiabatic Passage (STIRAP). STIRAP allows for transferring the population of particles between two quantum states by coupling them with two radiation fields via an intermediate state [72]. STIRAP suppresses losses due to spontaneous emission from the intermediate state by adiabatically transferring population through a laser-induced dark state that avoids occupation of the excited state, and has therefore found widespread use in atomic, molecular, and chemical physics since its first complete description in Ref. [73]. This method has been extensively used in experiments demonstrating the formation of ultracold molecules, optical waveguides, and adiabatic population transfer in specific solid-state systems [74].

Raman transitions, which are two-photon transitions, can also be used for cooling. Raman sideband cooling (RSC) techniques have been used to cool ions [75] and neutral atoms [76] in traps. The method requires a tightly confining trap (an ion trap, optical tweezers, or an optical lattice) and uses internal-state transitions that couple to the vibrational motion. RSC proceeds in two main steps. First, a motional-sideband–resolved two-photon Raman transition is driven, reducing the vibrational quantum number of the harmonic trap while simultaneously transferring the atom to a different internal state. Second, optical pumping (OP) returns the atom to its original internal state without altering its motional state. Repeating this cycle incrementally reduces the atom's translational energy and drives it toward the trap's ground state. Achieving efficient RSC requires resolving the motional sidebands in all three spatial dimensions and ensuring highly efficient optical pumping. The method has been shown to cool a sample of many atoms efficiently [77], as well as a single atom to its motional ground state [78, 79].

The diversity of the explored ultracold physical systems has driven the development of a correspondingly broad set of experimental methods. In this context, trapped, laser-cooled ions offer exciting opportunities in ultracold physics by enabling extraordinary control over colli-

sions and initial quantum states. Due to Earnshaw's theorem, one can not use static electric fields to confine charged particles. Hence, ion trapping relies on time-varying fields. The most common implementation is the linear Paul trap, which combines static and radio-frequency (rf) electric fields. Axial (z-direction) confinement is provided by a static quadrupole potential proportional to $-z$. Radial confinement in the x–y plane is generated by electrodes driven with a dc voltage U together with an rf voltage $V\cos(\Omega_{\mathrm{rf}}t)$, where Ω_{rf} is the drive frequency. The resulting oscillating quadrupole potential alternately focuses and defocuses ions in the transverse directions, producing a stable time-averaged trapping pseudopotential [80]. Motion along z remains purely harmonic. Ultracold ions have become a central part of ultracold physics and provided opportunities for the study and development of technologies such as atomic clocks [81], quantum computing and information [82, 83], few- and many-body quantum physics [84–87], cold controlled chemistry [88], and fundamental physics [89]. More recently, a breakthrough in laser cooling and trapping of $^{224}Ra^{+}$ was realized via two-step photoionization loading of radium into an ion trap [90]. The investigated ion is radioactive and short-lived. However, in the ultracold regime, it enabled uniquely sensitive tests of fundamental physics – especially charge-parity symmetry violation and the measurement of electric dipole moments.

Lastly, two more optical methods for cooling below the Doppler limit should be mentioned: sisyphus cooling and evaporative cooling. The sisyphus effect, or polarization gradient cooling, requires that atoms move in a polarization gradient. Counter-propagating laser beams with orthogonal polarizations create a standing wave with spatially varying polarization. Due to the AC Stark shift, the energy of levels is periodically modulated as an atom moves through regions of different polarization. In a perpendicular configuration, for example, the ground-state Zeeman levels change their energies depending on the atom's position in the trap, creating alternating maxima and minima in the potential energy. An atom moving towards the maximum of the potential loses its kinetic energy. Near the top, it is optically pumped into a different Zeeman level whose potential is shifted downward, resulting in a net loss of kinetic energy after spontaneous emission. A comprehensive theoretical treatment of this mechanism was provided in a study of laser cooling below the Doppler limit via polarization gradients [91, 92]. Modern studies have extensively used this method for cooling of ions [93] or atoms using clock states [94].

Once temperatures near the quantum regime are reached with laser-based techniques such as optical molasses and polarization-gradient cooling, evaporative cooling becomes the dominant method for achieving the temperatures necessary for quantum degeneracy. In evaporative cooling, atoms with the highest kinetic energy are selectively removed from a trap. Evaporative cooling is currently the primary method for achieving quantum degeneracy in many species. Still, it is relatively slow, and often lossy, because it relies on elastic collisions to rethermalize the ensemble as high-energy atoms are continuously removed from the system [95].

1.3. Ion-atom systems

Ultracold ion-atom systems exhibit relatively long-range, polarization-dominated interactions, making them a promising platform for studying quantum induction-driven collision dynamics. Highly controllable trapped ions are the perfect tool for experimental studies of collisions [96]. Other examples of fields of study that take advantage of trapped ions are quantum simulation [97–99], quantum information [100, 101], cold controlled chemistry [102–105], as well as few- and many-body quantum physics [106–108], and various other fundamental physics

aspects [109].

In ultracold gases, inelastic collisions are typically dominated by only a few processes. Three-body recombination and atom-molecule relaxation leading to recombination are the major processes that cause sample losses [110]. In ion-atom-atom systems in particular, it has been shown that the sample losses are dominated by three-body recombination (TBR) [111].

Classical and semi-classical theories for ion-atom-atom systems have provided an accurate description of the three-body recombination rates for temperatures well above the quantum regime [112]. However, a comparison between classical trajectory calculations and a quantum approach for collision-induced dissociation rates has shown significant differences at temperatures below the quantum regime [113]. Certain qualitative classical results allowed the authors to predict that predominantly molecular ions are formed in the inelastic process [114].

In most ion-atom systems, tracing quantum effects in observables describing collision dynamics is challenging, as they cannot be readily cooled to the s-wave regime. Combining Paul traps with methods for cooling atoms introduces several technical challenges. High-power lasers used for optical trapping can damage or charge the ion-trap electrodes, while the radio-frequency (rf) fields of the Paul trap can induce spin flips in nearby atoms, increasing loss rates. These losses may also lead to unwanted atom deposition on the electrodes, degrading trap performance. In addition, intrinsic ion micromotion – unavoidable in radiofrequency traps – sets a fundamental limit on attainable temperatures, as it is typically much larger than the residual motion of ultracold atoms. Using a Penning trap usually does not resolve these issues: collisions between ions and atoms disrupt the ions' cyclotron orbits, severely reducing sample lifetimes [115].

Reaching the quantum regime proved more feasible for systems containing a heavy ion and light atoms, where micromotion effects are less relevant and lead to less heating [116]. Recently, the s-wave Feshbach resonances were theoretically predicted and observed through ion losses [111]. Similar results were provided for ytterbium [117, 118], where $LiYb^+$ molecular ions were detected via mass spectrometry. Several of the observed resonances could not be modeled by two-body scattering theory. Thus, the focus of this work is to model the three-body physics in an ultracold, charged sample.

The theoretical description of few-body dynamics in dilute ultracold neutral atoms with near-resonant interactions has been well established. Tractable observables show limited dependence on the microscopic details of the problem and the particular choice of atomic species. These universal, low-energy properties of observables, such as recombination rates, mean that they depend only on two relevant length scales: the scattering length and the wavenumber. Furthermore, universal physics can generally be modeled by contact interactions [119]. Limits to universality have been studied for homonuclear [119, 120] and heteronuclear bosonic systems [121, 122].

One of the main objectives of this thesis is to characterize three-body processes occurring in a system consisting of a trapped ytterbium or barium ion immersed in a lithium gas. Our approach enables the prediction of specific collision pathways leading to different types of ion loss, thereby accounting for the previously unexplained loss mechanisms observed in the recently investigated barium–lithium system [111]. A key goal is to determine the collision rates for channels that involve the formation of Li_2 molecules accompanied by the loss of a free barium ion. In addition, we aim to predict the quantum states of $BaLi^+$ molecules formed during collisions between the ion and a Feshbach dimer, as recently reported in experiments. Understanding the dynamics of ion-dimer collisions that lead to ion losses is also highly relevant to ongoing studies with barium ions.

Chapter 2

Three-body physics

2.1. Experimental results

In the context of ultracold physics, the experimental and theoretical studies of few-body systems have recently provided profound insight into a wide range of physical problems. Quantum three-body physics investigates how finite-range interactions, quantum statistics, and dimensionality govern the formation, scattering, and decay of three interacting particles. Experimental methods for studying three-body interactions in ultracold gases generally do not differ significantly from those used in precision spectroscopy, collision measurements, and time-resolved dynamics, which allows researchers to reveal correlations and quantum properties of systems beyond two-body physics. What is more, advances in experimental and theoretical studies of the three-body problem with near-resonant two-body interactions have motivated a wide range of studies on *universal* few-body physics and the related *Efimov physics*, i.e., the study of weakly bound three-body resonant trimers (Efimov trimers). These topics are covered in more depth in Section 2.2 of this Chapter, while this section focuses on more general advances in experimental three-body physics.

A promising platform for studying the structure of weakly bound three-body molecules is provided by helium trimers. The van der Waals force between two helium atoms is weak and leads to unusually large spatial extension, placing the system in a regime dominated by universal few-body quantum behavior. The current understanding of $^4\mathrm{He}_3$ is based almost entirely on theoretical studies. Conventional experimental methods for determining molecular structure do not apply to these extremely fragile systems, as the centrifugal force already makes the first excited rotational state unbound. A recent study using Coulomb-explosion imaging of helium trimers directly mapped out the trimer geometry and wavefunction distributions, showing that the density distribution of the $^4\mathrm{He}_3$ is best described by a non-equilateral triangle and that $^3\mathrm{He}^4\mathrm{He}_2$ exists as a quantum halo state [123].

A comprehensive study of the three-body recombination dynamics in a representative system of bosonic ^{87}Rb is presented in Ref. [124]. This work was the first experimental setup allowing for the description of three-body recombination into specific reaction channels. Simplified theoretical treatments indicate that three-body recombination does not, in principle, have to favor the most weakly bound state [125]. However, for most physical systems studied experimentally to date, recombination predominantly populates the least-bound available channel [110].

By contrast, the first measurements of three-body loss coefficients for a *three-component* Fermi gas over magnetically tuned pairwise interactions were conducted for a system of ultracold ^{6}Li [126]. A three-spin-state mixture of atoms was prepared to enable s-wave collisions be-

tween the particles. The study concluded that three-body recombination in a three-component Fermi gas is highly tunable and dominates atom-loss processes. Three-body recombination can be suppressed, allowing for experimentally stable regimes when pairwise interactions are sufficiently weak. These results are shown to be non-universal.

Recently, an impactful study was published showing anomalous decay in a sample of polarized three-component Fermi gas of ^{6}Li [127]. It is a general expectation that three-body losses are the same for all spin components. However, near one of the Feshbach resonances, a significant qualitative difference has been demonstrated – the loss rates per spin were distinct, with the majority component showing significantly larger losses. One possible explanation for the anomalies is the cascade mechanism for reactions, in which secondary collisions occur between the products of three-body recombination and other atoms in the gas, leading to excess losses. Secondly, a few-body process could be quantitatively indistinguishable from a three-body loss, for example, if a multi-stage process is rate-limited by a three-body stage. This process depends on forming an intermediate bound state with a binding energy comparable to the trap depth. However, no such state has been identified to date. The studied effect was found not to be specific to homogeneous gases, and research into possible explanations of this phenomenon is required.

Expanding on recent research into ultracold Fermi gases in the context of three-body physics, the experimental investigation of the scaling of the three-body loss rate in a *two-component* ^{6}Li near a narrow Feshbach resonance has verified that the Fermi gas can be cooled to a higher phase-space density through three-body recombination. Unlike standard evaporative cooling, collisional cooling can use Feshbach resonances to selectively expel atoms with specific kinetic energy [128]. This study expanded on the previous, impactful research into the stability of a repulsive, quasi-homogeneous spin-1/2, i.e., two-component, Fermi gas with contact interactions. For the range of scattering lengths explored, the dominant mechanism of decay was shown to be a universal three-body recombination towards a Feshbach bound state [129].

For a *single-component* system of ultracold Fermi gases, only the p-wave collisions are statistically allowed. One of the first measurements of the three-body loss rates was reported in Ref. [130]. In addition to the modification of two-body elastic processes, the p-wave resonance primarily enhanced three-body inelastic loss rates. Theoretical studies found that the loss behavior exhibits n^3 and an anomalous n^2 density dependence for a ratio of elastic-to-inelastic three-body collision rate [131]. Interestingly, to describe losses in the latter regime and to explain experimental observations in ground-state ^{6}Li atoms near a p-wave Feshbach resonance, theoretical studies used a cascade model inspired by earlier work [132].

Finally, we could shift our focus to experimental results investigating three-body loss in an ultracold mixture of a thermal Bose gas and a degenerate Fermi gas [133]. At unitarity, the typical inverse-square temperature scaling of three-body loss seen in nondegenerate systems failed to describe the experimental results adequately. With increased Fermi degeneracy, the three-body losses decreased. While this reduction can be qualitatively captured by few-body scattering theory, an additional suppression pointed to long-range Ruderman-Kittel-Kasuya-Yosida (RKKY) interactions mediated by the fermions between bosons.

A general review of three- and higher-body interactions in the context of nuclear physics and related areas was given in Ref. [134]. This work focuses on the impact of three-body interactions within effective field theories, which are particularly prominent in strongly interacting quantum systems. One of the first experimental studies of short-range physics investigated three-body recombination in bosonic ^{7}Li. The study indicated that short-range, three-body physics is nuclear-spin-independent, although it used traces of Efimov physics to confirm this hypothesis [135].

Three-body physics has also been investigated in a system of magnetically trapped Bose-Einstein condensate (BEC) into a deep two-dimensional optical lattice [136]. 1D confinement dramatically changes correlation functions and three-body collision rates because particles cannot bypass each other. This effect is a genuine reduction in dimensionality, measurable in ultracold gases and distinct from the universal Efimov scaling.

Studies of three-body losses in three-dimensional bulk Bose gases, particularly in a representative system of ^{39}K, have experimentally verified the theoretically predicted general scaling laws governing particle loss and heating in the unitary regime [137]. These measurements, however, showed the non-negligible relevance of four-body decay processes on the negative side of the Feshbach resonance. For positive a, the measured unitary value of L_3 was approximately three times smaller than the universal theoretical upper bound, indicating a suppression of three-body loss due to the emergence of many-body correlations. This reduced loss rate made ^{39}K a promising candidate for experimental investigations of strongly correlated many-body physics in a unitary Bose gas.

Further research confirms that a Bose gas, namely ^{7}Li, exhibits a finite lifetime that is long enough to be experimentally resolved and studied [138]. This study focused on quantitatively determining the sample's limits of stability. Although Efimov resonances are clearly resolved as a function of scattering length at finite temperature and density, the overall decay rate in the unitary regime did not exhibit Efimov log-periodic scaling. Once the scattering length exceeded the interparticle distances and the relevant energy scale is set by density rather than temperature, the decay dynamics were shown to be governed by universal many-body correlations, similarly to Ref. [137]. Numerous further references provide the reader with a deeper understanding and show extensive research into the limits of Efimov physics and more generally, determining the stability and dynamics of ultracold Bose gases in the context of three- and many-body interactions and correlations [139–149].

2.2. Efimov effect

Strongly interacting systems present unique scattering properties and support weakly bound, resonant three-body states – the Efimov states. This purely quantum effect attracted significant theoretical research interest since its observation in the context of atomic ultracold gases [150]. The theoretical description of Efimov physics and the related few-body dynamics is generally greatly simplified in dilute, resonantly interacting samples. Physical observables such as the position of the Efimov resonance, the energy scaling between the excited Efimov states, or the trimer lifetime exhibit universal behavior, i.e., they are independent of the microscopic details of the system. A schematic representation of the so-called *Efimov scenario* is presented in Figure 2.1.

The observation mentioned above happened more than 40 years after Vitaly Efimov's theoretical prediction [151] that an infinite family of universal three-body states should emerge when the two-body scattering lengths are sufficiently large in magnitude. What followed were many subsequent experiments and studies into the universality, impact on three-body loss rates, and general properties of the Efimov states. One of the first series of works includes studies by the Ferlaino group [152–154]. Ref. [152] showed a measurement of the relaxation rate coefficient for decay to lower-lying molecular states and studied the dependence on scattering length and temperature for a binary collision between two halo dimers. This study laid the groundwork for future studies of few-body processes near Feshbach resonances. Ref. [153] included measurements of four-body recombination rates in an atomic gas. Using an ultracold sample of cesium atoms with negative scattering lengths, a resonant increase in particle losses

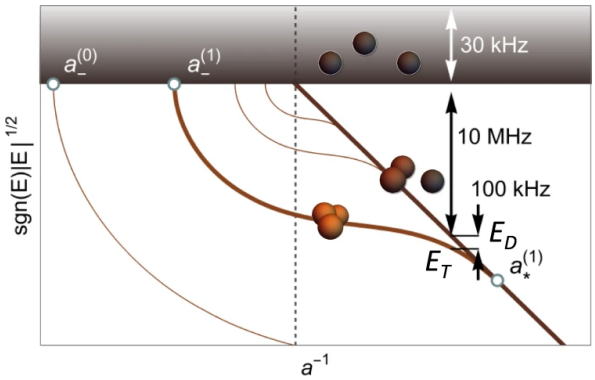

Figure 2.1: The binding energies of the Efimov trimers (solid curved lines) showing the discrete scale invariance of the three-body spectrum for three identical bosons. The energies are plotted against the inverse scattering length a^{-1}. The straight solid line originating at unitarity represents the universal dimer state. The gray region indicates the three-atom continuum. The n-th trimer appears from the three-body scattering threshold at $1/a_-^{(n)}$ and disappears into the particle-dimer scattering threshold at $1/a_*^{(n)}$. The presented energy scales are specific to the 894 G Feshbach resonance of the ^{7}Li. Adapted from [158] under the license CC BY 4.0 (https://creativecommons.org/licenses/by/4.0/).

was observed. This result provides strong evidence for two four-body bound states that are universally linked to Efimov trimers. In this context, the study expanded on the description of four-body processes from Ref. [152]. These results showed how the Efimov framework is extended when a fourth particle is added to the three-body problem. Finally, Ref. [154] presented comprehensive experimental measurements of triatomic Efimov resonances, atom-dimer Efimov resonances, and related four-body resonances, supporting and complementing the set of available data for ultracold cesium. The very first, direct observation of the Efimov spectrum through three-body losses was given in Ref. [155]. Further confirmation of a strong universal behavior of loss resonances and the three-body parameter in an ultracold gas of cesium was given in Refs. [156, 157].

The first experimental evidence of Efimov physics in a heteronuclear system was observed in a setup that used a mixture of ^{41}K and ^{87}Rb atoms cooled to a few hundred nanokelvin and confined in an optical dipole trap [159]. The study observed three distinct peaks of the inelastic collision rate of the mixture near an interspecies Feshbach resonance. Two of these peaks corresponded to Efimov resonances in both the KKRb and KRbRb channels.

Extensive experimental studies of the universality of Efimov physics were carried out by the group at Bar-Ilan University [135, 160, 161]. Their initial work demonstrated that the positions of Efimov resonances – identified through enhancements and suppressions of three-body recombination rates at negative and positive scattering lengths, respectively – are in excellent agreement with theoretical predictions [160]. The second study extended the previously reported universality in three-body recombination loss across a Feshbach resonance to the absolute ground state of ^{7}Li [135]. This study, cited above in the context of analysis of short-range physics, has shown that the positions and widths of recombination minima and Efimov resonances are identical for both analyzed nuclear-spin states. Both of these studies were summarized and extended upon in Ref. [161].

Further research identified a new experimental approach for analyzing the atom–dimer mixture coupled to the Efimov trimer. Namely, a resonance in atom–dimer scattering is observed, which manifests itself in resonantly enhanced inelastic decay [162]. Extended re-

search into this 'point of contact' between Efimov trimers and the atom-dimer mixture showed that we can magnetically control the energetic nature of the process, allowing it to be tuned from endoergic to exoergic. Unlike relaxation into more deeply bound molecular states, this exchange process does not cause trap loss [163].

A universal dimer formed via three-body recombination in an ultracold atomic cloud can undergo secondary collisions with surrounding atoms. Secondary collisions can obscure the connection between observed loss features and the true Efimov atom-dimer resonance, meaning that the scattering length associated with maximum secondary collisions does not necessarily indicate the Efimov resonance, which was shown in Ref. [164]. Hence, significant finite-range corrections to the first excited Efimov energy level should be accounted for in experimental setups.

In addition to Efimov trimers, the authors observed loss features consistent with four-body bound states (tetramers) that are universally tied to each Efimov trimer. Specifically, two tetramer states are associated with each trimer, as predicted by theory [165]. The positions of both three- and four-body loss resonances scale universally with the scattering length and are determined by the same three-body parameter. Interestingly, no independent four-body parameter is required.

A group from the Max-Planck-Institut in Heidelberg demonstrated that the observed magnetic-field dependence of three-body loss in a three-component ultracold ^{6}Li mixture can be accounted for by the existence of a universal trimer state. This mixture was analyzed in studies referenced above in the context of collisions in the ultracold Fermi gas [126]. By extending the theory provided in Ref. [166] for three identical bosons to three distinguishable fermions, an effective interaction parameter a_m constructed from the three scattering lengths a_{12}, a_{23}, and a_{13} was introduced to describe the observed features in terms of a proper characteristic length scale [167].

The work described in the previous paragraph laid the foundation for further investigations into the universality of these trimers. First, a proof-of-concept study demonstrated that the properties of the trimer could be probed through collisions between three different hyperfine spin states of ^{6}Li atoms and ^{6}Li$_2$ dimers [168]. Subsequent studies by a group at the University of Tokyo showed that the positions of the loss-rate peaks, when plotted against the scattering lengths, deviate from the predictions of universal theory in a manner that cannot be accounted for by non-universal two-body properties [169]. These findings were later confirmed through direct radiofrequency association measurements [170].

The determination of the position of the ^{85}Rb Efimov resonance was an additional outcome of a study of ultracold collisions in a BEC setting [171]. At the same time, the focus of the article was on finding the value of the *Tan's contact* – a universal quantity that quantifies the probability of finding two particles very close – essentially a measure of short-range correlations in a many-body system. Research showed the resonance position using three-body recombination rates. Expressed in units of the mean scattering length of the van der Waals potential for ^{85}Rb, the results appeared at a universal value as proposed by theory. These properties are described in more detail in Section 2.3.

Extending the experimental study of Efimov trimers to include mixtures of species rapidly became of particular interest to universal few-body physics. One of the first studies into this matter was a test of whether the observed van der Waals universality of Efimov three-body physics also applies to heteronuclear mixtures of different atomic species [172]. The work explored three-body loss in an ultracold trapped mixture of bosonic ^{87}Rb and fermionic ^{40}K atoms by measuring inelastic-collision loss rates as a function of the scattering length. An Efimov resonance in the loss rate for inelastic collisions between ^{40}K–^{87}Rb Feshbach molecules and ^{87}Rb atoms was shown. However, the study did not find any Efimov resonances in three-

atom losses, because the Rb–Rb interaction was relatively weak and not resonant. These observations were compared with previous measurements in other K-Rb isotopic mixtures and with theoretical predictions, providing insight into how universal three-body phenomena manifest in Bose-Fermi mixtures.

Differences between the ground and excited Efimov states were studied in a system of ultracold helium [173]. The authors reported the experimental observation of an Efimov state using Coulomb explosion imaging. The authors have found that the dominant structure of a ground Efimov state with positive two-body scattering length is a triangle with a relatively small acute angle, distinct from excited states and hinting at possible non-universality of the Efimov resonances.

Another study into the universality of the Efimov state was conducted and described in Ref. [174]. The authors directly compared the Efimov spectra in a mass-imbalanced ^{6}Li–^{133}Cs Cs mixture near two Feshbach resonances that are nearly identical except for their resonance strength (broad vs narrow). The result of the study showed a clear dependence of the absolute Efimov resonance position on Feshbach resonance strength, which is in contrast to the universal prediction. The experimental and theoretical results with respect to this phenomenon are described in more detail in the next Section 2.3.

Another interesting avenue of research concerns the *super-Efimov* effect. It is predicted to produce an infinite sequence of bound or resonant states in a system of three fermions confined to two dimensions. Compared with the conventional Efimov effect, the resulting spectrum exhibits a significantly lower density of states. So far, the studies carried out for this phenomenon were purely theoretical with no direct experimental confirmation [175–177].

2.3. Universality of the Efimov effect

As shown in Section 2.2, studies of the properties of Efimov states generally include measurements of three-body recombination. One of the first studies using a theoretical approach for spin-polarized atomic hydrogen was described in Ref. [178]. Applying the same framework for alkali atoms [179, 180] provided a prediction that the three-body recombination rate should scale approximately as a^2. But further studies showed that actually the rates scale vary much faster, proportionally to a^4 [17, 181, 182]. These studies also predicted an additional effect, namely the *Stückelberg interference*. This interference in three-body recombination rates occurs at positive values of a, where the Efimov state intersects the atom–dimer continuum – potentially beneficial for experiments where three-body loss needs to be minimized. Furthermore, Ref. [182] showed that the Efimov resonances for negative a lead to enhancements of the recombination rate – occurring where the Efimov states become unbound and merged into the three-body continuum. For homonuclear three-body recombination, these zero-energy Efimov resonances are expected to follow an approximate geometric progression in the scattering length, with each successive resonance appearing at a two-body scattering length roughly $e^{\pi/s_0} \approx 22.7$ times larger than the previous one. This effect is independent of the chosen atomic species or other microscopic parameters of the system and thus considered *universal*.

To give a broader idea of the concept of *universality*, we should state that the complete microscopic treatment of few- and many-body physics in an interacting gas is generally impossible. The description of few-body dynamics greatly simplifies in a dilute ultracold atomic gas with near-resonant interactions. In this regime, all physical observables can be expressed in terms of just two dimensionless parameters that quantify interaction strength and quantum degeneracy: na^3 and $n\lambda^3$, where n is the atomic density and λ is the thermal wavelength.

Continuous scaling transformations of the atomic density, scattering length, or thermal wavelength leave all observables and their dynamics unchanged when expressed in these rescaled units. This invariance defines the universal behavior, which is largely independent of the microscopic details of the interactions or the specific atomic species [119].

As mentioned, the Efimov effect occurs at $|a| \to \infty$, where a is the two-body scattering length. Exactly at unitarity, infinitely many Efimov bound states form as a result of resonant three-body interaction of the form $\sim -1/R^2$, where R is the hyperradius. A striking feature of the Efimov states is their universal properties, which emerge even at large but finite values of $|a|$. In such conditions, the number of Efimov states also becomes finite; their energies, however, preserve their near log-periodic behavior. Similarly, positions of the Efimov resonances $a_-^{(n)}$ follow the universal pattern in which each consecutive state becomes unbound at a value ca. 22.7 larger than the previous one, namely $a_-^{n+1}/a_-^n = e^{\pi/s_0} \approx 22.7$.

Conditions favorable for the Efimov effect require a to be larger than all length scales of the system, including the characteristic length of interaction, i.e., the van der Waals length r_{vdW}. Efimov bound states, therefore, appear in the vicinity of two-atom Feshbach resonances. Considerable scientific focus, both theoretical and experimental, has recently been placed on research into the limits of the universality of Efimov physics, governed by the specific properties of the underlying Feshbach resonances [158, 183]. The characteristic feature of a Feshbach resonance is its strength or width as measured by the dimensionless s_{res} parameter [14]. The s_{res} parameter is defined within the van der Waals theory of interatomic interactions and serves as a dimensionless measure characterizing the coupling strength and the extent to which the open-channel physics dominates a Feshbach resonance.

Theoretical studies have shown that the position of the first/ground Efimov resonance $a_-^0 = -9.7\, r_{\mathrm{vdW}}$ is also universal. However, experimental measurements fell within 20% of this value only in the regime of broad Feshbach resonances $s_{\mathrm{res}} \gg 1$. In the case of broad resonance, a universal repulsive wall appears in the effective three-body potentials at $R \approx 2r_{\mathrm{vdW}}$, tying the universality to long-range behavior of the underlying interaction. This universality allows us to predict the positions of all Efimov resonances. Recent experimental studies, however, have shown that the Efimov structure depends on the width of the Feshbach resonance; specifically, it loses its universal character as s_{res} decreases. Deviations from the universal value $-9.7\, r_{\mathrm{vdW}}$ have been confirmed in a precise study of two- and three-body interactions near an intermediate-strength ($s_{\mathrm{res}} \gtrsim 1$) Feshbach resonance in 39K at 33.5820(14) G [184].

One of the main goals of this thesis is to expand on research on three-body interactions presented in Ref. [158]. Investigating across a range of Feshbach resonance widths, we observe non-universal behavior of the Efimov trimer in the ground and excited states. It emerges from a repulsive interaction in the atom-dimer channel, which appears for narrow ($s_{\mathrm{res}} < 1$) resonances. The interplay between the length scales describing the short-range exchange and van der Waals interactions across a series of alkali-metal homonuclear samples is also likely an important factor in determining the universal behavior of the Efimov spectrum. Therefore, we estimate the strength of three-body forces in relevant few-body systems using ab initio quantum chemistry methods. We then compare the ground Efimov resonance location dependence on the s_{res} parameter for systems with varying strength of the Feshbach resonance.

Chapter 3

Three-body theory

In three-body physics, the most prominent approach for solving the Schrödinger equation is through the use of adiabatic hyperspherical coordinate methods. These techniques were essential to the early theoretical predictions and analytical calculations of the Efimov effect [151, 185–187]. Later, they were equally important in demonstrating that ultracold quantum gases are promising systems for observing universal Efimov physics. In particular, they directly linked the Efimov effect to three-body recombination losses. Hyperspherical methods have proven to be very versatile: they have been used both with zero-range, regularized interactions to produce simple analytical results [181, 188–193] and, on the other hand, as a basis for quantitative numerical solutions using finite range analytical or numerical three-body Hamiltonians [120, 182, 194–199].

One of the first uses of the adiabatic hyperspherical methods was shown in Ref. [200]. The theoretical framework allowed diagonalization of the system's Hamiltonian at each *hyperradius* R (a parameter measuring the system's size and described in more detail in the following Sections), yielding adiabatic potential curves that describe the system's energies as functions of R. These curves offer an immediate, dynamics-oriented depiction of the accessible reaction pathways for a given system, revealing the structure of bound and quasi-bound states, as well as their excitation and decay mechanisms. Coupling matrix elements between the adiabatic states can also be calculated, allowing for a systematic solution of the full three-body Schrödinger equation with a specific, numerical accuracy. The described approach applies to bound-state problems, two-body inelastic collisions, three-body collisions, and photon-assisted collision processes.

In this Chapter, we will briefly summarize the mathematical methods underlying the adiabatic hyperspherical approach and present the methodology for numerical calculations of three-body recombination rates, bound-state energies, and lifetimes. One of the primary achievements of this approach has been not only achieving quantitative accuracy but also, just as importantly, developing qualitative and quantitative insights into the dominant reaction pathways and the physical mechanisms that control them.

The adiabatic representation becomes increasingly challenging as the system's complexity and the number of coupled hyperradial equations grow. For such cases, reworking the problem into a set of diabatic equations using the *slow variable discretization* (SVD) method, introduced in Ref. [201], significantly increases computational efficiency. When propagation to very large hyperradii is needed to obtain precise scattering data, a hybrid approach has proven both accurate and efficient [202]. This method applies SVD at small to intermediate hyperradii while solving the directly coupled adiabatic equations at very large hyperradii. We will introduce the SVD method in Chapter 7, as it served as the basis for all referenced

calculations.

3.1. The Jacobi coordinates for N particles

The quantum-mechanical three-body problem involves solving the time-independent Schrödinger equation for a system of three interacting particles. However, before we reduce our considerations to three particles, it is prudent to start with a more general N-body system and show where specific mathematical constraints become either advantageous or restricting. For example, for N interacting particles, with masses m_i, separating the center-of-mass motion allows us to reduce the problem to a $d = 3N - 3$ dimensional partial differential equation in a lab-fixed, *relative* coordinate system [166].

Let us consider a Hamiltonian for a system of N particles, written in the lab-fixed, Cartesian coordinate system

$$\hat{H} = \sum_{i=1}^{N} \frac{\hat{\mathbf{p}}_i^2}{2m_i} + V\left(\mathbf{r}_1, \ldots, \mathbf{r}_N\right) \ , \tag{3.1}$$

where a set of vectors $\mathbf{r}_i$ represents the positions of the particles, $\hat{\mathbf{p}}_i = -i\hbar\nabla_{\mathbf{r}_i}$ is a set of N momentum operators, and V is the interaction potential. We introduce the standard, mass-scaled Jacobi coordinates used in few-body theory to separate the center-of-mass motion and greatly simplify the form of the kinetic operator

$$\boldsymbol{\rho}_j = \sqrt{\frac{\mu_j}{\mu}} \left(\mathbf{r}_j - \frac{1}{M_j} \sum_{i=1}^{j} m_i \mathbf{r}_i \right), \quad i = 1, \ldots, N-1 \ , \tag{3.2}$$

where $M_j = \sum_{i=1}^{j} m_i$ is the partial mass sum. Consistently, the total mass of the system is $M = M_N$. The Jacobi coordinates written this way are a set of recursively defined vectors, where each consecutive vector represents the distance of the next particle from the partial center of mass defined by a subset of previously considered particles. Each vector is normalized by a mass-dependent factor, whose importance will become relevant later. The reduced mass associated with each Jacobi coordinate is

$$\mu_j = \frac{M_j m_{j+1}}{M_{j+1}} \ , \tag{3.3}$$

and the overall N-body reduced mass is given by

$$\mu = \left(\prod_{i=1}^{N-1} \mu_j \right)^{1/(N-1)} \ . \tag{3.4}$$

Canonically, the total center of mass is the *N-th Jacobi vector*, and it is given by

$$\mathbf{R}_{\mathrm{CM}} = \sum_{i=1}^{N} \frac{m_i \mathbf{r}_i}{M} \ . \tag{3.5}$$

The full coordinate transformation is now given by

$$\{\mathbf{r}_1, \ldots, \mathbf{r}_N\} \to \{\boldsymbol{\rho}_1, \ldots, \boldsymbol{\rho}_{N-1}, \mathbf{R}_{\mathrm{CM}}\} \ . \tag{3.6}$$

This transformation is linear and invertible. Let us now consider how the kinetic energy operator transforms. We begin by using the chain rule

$$\begin{aligned}\frac{\partial}{\partial \mathbf{r}_i} &= \sum_{k=1}^{N-1} \frac{\partial \boldsymbol{\rho}_k}{\partial \mathbf{r}_i}\frac{\partial}{\partial \boldsymbol{\rho}_k} + \frac{\partial \mathbf{R}_{\mathrm{CM}}}{\partial \mathbf{r}_i}\frac{\partial}{\partial \mathbf{R}_{\mathrm{CM}}} \\ &= \sum_{k=1}^{N-1} a_{ik}\frac{\partial}{\partial \boldsymbol{\rho}_k} + \frac{m_i}{M}\frac{\partial}{\partial \mathbf{R}_{\mathrm{CM}}} \ .\end{aligned} \tag{3.7}$$

We calculate the coefficient

$$a_{ik} = \frac{\partial \boldsymbol{\rho}_k}{\partial \mathbf{r}_i} = \sqrt{\frac{\mu_k}{\mu}} \begin{cases} -\frac{m_i}{M_k}, & i < k+1 \\ 1, & i = k+1 \\ 0, & i > k+1 \end{cases} \ . \tag{3.8}$$

Thus, the kinetic energy operator in terms of the relative momenta $\hat{\boldsymbol{\pi}}_k = -i\hbar\nabla_{\boldsymbol{\rho}_k}$ and the center-of-mass momentum $\hat{\mathbf{P}}_{\mathrm{CM}} = -i\hbar\nabla_{\mathbf{R}_{\mathrm{CM}}}$ is given by

$$\begin{aligned}\hat{T} &= \sum_{i=1}^{N}\frac{\hat{\mathbf{p}}_i^2}{2m_i} = \sum_{i=1}^{N}\frac{1}{2m_i}\left(\sum_{k=1}^{N-1} a_{ik}\hat{\boldsymbol{\pi}}_k + \frac{m_i}{M}\hat{\mathbf{P}}_{\mathrm{CM}}\right)^2 = \\ &= \sum_{i=1}^{N}\frac{1}{2m_i}\left(\sum_{k=1}^{N-1} a_{ik}^2\hat{\boldsymbol{\pi}}_k^2 + \frac{m_i^2}{M^2}\hat{\mathbf{P}}_{\mathrm{CM}}^2 + \underbrace{2\sum_{1\le k<l\le N-1} a_{ik}a_{il}\hat{\boldsymbol{\pi}}_k\hat{\boldsymbol{\pi}}_l}_{} + \underbrace{2\sum_{k=1}^{N-1} a_{ik}\frac{m_i}{M}\hat{\boldsymbol{\pi}}_k\hat{\mathbf{P}}_{\mathrm{CM}}}_{}\right) \ .\end{aligned} \tag{3.9}$$

Both of the mixed terms are symmetric, because the set of operators $\{\hat{\boldsymbol{\pi}}_1 \ldots, \hat{\boldsymbol{\pi}}_{N-1}, \hat{\mathbf{P}}_{\mathrm{CM}}\}$ commutes, due to the mentioned linearity and invertibility of the proposed transformation. Let us focus on the first of the mixed, underlined terms

$$\sum_{1\le k<l\le N-1}^{N-1}\left(\sum_{i=1}^{N}\frac{a_{ik}a_{il}}{m_i}\right)\hat{\boldsymbol{\pi}}_k\hat{\boldsymbol{\pi}}_l \ . \tag{3.10}$$

Without loss of generality, we assumed $k < l$. From the definition of a_{ik}, we deduce that the bracketed sum over i ends at $k+1$. Terms $a_{ik}a_{il}$ with index $i : k+1 < i \le l+1$ are zero because a_{ik} is equal to zero. Let us expand this sum

$$\sum_{i=1}^{k+1}\frac{a_{ik}a_{il}}{m_i} = \sqrt{\frac{\mu_k}{\mu}}\sqrt{\frac{\mu_l}{\mu}}\left(\sum_{i=1}^{k}\frac{1}{m_i}\frac{m_i^2}{M_kM_l} - \frac{1}{m_{k+1}}\frac{m_{k+1}}{M_l}\right) = \sqrt{\frac{\mu_k}{\mu}}\sqrt{\frac{\mu_l}{\mu}}\left(\frac{M_k}{M_kM_l} - \frac{1}{M_l}\right) = 0 \ . \tag{3.11}$$

We will now prove that the second mixed term is also zero. We can simplify this term

$$\sum_{k=1}^{N-1}\sum_{i=1}^{N}\frac{a_{ik}}{M}\hat{\boldsymbol{\pi}}_k\hat{\mathbf{P}}_{\mathrm{CM}} \ . \tag{3.12}$$

Now, only the a_{ik} depends on the index i. This sum ends at $i = k+1$, due to the definition of a_{ik} and thus can also be expanded

$$\sum_{i=1}^{k+1} a_{ik} = \sqrt{\frac{\mu_k}{\mu}}\left(\sum_{i=1}^{k}\frac{-m_i}{M_k} + 1\right) = \sqrt{\frac{\mu_k}{\mu}}\left(\frac{-M_k}{M_k} + 1\right) = 0 \ . \tag{3.13}$$

Naturally, we also need to simplify the square terms in Eq. (3.9). First, let us consider the first of these terms

$$\sum_{k=1}^{N-1}\left(\sum_{i=1}^{N}\frac{a_{ik}^2}{2m_i}\right)\hat{\boldsymbol{\pi}}_k^2 \ . \tag{3.14}$$

We expand the bracketed sum, truncating it again due to the definition of a_{ik}

$$\begin{aligned}\sum_{i=1}^{N}\frac{a_{ik}^2}{2m_i} &= \frac{\mu_k}{\mu}\sum_{i=1}^{k+1}\frac{a_{ik}^2}{2m_i} = \frac{\mu_k}{\mu}\left(\sum_{i=1}^{k}\frac{m_i^2}{2m_iM_k^2}+\frac{1}{2m_{k+1}}\right)\\ &= \frac{\mu_k}{\mu}\left(\frac{M_k}{2M_k^2}+\frac{1}{2m_{k+1}}\right) = \frac{\mu_k}{2\mu}\frac{m_{k+1}+M_k}{M_km_{k+1}} = \frac{\mu_k}{2\mu}\frac{M_{k+1}}{M_km_{k+1}} = \frac{1}{2\mu}\ ,\end{aligned} \tag{3.15}$$

where we used the definition from Eq. (3.3). We can thus simplify the first of the squared terms to

$$\sum_{k=1}^{N-1}\frac{\hat{\boldsymbol{\pi}}_k^2}{2\mu}\ . \tag{3.16}$$

It is apparent now why the Jacobi coordinates were *mass-regularized* by multiplying the relative positions of the particles by the factor $\sqrt{\frac{\mu_j}{\mu}}$. This approach allows the sum in the kinetic energy operator to be dependent only on the N-body reduced mass μ. Other definitions of the overall reduced mass μ can be used and are occasionally adopted. Still, the choice made in Eq. (3.4) is especially advantageous in many situations, as it preserves the overall volume element. Simplifying the second squared term gives the final form of the kinetic energy operator and thus the whole Hamiltonian

$$\hat{H} = \left(\sum_{k=1}^{N-1}\frac{\hat{\boldsymbol{\pi}}_k^2}{2\mu}+\frac{\mathbf{P}_{\mathrm{CM}}^2}{2M}\right)+V(\boldsymbol{\rho}_1,\ldots,\boldsymbol{\rho}_{N-1},\mathbf{P}_{\mathrm{CM}})\ . \tag{3.17}$$

Most of the considered interaction potentials do not depend on the motion of the total center of mass $\mathbf{P}_{\mathrm{CM}}$, thus allowing for complete separation of variables and reducing the dimensionality of the considered set of differential equations by 3. In the next Section, we will build on this progress by introducing the so-called *adiabatic approach*, which allows us to rewrite the kinetic energy operator in terms of a single variable, namely the *hyperradius* R. We will, however, specifically consider the *three-body* hyperspherical coordinates in yet another Section, where careful conclusions must be drawn from the various symmetry constraints of our problem.

3.2. The hyperspherical coordinates for N particles

In the previous Section, we have successfully reduced the dimensionality of the stated problem by three – under the assumption that we can separate the motion of the total center-of-mass for N interacting particles, i.e., express the total wavefunction as a product $\Psi_{\mathrm{tot}} = \Psi_{\mathrm{CM}}(\mathbf{R}_{\mathrm{CM}})\Psi(\boldsymbol{\rho}_1,\ldots,\boldsymbol{\rho}_N)$. Thus, let us consider a $d = 3N-3$ dimensional partial differential equation in the relative coordinate system,

$$\hat{H} = \sum_{k=1}^{N-1}\frac{\hat{\boldsymbol{\pi}}_k^2}{2\mu}+V(\boldsymbol{\rho}_1,\ldots,\boldsymbol{\rho}_{N-1}) = -\frac{\hbar^2\Delta_{\boldsymbol{\rho}}}{2\mu}+V\ . \tag{3.18}$$

The Cartesian coordinates of the Jacobi vectors can be collected into a single d-dimensional vector $\mathbf{r} = \{r_1,\ldots,r_d\}$. In hyperspherical coordinates, one scalar variable—the hyperradius

R – introduced below – is treated separately in the adiabatic framework. The aim in the adiabatic approach is to introduce this variable in such a way that when the potential depends only on relative coordinates, the system is transformed into an infinite set of coupled ordinary differential equations in the single adiabatic coordinate R. Let us therefore consider a coordinate transformation in the lab-fixed frame

$$F : \{R, \alpha_1, \ldots, \alpha_{d-1}\} \to \{r_1, \ldots, r_{d-1}\} \ , \tag{3.19}$$

where we introduced a set of $d-1$ *hyperangles* α_i. Canonically. the map F is given by

$$\begin{aligned} r_d &= R\cos\alpha_{d-1} \ , \\ r_{d-1} &= R\sin\alpha_{d-1}\cos\alpha_{d-2} \ , \\ r_{d-2} &= R\sin\alpha_{d-1}\sin\alpha_{d-2}\cos\alpha_{d-3} \ , \\ &\vdots \\ r_2 &= R\prod_{i=2}^{d-1}\sin\alpha_i\cos\alpha_1 \ , \\ r_1 &= R\prod_{i=1}^{d-1}\sin\alpha_i \ . \end{aligned} \tag{3.20}$$

Naturally, we require the coordinate map F to be bijective. In general, all hyperangles would span the range $[0, 2\pi]$ to ensure the surjectivity of F. However, let us consider a point with hyperangle $\alpha_k \in [\pi, 2\pi] : 2 \leq k \leq d-1$. Now consider a symmetry projection

$$t : \{R, \alpha_1, \ldots, \alpha_{d-1}\} \to \{R, \alpha_1+\pi, \pi-\alpha_2, \pi-\alpha_3 \ldots, \pi-\alpha_{k-1}, 2\pi-\alpha_k, \alpha_k, \ldots, \alpha_{d-1}\} \ , \tag{3.21}$$

where by induction, we assume that all hyperangles $\alpha_l : 2 \leq l < k$ are in range $[0, \pi]$. Using the following trigonometric relations

$$\begin{aligned} \sin(2\pi-\alpha_k) &= -\sin\alpha_k \ , \\ \cos(2\pi-\alpha_k) &= \cos\alpha_k \ , \\ \sin(\pi-\alpha_l) &= \sin\alpha_l \ , \\ \cos(\pi-\alpha_l) &= -\cos\alpha_l \ , \\ \sin(\alpha_1+\pi) &= -\sin\alpha_1 \ , \\ \cos(\alpha_1+\pi) &= -\cos\alpha_1 \ , \end{aligned} \tag{3.22}$$

we can show that

$$F(t(R, \alpha_1, \ldots, \alpha_{d-1})) = F(R, \alpha_1, \ldots, \alpha_{d-1}) \ , \tag{3.23}$$

which means that by allowing α_k to be larger than π we do not ensure the injectivity of the map F. Hence, we can truncate the range of α_k to $[0, \pi]$. As mentioned, we provide this reasoning inductively for all $k : 2 \leq k \leq d-1$. Therefore, the ranges spanned by the hyperangles are

$$\alpha_1 \in [0, 2\pi] \, , \quad \alpha_k \in [0, \pi] \, , \quad k = 2, \ldots, d-1 \ . \tag{3.24}$$

We note that through such a definition of F, we have ensured the relation:

$$R = \sqrt{\sum_{i=1}^{d} x_i^2} \ , \tag{3.25}$$

which is equivalent to stating that the hyperradius R is the radius of the d-dimensional hypersphere. We will now show how the Laplacian becomes simplified in the hyperspherical coordinates $\{R, \Omega\}$, where we denote the hyperangles collectively as $\Omega = \{\alpha_1, \ldots, \alpha_{d-1}\}$.

3.2.1. The Laplacian in canonical hyperspherical coordinates

Beginning with the Voss-Weyl formula, one can derive the form of the Laplacian in Jacobi curvilinear coordinates

$$\Delta_{\boldsymbol{\rho}} = \frac{1}{\sqrt{\det g}} \frac{\partial}{\partial \xi^i} \left(\sqrt{\det g}\; g^{ij} \frac{\partial}{\partial \xi^j} \right) \ , \tag{3.26}$$

where g_{ij} is the metric tensor of the map F, we use a notation $\{\xi^1, \ldots, \xi^d\} = \{R, \alpha_1, \ldots, \alpha_{d-1}\}$ to describe the hyperspherical coordinates collectively, and we use the Einstein notation. In the case of map F the tensor g is diagonal

$$\begin{aligned}
g_{RR} =& \sum_{i=1}^{d} \left(\frac{\partial r_i}{\partial R} \right)^2 = \sum_{i=1}^{d} \frac{r_i^2}{R^2} = 1 \ , \\
g_{R\alpha_k} =& \sum_{i=1}^{d} \frac{\partial r_i}{\partial R} \frac{\partial r_i}{\partial \alpha_k} = \sum_{i=1}^{d} \frac{r_i}{R} \frac{\partial r_i}{\partial \alpha_k} = \sum_{i=1}^{d} \frac{1}{2R} \frac{\partial r_i^2}{\partial \alpha_k} = \frac{1}{2R} \frac{\partial}{\partial \alpha_k} \sum_{i=1}^{d} r_i^2 = \frac{1}{2R} \frac{\partial}{\partial \alpha_k} R = 0 \ , \\
g_{\alpha_k \alpha_k} =& \sum_{i=1}^{d} \left(\frac{\partial r_i}{\partial \alpha_k} \right)^2 = \mathcal{R}_k^2 \cos^2 \alpha_k \prod_{j=1}^{k-1} \sin^2 \alpha_j + \sum_{i=2}^{k} \mathcal{R}_k^2 \cos^2 \alpha_k \left(\prod_{j=i}^{k-1} \sin^2 \alpha_j \cos^2 \alpha_{i-1} \right) + \mathcal{R}_k^2 \sin^2 \alpha_k \\
=& \mathcal{R}_k^2 \cos^2 \alpha_k \left(\prod_{j=1}^{k-1} \sin^2 \alpha_j + \sum_{i=2}^{k} \prod_{j=i}^{k-1} \sin^2 \alpha_j \cos^2 \alpha_{i-1} \right) + \mathcal{R}_k^2 \sin^2 \alpha_k = \mathcal{R}_k^2 \ , \\
\frac{g_{\alpha_l \alpha_k}}{R^2} =& \frac{1}{R^2} \sum_{i=1}^{d} \frac{\partial r_i}{\partial \alpha_k} \frac{\partial r_i}{\partial \alpha_l} \ = \left(\prod_{j=l+1}^{d-1} \sin \alpha_j \right) \cos \alpha_l \left(\prod_{j=1}^{l-1} \sin \alpha_j \right) \left(\prod_{j=k+1}^{d-1} \sin \alpha_j \right) \cos \alpha_k \left(\prod_{j=1}^{k-1} \sin \alpha_j \right) + \\
&+ \sum_{i=2}^{k} \left(\prod_{j=l+1}^{d-1} \sin \alpha_j \right) \cos \alpha_l \left(\prod_{j=i}^{l-1} \sin \alpha_j \right) \left(\prod_{j=k+1}^{d-1} \sin \alpha_j \right) \cos \alpha_k \left(\prod_{j=i}^{k-1} \sin \alpha_j \right) \cos^2 \alpha_{i-1} + \\
&+ \left(\prod_{j=l+1}^{d-1} \sin \alpha_j \right) \cos \alpha_l \left(\prod_{j=k+1}^{l-1} \sin \alpha_j \right) \left(\prod_{j=k+1}^{d-1} \sin \alpha_j \right) (-\sin \alpha_k \cos \alpha_k) = \\
=& \left(\prod_{j=1, j \neq l,k}^{d-1} \sin^2 \alpha_j \right) \cos \alpha_l \cos \alpha_k \sin \alpha_k + \sum_{i=2}^{k} \left(\prod_{j=i, j \neq l,k}^{d-1} \sin^2 \alpha_j \right) \cos \alpha_l \cos \alpha_k \sin \alpha_k \cos^2 \alpha_{i-1} - \\
&- \left(\prod_{j=k+1, j \neq l}^{d-1} \sin^2 \alpha_j \right) \sin \alpha_k \cos \alpha_l \cos \alpha_k = \\
=& \left(\prod_{j=k+1, j \neq l}^{d-1} \sin^2 \alpha_j \right) \cos \alpha_l \cos \alpha_k \sin \alpha_k \left[\left(\prod_{j=1}^{k-1} \sin^2 \alpha_j + \sum_{i=1}^{k} \prod_{j=2}^{k-1} \sin^2 \alpha_j \cos^2 \alpha_{i-1} \right) - 1 \right] = 0 \ ,
\end{aligned} \tag{3.27}$$

where we defined $\mathcal{R}_k = R \prod_{j=k+1}^{d-1} \sin \alpha_j$, used $k < l$ without the loss of generality and used the identity

$$\prod_{j=1}^{k-1} \sin^2 \alpha_j + \sum_{i=2}^{k} \prod_{j=i}^{k-1} \sin^2 \alpha_j \cos^2 \alpha_{i-1} = 1 \ , \tag{3.28}$$

which can be proven by induction. For completeness, we can write the resulting line element ds^2, the volume element dV, and the differential surface area on the hypersphere $d\Omega$

$$\begin{aligned} ds^2 &= g_{ij} d\xi^i d\xi^j = dR^2 + R^2 \left[\sum_{k=1}^{d-1} \prod_{j=k+1}^{d-1} \sin^2 \alpha_j \, d\alpha_k^2 \right] , \\ dV &= \sqrt{\det g} \; d\xi^1, \ldots, \xi^d = R^{d-1} \left(\prod_{j=2}^{d-1} \sin^{j-1} \alpha_j \right) dR \, d\alpha_1 \ldots d\alpha_{d-1} , \\ dV &= R^{d-1} dR \, d\Omega , \\ d\Omega &= \prod_{j=2}^{d-1} \sin^{j-1} \alpha_j \; d\alpha_1 \ldots d\alpha_{d-1} . \end{aligned} \tag{3.29}$$

Finally, we derive the the hyperradial (Δ_R) and hyperangular (Δ_Ω) parts of Laplacian $\Delta_{\boldsymbol{\rho}} = \Delta_R + \Delta_\Omega$ in the hyperspherical coordinates – using Eq. (3.26)

$$\begin{aligned} \sqrt{\det g} &= R^{d-1} f(\Omega) , \\ \Delta_R &= \frac{1}{R^{d-1}} \frac{\partial}{\partial R} \left(R^{d-1} \frac{\partial}{\partial R} \right) = \frac{\partial^2}{\partial R^2} + \frac{d-1}{R} \frac{\partial}{\partial R} , \\ \Delta_\Omega &= \frac{1}{\sqrt{\det g}} \frac{\partial}{\partial \alpha_k} \left(\sqrt{\det g} \; g^{kl} \frac{\partial}{\partial \alpha_l} \right) = \frac{1}{f(\Omega)} \frac{\partial}{\partial \alpha_k} \left(f(\Omega) \mathcal{R}_k^{-2} \frac{\partial}{\partial \alpha_k} \right) = \\ &= \frac{1}{R^2 f(\Omega)} \frac{\partial}{\partial \alpha_k} \left[f(\Omega) \left(\prod_{j=k+1}^{d-1} \sin^{-2} \alpha_j \right) \frac{\partial}{\partial \alpha_k} \right] = -\frac{\boldsymbol{\Lambda}^2(\Omega)}{R^2} , \end{aligned} \tag{3.30}$$

where $f(\Omega) = \prod_{j=2}^{d-1} \sin^{j-1} \alpha_j$, k, l are indices ranging from 1 to $d-1$ describing only the hyperangles – for which we use the Einstein notation, and $\boldsymbol{\Lambda}^2$ is the *grand angular momentum* operator, which is an isotropic Casimir operator for the group SO(d) [203]. Using the calculated Laplacian, we can greatly simplify the form of the Hamiltonian given by Eq. (3.18)

$$\hat{H} = -\frac{\hbar^2 \Delta_R}{2\mu} + \frac{\hbar^2 \boldsymbol{\Lambda}^2}{2\mu R^2} + V(R, \Omega) . \tag{3.31}$$

3.2.2. The operator Λ^2 in canonical hyperspherical coordinates

We still need to derive the form of the operator $\boldsymbol{\Lambda}$. We will show that it is explicitly given by

$$\boldsymbol{\Lambda}^2 = -\sum_{i>j} \Lambda_{ij}^2 , \quad \Lambda_{ij} = r_i \frac{\partial}{\partial r_j} - r_j \frac{\partial}{\partial r_i} . \tag{3.32}$$

The operators λ_{ij} are the generators of rotations in the plane spanned by the Jacobi coordinates r_i and r_j, and thus represent a pseudo-angular momentum associated with rotations between two relative degrees of freedom of the system. Firstly, let us show that the operator

$\mathbf{\Lambda}^2$ follows a recursive equation

$$\begin{aligned}\mathbf{\Lambda}^2(\Omega) =& -\frac{1}{\prod_{j=2}^{d-1}\sin^{j-1}\alpha_j}\frac{\partial}{\partial\alpha_{d-1}}\left(\prod_{j=2}^{d-1}\sin^{j-1}\alpha_j\cdot 1\frac{\partial}{\partial\alpha_{d-1}}\right)-\\ &-\sum_{k=1}^{d-2}\frac{1}{\prod_{j=2}^{d-1}\sin^{j-1}\alpha_j}\frac{\partial}{\partial\alpha_k}\left(\prod_{j=2}^{d-1}\sin^{j-1}\alpha_j\cdot\prod_{j=k+1}^{d-1}\sin^{-2}\alpha_j\frac{\partial}{\partial\alpha_k}\right)=\\ =& -\frac{1}{\sin^{d-2}\alpha_{d-1}}(d-2)\sin^{d-3}\alpha_{d-1}\cos\alpha_{d-1}\frac{\partial}{\partial\alpha_{d-1}}-\frac{\partial^2}{\partial\alpha_{d-1}^2}-\\ &-\frac{1}{\sin^2\alpha_{d-1}}\sum_{k=1}^{d-2}\frac{1}{\prod_{j=2}^{d-2}\sin^{j-1}\alpha_j}\frac{\partial}{\partial\alpha_k}\left(\prod_{j=2}^{d-2}\sin^{j-1}\alpha_j\prod_{j=k+1}^{d-2}\sin^{-2}\alpha_j\frac{\partial}{\partial\alpha_k}\right)=\\ =& -\frac{\partial^2}{\partial\alpha_{d-1}^2}-(d-2)\cot\alpha_{d-1}\frac{\partial}{\partial\alpha_{d-1}}+\frac{\mathbf{\Lambda}^2(\Omega_{d-1})}{\sin^2\alpha_{d-1}}\ ,\end{aligned}\tag{3.33}$$

where $\mathbf{\Lambda}^2(\Omega_{d-1})$ follows the definition of the grand angular momentum operator for the metric $d\Omega_{d-1}$ in $d-2$ hyperangular dimensions (as opposed to $d-1$ hyperangular dimensions up to this point), i.e., neglecting the coordinate α_{d-1},

$$d\Omega^2 := d\Omega_d^2 = d\alpha_{d-1}^2 + \sin^2\alpha_{d-1}d\Omega_{d-1}\ .\tag{3.34}$$

Seeing the recursive relations given by Eq. (3.33) and Eq. (3.34), it is natural to follow up this reasoning by trying to obtain the eigenvalues of $\mathbf{\Lambda}^2(\Omega_d)$ through a recursive ansatz for the eigenfunctions $\mathcal{Y}(\Omega_d)$

$$\mathbf{\Lambda}^2(\Omega_d)\mathcal{Y}(\Omega_d) = \lambda_d\mathcal{Y}(\Omega_d)\ .\tag{3.35}$$

Thus, let us assume that we can separate the variables α_{d-1} and Ω_{d-1} and propose that the eigenfunctions are of the form

$$\mathcal{Y}(\Omega_d) = g(\alpha_{d-1})\mathcal{Y}_{d-1}(\Omega_{d-1})\ ,\quad \mathbf{\Lambda}^2(\Omega_{d-1})\mathcal{Y}_{d-1} = \lambda_{d-1}\mathcal{Y}_{d-1}\ .\tag{3.36}$$

for some function $g(\alpha_{d-1})$. Let us insert the recursive ansatz from Eq. (3.36) into Eq. (3.33)

$$\lambda_d\cdot g(\alpha_d) = -\frac{\partial^2 g(\alpha_{d-1})}{\partial\alpha_{d-1}^2}-(d-2)\cot\alpha_{d-1}\frac{\partial g(\alpha_{d-1})}{\partial\alpha_{d-1}}+g(\alpha_{d-1})\frac{\lambda_{d-1}}{\sin^2\alpha_{d-1}}\ .\tag{3.37}$$

Let us define $x = \cos\alpha_{d-1}$, $y(x) = g(\alpha_{d-1})$ and simplify the equations above, using the relations

$$\begin{aligned}\frac{\partial}{\partial\alpha_{d-1}} =& -\sin\alpha_{d-1}\frac{\partial}{\partial x}\ ,\\ \frac{\partial^2}{\partial\alpha_{d-1}^2} =& (1-x^2)\frac{\partial^2}{\partial x^2}-x\frac{\partial}{\partial x}\ .\end{aligned}\tag{3.38}$$

The recursive equation becomes

$$(1-x^2)y'' - (d-1)xy' + \left[\lambda_d - \frac{\lambda_{d-1}}{1-x^2}\right]y = 0\ .\tag{3.39}$$

The equation above is the *associated* Gegenbauer differential equation. We can regularize it through a substitution

$$y(x) = (1-x^2)^{\alpha/2}u(x)\ ,\tag{3.40}$$

for some value of α – to be determined later. First, let us calculate the derivatives of the regular term $(1-x^2)^{\alpha/2}$

$$\begin{aligned}\left((1-x^2)^{\alpha/2}\right)' &= -\alpha x(1-x^2)^{\alpha/2-1}\ ,\\ \left((1-x^2)^{\alpha/2}\right)'' &= \alpha(1-x^2)^{\alpha/2-2}((\alpha-1)x^2-1)\ .\end{aligned} \tag{3.41}$$

Now let us calculate the terms in Eq. (3.39)

$$\begin{aligned}(1-x^2)y'' =&(1-x^2)^{\alpha/2-1}\left[\alpha\left((\alpha-1)x^2-1\right)u-(1-x^2)2\alpha x u'+(1-x^2)^2u''\right]\ ,\\ -(d-1)xy' =&-(d-1)x(1-x^2)^{\alpha/2-1}\left(-axu+(1-x^2)u'\right)\ ,\\ \left[\lambda_d-\frac{\lambda_{d-1}}{1-x^2}\right]y =&(1-x^2)^{\alpha/2-1}\left[\lambda_d(1-x^2)-\lambda_{d-1}\right]\ .\end{aligned} \tag{3.42}$$

We proceed by collecting the terms near $u''(x)$, $u'(x)$ and $u(x)$. Eq. (3.39) becomes

$$\begin{aligned}0 =\ & u''(1-x^2)^{\alpha/2+1}+u'(1-x^2)^{\alpha/2-1}\left[(d-1)x-2\alpha x\right](1-x^2)+\\ &+u(1-x^2)^{\alpha/2-1}\left[\lambda_d(1-x^2)-\lambda_{d-1}+\alpha(\alpha-1)x^2-\alpha+(d-1)\alpha x^2\right]\ .\end{aligned} \tag{3.43}$$

We can divide it by the factor $(1-x^2)^{\alpha/2-1}$ (keeping in mind the regularization at $x=\pm1$, which we will discuss later) and collect terms next to x^2 in the $\sim u(x)$ term

$$\begin{aligned}0 =\ & u''(1-x^2)^2+u'\left[(d-1)x-2\alpha x\right](1-x^2)+\\ &+u\left[(\alpha(\alpha+d-2)-\lambda_d)x^2+(\lambda_d-\lambda_{d-1}-\alpha)\right]\ .\end{aligned} \tag{3.44}$$

Now, we express the $\sim u(x)$ term in a way that allows to extract the $(1-x^2)$ bracket

$$\begin{aligned}0 =\ & u''(1-x^2)^2+u'\left[(d-1)x-2\alpha x\right](1-x^2)+\\ &+u\left[(\lambda_d-\alpha(\alpha+d-2))(1-x^2)+(-\lambda_{d-1}+\alpha(\alpha+d-2)-\alpha)\right]\ .\end{aligned} \tag{3.45}$$

We can factor out the $(1-x^2)$, by requiring that the equation is regular at $x=\pm1$

$$\begin{aligned}0 &= -\lambda_{d-1}+\alpha(\alpha+d-2)-\alpha\ ,\\ \lambda_{d-1} &= \alpha(\alpha+d-3)\ .\end{aligned} \tag{3.46}$$

Thus, by inserting relation from Eq. (3.46) into Eq. (3.45) and dividing by $(1-x^2)$, we obtain the *regular* Gegenbauer equation

$$0=(1-x^2)\,u''(x)-(2\alpha-(d-1))x\,u'(x)+\left[\lambda_d-\alpha(\alpha+d-2)\right]u(x)\ . \tag{3.47}$$

The solutions of this equation are the Gegenbauer polynomials $C_n^{(\tilde{\alpha})}(x)$, for which the following relations are satisfied

$$\begin{aligned}\tilde{\alpha} &= \alpha+\frac{d-2}{2}\ ,\\ \lambda_d &= (n+\alpha)(n+\alpha+d-2)\ .\end{aligned} \tag{3.48}$$

The quantum numbers n and α represent the excitations to the grand angular momentum stemming from introducing an additional, single Jacobi coordinate – which *is not* equivalent to adding another interacting particle, because that would require adding three more Jacobi coordinates, each representing a Cartesian coordinate of the additional Jacobi vector. The

mathematical procedure of including another particle through three more Jacobi coordinates is called *clustering* and is described in greater detail in Ref. [203] and below. We notice, that by setting $\lambda_d := \lambda(\lambda + d - 2)$ for some value λ of the grand angular momentum in d dimensions – we can relate it to the value α, which represents the eigenvalue of the grand angular momentum in $d-1$ dimensions

$$\begin{aligned} \lambda_d &:= \lambda(\lambda + d - 2) = (n + \alpha)((n + \alpha) + d - 2) \ , \\ \lambda_{d-1} &:= \alpha(\alpha + d - 2) \ , \\ \lambda &= n + \alpha \ , \quad n = 0, 1, 2, \dots \ . \end{aligned} \tag{3.49}$$

Thus, the eigenfunctions of the grand angular momentum have the following recursive form

$$\mathcal{Y}(\alpha_{d-1}, \Omega_{d-1}) = \mathcal{N}(\sin\alpha_{d-1})^\alpha \, C_{\lambda-\alpha}^{\left(\alpha+\frac{d-2}{2}\right)}(\cos\alpha_{d-1}) \, \mathcal{Y}_{d-1}(\Omega_{d-1}), \tag{3.50}$$

where $\mathcal{N}$ is the norm of the solution. We can check the validity of Eq. (3.50) by applying it to $d = 2$ and $d = 3$ (that is, cases representing one- and two interacting particles, respectively). For $d = 2$ we have

$$\begin{aligned} \Omega_2 = \{\alpha_1\} &:= \{\varphi\} \ , \\ \mathbf{\Lambda}^2(\Omega_2) &= -\frac{d^2}{d\varphi^2} \ , \\ \mathcal{Y}(\varphi) &= \frac{1}{\sqrt{2\pi}} e^{im\varphi} \ , \\ \lambda_2 &:= m^2 \ , \end{aligned} \tag{3.51}$$

while for $d = 3$ we obtain

$$\begin{aligned} \Omega_3 = \{\alpha_2, \alpha_1\} &:= \{\theta, \varphi\} \ , \\ \mathbf{\Lambda}^2(\Omega_3) &= -\frac{1}{\sin\theta}\frac{\partial}{\partial\theta}\left(\sin\theta\frac{\partial}{\partial\theta}\right) - \frac{1}{\sin^2\theta}\frac{\partial^2}{\partial\varphi^2} \ , \\ \mathcal{Y}(\theta, \varphi) &\sim (\sin\theta)^{|m|} C_{l-|m|}^{\left(|m|+\frac{1}{2}\right)}(\cos\theta) e^{im\varphi} \sim Y_m^l(\theta, \varphi) \ , \\ \lambda_3 &:= l(l+1) \ . \end{aligned} \tag{3.52}$$

To see that the solutions $\mathcal{Y}(\theta, \varphi)$ are proportional to the spherical harmonics, one can use the relations between the associated Legendre polynomials, the Gegenbauer polynomials, and the Jacobi polynomials found in Ref. [204]

$$\begin{aligned} C_{l-|m|}^{\left(|m|+\frac{1}{2}\right)}(x) &= \frac{(2|m|+1)_{l-|m|}}{(|m|+1)_{l-|m|}} P_n^{(|m|,|m|)}(x) \ , \\ P_l^{|m|}(\cos\theta) &= 2^{-|m|}\frac{\Gamma(l+|m|+1)}{\Gamma(l+1)}(\sin\theta)^{|m|} P_{l-|m|}^{(|m|,|m|)}(\cos\theta) \ , \end{aligned} \tag{3.53}$$

where $(z)_n$ represents the rising factorial of z. Thus, for $d = 6$ (a case representing three interacting particles), the eigenvalues of the grand angular momentum take the form $\lambda_6 := \lambda(\lambda + 4)$.

The explicit form of Λ^2

Let us continue by proving Eq. (3.32). We will consider the sum of operators Λ_{ij} and use the shorthand notation $\partial_i := \frac{\partial}{\partial r_i}$

$$\sum_{i<j} \Lambda_{ij} = \sum_{i<j} (r_i\partial_j - r_j\partial_i)^2 = \sum_{i<j} r_i^2\partial_j^2 + r_j^2\partial_i^2 - 2r_ir_j\partial_i\partial_j - r_i\partial_i - r_j\partial_j \ . \tag{3.54}$$

The first term in Eq. (3.54) is equal to

$$\sum_{i<j}(r_i^2\partial_j^2 + r_j^2\partial_i^2) = \sum_j \left(\sum_{i\neq j} r_i^2\right)\partial_j^2 = \sum_{j=1}^{d}\left(R^2 - r_j^2\right)\partial_j^2 \ . \tag{3.55}$$

The term involving mixed derivatives is equal to

$$\sum_{i<j}(-2r_i r_j \partial_i\partial_j) = -\sum_{i\neq j} r_i r_j \partial_i\partial_j \ . \tag{3.56}$$

Summed up, all three terms give

$$\begin{aligned}\sum_{i<j}\Lambda_{ij}^2 =& \sum_{i<j} r_i^2\partial_j^2 + r_j^2\partial_i^2 - 2r_i r_j\partial_i\partial_j - r_i\partial_i - r_j\partial_j = \\ &= R^2\sum_k \partial_k^2 - \left(\sum_k r_k^2\partial_k^2 + \sum_{i\neq j} r_i r_j\partial_i\partial_j\right) - (d-1)\left(\sum_{k=1}^{d} r_k\partial_k\right) = \\ &= R^2\Delta_{\boldsymbol{\rho}} - \left(\sum_{k,l} r_k r_l \partial_k\partial_l\right) - (d-1)\left(\sum_{k=1}^{d} r_k\partial_k\right) \ .\end{aligned} \tag{3.57}$$

We shall now focus on the operator $\hat{E} = \sum_{k=1}^{d} r_k\partial_k$. It can be greatly simplified by recalling that the hyperangles α_i are scale-invariant. Let us consider the inverse map F^{-1}, which means the hyperangles to be functions of r_k , $k = 1, \ldots, d$, i.e., $\alpha_i(r_1, \ldots, r_d)$. We notice that the hyperangles are indeed scale-invariant, i.e.,

$$\alpha_i(c\,\mathbf{r}) = \alpha_i(\mathbf{r}) \ , \tag{3.58}$$

for some scaling factor c. The derivative of the equation above with respect to c is therefore equal to zero

$$\begin{aligned} 0 = \frac{d\alpha_i(c\,\mathbf{r})}{dc} &= \sum_k \frac{\partial\alpha_i}{\partial r_k}\frac{\partial(cr_k)}{\partial c} \ , \\ 0 &= \sum_{k=1}^{d} r_k\frac{\partial\alpha_i}{\partial r_k} \ . \end{aligned} \tag{3.59}$$

We should note that the scale invariance condition is independent of the *exact* choice of the trigonometric functions that define the hyperangles, as long as the scaling factor is served by the hyperangle $R = \sqrt{\sum_j r_j^2}$. We know move on to evaluating the $\hat{E}$ operator

$$\hat{E} = \sum_k r_k\partial_k = \sum_{k=1}^{d} r_k\left(\frac{\partial R}{\partial r_k}\frac{\partial}{\partial R} + \sum_{i=1}^{d-1}\frac{\partial\alpha_i}{\partial r_k}\frac{\partial}{\partial\alpha_i}\right) \ . \tag{3.60}$$

Using Eq. (3.59) and recalling the relation $R(\mathbf{r}) = \sqrt{\sum_j r_j^2}$, we can calculate the simplified and expanded forms of $\hat{E}$, and $\hat{E}^2$

$$\begin{aligned}
\hat{E} &= R\frac{\partial}{\partial R} + \sum_i \left(\sum_k r_k \frac{\partial \alpha_i}{\partial r_k}\right) \frac{\partial}{\partial \alpha_i} = R\frac{\partial}{\partial R} + 0 = R\frac{\partial}{\partial R} \\
\hat{E}^2 &= \left(R\frac{\partial}{\partial R}\right)^2 = R^2\frac{\partial^2}{\partial R^2} + R\frac{\partial}{\partial R} \\
\hat{E}^2 &= \left(\sum_k r_k \partial_k\right)^2 = \sum_{k,l} r_k \partial_k r_l \partial_l = \sum_{k,l} r_k \left(\partial_k r_l\right) \partial_l + r_k r_l \partial_k \partial_l = \\
&= \sum_k r_k \partial_k + \sum_{k,l} r_k r_l \partial_k \partial_l \ ,
\end{aligned} \tag{3.61}$$

where we used the relation $\partial_l r_k = \delta_{kl}$, which is true because the metric g is orthogonal. The relations above can be inserted into Eq. (3.57)

$$\begin{aligned}
\sum_{i<j} \Lambda_{ij}^2 &= R^2 \Delta_{\boldsymbol{\rho}} - \hat{E}^2 - (d-2)\hat{E} \ , \\
\sum_{i<j} \frac{\Lambda_{ij}^2}{R^2} &= \Delta_{\boldsymbol{\rho}} - \frac{\partial^2}{\partial R^2} - \frac{1}{R}\frac{\partial}{\partial R} - (d-2)\frac{1}{R}\frac{\partial}{\partial R} = \Delta_{\boldsymbol{\rho}} - \frac{\partial^2}{\partial R^2} - (d-1)\frac{1}{R}\frac{\partial}{\partial R} \ .
\end{aligned} \tag{3.62}$$

We notice that the equation above is equivalent to the equation, which allowed us to define the form of the Laplacian $\Delta_{\boldsymbol{\rho}}$ in hyperspherical coordinates, thus proving Eq. (3.32). We recall that the proven, explicit form of the grand angular momentum operator is true for all definitions of hyperspherical coordinates that preserve the hyperangular invariance upon scaling by a factor $\mathbf{r} \to \mathbf{r}c$ – as mentioned above.

3.2.3. The clustering method

Naturally, the canonical choice for the hyperspherical coordinates defined by the map F is not the only possible definition of hyperspherical coordinates that greatly simplifies the Laplacian, and thus the Hamiltonian in the lab-fixed frame. Below, we discuss a *clustering* method that allows us to interpret the values of the grand angular momentum in terms of partial angular momenta associated with the Jacobi vectors (rather than individual Jacobi coordinates). This approach provides a more intuitive physical description of λ rather than the crude, mathematical interpretation given by the explicit form of $\boldsymbol{\Lambda}^2$ in Eq. (3.32). This approach is provided in greater detail in Ref. [203].

Let us consider two sets of hyperspherical coordinates

- cluster $\mathbf{x} := (x_1, x_2, x_3) = (r_1, r_2, r_3)$
- the rest of the coordinate set $\mathbf{y} := (y_4, \ldots, y_d) = (r_4, \ldots, r_d)$

We should note that the exact choice of trigonometric functions defining the hyperangles is irrelevant for the considerations below. We only require that they are scale-invariant, which allows us to use the explicit form of $\boldsymbol{\Lambda}^2$. Let us define the lengths of these vectors and the relation between x and y, by introducing a *polar* hyperangle η

$$\begin{gathered}
x^2 = \sum_{i=1}^{3} r_i^2, \quad y^2 = \sum_{i=4}^{d} r_i^2, \quad x^2 + y^2 = R^2 \ , \\
x = R\cos\eta, \quad y = R\sin\eta \ .
\end{gathered} \tag{3.63}$$

Essentially, we could consider defining both the $d-4$ hyperspherical coordinates for y and 3 hyperspherical coordinates for x canonically and then multiplying each of the individual coordinates r_i by $\sin\eta$ or $\cos\eta$ appropriately

$$\begin{aligned}
r_d &= R\sin\eta\cos\alpha_{d-1}\ , \\
r_{d-1} &= R\sin\eta\sin\alpha_{d-1}\cos\alpha_{d-2}\ , \\
r_{d-2} &= R\sin\eta\sin\alpha_{d-1}\sin\alpha_{d-2}\cos\alpha_{d-3}\ , \\
&\vdots \\
r_5 &= R\sin\eta\prod_{i=5}^{d-1}\sin\alpha_i\cos\alpha_4\ , \\
r_4 &= R\sin\eta\prod_{i=4}^{d-1}\sin\alpha_i\ , \\
r_3 &= R\cos\eta\cos\theta_1\ , \\
r_2 &= R\cos\eta\sin\theta_1\cos\varphi_1\ , \\
r_1 &= R\cos\eta\sin\theta_1\sin\varphi_1\ .
\end{aligned} \tag{3.64}$$

In Cartesian coordinates, the Casimir operator $\mathbf{\Lambda}^2$ acts on the group SO(d) and can be represented as a sum of two Casimir operators $\mathbf{\Lambda}_x^2$ (acting on group SO(3) and $\mathbf{\Lambda}_y^2$ (acting on group SO($d-3$)), as well as a *mixing operator* term $\mathbf{\Lambda}_{xy}^2$

$$\mathbf{\Lambda}^2 = \mathbf{\Lambda}_x^2 + \mathbf{\Lambda}_y^2 + \mathbf{\Lambda}_{xy}^2\ , \tag{3.65}$$

where

$$\begin{aligned}
\mathbf{\Lambda}_x^2 &= -\sum_{1\le i<j\le 3}\Lambda_{ij}^2\ , \\
\mathbf{\Lambda}_y^2 &= -\sum_{4\le i<j\le d}\Lambda_{ij}^2\ , \\
\mathbf{\Lambda}_{xy}^2 &= -\sum_{i\le 3,\, j\ge 4}\Lambda_{ij}^2\ .
\end{aligned} \tag{3.66}$$

The Casimir operators $\mathbf{\Lambda}_x^2$, $\mathbf{\Lambda}_y^2$, and $\mathbf{\Lambda}^2$ commute

$$[\mathbf{\Lambda}_x^2, \mathbf{\Lambda}_y^2] = 0\ , \quad [\mathbf{\Lambda}^2, \mathbf{\Lambda}_y^2] = 0\ , \quad [\mathbf{\Lambda}^2, \mathbf{\Lambda}_x^2] = 0\ . \tag{3.67}$$

The first of these equations is apparent from the explicit forms of Λ_x^2 and Λ_y^2 (no overlap indices). The second and third equations are equivalent to stating that $[\mathbf{\Lambda}_x^2, \mathbf{\Lambda}_{xy}^2] = 0$, and $[\mathbf{\Lambda}_y^2, \mathbf{\Lambda}_{xy}^2] = 0$. By symmetry, we only need to justify the first of these commutation relations. Due to the commutation relations, we can write the eigenfunctions of the grand angular momentum in the following form

$$\psi(\Omega) = f(\eta)\mathcal{Y}_{l_x}(\Omega_x)\mathcal{Y}_{K_y}(\Omega_y)\ , \tag{3.68}$$

for some function $f(\eta)$ – to be determined later. Following the same convention as in the previous Section – the functions $\mathcal{Y}_{l_x}^{(x)}(\Omega_x)$ and $\mathcal{Y}_{K_y}(\Omega_y)$ are eigenfunctions of $\mathbf{\Lambda}_x^2$ and $\mathbf{\Lambda}_y^2$, respectively. Furthermore, the eigenvalues l_x and K_y are good quantum numbers.

The commutation relations between the Casimir operators

We aim to prove the commutation relation

$$0 = [\mathbf{\Lambda}_x^2, \mathbf{\Lambda}_{xy}^2] \ . \tag{3.69}$$

In order to do that, we will first prove the equation

$$[\Lambda_{ij}, \Lambda_{ka}] = \delta_{jk}\Lambda_{ia} - \delta_{ik}\Lambda_{ja}, \quad i,j,k \in I_x,\ a \in I_y \ , \tag{3.70}$$

where in our case the indices in set I_x are ranging from 1 to 3, and those in I_y – from 4 to $d-1$, but we only require that the sets I_x and I_y are disjoint. Eq. (3.70) is a special case of the more general equation

$$[\Lambda_{ij}, \Lambda_{kl}] = \delta_{jk}\Lambda_{il} - \delta_{ik}\Lambda_{jl} - \delta_{jl}\Lambda_{ik} + \delta_{il}\Lambda_{jk} \ , \tag{3.71}$$

which is true for the generators of Lie algebras $\mathfrak{so}(d)$. Let us compute the operators $\Lambda_{ij}\Lambda_{ka}$ and $\Lambda_{ka}\Lambda_{ij}$

$$\begin{aligned}\Lambda_{ij}\Lambda_{ka} =&(x_i\partial_{x_j} - x_j\partial_{x_i})(x_k\partial_{y_a} - y_a\partial_{x_k}) \\ =&x_i(\underbrace{\delta_{jk}\partial_{y_a}}+x_k\partial_{x_j}\partial_{y_a}) - x_iy_a\partial_{x_j}\partial_{x_k} - \\ &- x_j(\underbrace{\delta_{ik}\partial_{y_a}}+x_k\partial_{x_i}\partial_{y_a}) + x_jy_a\partial_{x_i}\partial_{x_k} \ ,\end{aligned} \tag{3.72}$$

where we use the orthogonality of the x_i, x_j, x_k and y_a coordinates. We also have

$$\begin{aligned}\Lambda_{ka}\Lambda_{ij} =&(x_k\partial_{y_a} - y_a\partial_{x_k})(x_i\partial_{x_j} - x_j\partial_{x_i}) = \\ =&x_k(x_i\partial_{y_a}\partial_{x_j} - x_j\partial_{y_a}\partial_{x_i}) - y_a(\underbrace{\delta_{ki}\partial_{x_j}}+x_i\partial_{x_k}\partial_{x_j})+ \\ &+ y_a(\underbrace{\delta_{kj}\partial_{x_i}}+x_j\partial_{x_k}\partial_{x_i}) \ .\end{aligned} \tag{3.73}$$

We note that the terms which include second derivatives are the same for $\Lambda_{ij}\Lambda_{ka}$ and $\Lambda_{ka}, \Lambda_{ij}$. Thus, in the commutator, we are left with the first-derivative terms only

$$[\Lambda_{ij}, \Lambda_{ka}] = \delta_{jk}(x_i\partial_{y_a} - y_a\partial_{x_i}) + \delta_{ik}(-x_j\partial_{y_a} + y_a\partial_{x_j}) = \delta_{jk}\Lambda_{ia} - \delta_{ik}\Lambda_{ja} \ , \tag{3.74}$$

proving Eq. (3.70). Now, let us use this knowledge to compute the commutator

$$\left[\Lambda_{ij}, \Lambda_{ka}^2\right] = \Lambda_{ka}\left[\Lambda_{ij}, \Lambda_{ka}\right] + \left[\Lambda_{ij}, \Lambda_{ka}\right]\Lambda_{ka} = \delta_{jk}\{\Lambda_{ia}, \Lambda_{ka}\} - \delta_{ik}\{\Lambda_{ja}, \Lambda_{ka}\} \ , \tag{3.75}$$

where $\{.,.\}$ is the anti-commutator. Now, let us consider the sum stemming from the definition of $\mathbf{\Lambda}_x^2$

$$\begin{aligned}\left[\mathbf{\Lambda}_x^2, \Lambda_{ka}^2\right] = -\sum_{i<j}\left[\Lambda_{ij}, \Lambda_{ka}^2\right] = -\sum_{i<j}(\delta_{jk}\{\Lambda_{ia}, \Lambda_{ka}\} - \delta_{ik}\{\Lambda_{ja}, \Lambda_{ka}\}) = \\ = -\sum_{i\neq k}\{\Lambda_{ia}, \Lambda_{ka}\} + \sum_{j\neq k}\{\Lambda_{ja}, \Lambda_{ka}\} = 0 \ ,\end{aligned} \tag{3.76}$$

where we use the fact that $\sum_{i<j}\delta_{ik}$ is the sum over all distinct pairs of i,j. The Kronecker delta inside forces the sum to run over all pairs that involve only k. Since the following terms do not depend on i – the sum simplifies to $\sum_{j\neq k}$. By symmetry of the indices i,j, the equation above is equal to zero. Finally, we obtain

$$\left[\mathbf{\Lambda}_x^2, \mathbf{\Lambda}_{xy}^2\right] = -\sum_{k,a}\left[\mathbf{\Lambda}_x^2, \Lambda_{ka}^2\right] = 0 \ . \tag{3.77}$$

The cluster operator

In the previous paragraph, we have justified the separation of variables η, $\mathbf{x}$, and $\mathbf{y}$ by analyzing the proper commutation relations between the Casimir and *mixing* operators. What remains is to separate the Laplacian in d dimensions into two Laplacians in 3 and $d-3$ dimensions, with the coupling depending on η. Thus, we will prove that

$$\Delta_{\boldsymbol{\rho}} = \Delta_x + \Delta_y, \tag{3.78}$$

where

$$\begin{aligned} \Lambda_x =& \partial_x^2 + \frac{2}{x}\partial_x - \frac{\mathbf{\Lambda}_x^2}{x^2} \ , \\ \Lambda_y =& \partial_y^2 + \frac{d-4}{y}\partial_y - \frac{\mathbf{\Lambda}_y^2}{y^2} \ . \end{aligned} \tag{3.79}$$

Additionally, we will find the form of the mixing operator in terms of η and R, keeping in mind the relation in Eq. (3.65).

Let us obtain the derivatives ∂_x, ∂_y and their powers in terms of η and R, recalling the definitions $x = R\cos\eta$ and $y = R\sin\eta$

$$\begin{aligned} \partial_x =& \cos\eta\,\partial_R - \frac{\sin\eta}{R}\,\partial_\eta \ , \\ \partial_y =& \sin\eta\,\partial_R + \frac{\cos\eta}{R}\,\partial_\eta \ , \\ \partial_x^2 =& \left(\cos\eta\,\partial_R - \frac{\sin\eta}{R}\,\partial_\eta\right)\left(\cos\eta\,\partial_R - \frac{\sin\eta}{R}\,\partial_\eta\right) = \\ =& \cos^2\eta\,\partial_R^2 + \frac{\cos\eta\sin\eta}{R^2}\partial_\eta - \frac{\cos\eta\sin\eta}{R}\partial_R\partial_\eta + \\ &+ \frac{\sin^2\eta}{R}\partial_R - \frac{\sin\eta\cos\eta}{R}\partial_R\partial_\eta + \frac{\sin\eta\cos\eta}{R^2}\partial_\eta + \frac{\sin^2\eta}{R^2}\partial_\eta^2 \\ =& \cos^2\eta\,\partial_R^2 + \frac{2\sin\eta\cos\eta}{R^2}\partial_\eta - \frac{2\sin\eta\cos\eta}{R}\partial_\eta\partial_R + \frac{\sin^2\eta}{R^2}\partial_\eta^2 + \frac{\sin^2\eta}{R}\partial_R \ , \\ \partial_y^2 =& \left(\sin\eta\,\partial_R + \frac{\cos\eta}{R}\,\partial_\eta\right)\left(\sin\eta\,\partial_R + \frac{\cos\eta}{R}\,\partial_\eta\right) = \\ =& \sin^2\eta\,\partial_R^2 - \frac{\sin\eta\cos\eta}{R^2}\partial_\eta + \frac{\cos\eta\sin\eta}{R}\partial_R\partial_\eta + \\ &+ \frac{\cos\eta\sin\eta}{R}\partial_\eta\partial_R + \frac{\cos^2\eta}{R}\partial_R + \frac{\cos^2\eta}{R^2}\partial_\eta^2 - \frac{\sin\eta\cos\eta}{R^2}\partial_\eta \\ =& \sin^2\eta\,\partial_R^2 - \frac{2\sin\eta\cos\eta}{R^2}\partial_\eta + \frac{\cos\eta\sin\eta}{R}\partial_\eta\partial_R + \frac{\cos^2\eta}{R^2}\partial_\eta^2 + \frac{\cos^2\eta}{R}\partial_R \ . \end{aligned} \tag{3.80}$$

Let us consider the sum $\Delta_x + \Delta_y$. The sum of the second derivatives is given by

$$\partial_x^2 + \partial_y^2 = \partial_R^2 + \frac{1}{R^2}\partial_\eta^2 + \frac{1}{R}\partial_R \ , \tag{3.81}$$

where the mixed-derivative terms and the $\sim \partial_\eta$ terms are canceled. The first-derivatives terms give

$$\begin{aligned} \frac{2}{x}\partial_x + \frac{d-4}{y}\partial_y &= \frac{2}{x}\left(\cos\eta\,\partial_R - \frac{\sin\eta}{R}\,\partial_\eta\right) + \frac{d-4}{y}\left(\sin\eta\,\partial_R + \frac{\cos\eta}{R}\,\partial_\eta\right) \\ &= \frac{d-2}{R}\partial_R + \frac{(d-4)\cos^2\eta - 2\sin^2\eta}{R^2\cos\eta\sin\eta}\partial_\eta \ . \end{aligned} \tag{3.82}$$

We finally obtain the separation of the Laplacian

$$\Delta = \Delta_x + \Delta_y = \partial_R^2 + \frac{d-1}{R}\partial_R - \frac{1}{R^2}\left[-\partial_\eta^2 - \frac{(d-4)\cos^2\eta - 2\sin^2\eta}{\cos\eta\sin\eta}\partial_\eta + \frac{\mathbf{\Lambda}_x^2}{\cos^2\eta} + \frac{\mathbf{\Lambda}_y^2}{\sin^2\eta}\right] . \tag{3.83}$$

Comparing with Eq. (3.31), the grand angular momentum operator is given by

$$\mathbf{\Lambda}^2 = -\partial_\eta^2 - \frac{(d-4)\cos^2\eta - 2\sin^2\eta}{\cos\eta\sin\eta}\partial_\eta + \frac{\mathbf{\Lambda}_x^2}{\cos^2\eta} + \frac{\mathbf{\Lambda}_y^2}{\sin^2\eta} . \tag{3.84}$$

This equation is found in Ref. [203], although modified to account for numerous clusters of three coordinates. The mixing operator in terms of R and η is given by

$$\mathbf{\Lambda}_{xy}^2 = -\partial_\eta^2 - \frac{(d-4)\cos^2\eta - 2\sin^2\eta}{R^2\cos\eta\sin\eta}\partial_\eta + \mathbf{\Lambda}_x^2\left(\frac{1}{\cos^2\eta} - 1\right) + \mathbf{\Lambda}_y^2\left(\frac{1}{\sin^2\eta} - 1\right) . \tag{3.85}$$

We now see that while $\mathbf{\Lambda}^2$, $\mathbf{\Lambda}_x^2$, $\mathbf{\Lambda}_y^2$, $\mathbf{\Lambda}_{xy}^2$ commute and Eq. (3.65) holds, $\mathbf{\Lambda}_{xy}^2$ is not independent of the other operators and its spectrum is therefore also constrained by the other eigenvalues. This statement is equivalent to the relation that the group $\mathrm{SO}(3) \times \mathrm{SO}(d-3)$ with its Lie algebra is embedded in $\mathrm{SO}(d)$.

We will proceed by inserting the ansatz from Eq. (3.68) for the eigenfunction $\psi(\Omega)$ into equation $\mathbf{\Lambda}\psi(\Omega) = \lambda_d\psi(\Omega)$. We remember that $\psi(\Omega)$ is *not equal* to $\mathcal{Y}(\Omega)$ because we are solving the eigenvalue problem in non-canonical hyperspherical coordinates.

$$0 = \left[-\frac{d^2}{d\eta^2} - \frac{(d-4)\cos^2\eta - 2\sin^2\eta}{\sin\eta\cos\eta}\frac{d}{d\eta} + \frac{l_x(l_x+1)}{\cos^2\eta} + \frac{K_y(K_y+d-5)}{\sin^2\eta} - \lambda_d\right] f(\eta) , \tag{3.86}$$

where we are justified to use the eigenvalues of $\mathbf{\Lambda}_x^2$ and $\mathbf{\Lambda}_y^2$ in the form $l_x(l_x+1)$, and $K_y(K_y+d-5)$, respectively, because individually they *are* defined on canonical hyperspherical coordinates – only multiplied by the coupling factor $\sin\eta$ or $\cos\eta$. The standard substition $f(\eta) = g(\eta)F(\eta) = (\cos\eta)^{l_x}(\sin\eta)^{K_y}F(\eta)$ allows us to regularize the terms with $\sin^2\eta$ and $\cos^2\eta$ in the denominator. We will conisder the relevant substitutions step by step. Firstly, let us calculate f'. We will go through a logarithmic derivative

$$\begin{aligned} \frac{g'}{g} &= (\ln g)' = \frac{d}{d\eta}\left(l_x \ln\cos\eta + K_y \ln\sin\eta\right) = -l_x\tan\eta + K_y\cot\eta , \\ f' &= g\left(F' + F\frac{g'}{g}\right) = g\left[F' + F(K_y\cot\eta - l_x\tan\eta)\right] . \end{aligned} \tag{3.87}$$

Let us set define $h = F' + F(K_y\cot\eta - l_x\tan\eta)$. Now, we evaluate the second derivative f''. It is equal to

$$\begin{aligned} f'' = (gh)' =& g\left[\frac{g'}{g}h + h'\right] = [(K_y\cot\eta - l_x\tan\eta)(F' + F(K_y\cot\eta - l_x\tan\eta)]g + \\ &+ [F'' - (K_y\csc^2\eta + l_x\sec^2\eta)F + (K_y\cot\eta - l_x\tan\eta)F']g = \\ =& g[F'' + F\left((K_y\cot\eta - l_x\tan\eta)^2 - K_y\csc^2\eta - \sec^2\eta\right) + 2F'(K_y\cot\eta - l_x\tan\eta)] . \end{aligned} \tag{3.88}$$

Now let us evaluate the second term in Eq. (3.86)

$$-\frac{(d-4)\cos^2\eta - 2\sin^2\eta}{\sin\eta\cos\eta}f' = -g[(d-4)\cot\eta - 2\tan\eta][F' + F(K_y\cot\eta - l_x\tan\eta)] . \tag{3.89}$$

The potential terms become

$$\left(l_x(l_x+1)\sec^2\eta + K_y(K_y+d-5)\csc^2\eta - \lambda_d\right) gF \ . \tag{3.90}$$

All results are proportional to g, thus we can divide both sides of Eq. (3.86) by $g(\eta)$ – keeping in mind that the result should be regular at $\eta = 0$ and $\eta = \pi/2$. We now move on to grouping the terms by order of the derivatives of F. Firstly, the second derivative has only one contribution in the equation, namely $-F''(\eta)$. Now the terms next to $F'(\eta)$ come from the first $(-f'')$, and the second term in Eq. (3.86)

$$[-2(K_y\cot\eta - l_x\tan\eta) - ((d-4)\cot\eta - 2\tan\eta)]\,F' = -[(2K_y+d-4)\cot\eta - 2(l_x+1)\tan\eta]F' \ . \tag{3.91}$$

Now we move on to the largest part of the equation, i.e. terms next to $F(\eta)$. To simplify this part, we will use the relations $\cot^2\eta = \csc^2\eta - 1$ and $\tan^2\eta = \sec^2\eta - 1$. The terms below are written in such a way, that each row corresponds to the first- $(-f'')$, second- and potential terms in Eq. (3.86), respectively

$$\begin{aligned} &-F[K_y^2\cot^2\eta + l_x^2\tan^2\eta - 2K_yl_x - K_y\csc^2\eta - l_x\sec^2\eta] - \\ &-F[(d-4)\cot\eta - 2\tan\eta][K_y\cot\eta - l_x\tan\eta] + \\ &+F[(l_x^2+l_x)\sec^2\eta + [K_y^2 + (d-4)K_y - K_y]\csc^2\eta - \lambda_d] \quad . \end{aligned} \tag{3.92}$$

The equation above can be greatly simplified, which is noticable after expanding all of the terms. The underlined, underbracketed and underbraced terms cancel with each other respectively

$$\begin{aligned} &-F[\underbrace{K_y^2\csc^2\eta + l_x^2\sec^2\eta}\,-K_y^2 - l_x^2 - 2K_yl_x - \underline{K_y\csc^2\eta - l_x\sec^2\eta}] - \\ &-F[\underbrace{(d-4)K_y\csc^2\eta}\,+\underline{2l_x\sec^2\eta} - (d-4)K_y - 2l_x - 2K_y - (d-4)l_x] \\ &+F[\underline{l_x\sec^2\eta} + \underbrace{l_x^2\sec^2\eta + K_y^2\csc^2\eta}\,+ \underbrace{(d-4)K_y\csc^2\eta}\, - \underline{K_y\csc^2\eta}\lambda_d] \ . \end{aligned} \tag{3.93}$$

We are left with

$$F\left(K_y^2 + l_x^2 + 2K_yl_x + (d-4)K_y + 2l_x + 2K_y + (d-4)l_x\right) = F(l_x+K_y)(l_x+K_y+d-2) \ . \tag{3.94}$$

Finally, we get the simplified form of Eq. (3.86)

$$F'' + [(2K_y+d-4)\cot\eta - (2l_x+2)\tan\eta]\,F' - [(l_x+K_y)(l_x+K_y+d-2) - \lambda_d]\,F = 0 \ . \tag{3.95}$$

This equation can be simplified further through substitution $t = \cos 2\eta$. We need to express the derivatives with respect to η in terms of derivatives with respect to t

$$\begin{aligned} \frac{d}{d\eta} &= -2\sin 2\eta\frac{d}{dt} \ , \\ \frac{d^2}{d\eta^2} &= -4\cos 2\eta\frac{d}{dt} + 4\sin^2 2\eta\frac{d^2}{dt^2} = 4(1-t^2)\frac{d^2}{dt^2} - 4t\frac{d}{dt} \ . \end{aligned} \tag{3.96}$$

The second derivative term becomes

$$\frac{d^2F}{d\eta^2} = 4(1-t^2)F''(t) - 4tF'(t) \ , \tag{3.97}$$

where the notation F' now means taking the derivative with respect to t, not η. The first-derivative term is equal to

$$\begin{aligned}&[(2K_y+d-4)\cot\eta-(2l_x+2)\tan\eta]\,\frac{dF}{d\eta}=\\&=-2\,[(2K_y+d-4)\cot\eta-(2l_x+2)\tan\eta]\sin 2\eta F'(t)=\\&=-2[(2K_y+d-4)(1+t)-(2l_x+2)(1-t)]F'(t)\ ,\end{aligned}\tag{3.98}$$

where we use the relaions $\cot\eta\sin 2\eta = 2\cos^2\eta = 1+t$ and $\tan\eta\sin 2\eta = 2\sin^2\eta = 1-t$. We group terms near $F''(t)$ and $F'(t)$

$$\begin{aligned}4(1-t^2)F''(t)-2[2t+(2K_y+d-4)(1+t)-(2l_x+2)(1-t)]F'(t)+CF(t)=&0\ ,\\(1-t^2)F''(t)-\frac{1}{2}[(2K_y-2l_x+d-6)+(2K_y+2l_x+d)t]F'(t)+\frac{C}{4}F(t)=&0\ ,\end{aligned}\tag{3.99}$$

where $C=\lambda_d-(l_x+K_y)(l_x+K_y+d-2)$. Eq. (3.99) is the Jacobi differential equation. Its solutions are the Jacobi polynomials $P_n^{(\tilde\alpha,\tilde\beta)}(t)$ for which the following relations are satisfied

$$\begin{aligned}\tilde\alpha=&K_y+\frac{d-5}{2}\ ,\\\tilde\beta=&l_x+\frac{1}{2}\ ,\\\lambda_d=&(2n+l_x+K_y)(2n+l_x+K_y+d-2)\ .\end{aligned}\tag{3.100}$$

Thus, we see that the form of $\lambda_d := \lambda(\lambda+d-2)$ in the clustered coordinates coincides with the result obtained in canonical hyperspherical coordinates. In this representation, the grand angular momentum is interpreted as a sum of three quantum states: the angular momentum associated with the *additional* Jacobi vector l_x, the grand angular momentum of the system of all *previous* particles – K_y, and angular excitations n

$$\lambda = l_x+K_y+2n,\quad n=0,1,2,\dots\ .\tag{3.101}$$

The eigenfunctions of the grand angular momentum have the following recursive form

$$\begin{aligned}\psi(\Omega)&=\mathcal{Y}_{l_x}(\Omega_3)\mathcal{Y}_{K_y}(\Omega_{d-3})f(\eta)\ ,\\f(\eta)&=\mathcal{N}_\lambda^{K_y,l_x}(\cos\eta)^{l_x}(\sin\eta)^{K_y}P^{\left(K_y+\frac{d-5}{2},l_x+\frac{1}{2}\right)}_{(\lambda-l_x-K_y)/2}(\cos 2\eta)\ ,\end{aligned}\tag{3.102}$$

where $\mathcal{N}_\lambda^{K_y,l_x}$ is the norm of the solution and can be derived from the orthogonality of the Jacobi polynomials. Let us find the norm by analyzing the integral equation

$$\int_0^{\pi/2}|f(\eta)|^2 w(\eta)d\eta = 1\ .\tag{3.103}$$

The volume element is given by $d\Omega = (\cos\eta)^2(\sin\eta)^{d-4}\,d\eta\,d\Omega_3\,d\Omega_{d-3}$, hence the weight function in the norm integral is given by $w(\eta) = (\cos\eta)^2(\sin\eta)^{d-4}$. It is clear that for the non-canonical map to be bijective, the range of η needs to be $\eta\in[0,\frac{\pi}{2}]$. The norm equation in the metric dt is thus given by

$$\frac{1}{2}\left(\mathcal{N}_\lambda^{K_y,l_x}\right)^2\int_{-1}^{1}\left(\frac{1+t}{2}\right)^{\tilde\beta}\left(\frac{1-t}{2}\right)^{\tilde\alpha}\left[P_n^{(\tilde\alpha,\tilde\beta)}(t)\right]^2 dt = 1\ ,\tag{3.104}$$

where we used the relations

$$\cos\eta = \sqrt{\frac{1+t}{2}}\ , \quad \sin\eta = \sqrt{\frac{1-t}{2}}\ , \quad d\eta = \frac{dt}{-2(1+z)(1-z)} \tag{3.105}$$

for $t = \cos 2\eta$. Using the known result for the norm of the (orthogonal) Jacobi polynomials

$$\int_{-1}^{1} (1+t)^{\tilde{\beta}} (1-t)^{\tilde{\alpha}} \left[P_n^{(\tilde{\alpha},\tilde{\beta})}(t)\right]^2 dt = \frac{2^{\tilde{\alpha}+\tilde{\beta}+1}}{2n+\tilde{\alpha}+\tilde{\beta}+1} \frac{\Gamma(n+\tilde{\alpha}+1)\Gamma(n+\tilde{\beta}+1)}{n!\Gamma(n+\tilde{\alpha}+\tilde{\beta}+1)}\ , \tag{3.106}$$

we get the norm of our solution

$$\mathcal{N}_\lambda^{l_x,K_y} = \left[\frac{(2n+\tilde{\alpha}+\tilde{\beta}+1)n!\Gamma(n+\tilde{\alpha}+\tilde{\beta}+1)}{\Gamma(n+\tilde{\alpha}+1)\Gamma(n+\tilde{\beta}+1)}\right]^{\frac{1}{2}}\ . \tag{3.107}$$

The clustering method for 3 interacting particles

The clustering procedure can be applied recursively, creating $N-1 = d/3$ clusters of three coordinates, each associated with one of the Jacobi vectors for N interacting particles. Taking $d = 6$, we obtain

$$\begin{aligned}
r_6 &= (\boldsymbol{\rho}_2)_z = R\sin\eta\cos\theta_2\ ,\\
r_5 &= (\boldsymbol{\rho}_2)_x = R\sin\eta\sin\theta_2\cos\varphi_2\ ,\\
r_4 &= (\boldsymbol{\rho}_2)_y = R\sin\eta\sin\theta_2\sin\varphi_2\ ,\\
r_3 &= (\boldsymbol{\rho}_1)_z = R\cos\eta\cos\theta_1\ ,\\
r_2 &= (\boldsymbol{\rho}_1)_x = R\cos\eta\sin\theta_1\cos\varphi_1\ ,\\
r_1 &= (\boldsymbol{\rho}_1)_y = R\cos\eta\sin\theta_1\sin\varphi_1\ .
\end{aligned} \tag{3.108}$$

The eigenfunctions of the grand angular momentum operator $\boldsymbol{\Lambda}^2$ are therefore given by

$$\mathcal{Y}_\lambda^{l_k,m_k,l_{ij},m_{ij}}(\Omega_6) = \mathcal{N}_\lambda^{l_k,l_{ij}} Y_{l_k}^{m_k}(\hat{\rho}_1) Y_{l_{ij}}^{m_{ij}}(\hat{\rho}_2)(\cos\eta)^{l_k}(\sin\eta)^{l_{ij}} P_{(\lambda-l_k-l_{ij})/2}^{(l_{ij}+\frac{1}{2},l_k+\frac{1}{2})}(\cos 2\eta)\ . \tag{3.109}$$

$Y_l^m(\hat{\rho}_i)$ are spherical harmonics on polar coordinates θ_i, φ_i of the Jacobi vector $\boldsymbol{\rho_i}$. The grand angular momentum is related to the partial momenta l_k and l_{ij} by the equation

$$\lambda = l_k + l_{ij} + 2n\ , \quad n = 0, 1, 2, \ldots\ . \tag{3.110}$$

The angular momentum for the particle k with respect to the center of mass of two particles ij is given by l_k, and the angular momentum of two particles i, j is given by l_{ij}.

3.3. The adiabatic approach for N particles

As mentioned in Section 3.2, using the solutions of the hyperangular part of the Hamiltonian, one can formally rewrite the d-dimensional partial differential equations, i.e., the time-independent Schrödinger equation with a potential energy that depends only on relative position coordinates, as an infinite set of coupled ordinary differential equations in a single adiabatic coordinate R – the hyperradius. The basic form of the adiabatic representation requires writing the Hamiltonian in the following form

$$\hat{H} = \hat{T}_R + \hat{H}_{\rm ad}(R;\Omega)\ , \tag{3.111}$$

where $\hat{T}_R$ is the kinetic energy operator, which introduces coupling between different hyperradii R, the $\hat{H}_{\rm ad}$ is the *adiabatic* Hamiltonian comprised of the interaction potential V, which represents a set of coupled potential surfaces at each R and the hyperangular part of the kinetic energy. The adiabatic Hamiltonian depends on R parametrically and is a Hermitian partial differential operator. In order to find the form of $\hat{H}_{\rm ad}$, let us recall that using the relation in Eq. (3.31) the N-body Schrödinger equation can be written in a quasi-separable form

$$\left[-\frac{\hbar^2}{2\mu}\left(\frac{\partial^2}{\partial R^2}+\frac{d-1}{R}\frac{\partial}{\partial R}\right)+\frac{\mathbf{\Lambda}^2(\Omega)}{2\mu R^2}+V(R,\Omega)\right]\Psi(R,\Omega)=E\,\Psi(R,\Omega)\ . \tag{3.112}$$

We can cancel out the first-derivative term in R through a substitution on the total wavefunction

$$\Psi(R,\Omega)=R^{-\frac{d-1}{2}}\psi(R,\Omega)\ . \tag{3.113}$$

The Schrödinger equation becomes

$$\left[-\frac{\hbar^2}{2\mu}\frac{\partial^2}{\partial R^2}+\frac{1}{4}\frac{(d-1)(d-3)}{2\mu R^2}+\frac{\mathbf{\Lambda}^2(\Omega)}{2\mu R^2}+V(R,\Omega)\right]\psi(R,\Omega)=E\,\psi(R,\Omega)\ . \tag{3.114}$$

The adiabatic Hamiltonian is therefore comprised of the hyperangular part of the kinetic energy or the grand angular momentum, the potential, and the *mock-centrifugal* term proportional to $\sim(d-1)(d-3)/2$

$$\hat{H}_{\rm ad}(R;\Omega)=\frac{\mathbf{\Lambda}^2(\Omega)+(d-1)(d-3)/4}{2\mu R^2}+V(R,\Omega)\ . \tag{3.115}$$

The adiabatic separation of the Hamiltonian is justified when the hyperangular Hamiltonian $\hat{H}_{\rm ad}(R;\Omega)$ is Hermitian with respect to the measure $d\Omega$. The eigenfunctions of this operator need to form a complete orthonormal set and depend smoothly on R. This allows us to expand the total wavefunction in the corresponding adiabatic *channel* functions. The resulting non-adiabatic coupling terms – arising from derivatives with respect to R – should be finite and well-defined. Thus, we impose the adiabatic expansion of the total wavefunction

$$\psi(R,\Omega)=\sum_\nu F_\nu(R)\Phi_\nu(R;\Omega)\ , \tag{3.116}$$

where $F_\nu(R)$ are the hyperradial functions, and $\Phi_\nu(R;\Omega)$ are the channel functions, and ν represents all quantum numbers necessary to specify a given channel. The channel functions satisfy the eigenvalue equation for the

$$\hat{H}_{\rm ad}\Phi_\nu(R;\Omega)=U_\nu(R)\Phi_\nu(R;\Omega)\ , \tag{3.117}$$

where the eigenvalues $U_\nu(R)$ are the N-body hyperspherical potentials or adiabatic potential energy curves. By substituting the adiabatic expansion from Eq. (3.116) into the Schrödinger equation, we obtain the *hyperradial Schrödinger equation* which is a set of coupled differential equations for $F_\nu(R)$

$$\left[-\frac{\hbar^2}{2\mu}\frac{d^2}{dR^2}+W_\nu(R)-E\right]F_\nu(R)-\frac{\hbar^2}{2\mu}\sum_{\nu'\neq\nu}W_{\nu\nu'}(R)F_{\nu'}(R)=0\ . \tag{3.118}$$

The equation above describes the motion of N particles under the influence of the *effective potentials* $W_\nu(R)$ and *non-adiabatic* couplings $W_{\nu\nu'}$ defined by

$$\begin{aligned} W_\nu(R) &= U_\nu(R) - \frac{\hbar^2}{2\mu} Q_{\nu\nu}(R) \ , \\ W_{\nu\nu'}(R) &= 2P_{\nu\nu'}(R)\frac{d}{dR} + Q_{\nu\nu'}(R) \ . \end{aligned} \tag{3.119}$$

The first- and second-derivative terms are defined through the hyperradial dependence of the channel functions

$$\begin{aligned} P_{\nu\nu'}(R) &= \left\langle\!\!\left\langle \Phi_\nu(R) \middle| \frac{\partial \Phi_{\nu'}(R)}{\partial R} \right\rangle\!\!\right\rangle \ , \\ Q_{\nu\nu'}(R) &= \left\langle\!\!\left\langle \Phi_\nu(R) \middle| \frac{\partial^2 \Phi_{\nu'}(R)}{\partial R^2} \right\rangle\!\!\right\rangle \ , \end{aligned} \tag{3.120}$$

where the double bracket notation signifies an integral with respect to the measure $d\Omega$. Physically, the adiabatic separation requires that the hyperradial motion is slow compared to the hyperangular dynamics, such that the adiabatic potential energy curves $U_\nu(R)$ are well separated in energy and the non-adiabatic couplings $P_{\nu\nu'}(R)$ and $Q_{\nu\nu'}(R)$ are small compared to the energy differences between the channels. The diagonal part of the non-adiabatic couplings $P_{\nu\nu}$ is equal to zero, because we require that the set of channel functions is orthonormal

$$\left\langle\!\!\left\langle \Phi_\nu(R) \middle| \Phi_{\nu'}(R) \right\rangle\!\!\right\rangle = \delta_{\nu\nu'} \ . \tag{3.121}$$

Taking a derivative (with respect to R) of this equation and further requiring that the imaginary part of the channel functions is zero – yields the mentioned result.

The resulting set of coupled equations from Eq. (3.118) can be simplified using the *hyperradial Born-Oppenheimer approximation*. Under this approximation, both the diagonal and non-diagonal coupling terms $W_{\nu\nu'}$ are neglected. In such a case, the system's dynamics are constrained to a single adiabatic potential curve, which prevents transitions between channels and prevents the modeling of inelastic collisions. Nevertheless, the approximation yields reasonable estimates for bound-state energies and scattering phase shifts in certain regimes. In general, improved accuracy is obtained by retaining at least the diagonal non-adiabatic contributions $W_\nu(R)$, except in the vicinity of sharp avoided crossings; this treatment is known as the *hyperspherical adiabatic approximation* [205].

In three-body physics, i.e., for $d = 6$, the system's dynamics is driven by the effective three-body potentials $W_\nu(R)$ given in Eq. (3.119). The structure of the three-body potential determines the system's characteristic properties. At large distances, where $R \to \infty$, the potentials below the $E = 0$ threshold converge asymptotically to the binding energy E_b of the diatomic molecule and the two-body centrifugal term

$$W_\nu(R) \simeq -E_b + \frac{\hbar^2 l(l+1)}{2\mu R^2} \ , \tag{3.122}$$

where l is the relative angular momentum between the molecule and the atom. Above the threshold, the effective potentials follow the expansion

$$W_\nu(R) \simeq \hbar^2 \frac{\lambda(\lambda+4)+15/4}{2\mu R^2} \ , \tag{3.123}$$

where λ is the eigenvalue of the grand angular operator $\mathbf{\Lambda}^2(\Omega)$.

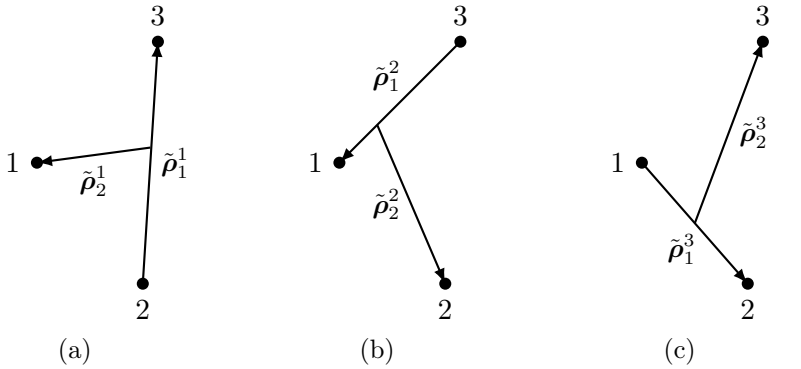

Figure 3.1: The three sets of Jacobi coordinate systems, which describe the relative positions of three interacting particles. The vectors presented in this plot are not mass-normalized, hence their relation to the mass-scaled Jacobi vectors is given by $\boldsymbol{\rho}_1^k = d_k^{-1}\tilde{\boldsymbol{\rho}}_1^k$, and $\boldsymbol{\rho}_2^k = d_k\tilde{\boldsymbol{\rho}}_2^k$. Panel (a) represents the case of the cyclic permutation $(i,j,k) = (2,3,1)$, panel (b) – $(i,j,k) = (3,1,2)$, and panel (c) – $(i,j,k) = (1,2,3)$.

3.4. The Johnson coordinates in the body-fixed frame

Let us now move on to the considerations of only three interacting particles. The equations in the previous Sections could therefore be considered with $N = 3$ and $d = 6$. There is a symmetry to the way we define the mass-normalized Jacobi vectors in Eq. (3.2). Namely, any one of the pairs of particles can be used to define the first Jacobi vector. Thus, we include an additional index i, j, or k in the superscript of the definition of the Jacobi vectors

$$\begin{aligned} \boldsymbol{\rho}_1^k &= d_k^{-1}(\mathbf{r}_j - \mathbf{r}_i) \ , \\ \boldsymbol{\rho}_2^k &= d_k \left(\mathbf{r}_k - \frac{m_i\mathbf{r}_i + m_j\mathbf{r}_j}{m_i + m_j} \right) \ . \end{aligned} \tag{3.124}$$

The indices (i,j,k) are a cyclic permutation of $(1,2,3)$. Eq. (3.124) defines three different sets of coordinates, which are presented schematically in Fig. 3.1. The mass-dependent coefficients are defined as follows

$$\begin{aligned} M &= m_1 + m_2 + m_3 \ , \\ \mu &= \left(\frac{m_1 m_2 m_3}{M} \right)^{\frac{1}{2}} \ , \\ d_k &= \left(\frac{m_k}{\mu} \left(\frac{m_i + m_j}{M} \right) \right)^{\frac{1}{2}} \ , \end{aligned} \tag{3.125}$$

and they are consistent with the definitions of the normalization factors dependent on μ_j and μ in Eq. (3.2). The canonical definition of the relation between the sets of vectors $(\boldsymbol{\rho}_1^i, \boldsymbol{\rho}_2^i)$ and $(\boldsymbol{\rho}_1^j, \boldsymbol{\rho}_2^j)$ is given by the so-called *kinematic rotation*

$$\begin{pmatrix} \boldsymbol{\rho}_1^j \\ \boldsymbol{\rho}_2^j \end{pmatrix} = \begin{pmatrix} \cos\beta_{ij} & \sin\beta_{ij} \\ -\sin\beta_{ij} & \cos\beta_{ij} \end{pmatrix} \begin{pmatrix} \boldsymbol{\rho}_1^i \\ \boldsymbol{\rho}_2^i \end{pmatrix} \ . \tag{3.126}$$

The *kinematic angle* β_{ij} follows relations, which are the result of the definitions given by Eq. (3.124). We will derive them by analyzing the expression

$$\begin{aligned}\boldsymbol{\rho}_1^j d_j = \mathbf{r}_i - \mathbf{r}_k = \mathbf{r}_i - \frac{m_j\mathbf{r}_j + m_k\mathbf{r}_k}{m_j + m_k} + \frac{m_j\mathbf{r}_j + m_k\mathbf{r}_k}{m_j + m_k} - \mathbf{r}_k = \\ = d_i^{-1}\boldsymbol{\rho}_2^i + \frac{m_j(\mathbf{r}_j - \mathbf{r}_k)}{m_j + m_k} = d_i^{-1}\boldsymbol{\rho}_2^i - \frac{m_j}{m_j + m_k} d_i\boldsymbol{\rho}_1^i \ .\end{aligned} \tag{3.127}$$

Comparing with the first row of the Eq. (3.126), this leads us to the equations

$$\begin{aligned}\sin\beta_{ij} =& d_i^{-1}d_j^{-1} \ , \\ \cos\beta_{ij} =& - d_i d_j^{-1}\frac{m_j}{m_j + m_k} = -d_i d_j^{-1} m_j \frac{m_i}{d_i^2\mu M} = \\ =& -d_i^{-1}d_j^{-1}\frac{m_i m_j}{\mu M}\cdot\frac{m_k}{m_k} = -d_i^{-1}d_j^{-1}\frac{\mu^2}{\mu\, m_k} = -d_i^{-1}d_j^{-1}\frac{\mu}{m_k} \ .\end{aligned} \tag{3.128}$$

This results in the following definition for the kinematic angle

$$\tan\beta_{ij} = -\frac{m_k}{\mu} \ . \tag{3.129}$$

Clearly, β_{ii} is equal to zero. Analysis of the inverse of the kinematic rotation matrix yields the result $\beta_{ij} = -\beta_{ji}$. Combining three kinematic rotations should result in the same set of Jacobi vectors, hence $\beta_{12} + \beta_{23} + \beta_{31} = 2\pi$. The kinematic angle should be in the range $\beta_{ij} \in [\pi/2, \pi]$, which can be deduced by analyzing the directions of the Jacobi vectors after the kinematic rotation.

In the previous Sections, we have shown that the N-particle interacting Hamiltonian can be expressed in the form given by Eq. (3.18). For three particles, it is therefore given by

$$\hat{H} = -\frac{\hbar^2}{2\mu}\left(\Delta_{\boldsymbol{\rho}_1} + \Delta_{\boldsymbol{\rho}_2}\right) + V(\boldsymbol{\rho}_1, \boldsymbol{\rho}_2) \ , \tag{3.130}$$

where $\Delta_{\boldsymbol{\rho}_2}$ and $\Delta_{\boldsymbol{\rho}_2}$ are the Laplacians given by the Jacobi vectors – regardless of the exact permutation (i, j, k). So far, we were able to simplify the Hamiltonian by parameterizing the *lab-fixed* coordinates of the Jacobi vectors. We should note that for a field-free problem, the potential V depends only on the relative positions of the three-interacting particles. By parametrizing the Jacobi vectors in the *particle-* or *body-fixed frame* – using the hyperradius R and two hyperangles θ and ϕ – we can reduce the problem's degrees of freedom by three hyperangles. These hyperangles define the rotation of the body-fixed frame with respect to the lab-fixed frame and are, by definition, the Euler angles α, β, γ. In this Section, we will provide the full reasoning for expressing the interacting Hamiltonian – especially the grand angular momentum operator – in variables R, θ, and ϕ as it was proposed in Refs. [187, 206, 207] by Prof. Johnson – based on the works of Prof. Smith and Prof. Whitten described in Refs. [208–210].

3.4.1. Rotation of the lab-fixed frame

The first step is parametrizing the Jacobi vectors in the body-fixed frame. This means that we must fix the index k describing one of the chosen sets of Jacobi vectors presented in Fig. 3.1 and, if needed, use the kinematic rotation to calculate the results in another set. We note that the rotation of the coordinate system by the Euler angles does not change the relation defining the hyperradius

$$R^2 = |\boldsymbol{\rho}_1^k|^2 + |\boldsymbol{\rho}_2^k|^2 \ . \tag{3.131}$$

Furthermore, using Eq. (3.126), one can also show that Eq. (3.131) is true for all $k = 1, 2, 3$ – hence the hyperradius is independent of the kinematic rotation.

The externals coordinates α, β, γ rotate a lab-fixed Cartesian coordinate system $\mathcal{O}x'y'z'$ into the moving, body-fixed coordinate system $\mathcal{O}xyz$. By convention, the $\mathcal{O}xyz$ system is oriented so that the axis z is positive in the direction of the vector

$$\mathbf{A} = \frac{1}{2}\left(\boldsymbol{\rho}_1^k \times \boldsymbol{\rho}_2^k\right) \ , \tag{3.132}$$

whose length is the area of the triangle formed by the three particles. In classical (rather than quantum) problems, the x and y axes of the body-fixed frame are canonically chosen to coincide with the principal axes of inertia of the three particles. There are many conventions for the exact definitions of rotations given by the Euler angles. The convention proposed in Refs. [187, 206, 207] is provided below. The axes of the stationary coordinate system $\mathcal{O}x'y'z'$ can be brought to coincide with the $\mathcal{O}xyz$ system by a series of three elementary (right-hand) rotations. The first of these operations is the rotation $\hat{R}_\alpha$ by an angle $\alpha \in [0, 2\pi]$ around the z' axis, followed by a rotation by $\beta \in [0, \pi]$ by the new $\tilde{y}$ axis, where $\tilde{y} = \hat{R}_\alpha\, y$. This operation brings the z' axis to the z axis. The last rotation is by an angle $\gamma \in [0, 2\pi]$ around the z axis.

Let us consider a partly-rotated coordinate system $\mathcal{O}\bar{x}\bar{y}\bar{z}$, which is obtained by rotating the stationary system by the Euler angles $\alpha = \phi_{\mathbf{A}}$, $\beta = \theta_{\mathbf{A}}$ and $\gamma = 0$, where $\theta_{\mathbf{A}}$ and $\phi_{\mathbf{A}}$ are the spherical polar angles of the vector $\mathbf{A}$. By construction, the three particles lie in the $\bar{x}\bar{y}$ plane. In order to keep this Section self-contained, we will calculate the angle γ, which rotates the system $\mathcal{O}\bar{x}\bar{y}\bar{z}$ into $\mathcal{O}xyz$, such that the axes xy coincide with the principal axes of inertia of the three particles. We will notice that for the rotation of the Laplacian in the quantum three-body problem, such considerations are not strictly necessary. However, it is prudent to consider the form of the classical equations of motion first before solving the quantum three-body problem in the body-fixed frame; therefore, we will continue this reasoning.

We would like to express the only non-zero elements of the inertia tensor in the $\mathcal{O}\bar{x}\bar{y}\bar{z}$ system, namely

$$\begin{aligned} I_{\bar{x}\bar{x}} &= \sum_l m_l \mathbf{r}_{l,\bar{y}}^2 \ , \\ I_{\bar{y}\bar{y}} &= \sum_l m_l \mathbf{r}_{l,\bar{x}}^2 \ , \\ I_{\bar{x}\bar{y}} &= -\sum_l m_l \mathbf{r}_{l,\bar{x}} \mathbf{r}_{l,\bar{y}} \ , \end{aligned} \tag{3.133}$$

where $l = 1, 2, 3$ denotes a given particle – in terms of the Jacobi vectors $(\boldsymbol{\rho}_1^k, \boldsymbol{\rho}_2^k)$ and the total center of mass $\mathbf{R}_{\mathrm{CM}}$. Although we keep in mind that by definition given in Eq. (3.18) we choose all coordinate systems such that $\mathbf{R}_{\mathrm{CM}} = 0$. For simplicity, we neglect the z components of all of these vectors, since in $\mathcal{O}\bar{x}\bar{y}\bar{z}$ they are equal to zero anyway. We aim to prove the identity

$$\langle \xi | \zeta \rangle_E = \langle \mathcal{A}\xi | \mathcal{A}\zeta \rangle_E \ , \tag{3.134}$$

where $\xi, \zeta \in \mathbb{R}^3$, $\langle \cdot | \cdot \rangle_E$ is the standard Euclidean inner product in $\mathbb{R}^3$, and $\mathcal{A} : \mathbb{R}^3 \to \mathbb{R}^3$ is a linear transformation given by $\mathcal{A} : (\mathbf{r}_1, \mathbf{r}_2, \mathbf{r}_3) \to (\sqrt{\mu_1}\tilde{\boldsymbol{\rho}}_1^k, \sqrt{\mu_2}\tilde{\boldsymbol{\rho}}_2^k, \sqrt{M}\mathbf{R}_{\mathrm{CM}})$, where μ_1, and μ_2 are defined in Eq. (3.3) and where $\tilde{\boldsymbol{\rho}}_1^k = \mathbf{r}_j - \mathbf{r}_i$, $\tilde{\boldsymbol{\rho}}_2^k = \mathbf{r}_k - (m_i\mathbf{r}_i + m_j\mathbf{r}_j)/(m_i + m_j)$ are the Jacobi vectors without the mass-scaling, i.e., $\boldsymbol{\rho}_1^k = \sqrt{\mu_1/\mu}\,\tilde{\boldsymbol{\rho}}_1^k$, and $\boldsymbol{\rho}_2^k = \sqrt{\mu_2/\mu}\,\tilde{\boldsymbol{\rho}}_2^k$. In other words, we aim to prove that the transformation $\mathcal{A}$ is orthogonal.

We notice that if true, for $\mathbf{R}_{\mathrm{CM}} = 0$, this result immediately gives the desired expression

for the initial tensor elements

$$\begin{aligned} I_{\bar{x}\bar{x}} =& \mu_1(\tilde{\boldsymbol{\rho}}_1^k)_{\bar{y}}^2 + \mu_2(\tilde{\boldsymbol{\rho}}_2^k)_{\bar{y}}^2 = \mu\left[(\boldsymbol{\rho}_1^k)_{\bar{y}}^2 + (\boldsymbol{\rho}_2^k)_{\bar{y}}^2\right] \ , \\ I_{\bar{y}\bar{y}} =& \mu_1(\tilde{\boldsymbol{\rho}}_1^k)_{\bar{x}}^2 + \mu_2(\tilde{\boldsymbol{\rho}}_2^k)_{\bar{x}}^2 = \mu\left[(\boldsymbol{\rho}_1^k)_{\bar{x}}^2 + (\boldsymbol{\rho}_2^k)_{\bar{x}}^2\right] \ , \\ I_{\bar{x}\bar{y}} =& -\mu_1(\tilde{\boldsymbol{\rho}}_1^k)_{\bar{x}}(\tilde{\boldsymbol{\rho}}_1^k)_{\bar{y}} - \mu_2(\tilde{\boldsymbol{\rho}}_2^k)_{\bar{x}}(\tilde{\boldsymbol{\rho}}_2^k)_{\bar{y}} = -\mu\left[(\boldsymbol{\rho}_1^k)_{\bar{x}}(\boldsymbol{\rho}_1^k)_{\bar{y}} + (\boldsymbol{\rho}_2^k)_{\bar{x}}(\boldsymbol{\rho}_2^k)_{\bar{y}}\right] \ . \end{aligned} \tag{3.135}$$

These equations are equivalent to Eq. (3.134), for the following sets of vectors ξ, ζ: the first equation for $\xi^T = \zeta^T = (\sqrt{m_i}, r_{i,\bar{y}}, \sqrt{m_j}, r_{j,\bar{y}}, \sqrt{m_k}, r_{k,\bar{y}})$, the second equation for $\xi^T = \zeta^T = (\sqrt{m_i}, r_{i,\bar{x}}, \sqrt{m_j}, r_{j,\bar{x}}, \sqrt{m_k}, r_{k,\bar{x}})$, and the third equation for

$$\begin{aligned} \xi^T &= -(\sqrt{m_i}, r_{i,\bar{x}}, \sqrt{m_j}, r_{j,\bar{x}}, \sqrt{m_k}, r_{k,\bar{x}}) \ , \\ \zeta^T &= (\sqrt{m_i}, r_{i,\bar{y}}, \sqrt{m_j}, r_{j,\bar{y}}, \sqrt{m_k}, r_{k,\bar{y}}) \ , \end{aligned} \tag{3.136}$$

respectively. To prove that $\mathcal{A}$ is orthogonal, it is enough to show that $[\mathcal{A}]^T[\mathcal{A}] = \mathbb{I}$, where $[\mathcal{A}]$ is the matrix of the transformation given in the standard basis by

$$[\mathcal{A}] = \begin{pmatrix} -\sqrt{\frac{\mu_1}{m_i}} & \sqrt{\frac{\mu_1}{m_j}} & 0 \\ -\frac{\sqrt{m_i\mu_2}}{m_i+m_j} & -\frac{\sqrt{m_j\mu_2}}{m_i+m_j} & \sqrt{\frac{\mu_2}{m_k}} \\ \sqrt{\frac{m_i}{M}} & \sqrt{\frac{m_j}{M}} & \sqrt{\frac{m_k}{M}} \end{pmatrix} \ , \tag{3.137}$$

This derivation requires extensive, but routine, algebra.

Rotating the coordinate system $\mathcal{O}\bar{x}\bar{y}\bar{z}$ by the γ around the $\bar{z}$ axis transforms the $\bar{x}$, and $\bar{y}$ coefficients of all the vectors in Eq. (3.135), and thus results in the following relations

$$\begin{aligned} I_{xx} =& I_{\bar{x}\bar{x}}\cos^2\gamma + I_{\bar{y}\bar{y}}\sin^2\gamma - 2I_{\bar{x}\bar{y}}\sin\gamma\cos\gamma \ , \\ I_{yy} =& I_{\bar{x}\bar{x}}\sin^2\gamma + I_{\bar{y}\bar{y}}\cos^2\gamma + 2I_{\bar{x}\bar{y}}\sin\gamma\cos\gamma \ , \\ I_{xy} =& (I_{\bar{x}\bar{x}} - I_{\bar{y}\bar{y}})\sin\gamma\cos\gamma + I_{\bar{x}\bar{y}}\left(\cos^2\gamma - \sin^2\gamma\right) \ , \end{aligned} \tag{3.138}$$

where we notice that the subscripts now indicate that the moments of inertia are calculated in the $\mathcal{O}xyz$ system. As shown in Ref. [209], but what is also apparent from the form of the Eq. (3.138), the following variables

$$\begin{aligned} s &= \frac{I_x - I_y}{\mu} \ , \\ t &= 2\frac{I_{xy}}{\mu} \ , \end{aligned} \tag{3.139}$$

transform under the γ rotation in the following way

$$\begin{aligned} s =& \bar{s}\cos(2\gamma) + \bar{t}\sin(2\gamma) \ , \\ t =& -\bar{s}\sin(2\gamma) + \bar{t}\cos(2\gamma) \ , \end{aligned} \tag{3.140}$$

where $\bar{s}$ and $\bar{t}$ are the analogous variables in the $\mathcal{O}\bar{x}\bar{y}\bar{z}$ system. Thus, the quantities s, t behave like components of a vector rotated by an angle (-2γ). The length $Q = \sqrt{t^2 + s^2}$ of this abstract vector is preserved in both coordinate systems. By definition, the mixed element of the inertia tensor I_{xy} is zero in the $\mathcal{O}xyz$ coordinate system, which is equivalent to setting $t = 0$. By convention [209], the larger of the tensor elements is labeled I_y, hence $Q = s = (I_y - I_x)/\mu > 0$. The relation in Eq. (3.140) can be easily inverted

$$\begin{aligned} \bar{s} =& s\cos(2\gamma) - t\sin(2\gamma) \ , \\ \bar{t} =& s\sin(2\gamma) + t\cos(2\gamma) \ . \end{aligned} \tag{3.141}$$

The following relations therefore define the angle γ

$$\begin{aligned} \cos(2\gamma) &= \frac{\bar{s}}{Q} \ , \\ \sin(2\gamma) &= \frac{\bar{t}}{Q} \ , \end{aligned} \tag{3.142}$$

which result from inserting the condition that $t = 0$ into Eq. (3.141). By definition, the Euler angle is in the range $\gamma \in [0, 2\pi]$. However the obtained conditions for γ have two solutions in this range, one such that $\gamma_1 \in [0, \pi]$, and the other $\gamma_2 = (\gamma_1 + \pi) \in [\pi, 2\pi]$. These two solutions define equivalent coordinate systems that are rotated by π with respect to each other.

3.4.2. Parametrization of the Jacobi vectors in the body-fixed frame

We can now move on to defining the internal coordinates proposed in Ref. [210], called the symmetric *Smith-Whitten* internal coordinates R, Θ, Φ^k in the $\mathcal{O}xyz$ coordinate system

$$\begin{aligned} (\boldsymbol{\rho}_1^k)_x &= R\cos\Theta\cos\Phi^k \ , \\ (\boldsymbol{\rho}_1^k)_x &= -R\sin\Theta\sin\Phi^k \ , \\ (\boldsymbol{\rho}_2^k)_x &= R\cos\Theta\sin\Phi^k \ , \\ (\boldsymbol{\rho}_2^k)_y &= R\sin\Theta\cos\Phi^k \ , \\ (\boldsymbol{\rho}_1^k)_z &= (\boldsymbol{\rho}_2^k)_z = 0 \ . \end{aligned} \tag{3.143}$$

In classical physics, these relations satisfy that the product of inertia is zero in the principal axes system, namely

$$I_{xy} = \mu\left[(\boldsymbol{\rho}_2^k)_y(\boldsymbol{\rho}_2^k)_x + (\boldsymbol{\rho}_1^k)_x(\boldsymbol{\rho}_1^k)_y\right] = 0 \ . \tag{3.144}$$

We notice that the square sum of the components gives

$$(\boldsymbol{\rho}_1^k)_x^2 + (\boldsymbol{\rho}_1^k)_y^2 + (\boldsymbol{\rho}_2^k)_x^2 + (\boldsymbol{\rho}_2^k)_y^2 = R^2 \ . \tag{3.145}$$

The length of vectors is invariant under the Euler rotations, so the R is the same hyperradius that was defined previously in Eq. (3.131). The length of the vector $\mathbf{A}$ given in Eq. (3.132) is easily evaluated

$$|\mathbf{A}| = \frac{1}{2}\left[(\boldsymbol{\rho}_1^k)_x(\boldsymbol{\rho}_2^k)_y - (\boldsymbol{\rho}_1^k)_y(\boldsymbol{\rho}_2^k)_x\right] = \frac{R^2\sin(2\Theta)}{4} \ . \tag{3.146}$$

In order to evaluate the range of the angle Θ, we need another constraint. We recall that the value Q is given in the principal axes coordinate system by

$$Q = s = \frac{1}{\mu}(I_y - I_x) = (\boldsymbol{\rho}_1^k)_x^2 + (\boldsymbol{\rho}_2^k)_x^2 - (\boldsymbol{\rho}_1^k)_y^2 - (\boldsymbol{\rho}_2^k)_y^2 = R^2\cos(2\Theta) \ . \tag{3.147}$$

Since R, $|\mathbf{A}|$ and Q are all nonnegative, the range is $\Theta \in [0, \pi/4]$. Using Eq. (3.135), the moments of inertia can be expressed in terms of R, and Θ

$$\begin{aligned} I_{xx} &= \mu R^2\sin^2\Theta \ , \\ I_{yy} &= \mu R^2\cos^2\Theta \ , \\ I_{zz} &= I_{xx} + I_{zz} = \mu R^2 \ . \end{aligned} \tag{3.148}$$

The calculation of Φ^k could be performed by introducing two scalar quantities, namely $2\boldsymbol{\rho}_1^k \cdot \boldsymbol{\rho}_2^k$, and $|\boldsymbol{\rho}_1^k|^2 - |\boldsymbol{\rho}_2^k|^2$. A quick calculation gives the relation between them and the Smith-Whitten coordinates

$$\begin{aligned} 2\boldsymbol{\rho}_1^k \cdot \boldsymbol{\rho}_2^k &= R^2 \cos(2\Theta) \sin(2\Phi^k) \\ |\boldsymbol{\rho}_1^k|^2 - |\boldsymbol{\rho}_2^k|^2 &= R^2 \cos(2\Theta) \cos(2\Phi^k) \ . \end{aligned} \tag{3.149}$$

The angle Φ^k is in principle defined in the range $\Phi^k \in [0, 2\pi]$. However, the equation above have two solutions $\Phi_1^k \in [0, \pi]$ and $\Phi_2^k = \Phi_1^k + \pi \in [\pi, 2\pi]$, same as the Euler angle γ. Each of the solutions Φ_1^k and Φ_2^k is associated with one of the solutions γ_1 and γ_2. To properly pair these solutions, one should insert a given solution Φ_1^k or Φ_2^k into the definitions in Eq. (3.143), then evaluate the positions of the three particles and evaluate the angle for axes rotation with the correct algebraic sign, thus assigning the correct value of γ. Thus, hyperspherical coordinate space is divided into two branches.

The kinematic rotation in the Smith-Whitten coordinates is given by

$$\Phi^j = \Phi^i - \beta_{ij} \ , \tag{3.150}$$

which can be easily verified by inserting the definitions from Eq. (3.143) into Eq. (3.126). Using the Smith-Whitten coordinates and the definition given by Eq. (3.124), the following formula for the interparticle distances can be derived

$$\begin{aligned} |\mathbf{r}_j - \mathbf{r}_i| =& d_k |\boldsymbol{\rho}_1^k| = d_k \sqrt{(\boldsymbol{\rho}_1^k)_x^2 + (\boldsymbol{\rho}_1^k)_y^2} = d_k R \sqrt{\cos^2\Theta \cos^2\Phi^k + \sin^2\Theta \sin^2\Phi^k} = \\ =& d_k R \sqrt{\frac{1}{2}\cos^2\Theta\cos^2\Phi^k + \frac{1}{2}\underbrace{\cos^2\Theta}\sin^2\Phi^k + \frac{1}{2}\sin^2\Theta\sin^2\Phi^k + \frac{1}{2}\underbrace{\sin^2\Theta}\sin^2\Phi^k} = \\ =& d_k R \sqrt{\frac{1}{2}\left(\cos^2\Phi^k + \sin^2\Phi^k\right) + \frac{1}{2}\left(\cos^2\Theta - \sin^2\Theta\right)\left(\cos^2\Phi^k - \sin^2\Phi^k\right)} = \\ =& \frac{d_k R}{\sqrt{2}} \sqrt{1 + \cos(2\Theta)\cos(2\Phi^k)} \ , \end{aligned} \tag{3.151}$$

where we substitute the underbaced terms using the trigonometric identity.

Ref. [187] introduces a slightly modified version of the Smith-Whitten coordinates, called the *Johnson* coordinates θ, ϕ, given by

$$\begin{aligned} \theta &= \frac{\pi}{2} - 2\Theta \ , \\ \phi^k &= \frac{\pi}{2} - 2\Phi^k \ . \end{aligned} \tag{3.152}$$

The hyperradius remains unmodified. The ranges of the Smith-Whitten coordinates are as follows $R \in [0, \infty]$, $\Theta \in [0, \pi/4]$, $\Phi^k \in [0, 2\pi]$, hence the Johnson coordinates have the following ranges $R \in [0, \infty]$, $\theta \in [0, \pi/2]$, $\phi^k \in [0, 4\pi]$. What immediately follows is a slight simplification of the relations derived in this Section

$$\begin{aligned} |\mathbf{A}| = \frac{1}{2}\left(\boldsymbol{\rho}_1^k \times \boldsymbol{\rho}_2^k\right) &= \frac{1}{4} R^2 \cos\theta \ , \\ 2(\boldsymbol{\rho}_1^k \cdot \boldsymbol{\rho}_2^k) &= R^2 \sin\theta \cos\phi^k \ , \\ |\boldsymbol{\rho}_1^k|^2 - |\boldsymbol{\rho}_2^k|^2 &= R^2 \sin\theta \sin\phi^k \ , \\ |\mathbf{r}_j - \mathbf{r}_i| &= \frac{d_k R}{2^{1/2}} \left(1 + \sin\theta \sin\phi^k\right)^{\frac{1}{2}} \ . \end{aligned} \tag{3.153}$$

We recall that the potential energy in a field-free problem depends only on the internal Jacobi coordinates. It is useful to map these coordinates into some abstract, *configuration space*

$\mathcal{O}_c\, x_c y_c z_z$, which is not the body-fixed frame $\mathcal{O}xyz$. As proposed in Ref. [187], a simple mapping of the internal configuration of the triangle formed by the three particles can be defined as follows. We define R, θ and ϕ^k to be the spherical polar coordinates of a given point (x_c^k, y_c^k, z_c) in the configuration space

$$\begin{aligned} x_c^k &= R\sin\theta\cos\phi^k \ , \\ y_c^k &= R\sin\theta\sin\phi^k \ , \\ z_c &= R\cos\theta \ . \end{aligned} \tag{3.154}$$

There are three configuration spaces for each Jacobi choice, marked by the index k. The kinematic rotation in Jacobi coordinates is given by

$$\phi^j = \phi^i - 2\eta_{ij} \ , \tag{3.155}$$

where $\eta_{ij} = -\beta_{ij} = \arctan(m_k/\mu)$.

So far, we have considered all equations in a general form, using the index k marking the choice of the Jacobi coordinate system. We can make the choice that $k = 1$, i.e., particles 2 and 3 are paired, and particle 1 is separate. The distance formulas become

$$\begin{aligned} |\mathbf{r}_2 - \mathbf{r}_3| &= \frac{Rd_1}{2^{1/2}}\left[1 + \sin\theta\sin\phi\right]^{\frac{1}{2}} \ , \\ |\mathbf{r}_3 - \mathbf{r}_1| &= \frac{Rd_2}{2^{1/2}}\left[1 + \sin\theta\sin\left(\phi - 2\arctan\left(m_2/\mu\right)\right)\right]^{\frac{1}{2}} \ , \\ |\mathbf{r}_1 - \mathbf{r}_2| &= \frac{Rd_3}{2^{1/2}}\left[1 + \sin\theta\sin\left(\phi + 2\arctan\left(m_3/\mu\right)\right)\right]^{\frac{1}{2}} \ , \end{aligned} \tag{3.156}$$

where we set $\phi^1 := \phi$.

3.4.3. The operator Λ^2 in Johnson coordinates

We aim to derive the Laplacian – and thus the quantum Hamiltonian – in the Johnson coordinates. We will proceed in two steps, following the procedure proposed in Refs. [206, 207] by Prof. Johnson. First, we will consider a transformation of the classical kinetic energy T in the context of Hamiltonian mechanics. We will show that this transformation allows us to find the metric tensor of the Johnson coordinate map in the $\mathcal{O}xyz$ system. In the second step, we will use the familiar formula for the Laplacian in curvilinear coordinates given by Eq. (3.26) and calculate the Laplacian using our knowledge of the metric tensor g_{ij}. In this Section, we will use the Einstein notation for summation, wherever appropriate. Furthermore, in this Section, we choose the Jacobi coordinate set: $(i, j, k) = (2, 3, 1)$, i. e., $(\boldsymbol{\rho}_1, \boldsymbol{\rho}_2) := (\boldsymbol{\rho}_1^1, \boldsymbol{\rho}_2^1) = (\boldsymbol{\rho}_1^k, \boldsymbol{\rho}_2^k)$, without loss of generality.

Let us express the classical kinetic energy T' in the stationary $\mathcal{O}x'y'z'$ system in terms of the Jacobi vectors $(\boldsymbol{\rho}_1, \boldsymbol{\rho}_2)$. Let us consider a linear transformation $\mathcal{A}_t : \mathbb{R}^3 \to \mathbb{R}^3$ given by $\mathcal{A}_t : (\dot{\mathbf{r}}_1, \dot{\mathbf{r}}_2, \dot{\mathbf{r}}_3) \to (\sqrt{\mu_1}\dot{\tilde{\boldsymbol{\rho}}}_1, \sqrt{\mu_2}\dot{\tilde{\boldsymbol{\rho}}}_2, \sqrt{M}\dot{\mathbf{R}}_{\mathrm{CM}})$, which is analogous to the linear transformation $\mathcal{A}$ given in the previous Section. In fact, the matrix of the transformation $\mathcal{A}_t$ is equal to that of $\mathcal{A}$ given by Eq. (3.137). This can be verified by taking the time-derivative of Eq. (3.124). This means that $\mathcal{A}_t$ is orthogonal. The standard expression for the kinetic energy in the stationary system $\mathcal{O}x'y'z'$ is

$$T' = \sum_l \frac{m_l \dot{\mathbf{r}}_l^2}{2} \ . \tag{3.157}$$

Since $\mathcal{A}_t$ preserves the inner product, similarly to $\mathcal{A}$ in Eq. (3.134), we can use this relation by setting $\xi^T = \zeta^T = (\sqrt{m_i}\dot{\mathbf{r}}_{i,\nu}, \sqrt{m_j}\dot{\mathbf{r}}_{j,\nu}, \sqrt{m_k}\dot{\mathbf{r}}_{k,\nu})$, resulting in the following expression

$$\sum_l m_l \dot{\mathbf{r}}_{l,\nu}^2 = \mu_1 (\dot{\boldsymbol{\rho}}_1)_\nu^2 + \mu_1 (\dot{\boldsymbol{\rho}}_2)_\nu^2 \ , \quad \nu = x', y', z' \ , \tag{3.158}$$

We recall that the origin of $\mathcal{O}x'y'z'$ is set such that $\mathbf{R}_{\mathrm{CM}} = \dot{\mathbf{R}}_{\mathrm{CM}} = 0$. Taking Eq. (3.158) and summing over all indices $\nu = x', y', z'$, we get

$$T' = \frac{\mu_1}{2}\dot{\boldsymbol{\rho}}_1 \cdot \dot{\boldsymbol{\rho}}_1 + \frac{\mu_2}{2}\dot{\boldsymbol{\rho}}_2 \cdot \dot{\boldsymbol{\rho}}_2 = \frac{\mu}{2}\left[\dot{\boldsymbol{\rho}}_1 \cdot \dot{\boldsymbol{\rho}}_1 + \dot{\boldsymbol{\rho}}_2 \cdot \dot{\boldsymbol{\rho}}_2\right] \ . \tag{3.159}$$

Let us now consider a curvilinear transformation of coordinates $y \to q$ given by the metric tensor g_{ij}

$$y^\alpha = y^\alpha(q^1 \ldots, q^n) \ , \quad \alpha = 1, \ldots, n \ , \tag{3.160}$$

for some $n \in \mathbb{N}$. Using the chain rule for derivation, we get

$$\dot{y}^\alpha = \frac{\partial y^\alpha}{\partial q^i}\dot{q}^i \ . \tag{3.161}$$

Inserting it into a general expression for T, we obtain

$$T = \frac{\mu}{2}\dot{y}^\alpha \dot{y}^\beta \delta_{\alpha\beta} = \frac{\mu}{2}\frac{\partial y^\alpha}{\partial q^i}\frac{\partial y^\beta}{\partial q^j}\delta_{\alpha\beta}\,\dot{q}^i\dot{q}^j = \frac{\mu}{2}g_{ij}\dot{q}^i\dot{q}^j = \frac{\mu}{2}\mathbf{q}^T\mathbf{g}\mathbf{q} \ . \tag{3.162}$$

Thus, by considering a transformation for $n = 6$, such that

$$y = \begin{pmatrix} (\dot{\boldsymbol{\rho}}_1)_x \\ (\dot{\boldsymbol{\rho}}_1)_y \\ (\dot{\boldsymbol{\rho}}_1)_z \\ (\dot{\boldsymbol{\rho}}_2)_x \\ (\dot{\boldsymbol{\rho}}_2)_y \\ (\dot{\boldsymbol{\rho}}_2)_z \end{pmatrix} \to \begin{pmatrix} \dot{R} \\ \dot{\Theta} \\ \dot{\Phi} \\ \omega_x \\ \omega_y \\ \omega_z \end{pmatrix} = q \ , \tag{3.163}$$

we will be able to find the metric tensor by calculating T' in the new coordinates and using Eq. (3.162), where R, Θ, Φ are the Smith-Whitten coordinates (parameters in the rotating $\mathcal{O}xyz$ frame), and $\omega_\nu := \dot{\Omega}_\nu$, for $\nu = x, y, z$ are the instantaneous angular velocity coordinates of the rotating axes $\mathcal{O}xyz$. They are not equal to time derivatives of the Euler angles.

The classical Hamiltonian

We have derived the expression for the classical Hamiltonian in the stationary coordinate system in Eq. (3.159). Let us recall the expressions for the time derivative of the Jacobi vectors between the two frames

$$\dot{\boldsymbol{\rho}}_1{}' = \dot{\boldsymbol{\rho}}_1 + \omega \times \boldsymbol{\rho}_1 \ , \tag{3.164}$$

where ω defines the vector of angular velocity of the rotating frame. The same relation is true for the second Jacobi vector $\boldsymbol{\rho}_2$ and any other vector measured in both frames. The superscript $'$ indicates the measurement in the stationary frame. The superscript $'$ next to the Jacobi vectors was omitted in Eqs. (3.157)-(3.159) and in Eq. (3.163) for greater clarity. Using definitions from Eq. (3.143) and the relation above for coordinates in the body-frame

(so the left-hand side is the velocity *measured* in the stationary frame but *expressed* in the body-frame coordinates), we can derive the curvilinear map

$$\begin{pmatrix} (\dot{\boldsymbol{\rho}}_1{}')_x \\ (\dot{\boldsymbol{\rho}}_1{}')_y \\ (\dot{\boldsymbol{\rho}}_1{}')_z \\ (\dot{\boldsymbol{\rho}}_2{}')_x \\ (\dot{\boldsymbol{\rho}}_2{}')_y \\ (\dot{\boldsymbol{\rho}}_2{}')_z \end{pmatrix} = \begin{pmatrix} c_\Theta c_\Phi & -s_\Theta c_\Phi & -c_\Theta s_\Phi & 0 & 0 & s_\Theta s_\Phi \\ -s_\Theta s_\Phi & -c_\Theta s_\Phi & -s_\Theta c_\Phi & 0 & 0 & c_\Theta c_\Phi \\ 0 & 0 & 0 & -s_\Theta s_\Phi & -c_\Theta c_\Phi & 0 \\ c_\Theta s_\Phi & -s_\Theta s_\Phi & c_\Theta c_\Phi & 0 & 0 & -s_\Theta c_\Phi \\ s_\Theta c_\Phi & c_\Theta c_\Phi & -s_\Theta s_\Phi & 0 & 0 & c_\Theta s_\Phi \\ 0 & 0 & 0 & s_\Theta c_\Phi & -c_\Theta s_\Phi & 0 \end{pmatrix} \begin{pmatrix} \dot{R} \\ R\dot{\Theta} \\ R\dot{\Phi} \\ R\omega_x \\ R\omega_y \\ R\omega_z \end{pmatrix} , \tag{3.165}$$

where $c_\Theta = \cos\Theta$, $c_\Phi = \cos\Phi$, $s_\Theta = \sin\Theta$, and $s_\Phi = \sin_\Phi$. The first three columns are direct derivatives of the expressions given by Eq. (3.143), while the last three columns of the matrix were obtained by calculating the value $\omega \times \boldsymbol{\rho}_1$ and $\omega \times \boldsymbol{\rho}_2$. Multiplying the equation above by its transpose immediately returns the expression for T' derived in Eq. (3.159) on the left-hand side. This is because the lengths of the velocity vectors *measured* in the stationary frame ($|\dot{\boldsymbol{\rho}}_1{}'|, |\dot{\boldsymbol{\rho}}_2|'$)– but *expressed* in coordinates of both the body- and stationary-frames – are equal.

The right-hand side of this equation requires finding the transpose of the matrix $[\mathcal{M}]$ in Eq. (3.165). The calculation is quite extensive, but eventually yields

$$[\mathcal{M}]^T = \begin{pmatrix} 1 & 0 & 0 & 0 & 0 & 0 \\ 0 & 1 & 0 & 0 & 0 & 0 \\ 0 & 0 & 1 & 0 & 0 & -\sin(2\Theta) \\ 0 & 0 & 0 & \sin^2\Theta & 0 & 0 \\ 0 & 0 & 0 & 0 & \cos^2\Theta & 0 \\ 0 & -\sin(2\Theta) & 0 & 0 & 0 & 1\,. \end{pmatrix} . \tag{3.166}$$

We can thus derive the classical Hamiltonian in the *time-derivative of the Smith-Whitten+ω* coordinates

$$T' = \frac{\mu}{2}\left[\dot{R}^2 + R^2\left(\dot{\Theta}^2 + \dot{\Phi}^2 + \omega_z^2 + \omega_y^2\cos^2\Theta + \omega_x^2\sin^2\Theta - 2\dot{\Phi}\omega_z\sin(2\Theta)\right)\right] . \tag{3.167}$$

We now make the substitution of the Smith-Whitten into Johnson coordinates, which is given by Eq. (3.152) and the simple relations

$$\begin{aligned} \dot{\Theta} &= -\frac{1}{2}\dot{\theta} , \\ \dot{\Phi} &= -\frac{1}{2}\dot{\phi} . \end{aligned} \tag{3.168}$$

Eq. (3.167) in Johnson coordinates is given by

$$\frac{\mu}{2}\left[\dot{R}^2 + \frac{R^2}{4}(\dot{\theta}^2 + \dot{\phi}^2)\right] + \frac{1}{2}\left(I_{xx}\omega_x^2 + I_{yy}\omega_y^2 + I_{zz}\omega_z^2 + I_{zz}\cos\theta\omega_z\dot{\phi}\right) , \tag{3.169}$$

where we used the definitions of the principal moments of inertia given by Eq. (3.148). The first term in the obtained equation is the translational kinetic energy, and the second term is comprised of the rotational kinetic energy and the Coriolis energy. Comparing with Eq. (3.162) we can finally derive the metric tensor $g_{ij} = \mathbf{g}$

$$\mathbf{g} = \begin{pmatrix} \mathbf{G} & \mathbf{C} \\ \mathbf{C}^T & \mathbf{K} \end{pmatrix} , \tag{3.170}$$

where the component block matrices are given by

$$\begin{aligned}
\mathbf{G} &= \begin{pmatrix} 1 & 0 & 0 \\ 0 & \frac{R^2}{4} & 0 \\ 0 & 0 & \frac{R^2}{4} \end{pmatrix} , \\
\mathbf{C} &= \begin{pmatrix} 0 & 0 & 0 \\ 0 & 0 & 0 \\ 0 & 0 & \frac{R^2}{2}\cos\theta \end{pmatrix} , \\
\mathbf{K} &= \frac{R^2}{2} \begin{pmatrix} 1-\sin\theta & 0 & 0 \\ 0 & 1+\sin\theta & 0 \\ 0 & 0 & 2 \end{pmatrix} .
\end{aligned} \tag{3.171}$$

Naturally, we see that $C^T = C$. Thus, we will omit the superscript indicating the transpose wherever appropriate, since it was included in Eq. (3.170) by convention. The derivation of the matrix $\mathbf{K}$ required the following simple transformation

$$\begin{aligned}
I_{xx} &= \mu R^2 \sin^2\Theta = \frac{1}{2}\mu R^2(1-\sin\theta) , \\
I_{yy} &= \mu R^2 \cos^2\Theta = \frac{1}{2}\mu R^2(1+\sin\theta) .
\end{aligned} \tag{3.172}$$

The quantum Hamiltonian

Let us recall the formula for the Laplacian in curvilinear coordinates given in Eq. (3.26). We aim to use the metric tensor g_{ij} to derive the Laplacian in the Johnson coordinates. Using Eq. (3.26), let us write the kinetic energy operator

$$\hat{T} = -\frac{\hbar^2}{2\mu}\Delta_{\boldsymbol{\rho}} = -\frac{\hbar^2}{2\mu}\frac{1}{\sqrt{\det g}}\frac{\partial}{\partial q^i}\left(\sqrt{\det g}\; g^{ij}\frac{\partial}{\partial q^j}\right) . \tag{3.173}$$

It will be useful to define a column vector of operators

$$\mathbf{p} = -i\hbar \begin{pmatrix} \frac{\partial}{\partial q_1} \\ \vdots \\ \frac{\partial}{\partial q_n} \end{pmatrix} , \tag{3.174}$$

and the result of this operator acting on $(\det g)$

$$\mathbf{p}_{\det} = \frac{1}{2(\det g)}\mathbf{p}(\det g) . \tag{3.175}$$

Thus, Eq. (3.173) in matrix notation is given by

$$2\mu\hat{T} = -\hbar^2\Delta_{\boldsymbol{\rho}} = (\mathbf{p}+\mathbf{p}_{\det})^T\mathbf{g}^{-1}\mathbf{p} , \tag{3.176}$$

where we used the chain rule for derivatives. Thus far, the equation is true for any curvilinear coordinates. Let us now calculate the inverse of the matrix $\mathbf{g}$. Let us first recall a few simple relations, true for any block matrices, the first of which is

$$\begin{pmatrix} \mathbf{I} & \mathbf{0} \\ -\mathbf{C}^T\mathbf{G}^{-1} & \mathbf{I} \end{pmatrix}\begin{pmatrix} \mathbf{G} & \mathbf{C} \\ \mathbf{C}^T & \mathbf{K} \end{pmatrix} = \begin{pmatrix} \mathbf{G} & \mathbf{C} \\ \mathbf{0} & \mathbf{S} \end{pmatrix} = \begin{pmatrix} \mathbf{G} & \mathbf{0} \\ \mathbf{0} & \mathbf{S} \end{pmatrix}\begin{pmatrix} \mathbf{I} & \mathbf{G}^{-1}\mathbf{C} \\ \mathbf{0} & \mathbf{I} \end{pmatrix} , \tag{3.177}$$

where $\mathbf{I}$ is the identity matrix and $\mathbf{S} = \mathbf{K} - \mathbf{C}^T\mathbf{G}^{-1}\mathbf{C}$. This equation allows us to get rid of the off-diagonal parts of the matrix $\mathbf{g}$. The second identity is the inverse of the upper-and lower-triangular matrices

$$\begin{aligned}\begin{pmatrix}\mathbf{I} & \mathbf{0}\\ -\mathbf{C}^T\mathbf{G}^{-1} & \mathbf{0}\end{pmatrix}^{-1} &= \begin{pmatrix}\mathbf{I} & \mathbf{0}\\ \mathbf{C}^T\mathbf{G}^{-1} & \mathbf{0}\end{pmatrix}\,,\\ \begin{pmatrix}\mathbf{I} & \mathbf{G}^{-1}\mathbf{C}\\ \mathbf{0} & \mathbf{0}\end{pmatrix}^{-1} &= \begin{pmatrix}\mathbf{I} & -\mathbf{G}^{-1}\mathbf{C}\\ \mathbf{0} & \mathbf{0}\end{pmatrix}\,.\end{aligned} \tag{3.178}$$

Taking the inverse of Eq. (3.177) and using Eq. (3.178), we obtain

$$\begin{aligned}\mathbf{g}^{-1} &= \begin{pmatrix}\mathbf{G} & \mathbf{C}\\ \mathbf{C}^T & \mathbf{K}\end{pmatrix}^{-1} = \left(\begin{pmatrix}\mathbf{I} & \mathbf{0}\\ -\mathbf{C}^T\mathbf{G}^{-1} & \mathbf{I}\end{pmatrix}^{-1}\begin{pmatrix}\mathbf{G} & \mathbf{0}\\ \mathbf{0} & \mathbf{S}\end{pmatrix}\begin{pmatrix}\mathbf{I} & \mathbf{G}^{-1}\mathbf{C}\\ \mathbf{0} & \mathbf{I}\end{pmatrix}\right)^{-1} =\\ &= \begin{pmatrix}\mathbf{I} & \mathbf{G}^{-1}\mathbf{C}\\ \mathbf{0} & \mathbf{I}\end{pmatrix}^{-1}\begin{pmatrix}\mathbf{G} & \mathbf{0}\\ \mathbf{0} & \mathbf{S}\end{pmatrix}^{-1}\begin{pmatrix}\mathbf{I} & \mathbf{0}\\ -\mathbf{C}^T\mathbf{G}^{-1} & \mathbf{I}\end{pmatrix} =\\ &= \begin{pmatrix}\mathbf{I} & -\mathbf{G}^{-1}\mathbf{C}\\ \mathbf{0} & \mathbf{I}\end{pmatrix}\begin{pmatrix}\mathbf{G}^{-1} & \mathbf{0}\\ \mathbf{0} & \mathbf{S}^{-1}\end{pmatrix}\begin{pmatrix}\mathbf{I} & \mathbf{0}\\ -\mathbf{C}^T\mathbf{G}^{-1} & \mathbf{I}\end{pmatrix} = \begin{pmatrix}\mathbf{I} & -\mathbf{G}^{-1}\mathbf{C}\\ \mathbf{0} & \mathbf{I}\end{pmatrix}\begin{pmatrix}\mathbf{G}^{-1} & \mathbf{0}\\ -\mathbf{U}\mathbf{C}^T\mathbf{G}^{-1} & \mathbf{U}\end{pmatrix} =\\ &= \begin{pmatrix}\mathbf{G}^{-1}+\mathbf{G}^{-1}\mathbf{C}\mathbf{U}\mathbf{C}^T\mathbf{G}^{-1} & -\mathbf{G}^{-1}\mathbf{C}\mathbf{U}\\ -\mathbf{U}\mathbf{C}^T\mathbf{G}^{-1} & \mathbf{U}\end{pmatrix}\,,\end{aligned} \tag{3.179}$$

where $\mathbf{U} = \mathbf{S}^{-1} = (\mathbf{K} - \mathbf{C}^T\mathbf{G}^{-1}\mathbf{C})^{-1}$. Taking the determinant of Eq. (3.177), we get

$$1\cdot\det g = \det\begin{pmatrix}\mathbf{I} & \mathbf{0}\\ -\mathbf{C}^T\mathbf{G}^{-1} & \mathbf{I}\end{pmatrix}\det\begin{pmatrix}\mathbf{G} & \mathbf{C}\\ \mathbf{C}^T & \mathbf{K}\end{pmatrix} = \det\begin{pmatrix}\mathbf{G} & \mathbf{C}\\ \mathbf{0} & \mathbf{S}\end{pmatrix} = \det\mathbf{G}\cdot\det\mathbf{S}\,. \tag{3.180}$$

The matrix $\mathbf{S}$ is given by

$$\mathbf{S} = \frac{R^2}{2}\begin{pmatrix}1-\sin\theta & 0 & 0\\ 0 & 1+\sin\theta & 0\\ 0 & 0 & 2\sin^2\theta\end{pmatrix}\,. \tag{3.181}$$

Thus, the determinant of the metric tensor is equal to

$$\det g = \frac{R^4}{16}\cdot\frac{R^6}{8}\left(2\cos^2\theta\sin^2\theta\right) = \frac{R^{10}}{64}\sin^2\theta\cos^2\theta\,. \tag{3.182}$$

Finally, we can derive the inverse of $\mathbf{g}$ using Eq. (3.179). Below, we calculate a few intermediate steps

$$\begin{aligned}\mathbf{C}\mathbf{U}\mathbf{C}^T = \mathbf{C}\mathbf{U}\mathbf{C} &= \begin{pmatrix}0 & 0 & 0\\ 0 & 0 & 0\\ 0 & 0 & \frac{R^2}{4}\cot^2\theta\end{pmatrix}\,,\\ \mathbf{G}^{-1}+\mathbf{G}^{-1}\mathbf{C}\mathbf{U}\mathbf{C}^T\mathbf{G}^{-1} &= \begin{pmatrix}1 & 0 & 0\\ 0 & \frac{4}{R^2} & 0\\ 0 & 0 & \frac{4}{R^2}\csc^2\theta\end{pmatrix}\,,\\ -\mathbf{U}\mathbf{C}^T\mathbf{G}^{-1} = -\mathbf{U}\mathbf{C}\mathbf{G}^{-1} &= \begin{pmatrix}0 & 0 & 0\\ 0 & 0 & 0\\ 0 & 0 & -\frac{2}{R^2}\frac{\cos\theta}{\sin^2\theta}\end{pmatrix} = -\mathbf{G}^{-1}\mathbf{C}\mathbf{U}\,,\\ \mathbf{U} &= \begin{pmatrix}\frac{2}{R^2(1-\sin\theta)} & 0 & 0\\ 0 & \frac{2}{R^2(1+\sin\theta)} & 0\\ 0 & 0 & \frac{\csc^2\theta}{R^2}\end{pmatrix}\,.\end{aligned} \tag{3.183}$$

Finally, we get

$$\mathbf{g}^{-1} = \begin{pmatrix} 1 & 0 & 0 & 0 & 0 & 0 \\ 0 & \frac{4}{R^2} & 0 & 0 & 0 & 0 \\ 0 & 0 & \frac{4}{R^2}\csc^2\theta & 0 & 0 & -\frac{2}{R^2}\frac{\cos\theta}{\sin^2\theta} \\ 0 & 0 & 0 & \frac{2}{R^2(1-\sin\theta)} & 0 & 0 \\ 0 & 0 & 0 & 0 & \frac{2}{R^2(1+\sin\theta)} & 0 \\ 0 & 0 & -\frac{2}{R^2}\frac{\cos\theta}{\sin^2\theta} & 0 & 0 & \frac{\csc^2}{R^2} \end{pmatrix} . \tag{3.184}$$

We will compare this result with Eq. (3.176) for

$$\mathbf{p} = \begin{pmatrix} \mathbf{P} \\ \mathbf{J} \end{pmatrix} , \quad \mathbf{P} = -i\hbar \begin{pmatrix} \frac{\partial}{\partial R} \\ \frac{\partial}{\partial\theta} \\ \frac{\partial}{\partial\phi} \end{pmatrix} , \quad \mathbf{J} = -i\hbar \begin{pmatrix} \frac{\partial}{\partial\Omega_x} \\ \frac{\partial}{\partial\Omega_y} \\ \frac{\partial}{\partial\Omega_z} \end{pmatrix} . \tag{3.185}$$

The differentials $\delta\Omega_x$, $\delta\Omega_y$, $\delta\Omega_z$ do not correspond to the differentials of any true coordinates. Rather, they depend on the Euler angles and are considered quasi-coordinates. Nevertheless, they define the generators of the appropriate Hermitian operators of rotation in the body-fixed frame

$$\hat{U}(\delta\Omega_\nu) = \exp\left(-\frac{i}{\hbar}\delta\Omega_\nu J_\nu\right) \approx\hat{}\, -\frac{i}{\hbar}\delta\Omega_\nu \hat{J}_\nu , \quad \nu = x, y, z , \tag{3.186}$$

and thus the operators $\hat{J}_x = -i\hbar\partial_{\Omega_x}$, $\hat{J}_y = -i\hbar\partial_{\Omega_y}$, $\hat{J}_z = -i\hbar\partial_{\Omega_z}$ are the total angular momentum operators in the body-fixed frame. Their dependence on the Euler angles, along with the calculation of the volume element of the Johnson coordinates, is shown in Section 3.4.4.

Let us now evaluate the two main terms in Eq. (3.176)

$$\begin{aligned} \mathbf{p}^T\mathbf{g}^{-1}\mathbf{p} =& -\hbar^2\left[\frac{\partial^2}{\partial R^2} + \frac{4}{R^2}\left(\frac{\partial^2}{\partial\theta^2} + \frac{1}{\sin^2\theta}\frac{\partial^2}{\partial\phi^2}\right)\right] + \frac{2}{R^2}\left(\frac{\hat{J}_x^2}{1-\sin\theta} + \frac{\hat{J}_y^2}{1+\sin\theta} + \frac{\hat{J}_z^2}{2\sin^2\theta}\right) + \\ &+ 4i\hbar\frac{\cos\theta\hat{J}_z}{R^2\sin^2\theta}\frac{\partial}{\partial\phi} , \\ \mathbf{p}_{\text{det}}^T\mathbf{g}^{-1}\mathbf{p} =& \left(\frac{1}{2\det g}\mathbf{p}\det g\right)^T\mathbf{g}^{-1}\mathbf{p} = \left(\frac{64}{2R^{10}\sin^2\theta\cos^2\theta}\mathbf{p}\left(\frac{R^{10}\sin^2\theta\cos^2\theta}{64}\right)\right)^T\mathbf{g}^{-1}\mathbf{p} = \\ =& \left(\begin{pmatrix} 10/R \\ \frac{4\sin(2\theta)\cos(2\theta)}{\sin^2(2\theta)} \\ \mathbf{0}_4 \end{pmatrix}\right)^T\mathbf{g}^{-1}\mathbf{p} = -\hbar^2\left[\frac{5}{R}\frac{\partial}{\partial R} + \frac{4}{R^2}2\cot(2\theta)\frac{\partial}{\partial\theta}\right] , \end{aligned} \tag{3.187}$$

where $\mathbf{0}_4$ is a 4-dimensional zero vector. Combining the results above, we can obtain the kinetic energy operator in the Johnson coordinates

$$\begin{aligned} \hat{T} =& \frac{1}{2\mu}\left(\mathbf{p}^T\mathbf{g}^{-1}\mathbf{p} + \mathbf{p}_{\text{det}}^T\mathbf{g}^{-1}\mathbf{p}\right) + V(R,\theta,\phi) = \\ =& -\frac{\hbar^2}{2\mu}\left[\frac{\partial^2}{\partial R^2} + \frac{5}{R}\frac{\partial}{\partial R}\right] - \frac{\hbar^2 2}{\mu R^2}\left(\frac{\partial^2}{\partial\theta^2} + 2\cot(2\theta)\frac{\partial}{\partial\theta} + \frac{1}{\sin^2\theta}\frac{\partial^2}{\partial\phi^2}\right) + \\ &+ \frac{1}{\mu R^2}\left(\frac{\hat{J}_x^2}{1-\sin\theta} + \frac{\hat{J}_y^2}{1+\sin\theta} + \frac{\hat{J}_z^2}{2\sin^2\theta}\right) + 4i\hbar\frac{\cos\theta\hat{J}_z}{2\mu R^2\sin^2\theta}\frac{\partial}{\partial\phi} \\ =& -\frac{\hbar^2\Delta_R}{2\mu} + \frac{\hbar^2\mathbf{\Lambda}^2(\theta,\phi)}{2\mu R^2} , \end{aligned} \tag{3.188}$$

where

$$\begin{aligned}\mathbf{\Lambda^2}(\theta,\phi) = &-4\left[\frac{1}{\sin(2\theta)}\frac{\partial}{\partial\theta}\sin(2\theta)\frac{\partial}{\partial\theta}+\frac{1}{\sin^2\theta}\frac{\partial^2}{\partial\phi^2}\right]+\\ &+\frac{2}{\hbar^2}\left(\frac{\hat{J}_x^2}{1-\sin\theta}+\frac{\hat{J}_y^2}{1+\sin\theta}+\frac{\hat{J}_z^2}{2\sin^2\theta}\right)+\\ &+4i\frac{\cos\theta\hat{J}_z}{\hbar\sin^2\theta}\frac{\partial}{\partial\phi}\ ,\end{aligned} \tag{3.189}$$

Δ_R was defined in Eq. (3.30), and we used the relation

$$\frac{\partial^2}{\partial\theta^2}+2\cot(2\theta)\frac{\partial}{\partial\theta}=\frac{1}{\sin(2\theta)}\left(\frac{\partial}{\partial\theta}\sin(2\theta)\frac{\partial}{\partial\theta}\right)\ . \tag{3.190}$$

The last term in Eq. (3.189) represents the Coriolis energy. Naturally, the Hamiltonian is equal to $\hat{H}=\hat{T}+V(R,\theta,\phi)$.

3.4.4. The quasi-coordinates and the Euler angles

We begin our considerations of the relation between the quasi-coordinates Ω_ν, for $\nu=x,y,z$, and the Euler angles α, β, γ by recalling that the time-derivative of the curvilinear coordinates transforms in the following way

$$\dot{y}^\alpha=\frac{\partial y^\alpha}{\partial q^i}\dot{q}^i\ , \tag{3.191}$$

where we used the Einstein notation for i. Naturally, this transformation uses the inverse of the Jacobian for the transformation between the derivative operators

$$\partial_{y^\alpha}=\frac{\partial q^i}{\partial y^\alpha}\partial_{q^i}\ . \tag{3.192}$$

Let us now consider the curvilinear transformation $y\to q$ between the considered variables

$$y=\begin{pmatrix}\Omega_x\\ \Omega_y\\ \Omega_z\end{pmatrix}\to\begin{pmatrix}\alpha\\ \beta\\ \gamma\end{pmatrix}=q\ . \tag{3.193}$$

Once we find the coefficient of the matrix $[\mathbb{Y}]_{\alpha i}:=\partial y^\alpha/\partial q^i$ thanks to relation in Eq. (3.191), we will be able to use Eq. (3.192) to calculate the expressions for $\hat{J}_\nu\sim\partial_\nu$, for $\nu=\Omega_x,\Omega_y,\Omega_z$ in terms of the Euler angles. Similarly, to find the metric tensor g_{ij} of the transformation $y\to q$, it is enough to find the relation between the classical vector, the length, and volume elements in the Johnson coordinate system.

Consider a point which is defined by a vector $\mathbf{x}(t)$ measured in the stationary frame and which is rotating with the angular velocity $\boldsymbol{\omega}$. The motion of this vector is generated by a time-dependent rotation matrix $\mathbf{R}(t)\in\mathrm{SO}(3)$

$${}^s\mathbf{x}(t)=\mathbf{R}(t)\,{}^b\mathbf{x}(0)\ . \tag{3.194}$$

The left superscripts s,b indicate whether the vector is *expressed* (as opposed to *measured*) in the stationary (s) or body/rotating (b) frame. Differentiating with respect to time gives

$${}^s\dot{\mathbf{x}}(t)=\dot{\mathbf{R}}(t)\,{}^b\mathbf{x}(0)=\dot{\mathbf{R}}(t)\mathbf{R}^T(t)\,{}^s\mathbf{x}(t)\ . \tag{3.195}$$

Naturally, the rotation matrix satisfies the relation $\mathbf{R}\mathbf{R}^T = \mathbf{I}$, where $\mathbf{I}$ is the identity matrix. Let us differentiate this relation with respect to time. The right-hand side becomes zero, and the chain rule for the left-hand side gives

$$\dot{\mathbf{R}}\mathbf{R}^T = -\mathbf{R}\dot{\mathbf{R}}^T = -(\dot{\mathbf{R}}\mathbf{R}^T)^T \ . \tag{3.196}$$

So, the matrix $\dot{\mathbf{R}}\mathbf{R}^T$ is anti-symmetric and allows us to find the velocity of the vector $\dot{\mathbf{x}}'(t)$ with respect to its position $\mathbf{x}'(t)$ in the stationary frame. Derivative of the equation $\mathbf{R}^T\mathbf{R} = \mathbf{I}$ implies that the matrix $\mathbf{R}^T\dot{\mathbf{R}}$ is also anti-symmetric. The effect of this matrix is discussed below. Let us write the general expression for the matrices $\dot{\mathbf{R}}\mathbf{R}^T$ and $\mathbf{R}^T\dot{\mathbf{R}}$ stemming from their anti-symmetric properties

$$\dot{\mathbf{R}}\mathbf{R}^T = \begin{pmatrix} 0 & -c & b \\ c & 0 & -a \\ -b & a & 0 \end{pmatrix} \ , \quad \mathbf{R}^T\dot{\mathbf{R}} = \begin{pmatrix} 0 & -f & e \\ f & 0 & -d \\ -e & d & 0 \end{pmatrix} \ . \tag{3.197}$$

We recall that for all vectors, the transformation of the velocity measurement between the rotating and the stationary frame is given by

$$\dot{\mathbf{x}}'(t) = \dot{\mathbf{x}}(t) + \boldsymbol{\omega} \times \mathbf{x}(t) \ , \tag{3.198}$$

which is true when expressed in any of the frames. Superscript $'$ indicates the measurement in the stationary frame. But by definition, we have

$$\left(\mathbf{R}^{-1}\right) \cdot {}^s\dot{\mathbf{x}}(t) = {}^b\dot{\mathbf{x}}(t) = \frac{d}{dt}\,{}^b\mathbf{x}(t) = \frac{d}{dt}\,{}^b\mathbf{x}(0) = \mathbf{0} \ . \tag{3.199}$$

So the velocity measured in the body frame is equal to zero when expressed in both frames, i.e., ${}^b\dot{\mathbf{x}}(t) = {}^s\dot{\mathbf{x}}(t) = \mathbf{0}$. Comparing Eq. (3.198) with Eq. (3.195), we deduce that the operator $\dot{\mathbf{R}}\mathbf{R}^T$ must have the same effect as the vector product $(\boldsymbol{\omega}\times)$ when ${}^s\boldsymbol{\omega}$ is expressed in the stationary frame. Thus the following result is true: $a = \omega_{x'}$, $b = \omega_{y'}$, and $c = \omega_{z'}$. Let us now consider Eq. (3.198) expressed in the body-fixed coordinates

$$\begin{aligned} {}^b\mathbf{x}'(t) &= {}^b\boldsymbol{\omega} \times {}^b\mathbf{x}(t) \ , \\ \left(\mathbf{R}^{-1}\right) \cdot {}^s\mathbf{x}'(t) &= {}^b\boldsymbol{\omega} \times {}^b\mathbf{x}(0) \ , \\ \left[\mathbf{R}^T \cdot {}^s\mathbf{x}'(t)\right] &= {}^b\boldsymbol{\omega} \times {}^b\left[\mathbf{R}^T \cdot {}^s\mathbf{x}'(t)\right] \ . \end{aligned} \tag{3.200}$$

Now, let us multiply Eq. (3.195) by $\mathbf{R}^T$ from the left

$$\left[\mathbf{R}^T(t)\,{}^s\mathbf{x}(t)\right] = \mathbf{R}^T\dot{\mathbf{R}}\left[\mathbf{R}^T(t)\,{}^s\mathbf{x}(t)\right] \ . \tag{3.201}$$

Comparing Eq. (3.201) and Eq. (3.200) we deduce that the operator $\mathbf{R}^T\dot{\mathbf{R}}$ must have the same effect as the vector product $(\boldsymbol{\omega}\times)$ when ${}^b\boldsymbol{\omega}$ is expressed in the body frame . Thus the following result is true: $d = \omega_x$, $e = \omega_y$, and $f = \omega_z$.

We need to define the matrix of rotation $\mathbf{R}$ in terms of the Euler angles and then calculate the matrix $\dot{\mathbf{R}}\mathbf{R}^T$ to find the expressions for ω_ν, where $\nu = x', y', z'$ as well as matrix $\mathbf{R}^T\dot{\mathbf{R}}$ to do the same for $\nu = x, y, z$. As we recall, we follow the $z-y-z$ convention for the Euler angle rotation between the stationary $\mathcal{O}x'y'z'$ and rotating $\mathcal{O}xyz$ coordinate systems. By this definition, we combine the matrix of rotation $\mathbf{R}$ from three right-handed rotations about the Euler angles, i.e.,

$$\mathbf{R} = \begin{pmatrix} \cos\alpha(t) & -\sin\alpha(t) & 0 \\ \sin\alpha(t) & \cos\alpha(t) & 0 \\ 0 & 0 & 1 \end{pmatrix} \begin{pmatrix} \cos\beta(t) & 0 & \sin\beta(t) \\ 0 & 1 & 0 \\ -\sin\beta(t) & 0 & \cos\beta(t) \end{pmatrix} \begin{pmatrix} \cos\gamma(t) & -\sin\gamma(t) & 0 \\ \sin\gamma(t) & \cos\gamma(t) & 0 \\ 0 & 0 & 1 \end{pmatrix} \ . \tag{3.202}$$

We recall that in Eq. (3.194) we define $\mathbf{R}$ as the rotation from the rotating to the stationary frame. The calculation of $\dot{\mathbf{R}}\mathbf{R}^T$ and $\mathbf{R}^T\dot{\mathbf{R}}$ is slightly extensive, but eventually yields

$$\dot{\mathbf{R}}\mathbf{R}^T = \begin{pmatrix} 0 & -\dot{\alpha} - (\cos\beta)\dot{\gamma} & (\cos\alpha)\dot{\beta} + (\sin\alpha\cos\gamma)\dot{\gamma} \\ \dot{\alpha} + (\cos\beta)\dot{\gamma} & 0 & (\sin\alpha)\dot{\beta} - (\cos\alpha\sin\beta)\dot{\gamma} \\ -(\cos\alpha)\dot{\beta} - (\sin\alpha\sin\beta)\dot{\gamma} & -(\sin\alpha)\dot{\beta} + (\cos\alpha\sin\beta)\dot{\gamma} & 0 \end{pmatrix} , \tag{3.203}$$

$$\mathbf{R}^T\dot{\mathbf{R}} = \begin{pmatrix} 0 & -(\cos\beta)\dot{\alpha} - \dot{\gamma} & (\sin\beta\sin\gamma)\dot{\alpha} + (\cos\gamma)\dot{\beta} \\ (\cos\beta)\dot{\alpha} + \dot{\gamma} & 0 & (\cos\gamma\sin\beta)\dot{\alpha} - (\sin\gamma)\dot{\beta} \\ -(\sin\beta\sin\gamma)\dot{\alpha} - (\cos\gamma)\dot{\beta} & -(\cos\gamma\sin\beta)\dot{\alpha} + (\sin\gamma)\dot{\beta} & 0 \end{pmatrix} . \tag{3.204}$$

Thus, we finally obtain the relations

$$\begin{pmatrix} \dot{\Omega}_{x'} \\ \dot{\Omega}_{y'} \\ \dot{\Omega}_{z'} \end{pmatrix} = \begin{pmatrix} 0 & -\sin\alpha & \cos\alpha\sin\beta \\ 0 & \cos\alpha & \sin\alpha\sin\beta \\ 1 & 0 & \cos\beta \end{pmatrix} \begin{pmatrix} \dot{\alpha} \\ \dot{\beta} \\ \dot{\gamma} \end{pmatrix} =: [\mathbb{Y}'] \cdot \begin{pmatrix} \dot{\alpha} \\ \dot{\beta} \\ \dot{\gamma} \end{pmatrix} , \tag{3.205}$$

$$\begin{pmatrix} \dot{\Omega}_{x} \\ \dot{\Omega}_{y} \\ \dot{\Omega}_{z} \end{pmatrix} = \begin{pmatrix} -\sin\beta\cos\gamma & \sin\gamma & 0 \\ \sin\beta\sin\gamma & \cos\gamma & 0 \\ \cos\beta & 0 & 1 \end{pmatrix} \begin{pmatrix} \dot{\alpha} \\ \dot{\beta} \\ \dot{\gamma} \end{pmatrix} =: [\mathbb{Y}] \cdot \begin{pmatrix} \dot{\alpha} \\ \dot{\beta} \\ \dot{\gamma} \end{pmatrix} . \tag{3.206}$$

Following the discussion at the beginning of this Section, we will now invert the Jacobian $[\mathbb{Y}]_{\alpha i}$. First, let us recall that

$$\dot{q}^i = \frac{\partial q^i}{\partial y^\alpha}\dot{y}^\alpha = [\mathbb{Y}^{-1}]_{i\alpha}\dot{y}^\alpha = [(\mathbb{Y}^{-1})^T]_{\alpha i}\dot{y}^\alpha . \tag{3.207}$$

Comparing with Eq. (3.192) we deduce that

$$\partial_{y^\alpha} = [(\mathbb{Y}^{-1})^T]_{\alpha i}\partial_{q^i} , \tag{3.208}$$

which is an equation we can write in matrix form, as long as we can find the transpose of the inverse of matrix $[\mathbb{Y}]$, i.e.,

$$\begin{pmatrix} \partial_{\Omega_x} \\ \partial_{\Omega_y} \\ \partial_{\Omega_z} \end{pmatrix} = \left([\mathbb{Y}]^{-1}\right)^T \cdot \begin{pmatrix} \dot{\alpha} \\ \dot{\beta} \\ \dot{\gamma} \end{pmatrix} = \begin{pmatrix} -\csc\beta\cos\gamma & \sin\gamma & \cos\beta\cos\gamma \\ \csc\beta\sin\gamma & \cos\gamma & -\cot\beta\sin\gamma \\ 0 & 0 & 1 \end{pmatrix} \cdot \begin{pmatrix} \dot{\alpha} \\ \dot{\beta} \\ \dot{\gamma} \end{pmatrix} . \tag{3.209}$$

Similarly,

$$\begin{pmatrix} \partial_{\Omega_{x'}} \\ \partial_{\Omega_{y'}} \\ \partial_{\Omega_{z'}} \end{pmatrix} = \left([\mathbb{Y}']^{-1}\right)^T \cdot \begin{pmatrix} \partial_{\alpha} \\ \partial_{\beta} \\ \partial_{\gamma} \end{pmatrix} = \begin{pmatrix} -\cos\alpha\cot\beta & -\sin\alpha & \cos\alpha\csc\beta \\ -\cot\beta\sin\alpha & \cos\alpha & -\csc\beta\sin\alpha \\ 1 & 0 & 0 \end{pmatrix} \cdot \begin{pmatrix} \partial_{\alpha} \\ \partial_{\beta} \\ \partial_{\gamma} \end{pmatrix} . \tag{3.210}$$

Multiplying the equation above by $-i\hbar$ gives the formulae for $\hat{J}_x$, $\hat{J}_y$, $\hat{J}_z$ (body-fixed frame) and $\hat{J}_{x'}$, $\hat{J}_{y'}$, $\hat{J}_{z'}$ (lab-fixed frame) in terms of derivatives with respect to the Euler angles ∂_α, ∂_β, ∂_γ in the $z-y-z$ convention used in this Chapter. Using these relations, one can show that the space-fixed operators follow the standard commutation relations

$$[\hat{J}_{i'}, \hat{J}_{j'}] = i\hat{J}_{k'} , \tag{3.211}$$

where (i', j', k') is a cyclic permutation of (x', y', z'). The body-fixed angular momenta follow the *anomalous* commutation relations

$$[\hat{J}_i, \hat{J}_j] = -i\hat{J}_k \ , \tag{3.212}$$

where (i, j, k) is a cyclic permutation of (x, y, z). Furthermore, the two sets mutually commute $[\hat{J}_{\nu'}, \hat{J}_\nu] = 0$ for $\nu = x, y, z$ and the total angular momentum is equal in both frames, i.e.,

$$\hat{J}^2 = \hat{J}^2_{x'} + \hat{J}^2_{y'} + \hat{J}^2_{z'} = \hat{J}^2_x + \hat{J}^2_y + \hat{J}^2_z \ . \tag{3.213}$$

To complete the discussion, we shall calculate the volume element in the Johnson coordinates. Recall that,

$$dv = \sqrt{\det g} \prod_{i=1}^{n} dq^i \ . \tag{3.214}$$

In the case of coordinate set $(R, \theta, \phi, \Omega_x, \Omega_y, \Omega_z)$ it could readily be found

$$dv = \frac{R^5}{8} \sin\theta \cos\theta \, dR \, d\theta \, d\phi \, d\Omega_x \, d\Omega_y \, d\Omega_z \ , \tag{3.215}$$

where we used Eq. (3.182). However, Ω_ν for $\nu = x, y, z$ are pseudo-coordinates, and we need to express the volume element in terms of the Euler differentials. It can be easily verified that the differentials $d\Omega_\nu$, where $\nu = x, y, z$ transform in the same way as $\dot{\Omega}_\nu$, i.e.,

$$\begin{pmatrix} d\Omega_x \\ d\Omega_y \\ d\Omega_z \end{pmatrix} = [\mathbb{Y}] \cdot \begin{pmatrix} d\alpha \\ d\beta \\ d\gamma \end{pmatrix} \ . \tag{3.216}$$

Matrix $[\mathbb{Y}]^T[\mathbb{Y}]$ is therefore the metric tensor of the transformation from the pseudo-coordinates Ω_ν to Euler angles – discussed in this Section. Its determinant $\det[\mathbb{Y}] = -\sin\beta$ factors into the overall volume element as $\sqrt{\det([\mathbb{Y}]^T[\mathbb{Y}])} = |\det[\mathbb{Y}]| = \sin\beta$

$$dv = dv = \frac{R^5}{8} \sin\theta \cos\theta \sin\beta \, dR \, d\theta \, d\phi \, d\alpha \, d\beta \, d\gamma \ , \tag{3.217}$$

for $\beta \in [0, \pi]$.

3.4.5. The expansion of the wavefunction

Let us recall and slightly modify the expression for $\mathbf{\Lambda}^2$ in the Johnson coordinates given in Eq. (3.189),

$$\begin{aligned} \mathbf{\Lambda^2}(\theta, \phi) =& -4\left[\frac{1}{\sin(2\theta)}\frac{\partial}{\partial\theta}\sin(2\theta)\frac{\partial}{\partial\theta}\right] - \frac{1}{\sin^2\theta}\left[i\frac{\hat{J}_z}{\hbar}\cos\theta - 2\frac{\partial}{\partial\phi}\right]^2 + \frac{\hat{J}_z^2}{\hbar^2} + \\ &+ \frac{2}{\hbar^2}\left(\frac{\hat{J}_x^2(1+\sin\theta) + \hat{J}_y^2(1-\sin\theta)}{1-\sin^2\theta}\right) = \\ =& -4\left[\frac{1}{\sin(2\theta)}\frac{\partial}{\partial\theta}\sin(2\theta)\frac{\partial}{\partial\theta}\right] + \frac{1}{\sin^2\theta}\left[\frac{\hat{J}_z}{\hbar}\cos\theta - 2i\frac{\partial}{\partial\phi}\right]^2 + \frac{\hat{J}_z^2}{\hbar^2} + \\ &+ \frac{2}{\hbar^2\cos^2\theta}\left(\hat{J}^2 - \hat{J}_z^2 + \frac{\sin\theta}{2}\left(\hat{J}_+^2 + \hat{J}_-^2\right)\right) \ . \end{aligned} \tag{3.218}$$

The ladder operators in the body-fixed frame are defined with inverse signs with respect to the lab-fixed frame

$$\hat{J}_{\pm} = \hat{J}_x \mp \hat{J}_y \ , \tag{3.219}$$

due to the anomalous commutation relations mentioned in the previous Section. From the form of the operator $\mathbf{\Lambda}^2$, it can be seen that it commutes with $-i\frac{\partial}{\partial\phi}$ and $\hat{J}^2$. It also commutes with the space-fixed (x', y', z') components of the angular momentum operator $\hat{J}$ as it only describes the internal rotations. The good quantum numbers are therefore J (total angular momentum), m' (z' component of the angular momentum in the space-fixed frame), v (projection of $-2i\partial_\phi$) – as long as the potential $V(R, \theta, \phi)$ does not depend on ϕ, the grand angular momentum λ and the parity quantum number Π, which we discuss below. The natural way to expand the total wavefunction Ψ is therefore

$$\Psi^{\lambda\Pi v}_{Jm'}(R, \theta, \phi, \alpha, \beta, \gamma) = \sum_{m=-J}^{J} f_m(\lambda, \Pi, v, J, m'|R, \theta, \phi) D^J_{m'm}(\alpha, \beta, \gamma) \ , \tag{3.220}$$

where $D^J_{m'm}(\alpha, \beta, \gamma)$ are the *Wigner D-matrices* defined through the rotation operators as

$$\begin{aligned} D^J_{m'm}(\alpha, \beta, \gamma) =& \langle Jm'|e^{-i\alpha\hat{J}_{z'}} e^{-i\beta\hat{J}_{\bar{y}}} e^{-i\gamma\hat{J}_z}|Jm\rangle \ , \\ D^J_{m'm}(\alpha, \beta, \gamma) =& e^{-im'\alpha}\langle Jm'|e^{-i\beta\hat{J}_{\bar{y}}}|Jm\rangle e^{-im\gamma} =: e^{-im'\alpha} d^J_{m'm}(\beta) e^{-im\gamma} \ . \end{aligned} \tag{3.221}$$

We note, that the middle operator $-i\hbar\partial_\beta$ is the $\bar{y}$ component of the total angular momentum in the intermediate, $\mathcal{O}\bar{x}\bar{y}\bar{z}$ frame – discussed in Section 3.4.1. From its expansion, it is seen that the total wavefunction is an eigenfunction of $\hat{J}^2$ and $\hat{J}_{z'} = -i\hbar\partial_\alpha$ with quantum numbers J and m', respectively. Once the total wavefunction is substituted into the Schrödinger equation, it can be multiplied by $D^{J*}_{m'n}(\alpha, \beta, \gamma)$ and integrated over all Euler angles. The result is a set of coupled partial differential equations for the functions $f_m(\lambda, \Pi, v, J, m'|R, \theta, \phi)$, where $-J \leq m \leq J$. The coupling is introduced only due to the ladder operators $\hat{J}^2_+ + J^2_-$. The f_m functions are coupled with the $f_{m\pm2}$ functions. Thus, the wavefunctions with m even and odd are separately coupled, and the two sets do not couple to each other.

Let us consider the eigenfunctions $\psi^{\lambda\Pi v}_{Jm'}(\theta, \phi, \alpha, \beta, \gamma)$ of the grand angular momentum $\mathbf{\Lambda}^2$. As we have already established, their eigenvalues satisfy the following equation

$$\mathbf{\Lambda}^2 \, \psi^{\lambda\Pi v}_{Jm'} = \lambda(\lambda + 4) \ \psi^{\lambda\Pi v}_{Jm'} \ . \tag{3.222}$$

The eigenvalues of $-i\partial_\phi$ are also easily separable

$$-i\frac{\partial}{\partial\phi} \, \psi^{\lambda\Pi v}_{Jm'} = \frac{v}{2} \, \psi^{\lambda\Pi v}_{Jm'} \ , \tag{3.223}$$

which is not the case for $\hat{J}$ and its components. The following boundary conditions are satisfied between the quantum numbers

$$\lambda = J, J+1, \dots \ ; \quad v = K, K-2, \dots, -K+2, -K \ . \tag{3.224}$$

These relations have been derived, e.g., in Ref. [211]. Furthermore, the same article presents the first computationally feasible algorithm for calculating the eigenfunctions of the grand angular momentum $\mathbf{\Lambda}^2$. In principle, this problem has been solved analytically [210, 212, 213] – but the methods involved are not easily adaptable for numerical computations. Similarly to the total wavefunction, the eigenfunctions of $\mathbf{\Lambda}^2$ are expanded into the Wigner D-matrices

$$\psi^{\lambda\Pi v}_{Jm'}(\theta, \phi, \alpha, \beta, \gamma) = e^{i\frac{v}{2}\phi} \sum_{m=-J}^{J} F^{\lambda\Pi v}_m(\theta) \, D^J_{m'm}(\alpha, \beta, \gamma) \ , \tag{3.225}$$

and the coupled partial differential equations are solved for $F_m^{\lambda\Pi v}(\theta)$.

Lastly, we shall discuss the parity quantum number. From the form of the total wavefunction given in Eq. (3.220), it is clear that the parity operator $\hat{P} : \mathbf{r}_i \to -\mathbf{r}_i \ , \forall_{i\in\{1,2,3\}}$ acts in the following way

$$\hat{P} D^J_{m'm}(\alpha,\beta,\gamma) = D^J_{m'm}(\alpha+\pi,\pi-\beta,-\gamma) = (-1)^J D^J_{m'-m}(\alpha,\beta,\gamma) \ . \tag{3.226}$$

The second equation is easily derived from the definitions of the Wigner D-matrices in Eq. (3.221) and from the relation

$$d^J_{m',m}(\pi-\beta) = (-1)^{J+m'} d^J_{m',-m} \ . \tag{3.227}$$

As was shown in Section 3.2.3, the total angular momentum J could be considered as the sum of the angular momenta of the pair of particles (l_{ij}) and the relative motion of the third (l_k) particle with respect to the center of mass of the original pair. These quantities satisfy the rules for angular momentum addition: $|l_{ij} - l_k| \leq J \leq l_{ij} + l_k$ and $m' = m'_{ij} + m'_k$. The z component (body-fixed) of the total angular momentum takes the values $m = J, J-2, \ldots, -J+2, -J$ for the *parity-favored* case $\Pi = (-1)^J$ and $m = J-1, J-3, \ldots, -(J-3), -(J-1)$ for the *parity-unfavored* case $\Pi = (-1)^{J+1}$. The parity quantum number $\Pi = (-1)^J$ allows us to define the Bose/Fermi symmetry.

Chapter 4

Universality

As mentioned in Chapter 1, the theoretical description of few- and many-body interactions in dilute ultracold gases can be greatly simplified whenever the scattering length greatly exceeds all the characteristic interaction lengths and all other relevant length scales of the system, including the average spacing or the de Broglie wavelength. In rescaled units, measured physical quantities do not depend on the masses of the chosen species nor on the short-range physics of the interaction that governs the chemical quantum transitions. In these conditions, the three- and many-body observables become insensitive to the microscopic details of the problem, and the behavior is considered *universal*.

In this Chapter, we will provide a brief overview of the main theoretical concepts and effects that exhibit universal properties, such as the Efimov effect, three-body dynamics, and background two-body effects that lead to few-body universality. To keep this Thesis self-contained, we will derive some of the known results in three-body physics, wherever analytical or semi-analytical – rather than numerical – calculations provide relevant and informative conclusions with respect to the main topic of this Chapter. In each of the following Sections, we will refer to the pertinent literature to show the limits of universality and its breakdown due to thermal or quantum resonance effects.

4.1. The Efimov effect

In 1970, Vitaly Efimov predicted an extraordinary effect in the quantum spectrum of a three-particle system. He studied particles that interact via short-range attractive forces close to resonance. *Short-range* refers to interactions that decrease faster than $\sim 1/r^3$, where r is the interparticle distance. *Nearly resonant* describes attractive interactions that are just strong enough – or almost strong enough – to form a weakly bound two-body state. We discuss the classification of the short- and long-range potentials in greater detail in Section 4.3.

Under these conditions, V. Efimov demonstrated that an effective long-range attraction appears between three particles. This interaction supports an infinity of three-body bound states – now known as Efimov states or Efimov trimers. The amplitude of the three-body wavefunction of the trimers is large at progressively larger separations – well beyond the range of their underlying interactions. The effect can be described as an induced long-range three-body interaction, which, incredibly, is supported by a short-range potential – as already mentioned. Furthermore, at resonance, the trimers form as a result of an exchange interaction with no characteristic length scale, because the scattering length tends to infinity. Remarkably, the three-body system becomes scale-invariant. The resonant trimers can form even when the two-body interaction is not strong enough to support a single two-body s-wave bound state.

It is well-known from quantum scattering theory that the two-body dynamics of interacting particles is described by the partial-wave expansion of the *scattering wavefunction*, which in spherical coordinates (r, θ, φ) takes the form

$$\psi(\mathbf{r}) = \psi(r, \theta, \varphi) = e^{im\varphi} \sum_{l=0}^{\infty} \frac{u_l(r)}{r} P_l(\cos\theta) \ , \tag{4.1}$$

where $P_l(\cos\theta)$ are the Legendre polynomials, r is the interparticle distance, l is the angular momentum, and m – its projection on the quantization axis. The radial part of the wavefunction $u_l(r)$ approaches the asymptotic solutions

$$u_l(0) = 0, \ u_l(r) \to k^l \left[\cot\delta_l kr j_l(kr) - kr n_l(kr)\right], \ r \to \infty \ , \tag{4.2}$$

where $j_l(kr)$ and $n_l(kr)$ are the spherical Bessel functions – as long as the interacting potential is short-range. The form of the solutions given in Eq. (4.2) can be translated to

$$u_l(r) \to \sin\left(kr - l\frac{\pi}{2} + \delta_l\right) \ , \quad r \to \infty \ , \tag{4.3}$$

where k is the wavenumber. The Efimov effect arises when two-body interaction is near-resonant in the s-wave ($l = 0$) partial wave. In this regime, the phase shift δ_0 is close to $\frac{\pi}{2}$ and is related to the scattering length a via the expression

$$\lim_{k\to 0} k \cot\delta_0 = -\frac{1}{a} \ . \tag{4.4}$$

The two-body interaction becomes resonant when the scattering length is larger than the characteristic length of interaction β.

In the limit $k \to 0$, the scattering cross section σ is dominated by the $l = 0$ partial wave, i.e., the first component of the expansion

$$\sigma = \frac{4\pi}{k^2} \sum_{l=0}^{\infty} (2l+1) \sin^2\delta_l \ . \tag{4.5}$$

If we further set the conditions for near-resonant interaction, i.e., $a \to \infty$, then the scattering cross section $\sigma \to \frac{4\pi}{k^2}\sin^2\delta_0$ approaches its maximal value $\sin^2\delta_0 \to 1$. In this regime, the S-matrix becomes unitary, a property often called *unitarity*. Near unitarity, the scattering length becomes the dominant parameter controlling the physics of the collision. As already mentioned, the positive energy determines the scattering cross section. For negative energy – a weakly bound state forms below the $k = 0$ threshold whose energy is given by Eq. (1.7).

Deriving semi-analytical solutions to the quantum three-body problem requires using a relatively simple model of the interaction potential. The original derivation of V. Efimov considered equations describing the resonant interaction outside its range, i.e., $r \gg \beta$ [186]. In essence, this approach is equivalent to a model of a contact-interaction between pairs of particles, where the short-range two-body interaction is represented by a zero-range *Fermi pseudopotential* [214]. The pseudo-potential takes the form of a *renormalized* Dirac-δ function [215]

$$v(r_{ij}) = \frac{4\pi\hbar^2 a_{ij}}{2\mu_{ij}} \delta^{(3)}(\mathbf{r}_{ij}) \frac{\partial}{\partial r_{ij}} r_{ij} \ , \tag{4.6}$$

where μ_{ij} is the two-body reduced mass, a_{ij} – the scattering length for the interaction of the particle pair ij, and $r_{ij} = |\mathbf{r}_j - \mathbf{r}_i| = |\mathbf{r}_{ij}|$ is the interparticle distance. The presented

model differs from the more standard approach of using a single three-dimensional Dirac-δ function, because the radial part of the two-body scattering wavefunction $\mathcal{R}(r_{ij})$ is singular in the zero-range limit $r_{ij} \to 0$

$$\mathcal{R}(r_{ij}) = \frac{u_0(r_{ij})}{r_{ij}} \sim \frac{1}{r_{ij}} - \frac{1}{a_{ij}} \,. \tag{4.7}$$

This relation is described in more detail in Section 4.3 in the context of solutions of the free Schrödinger equation at large interparticle distances and for $k \to 0$. In the contact-interaction model, the form of the two-body wavefunction ψ is reproduced by the *Bethe-Peierls boundary condition* [216]

$$-\frac{1}{r_{ij}\Psi}\frac{\partial}{\partial r_{ij}}(r_{ij}\Psi) \to \frac{1}{a_{ij}} \,, \quad r_{ij} \to 0, \tag{4.8}$$

which is imposed on the many-particle wavefunction Ψ along with the corresponding boundary conditions on the pairs jk and ki. The Bethe-Peierls boundary condition for all three pairs of particles represents all interactions in the problem, and it can be shown that the effect of the pseudopotential is entirely captured by Eq. (4.8).

The three-body interaction is usually represented as a pairwise sum of the two-body interaction potentials

$$V(R,\Omega) = v(r_{ij}) + v(r_{jk}) + v(r_{ki}) \,, \tag{4.9}$$

where v are the two-body potentials for each of the pairs of particles (i,j,k). The three-body forces, dependent on the positions of all of the particles simultaneously, are generally excluded from models due to their rapid decay, which falls proportionally to $V(R,\Omega) \sim R^{-9}$ [217]. The same approach is used in solving the three-body problem for near-resonant interactions. As we have shown in Chapter 3, the three-body Schrödinger equation is solved using the hyperspherical adiabatic approach, where the dynamics of the system is driven by the effective three-body potentials given by Eq. (3.122)-(3.123). The Efimov derivation showed that the three-body potentials are universal and take the long-range form proportional to $\sim R^{-2}$ for $\beta \ll R \ll |a|$,

$$W_\nu(R) = \hbar^2 \frac{\xi_\nu^2 - 1/4}{2\mu R^2} \,, \tag{4.10}$$

where ξ_ν is a universal parameter that characterizes the properties of the underlying three-body interactions, whether attractive or repulsive. The parameter ξ_ν depends on the general properties of the system and the good quantum numbers given in Eq. (3.220), where ν denotes all the quantum numbers required for the proper description of the system as discussed in Section 3.3. The repulsive interaction above the threshold given in Eq. (3.123) is realized for the value $\xi_\nu = \lambda + 2$. V. Efimov's derivation focused on the attractive case, which is obtained for $\xi_\nu = is_0$, where s_0 is another universal parameter that defines the scaling properties of the Efimov effect.

4.1.1. The Faddeev expansion of the wavefunction

Thus, we will show that the key quantity controlling the Efimov physics is the parameter ξ_ν, which depends on the good quantum numbers and the mass ratios of the particles involved. The standard approach is to use the *Faddeev expansion* of the three-body wavefunction [218, 219]

$$\Psi(R,\Omega) = c_1\Psi^i(\boldsymbol{\rho}_1^i,\boldsymbol{\rho}_2^i) + c_2\Psi^j(\boldsymbol{\rho}_1^j,\boldsymbol{\rho}_2^j) + c_3\Psi^k(\boldsymbol{\rho}_1^k,\boldsymbol{\rho}_2^k) \,. \tag{4.11}$$

Each Faddeev component $\Psi^{i,j,k}$ favorably describes the configuration of the three-body system defined by the kinematic variables given in Eq. (3.124). The mass-scaled Jacobi vectors are

related by the kinematic rotation given in Eq. (3.126). Within the hyperspherical approach, the hyperradius is independent of the exact choice of the hyperspherical map of the Jacobi coordinates, as summarized in Eq. (3.63) – with $\eta_{i,j,k} \in [0, \pi/2]$, being the polar hyperangle, which couples the motion of the two Jacobi vectors for every kinematic configuration i, j, k, which for three particles ($d = 6$) takes the form

$$\begin{aligned} |\boldsymbol{\rho}_1^k| =& R \sin\eta_k \ , \\ |\boldsymbol{\rho}_2^k| =& R \cos\eta_k \ . \end{aligned} \tag{4.12}$$

The general approach to deriving the Efimov effect involves considering the clustering method as discussed in Section 3.2.3. The total three-body wavefunction is still expanded adiabatically

$$\Psi(R.\Omega) = \sum_\nu F_\nu(R)\Phi_\nu(R;\Omega) \ , \tag{4.13}$$

but the adiabatic eigenfunctions $\Phi_\nu(R;\Omega)$ are subjected to the Faddeev expansion

$$\Phi_\nu(R;\Omega) = c_i\phi^i(R;\Omega_i) + c_j\phi^j(R;\Omega_j) + c_k\phi^k(R;\Omega_k) \ , \tag{4.14}$$

where $\Omega_{i,j,k}$ defines the full hyperangular configuration space associated with the Jacobi vectors $\boldsymbol{\rho}_1^{i,j,k}$ and $\boldsymbol{\rho}_2^{i,j,k}$. Each of the Faddeev components is determined by solving the eigenvalue problem given by Eq. (3.117), which takes the form

$$\left[\frac{\boldsymbol{\Lambda}^2(\Omega_k) + 15/4}{2\mu R^2}\right] \phi^k(R;\Omega_k) = U_\nu(R)\phi^k(R;\Omega_k) \ . \tag{4.15}$$

The equation above and all further equations in this Section are analogous for i and j. The grand angular momentum operator is given by

$$\boldsymbol{\Lambda}^2(\Omega_k) = -\partial^2_{\eta_k} - 2(\cot\eta_k - \tan\eta_k)\partial_{\eta_k} + \frac{\hat{L}^2_{ij}\left(\hat{\boldsymbol{\rho}}_1^k\right)}{\sin^2\eta_k} + \frac{\hat{L}^2_{k}\left(\hat{\boldsymbol{\rho}}_2^k\right)}{\cos^2\eta_k} \ , \tag{4.16}$$

as it was derived in Eq. (3.84), and where $\hat{L}^2_{ij}$, $\hat{L}^2_k$ are the angular momemtum operators for the pair ij and the relative moiton of the k particles with respect to the center of mass of ij, and where $\hat{\boldsymbol{\rho}}_1^k$ and $\hat{\boldsymbol{\rho}}_1^k$ are the hyperangular parts – or spherical angles – of the Jacobi vectors defined, e.g., in Eq. (3.108).

4.1.2. The eigenvalue problem for Λ^2

In the Bethe-Peierls approach, the effect of the potential, and thus the hyperradial dependence in Eq. (4.15) is entirely covered by the Bethe-Peierls boundary condition, which now takes the form

$$\begin{aligned} -\frac{1}{d_k R\sin\eta_k\Phi_\nu}\frac{\partial}{\partial(d_k R\sin\eta_k)}(d_k R\sin\eta_k\Phi_\nu) =& \frac{1}{a_{ij}} \ , \\ -\frac{1}{\sin\eta_k\Phi_\nu}\frac{1}{\cos\eta_k}\frac{\partial}{\partial\eta_k}(\sin\eta_k\Phi_\nu) =& \frac{d_k R}{a_{ij}} \ , \\ -\frac{1}{\sin\eta_k\Phi_\nu}\frac{\partial}{\partial\eta_k}(\sin\eta_k\Phi_\nu) =& \frac{d_k R}{a_{ij}} \ , \quad \eta_k \to 0 \ , \end{aligned} \tag{4.17}$$

where we use the relation $r_{ij} = |\mathbf{r}_j - \mathbf{r_i}| = d_k|\boldsymbol{\rho}_1^k| = d_k R\sin\eta_k$, we treat R as a parameter, and we use the limit $1/(\cos\eta_k) \to 1$, which is regular for $\eta_k \to 0$ as opposed to the term $1/(\sin\eta_k)$.

More generally, when the atoms interact through some finite-range potential, each of the Faddeev components of the channel functions should be expanded in a basis set comprised of the eigenfunctions of the $\hat{L}_{ij}^2$, $\hat{L}_k^2$ operators (expanded using the Clebsh-Gordan coefficients) or in terms of the eigenfunctions of the grand angular momentum given by Eq. (3.109). As we mentioned at the end of Section 3.2.3, the grand angular momentum quantum number λ is tightly linked to the angular momentum l_k for the particle k with respect to the center of mass of two particles ij and the angular momentum l_{ij} of two particles i, j. Both of these quantum numbers satisfy the standard rules of quantum angular momentum addition: $|l_{ij} - l_k| \leq J \leq l_{ij} + l_k$ and $m'_J = m'_{ij} + m'_k$, where J is the total angular momentum and m'_J denotes the projection of J on the quantization axis in the lab-fixed frame. In the s-wave regime, which, as we mentioned, is dominant for near-resonant interactions, only states with $l_{ij} = 0$ and $l_k = J$ interact. As we have shown in Section 3.4.5, the restrictions on coupling between consequent values of m'_J result in only quantum states with parity $(-1)^J$ (parity-favored case) to be relevant for scattering. We can finally expand the Faddeev component ϕ^k into proper eigenfunctions of the angular momentum operators

$$\phi^k(R; \eta_k, \hat{\boldsymbol{\rho}}_1^k, \hat{\boldsymbol{\rho}}_2^k) = u_\xi^J(\eta_k)\, Y_0^0(\hat{\boldsymbol{\rho}}_1^k)\, Y_J^{m'_J}(\hat{\boldsymbol{\rho}}_2^k) \,, \tag{4.18}$$

where Y_l^m are the spherical harmonic functions of degree l and order m, and $u_{\xi_\nu}^J(\eta_k)$ is the yet-to-be-determined eigenfunction of the operator given in Eq. (4.16). We shall now determine the function $u_\xi^J(\eta_k)$, where – for simplicity – we will omit the index ν. Let us write the effect of the operator given in Eq. (4.16) acting on functions given by Eq. (4.18)

$$\boldsymbol{\Lambda}^2(\Omega_k) u_\xi^J = \left[-\partial_{\eta_k}^2 - 2(\cot\eta_k - \tan\eta_k)\partial_{\eta_k} + \frac{J(J+1)}{\cos^2\eta_k} \right] u_\xi^J =: s^2 u_\xi^J \,, \tag{4.19}$$

for some eigenvalue s. Let us first consider a substitution

$$u_\xi^J(\eta_k) = \frac{\varphi_\xi^J(\eta_k)}{\sin\eta_k \cos\eta_k} \,. \tag{4.20}$$

The effect of the first-derivative operator ∂_{η_k} on this function is given by

$$\frac{\partial}{\partial\eta_k} \frac{\varphi_\xi^J(\eta_k)}{\sin\eta_k\cos\eta_k} = -4\cot(2\eta_k)\csc(2\eta_k)\,\varphi_\xi^J(\eta_k) + \frac{\dot{\varphi}_\xi^J(\eta_k)}{\sin\eta_k\cos\eta_k} \,, \tag{4.21}$$

where the dot represents the derivative over η_k. The second-derivative term is equal to

$$\begin{aligned}
\frac{\partial^2}{\partial\eta_k^2} \frac{\varphi_\xi^J(\eta_k)}{\sin\eta_k\cos\eta_k} =& \frac{\partial}{\partial\eta_k} \left[\frac{\dot{\varphi}_\xi^J(\eta_k)}{\sin\eta_k\cos\eta_k} - 4\cot(2\eta_k)\csc(2\eta_k)\,\varphi_\xi^J(\eta_k) \right] \\
=& -4\cot(2\eta_k)\csc(2\eta_k)\,\dot{\varphi}_\xi^J(\eta_k) + \frac{\ddot{\varphi}_\xi^J(\eta_k)}{\sin\eta_k\cos\eta_k} + \\
&+ 8\csc^3(2\eta_k)\varphi_\xi^J(\eta_k) + 8\cot^2(2\eta_k)\csc(\eta_k)\varphi_\xi^J(\eta_k) - \\
&- 4\cot(2\eta_k)\csc(2\eta_k)\,\dot{\varphi}_\xi^J(\eta_k) \\
=& \underbrace{-8\cot(2\eta_k)\csc(2\eta_k)\,\dot{\varphi}_\xi^J(\eta_k)} + \frac{\ddot{\varphi}_\xi^J(\eta_k)}{\sin\eta_k\cos\eta_k} + \\
&+ \underbrace{8\csc^3(2\eta_k)\varphi_\xi^J(\eta_k) + 8\cot^2(2\eta_k)\csc(\eta_k)\varphi_\xi^J(\eta_k)} \,,
\end{aligned} \tag{4.22}$$

Let us now calculate the second term in Eq. (4.19) and compare with $-\partial_{\eta_k}^2 u_\xi^J$

$$-2(\cot\eta_k - \tan\eta_k)\frac{\partial}{\partial\eta_k}\frac{\varphi_\xi^J(\eta_k)}{\sin\eta_k\cos\eta_k} = -4\cot(2\eta_k)\left[\frac{\dot\varphi_\xi^J(\eta_k)}{\sin\eta_k\cos\eta_k} - 4\cot(2\eta_k)\csc(2\eta_k)\,\varphi_\xi^J(\eta_k)\right] = \\ = \underbrace{-8\frac{\cos(2\eta_k)}{\sin^2(2\eta_k)}\dot\varphi_\xi^J} + \underbrace{16\cot^2(2\eta_k)\csc(2\eta_k)\,\varphi_\xi^J}\ . \tag{4.23}$$

The underbracketed terms in Eqs. (4.22) and (4.23) cancel out (keeping in mind the minus before the second derivative), while the underbraced terms proportional to φ_ξ^J are equal to

$$\begin{aligned} 8\,\varphi_\xi^J(\eta_k)\left[-\csc^3(2\eta_k) + \cot^2(2\eta_k)\csc(2\eta_k)\right] &= 8\,\varphi_\xi^J(\eta_k)\csc(2\eta_k)\left[\frac{\cos^2(2\eta_k)-1}{\sin^2(2\eta_k)}\right] = \\ &= 8\,\varphi_\xi^J(\eta_k)\frac{1}{2\sin\eta_k\cos\eta_k}[-1] = \\ &= -4\frac{\varphi_\xi^J(\eta_k)}{\sin\eta_k\cos\eta_k}\ . \end{aligned} \tag{4.24}$$

Using the results given in Eqs. (4.22) and (4.24) we are able to simplify the eigenvalue equation

$$\left[-\frac{\partial^2}{\partial\eta_k^2} + \frac{J(J+1)}{\cos^2\eta_k}\right]\varphi_\xi^J(\eta_k) = (s^2+4)\varphi_\xi^J(\eta_k)\ . \tag{4.25}$$

In further derivations, we will require the following operator definitions

$$\begin{aligned} H_J &= \frac{\partial^2}{\partial\eta_k^2} + \frac{J(J+1)}{\cos^2\eta_k}\ , \\ A_J &= (\cos\eta_k)^J\left[\frac{\partial}{\partial\eta_k}\frac{1}{\cos\eta_k}\right]^J\ , \\ B_J &= \frac{\partial}{\partial\eta_k} + J\tan\eta_k\ , \\ B_J^\dagger &= -\frac{\partial}{\partial\eta_k} + J\tan\eta_k\ , \end{aligned} \tag{4.26}$$

where we use the adjoint operator $-\partial_{\eta_k}$ to represent the hermitian conjugate of ∂_{η_k} and the power J in the operator A_J means applying it J-times. The operator A_J acting on the wavefunction behaves in a regular way as long as the wavefunction satisfies the boundary conditions such that it tends to zero at the endpoints of the domain interval of $\eta_k \in [0, \pi/2]$. The structure of H_J reproduces the so-called Pöschl–Teller potential. Let us first consider the solutions to the eigenvalue problem for $J = 0$

$$-\ddot\varphi_\xi^0(\eta_k) = \xi^2\varphi_\xi^0(\eta_k)\ , \tag{4.27}$$

where we set $\xi^2 = s^2 + 4$ – so far without the loss of generality as we are still to derive the relation given by Eq. (4.10). The solution to Eq. (4.27) is naturally

$$\varphi_\xi^0(\eta_k) = \sin\left[\xi\left(\frac{\pi}{2} - \eta_k\right)\right]\ , \tag{4.28}$$

where we introduced the substitution $\left(\frac{\pi}{2} - \eta_k\right)$ to satisfy the boundary condition $\varphi(\pi/2) = 0$, and where we omitted a global scaling factor for the sake of simplicity in the discussion. Let

us now consider the operator

$$\begin{aligned} B_J^\dagger B_J &= \left[-\frac{\partial}{\partial\eta_k} + J\tan\eta_k\right]\left[\frac{\partial}{\partial\eta_k} + J\tan\eta_k\right] = \\ &= -\frac{\partial^2}{\partial\eta_k^2} + J\tan\eta_k\frac{\partial}{\partial\eta_k} - J\frac{1}{\cos^2\eta_k} - J\tan\eta_k\frac{\partial}{\partial\eta_k} + J^2\tan^2\eta_k = \\ &= -\frac{\partial^2}{\partial\eta_k^2} + \frac{J(J-1)}{\cos^2\eta_k} - J^2\ . \end{aligned} \tag{4.29}$$

From the equation above it follows that,

$$H_{J-1} = B_J^\dagger B_J + J^2\mathbb{I}\ . \tag{4.30}$$

Similarly, we can show that

$$H_J = B_J B_J^\dagger + J^2\mathbb{I}\ . \tag{4.31}$$

Using these relations, let us show the so-called intertwining relation between H_J and H_{J-1}

$$\begin{aligned} H_{J-1} - J^2 &= B_J^\dagger B_J\ , \\ B_J(H_{J-1} - J^2\mathbb{I}) &= B_J B_J^\dagger B_J\ , \\ B_J(H_{J-1} - J^2\mathbb{I}) &= (H_J - J^2\mathbb{I})B_J\ , \\ B_J H_{J-1} &= H_J B_J\ . \end{aligned} \tag{4.32}$$

Using the intertwining relation allows us to solve the eigenvalue problem for the H_J operator recursively. We already know that the function φ_ξ^0 satisfies $H_0\varphi_\xi^0 = \xi^2\varphi_\xi^0$. Let us now consider the equation

$$\left(\prod_{j=1}^{J} B_m\right) H_0\varphi_\xi^0 = H_J\left(\prod_{j=1}^{J} B_m\right)\varphi_\xi^0\ , \tag{4.33}$$

where the symbol $\prod$ denotes a product of operators in decreasing order, and where for the operators H_i the value of i increased by 1 each time it commuted with B_k. Therefore, we deduce that the function $\left(\prod_{k=1}^{J} B_k\right)\varphi_\xi^0$ solves the eigenvalue problem for operator H_J with the same eigenvalue ξ^2 used for $H_0 = -\partial_{\eta_k}^2$. We will now express the operator product B_k as a *telescopic* series to show its relation to A_J. Let us consider the operator B_k

$$B_m = \frac{\partial}{\partial\eta_k} + m\tan\eta_k = \frac{\partial}{\partial\eta_k} - \left[m\cos^{-m-1}(\eta_k)(-\sin(\eta_k))\right]\cos^m(\eta_k) = \cos^m(\eta_k)\frac{\partial}{\partial\eta_k}\cos^{-m}(\eta_k)\ , \tag{4.34}$$

where in the last equation we used the product rule for derivatives. We now see that the product of operators is given by

$$\prod_{j=1}^{J} B_m = \prod_{j=1}^{J}\left[\cos^m(\eta_k)\partial_{\eta_k}\cos^{-m}(\eta_k)\right] = \cos^J(\eta_k)\left[\frac{\partial}{\partial\eta_k}\frac{1}{\cos\eta_k}\right]^J = A_J\ , \tag{4.35}$$

where in the last equation we consider that for each index m the consecutive product term $m-1$ factors out in the following way

$$\begin{aligned} &\left[\prod_{m'=m+1}^{J} B_{m'}\right]\cos^m(\eta_k)\frac{\partial}{\partial\eta_k}\cos^{-m}(\eta_k)\cos^{m-1}(\eta_k)\frac{\partial}{\partial\eta_k}\cos^{-(m-1)}(\eta_k)\left[\prod_{m'=1}^{m-2} B_{m'}\right] = \\ &= \left[\prod_{m'=m+1}^{J} B_{m'}\right]\cos^m(\eta_k)\frac{\partial}{\partial\eta_k}\cos^{-1}(\eta_k)\frac{\partial}{\partial\eta_k}\cos^{-(m-1)}(\eta_k)\left[\prod_{m'=1}^{m-2} B_{m'}\right]\ . \end{aligned} \tag{4.36}$$

We finally obtain the eigenfunctions $\varphi_\xi^J(\eta_k)$ of the H_J operator in the same form as proposed by V. Efimov in Ref. [186]

$$\varphi_\xi^J(\eta_k) = \left(\prod_{m=1}^{J} B_m\right)\varphi_\xi^0(\eta_k) = A_J\varphi_\xi^0(\eta_k) = \cos^J(\eta_k)\left[\frac{\partial}{\partial\eta_k}\frac{1}{\cos\eta_k}\right]^J \sin\left[\xi\left(\frac{\pi}{2}-\eta_k\right)\right] \ , \tag{4.37}$$

and the solutions to the eigenvalue problem for $\mathbf{\Lambda}^2(\Omega_k)$ with and R-dependent eigenvalue $\xi^2(R)$. Eq. (4.10) follows immediately. We now derive the Faddeev component

$$\phi^k(R;\eta_k,\hat{\boldsymbol{\rho}}_1^k,\hat{\boldsymbol{\rho}}_2^k) = \frac{Y_0^0(\hat{\boldsymbol{\rho}}_1^k)\,Y_J^{m'_J}(\hat{\boldsymbol{\rho}}_2^k)}{\sin\eta_k\cos\eta_k}\cos^J(\eta_k)\left[\frac{\partial}{\partial\eta_k}\frac{1}{\cos\eta_k}\right]^J \sin\left[\xi\left(\frac{\pi}{2}-\eta_k\right)\right] \ . \tag{4.38}$$

4.1.3. The Bethe-Peierls boundary condition

Let us use the solutions and the expansion in Eq. (4.14) and insert them into the Bethe-Peierls boundary condition given in Eq. (4.17)

$$\begin{aligned}\frac{\partial}{\partial(\sin\eta_k)}\left[c_i\phi^i\sin\eta_k + c_j\phi^j\sin\eta_k + c_k\phi^k\sin\eta_k\right] &= -\frac{d_kR}{a_{ij}}\left[c_i\phi^i\sin\eta_k + c_j\phi^j\sin\eta_k + c_k\phi^k\sin\eta_k\right] \ , \\ \left[c_i\phi^i + c_j\phi^j + c_k\frac{\partial}{\partial(\sin\eta_k)}\left(\phi^k\sin\eta_k\right)\right] &= -\frac{d_kR}{a_{ij}}\left[c_i\phi^i\sin\eta_k + c_j\phi^j\sin\eta_k + c_k\phi^k\sin\eta_k\right] \ .\end{aligned} \tag{4.39}$$

Let us take the limit $\eta_k \to 0$ and use the regularization $\frac{\partial}{\partial\sin\eta_k} \to \frac{\partial}{\partial\eta_k}$ shown in Eq. (4.17)

$$\left[c_i\phi^i + c_j\phi^j + c_k\frac{\partial}{\partial\eta_k}\left(\phi^k\sin\eta_k\right)\right] = -\frac{d_kR}{a_{ij}}\left[c_k\phi^k\sin\eta_k\right] \ , \tag{4.40}$$

where we inserted the form of the solutions given in Eq. (4.38) for each index i,j,k. Dividing by a constant function $Y_0^0(\hat{x})$ – for an angular part of any vector $\hat{x}$, Eq. (4.39) becomes

$$\begin{aligned}-\frac{d_kR}{a_{ij}}\left[c_k\frac{\varphi_\xi^J(\eta_k)}{\cos\eta_k}Y_J^{m'_J}(\hat{\boldsymbol{\rho}}_2^k)\right] =& c_i\frac{\varphi_\xi^J(\eta_i)Y_J^{m'_J}(\hat{\boldsymbol{\rho}}_2^i)}{\sin\eta_i\cos\eta_i} + c_j\frac{\varphi_\xi^J(\eta_j)Y_J^{m'_J}(\hat{\boldsymbol{\rho}}_2^j)}{\sin\eta_i\cos\eta_i} + \\ &+ c_kY_J^{m'_J}(\hat{\boldsymbol{\rho}}_2^k)\left[\frac{\tan\eta_k}{\cos\eta_k}\varphi_\xi^J(\eta_k) + \frac{\dot{\varphi}_\xi^J(\eta_k)}{\cos\eta_k}\right] \ .\end{aligned} \tag{4.41}$$

Let us briefly recall the definitions of the Jacobi vectors to see their behavior at $\eta_k \to 0$. The definitions for three particles stem from the Eq. (3.2)

$$\begin{aligned}\boldsymbol{\rho}_1^k &= \sqrt{\frac{m_im_j}{(m_i+m_j)\mu}}\left(\mathbf{r}_j - \mathbf{r}_i\right) \ , \\ \boldsymbol{\rho}_2^k &= \sqrt{\frac{m_k(m_i+m_j)}{M\mu}}\left(\mathbf{r}_k - \frac{m_i\mathbf{r}_i + m_j\mathbf{r}_j}{m_i+m_j}\right) \ ,\end{aligned} \tag{4.42}$$

where $\mu^2 = m_i m_j m_k/M$, and M is the total mass, and there exists a relation between the mass-scaling coefficients

$$\begin{aligned}\sqrt{\frac{m_k(m_i+m_j)}{M\mu}} &=: d_k \ , \\ \sqrt{\frac{m_i m_j}{(m_i+m_j)\mu}} &= \sqrt{\frac{\sqrt{M}}{\sqrt{m_i m_j m_k}}\frac{m_i m_j}{(m_i+m_j)}} = \\ &= \sqrt{\frac{M}{\sqrt{M}}\frac{\sqrt{m_i m_j m_k}}{m_k(m_i+m_j)}} = d_k^{-1} \ ,\end{aligned} \tag{4.43}$$

From Eq. (4.12), it follows that at for $\eta_k = 0$ we get,

$$\begin{aligned}|\boldsymbol{\rho}_1^k| = 0 &\implies \mathbf{r}_i = \mathbf{r}_j \ , \\ (\mathbf{r}_i = \mathbf{r}_j) &\implies \boldsymbol{\rho}_2^k = d_k\,(\mathbf{r}_k - \mathbf{r}_i) \ , \\ (|\boldsymbol{\rho}_2^k| = R) \wedge (\mathbf{r}_i = \mathbf{r}_j) &\implies r_{ki} = d_i|\boldsymbol{\rho}_1^i| = d_j|\boldsymbol{\rho}_1^j| = d_k^{-1}R \ .\end{aligned} \tag{4.44}$$

A simple calculation also yields that for $\eta_k = 0$,

$$\boldsymbol{\rho}_2^j = d_j\left[\mathbf{r}_j - \frac{m_i\mathbf{r}_i + m_k\mathbf{r}_k}{m_i+m_k}\right] = d_j\left[\frac{m_k(\mathbf{r}_i - \mathbf{r}_k)}{m_i+m_k}\right] \ . \tag{4.45}$$

The relation is analogous for $\boldsymbol{\rho}_2^i$.

Let us insert these limits into the kinematic rotation given by Eq. (3.126). We consider a kinematic rotation between vectors for k (left-hand side) and j (vectors undergoing the rotation on the right-hand side) at $\eta_k = 0$,

$$\begin{aligned}0 &= \cos\beta_{jk}\, d_j^{-1}(-\mathbf{r}_{ki}) + \sin\beta_{jk}\, d_j \frac{m_k}{m_i+m_k}(-\mathbf{r}_{ki}) \ , \\ d_k\mathbf{r}_{ki} &= -\sin\beta_{jk} d_j^{-1}(-\mathbf{r}_{ki}) + \cos\beta_{jk}\, d_j \frac{m_k}{m_i+m_k}(-\mathbf{r}_{ki}) \ ,\end{aligned} \tag{4.46}$$

where we use the short-hand notation $\mathbf{r}_{mn} = \mathbf{r}_m - \mathbf{r}_n$, we use Eqs. (4.44) and (4.45), and we keep in mind that (i,j,k) is a cyclic permutation of $(1,2,3)$. Solving these equations for β_{jk} gives

$$\begin{aligned}d_k\mathbf{r}_{ki} &= \sin\beta_{jk}\, d_j^{-1}\mathbf{r}_{ki} + \frac{\cos^2\beta_{jk}}{\sin\beta_{jk}} d_j^{-1}\mathbf{r}_{ki} \ , \\ 0 < \sin\beta_{jk} d_k d_j &= 0\sin^2\beta_{jk} + \cos^2\beta_{jk} = 1 \ , \\ \cos\beta_{jk} &= -\frac{m_k}{m_i+m_k} d_j d_k^{-1} < 0 \ .\end{aligned} \tag{4.47}$$

These results were already derived in Eq. (3.128), and due to opposing signs of cosine and sine, mean that $\beta_{jk} \in [\pi/2, \pi]$. Using the last of relations in Eq. (4.44) and the defining relation for η_j we show that

$$\begin{aligned}|\boldsymbol{\rho}_1^j| = R\sin\eta_j &= d_j^{-1} d_k^{-1} R \ , \\ \sin\eta_j\, d_j d_k &= 1 \ .\end{aligned} \tag{4.48}$$

Hence,

$$\sin\eta_j = \sin\beta_{jk} \ , \quad \eta_j \in \left[0, \frac{\pi}{2}\right] , \quad \beta_{jk} \in [\pi/2, \pi] \ , \tag{4.49}$$

which leads us to the relation

$$-\eta_j + \pi = \beta_{jk} \ . \tag{4.50}$$

Similarly, we can show that $\pi - \eta_i = \beta_{ki}$. Eq. (4.45) shows us that $\boldsymbol{\rho}_2^{i,j} \sim -\mathbf{r}_{ki}$, while the second equation in Eq. (4.44) means that $\boldsymbol{\rho}_2^{k} \sim \mathbf{r}_{ki}$. Thus, the spherical or angular parts of the second Jacobi vectors, which determine their orientation, must follow the simple relation $-\hat{\boldsymbol{\rho}}_2^k = \hat{\boldsymbol{\rho}}_2^j = \hat{\boldsymbol{\rho}}_2^i$. Therefore, the Eq. (4.41) at $\eta_k \to 0$ becomes

$$-c_i \frac{\varphi_\xi^J(\pi - \beta_{ki})(-1)^J}{\sin\beta_{ki}\cos\beta_{ki}} - c_j \frac{\varphi_\xi^J(\pi - \beta_{jk})(-1)^J}{\sin\beta_{kj}\cos\beta_{kj}} + c_k\, \dot{\varphi}_\xi^J(0) = -\frac{d_k R}{a_{ij}} c_k\, \varphi_\xi^J(0) \ , \tag{4.51}$$

where $\cos\beta_{jk} < 0$ and $\cos\beta_{ki} < 0$, and where we used the parity relation $Y_l^m(-\hat{x}) = (-1)^l Y_l^m(\hat{x})$ for a given set of spherical angles $\hat{x}$. We note that for near-resonant interactions and in the range $R \ll |a_{ij}|$, the parameter ξ – which drives the systems' dynamics and properties through the corresponding effective potential in Eq. (4.10) – is independent of R. Therefore, the three-body physics in this regime becomes *universal* – dependent only on the broad structural features of the system like symmetries, dimensionality, and the conserved quantities. The full description of the Efimov physics in resonantly interacting ultracold quantum gases is given in Ref. [119, 214]. As an example, we will consider a system of three identical bosons. Naturally, for such a system, all three Faddeev components have equal weights, $c_i = c_j = c_k$. Similarly, all mass-coefficients are equal $d_i = d_j = d_k = 2^{1/2}/3^{1/4}$ and using Eq. (4.48), we deduce that $\beta_{ki} = \beta_{jk} = 2\pi/3$. Introducing an angle $\beta = \pi - \beta_{jk} = \pi - \beta_{ki} \in [0, \pi/2]$ the Bethe-Peierls boundary condition takes the following form for $R \ll |a_{ij}|$,

$$\dot{\varphi}_\xi^J(0) + 2\frac{(-1)^J \varphi_\xi^J(\beta)}{\sin\beta\cos\beta} = 0 \ , \tag{4.52}$$

where $\cos\beta > 0$.

4.1.4. Explicit formula of the solution of the eigenvalue problem for Λ^2

To proceed with the derivation, we need to evaluate the values of the functions $\varphi_\xi^J(\eta_k)$ and $\dot{\varphi}_\xi^J(\eta_k)$ at any η_k with the help of some explicit formula. For this, let us consider a variable substitution $u = \pi/2 - \eta_k$ and insert it into the result given in Eq. (4.37)

$$\varphi_\xi^J(u) = (-1)^J \sin^J(u) \left[\frac{\partial}{\partial u}\frac{1}{\sin u}\right]^J \sin(\xi u) \ , \tag{4.53}$$

where, naturally, $\partial_{\eta_k} = -\partial_u$. In principle, for $\xi \in \mathbb{N}$, the solutions above could be simplified by the standard Chebyshev polynomials of the second kind $U_{\xi-1}(x)$. However, the recursively defined functions could be simplified *and* generalized to any $\xi \in \mathbb{Z}$ using the generalized form of the Chebyshev polynomials of the second-kind – $U_{\xi-1}(z)$. The $U_{\xi-1}(z)$ functions are defined using the *hypergeometric functions* ${}_2F_1(a, b; c; z)$, and they satisfy the closed-form relation [220, 221]

$$\begin{aligned} U_{\xi-1}(z) :=& \xi\, {}_2F_1\left(-\xi+1, \xi+1; \frac{3}{2}; \frac{1-z}{2}\right) \ , \\ U_\xi(z) =& \frac{\sin((\xi+1)\cdot\arccos z)}{\sqrt{1-z^2}} \ . \end{aligned} \tag{4.54}$$

The relation in the second equation can be proved by expressing the generalized Chebyshev polynomials as a special case of the generalized Gegenbauer functions of a non-integer order [220]. Let us now consider a substitution $u = \arccos(t)$, $\partial_u = -\sqrt{1-t^2}\partial_t$, and use it in

Eq. (4.53) along with the relation given by Eq. (4.54),

$$\begin{aligned}\varphi_\xi^J(t) =&(-1)^{2J}\left(\sqrt{1-t^2}\right)^J\left[\sqrt{1-t^2}\frac{\partial}{\partial t}\frac{1}{\sqrt{1-t^2}}\right]^J\sin(\xi\arccos(t)) = \\ =&\left(\sqrt{1-t^2}\right)^J\left[\sqrt{1-t^2}\frac{\partial}{\partial t}\frac{1}{\sqrt{1-t^2}}\right]^J\left(\sqrt{1-t^2}U_{\xi-1}(t)\right) = \\ =&\left(\sqrt{1-t^2}\right)^{J+1}\frac{\partial^J}{\partial t^J}U_{\xi-1}(t)\ ,\end{aligned} \tag{4.55}$$

where we use the relation $\sin(\arccos(t)) = \sqrt{1-t^2}$ and an additional coefficient $(-1)^J$ is an effect of the derivative substitution. In the last equation, the telescopic operator simplified drastically, thanks to the cancellation of the $\sqrt{1-t^2} = \sin(u)$ terms. We can calculate the J-th derivative of the $U_{\xi-1}(t)$ functions using their definitions in Eq. (4.54) and a variable change $w = (1-t)/2$, $\partial_t = (-1/2)\partial_w$

$$\begin{aligned}\frac{\partial^J}{\partial t^J}U_{\xi-1}(t) =&\xi\left(\frac{-1}{2}\right)^J\frac{\partial^J}{\partial w^J}\,{}_2F_1\left(-\xi+1,\xi+1;\frac{3}{2};w\right) = \\ =&\xi(-1)^J2^{-J}\frac{(-\xi+1)_J(\xi+1)_J}{(3/2)_J}\,{}_2F_1\left(-\xi+1+J,\xi+1+J;\frac{3}{2}+J;w\right)\ ,\end{aligned} \tag{4.56}$$

where $(a)_n$ is the (rising) Pochhammer symbol equal to $\Gamma(a+n)/\Gamma(a)$ and we used the known formula for the J-th derivative of the ${}_2F_1$ function [222]. The result turns out to be a generalized Gegenbauer polynomial $C_n^{(\alpha)}$

$${}_2F_1\left(-\xi+1+J,\xi+1+J;\frac{3}{2}+J;\frac{1-t}{2}\right) = \frac{(\xi-1-J)!}{(2(J+1))_{\xi-J-1}}C^{(J+1)}_{\xi-1-J}(t)\ . \tag{4.57}$$

The coefficient in front of this solution can be simplified

$$\begin{aligned}&(-2)^{-J}\xi\frac{(-\xi+1)_J(\xi+1)_J}{(3/2)_J}\frac{(\xi-1-J)!}{(2(J+1))_{\xi-J-1}} = \\ &= (-2)^{-J}\xi\frac{\Gamma(-\xi+1+J)\Gamma(\xi+1+J)\Gamma(3/2)}{\Gamma(1-\xi)\Gamma(\xi+1)\Gamma(3/2+J)}\frac{\Gamma(\xi-J)\Gamma(2J+2)}{\Gamma(\xi+J+1)} = \\ &= (-2)^{-J}\frac{\Gamma(2J+2)\Gamma(\xi-J)\Gamma(-\xi+1+J)\Gamma(3/2)}{\Gamma(1-\xi)\Gamma(\xi)\Gamma(3/2+J)} = \\ &= (-2)^{-J}\frac{\sin(\xi\pi)}{\sin(\pi(\xi-J))}\frac{\Gamma(2J+2)\Gamma(3/2)}{\Gamma(3/2+J)} = (-2)^{-J}(-1)^J2^{2J}\Gamma(J+1) = 2^JJ!\ ,\end{aligned} \tag{4.58}$$

where we used the Euler's reflection formula $\Gamma(z)\Gamma(1-z) = \pi/\sin(\pi z)$ for $z = \xi - J$ and $z = \xi$ and the duplication formula $\Gamma(3/2)\Gamma(2J+2) = 2^{2J}\Gamma(J+1)\Gamma(J+3/2)$. So, the solutions $\varphi_\xi^J(\eta_k)$ are equal to

$$\varphi_\xi^J(\eta_k) = 2^JJ!(\cos\eta_k)^{J+1}C^{(J+1)}_{\xi-J-1}(\sin\eta_k)\ . \tag{4.59}$$

A simple calculation yields its derivative

$$\begin{aligned}\dot\varphi_\xi^J(\eta_k) =&2^JJ!(\cos\eta_k)^J\left[-(J+1)\sin\eta_kC^{(J+1)}_{\xi-J-1}(\sin\eta_k)+(\cos\eta_k)^2\,2(J+1)C^{(J+2)}_{\xi-J-2}(\sin\eta_k)\right] = \\ =&2^J(J+1)!\left[-\sin\eta_kC^{(J+1)}_{\xi-J-1}(\sin\eta_k)+2(\cos\eta_k)^2\,C^{(J+2)}_{\xi-J-2}(\sin\eta_k)\right](\cos\eta_k)^J\ ,\end{aligned} \tag{4.60}$$

where we use the relation $\partial_xC_n^{(\alpha)}(x) = 2\alpha\,C_{n-1}^{(\alpha+1)}(x)$, which was already derived in Eqs. (4.56) and (4.57). At $\eta_k = 0$ this equation is simply,

$$\dot\varphi_\xi^J(0) = 2^{J+1}(J+1)!C^{(J+2)}_{\xi-J-2}(0)\ . \tag{4.61}$$

Relation to the Gegenbauer differential equation

The explicit form of the solution φ_ξ^J indicates that Eq. (4.25) can be reduced to the Gegenbauer differential equation. In fact, we can apply two substitutions in Eq. (4.25). The first of them is the following regularization for some function $f_\xi^J =: f$

$$\varphi_\xi^J(\eta_k) = (\cos\eta_k)^{J+1} f_\xi^J(\eta_k) \ , \tag{4.62}$$

which, after some algebra, results in Eq. (4.25) taking the following form

$$((J+1)^2 - \xi^2) f(\eta_k) + 2(J+1)\tan(\eta_k)\frac{\partial}{\partial\eta_k} f(\eta_k) - \frac{\partial^2}{\partial\eta_k^2} f(\eta_k) = 0 \ . \tag{4.63}$$

The next step is considering a variable change $x = \sin\eta_k$. Then, $\partial_{\eta_k} = \cos\eta_k\,\partial_x$ and $\partial^2_{\eta_k} = (1-x^2)\partial_x^2 - x\partial_x$. So Eq. (4.63) becomes

$$(\xi^2 - (J+1)^2) f(x) - (2J+3) x f'(x) + (1-x^2) f''(\eta_k) = 0 \ , \tag{4.64}$$

which is precisely the Gegenbauer differential equation with solutions $C_n^{(\alpha)}(x)$, such that

$$\begin{aligned} \alpha &= J+1 \ , \\ n &= \xi - J - 1 \ . \end{aligned} \tag{4.65}$$

Using the explicit solution in the Bethe-Peierls boundary condition

Let us find an exact formula for the value $\dot\varphi_\xi^J(0)$ given in Eq. (4.61). using the definition of the generalized Gegenbauer polynomial from Eq. (4.57). There exists a closed-form of the hypergeometric function at $z = \frac{1}{2}$, [223]

$${}_2F_1\left(a, b; \frac{1+a+b}{2}; \frac{1}{2}\right) = \frac{\Gamma\left(\frac{1}{2}\right)\Gamma\left(\frac{1}{2}(1+a+b)\right)}{\Gamma\left(\frac{1}{2}(1+a)\right)\Gamma\left(\frac{1}{2}(1+b)\right)} \ . \tag{4.66}$$

If we take $a = -\xi + J + 2$, and $b = \xi + 2 + J$, we can simplify Eq. (4.61)

$$\begin{aligned} \dot\varphi_\xi^J(0) =& 2^{J+1}(J+1)! C^{(J+2)}_{\xi-J-2}(0) = \\ =& 2^{J+1}(J+1)! \frac{\Gamma(\xi+J+2)}{\Gamma(\xi-J-1)\Gamma(2J+4)}\, {}_2F_1\left(-\xi+J+2, \xi+J+2; \frac{5}{2}+J; \frac{1}{2}\right) = \\ =& \frac{\Gamma(\xi+J+2)}{\Gamma(\xi-J-1)\Gamma(2J+4)} \frac{2^{J+1}(J+1)!\sqrt{\pi}\,\Gamma\left(\frac{5}{2}+J\right)}{\Gamma\left(\frac{1}{2}+\frac{1}{2}(2+J-\xi)\right)\Gamma\left(\frac{1}{2}+\frac{1}{2}(2+J+\xi)\right)} = \\ =& \frac{\Gamma(\xi+J+2)}{\Gamma(\xi-J-1)\Gamma(2J+4)} \frac{2^{-J-2}\,\pi\,\Gamma(2J+4)}{\Gamma\left(\frac{3+J-\xi}{2}\right)\Gamma\left(\frac{3+J+\xi}{2}\right)} = \frac{2^{-J-2}\,\pi(\xi-J-1)_{2J+3}}{\Gamma\left(\frac{3+J-\xi}{2}\right)\Gamma\left(\frac{3+J+\xi}{2}\right)} \ , \end{aligned} \tag{4.67}$$

where we used the Gamma duplication formula for $z = J + 2$. The resulting polynomial in ξ has a very simple structure,

$$\begin{aligned}\dot{\varphi}^J_\xi(0) =& \frac{2^{-J-2}\,\pi\,(\xi - J - 1)_{2J+3}}{\Gamma\left(\frac{3+J-\xi}{2}\right)\Gamma\left(\frac{3+J+\xi}{2}\right)} = \frac{2^{-J-2}\,\pi\,(\xi - J - 1)_{2J+3}}{\Gamma\left((1+J)+\frac{1-J-\xi}{2}\right)\Gamma\left(1+\frac{1+J+\xi}{2}\right)} = \\ =& \frac{2^{-J-2}\,\pi\,(\xi - J - 1)_{2J+3}}{\Gamma\left(\frac{1-J-\xi}{2}\right)\Gamma\left(\frac{1+J+\xi}{2}\right)\left(\frac{1-J-\xi}{2}\right)_{J+1}\left(\frac{1+J+\xi}{2}\right)} = \\ =& \cos\left(\frac{\pi}{2}(J+\xi)\right)(\xi - J - 1)_{2J+3}\left[2^{J+2}(-1)^{J+1}\left(\frac{\xi-1-J}{2}\right)_{J+1}\left(\frac{1+\xi+J}{2}\right)\right]^{-1} \\ =& (-1)^{J+1}\cos\left(\frac{\pi}{2}(J+\xi)\right)\left[\prod_{k=0}^{2J+2}(\xi - (J+1) + k)\right] / \left[\prod_{k=0}^{J+1}(\xi - (J+1) + 2k)\right] = \\ =& (-1)^{J+1}\cos\left(\frac{\pi}{2}(J+\xi)\right)\prod_{k=0}^{J}(\xi - J + 2k) = (-1)^{J+1}\cos\left(\frac{\pi}{2}(J+\xi)\right)A_{J+1}(\xi)\ ,\end{aligned} \tag{4.68}$$

where we used the Euler's reflection formula for $z = (1 - J - \xi)/2$, and the formula for the Pochhammer symbol with negative argument $(-a)_n = (-1)^n(a - n + 1)_n$ for $n = J + 1$ and $a = -(1 - J - \xi)/2$. Thus, $\dot{\varphi}^J_\xi(0)$ is proportional to a factorized polynomial $A_{J+1}(\xi)$ of order $J + 1$, with roots $\xi_0 = -J, -J + 2, \ldots, J - 2, J$. The behavior of the $\varphi^J_\xi(\beta)$ function at $\beta = 0$ can be derived entirely analogously to the calculations presented in Eqs. (4.67), and (4.68). Thus, it is given by

$$\varphi^J_\xi(0) = (-1)^J\cos\left(\frac{\pi}{2}(J-1+\xi)\right)\prod_{k=0}^{J-1}(\xi - (J-1) + 2k) = (-1)^J\cos\left(\frac{\pi}{2}(J-1+\xi)\right)A_J(\xi)\ . \tag{4.69}$$

The imaginary solutions to the Bethe-Peierls boundary condition

So far, we have not specified whether the parameter ξ is real or complex. Naturally, if $\xi \in \mathbb{R}$, the solutions reproduce the known solutions to the eigenvalue problem given in Eq. (4.19). In such case, we obtain that $\lambda(\lambda + 4) = s^2 = \xi^2 - 4$ or $\xi = 2 + \lambda$, for $\lambda = J + 2n$, where $n \in \mathbb{N}$ (see: Eq. (3.101)). Since ξ^2 is an eigenvalue of a self-adjoint operator defined in Eq. (4.25), then $\xi^2 \in \mathbb{R}$. Thus, another possible solution is purely imaginary, i.e., $\xi = is_0$ for $s_0 \in \mathbb{R}$.

The function $\varphi^J_\xi(\eta_k)$ is defined in range $\eta_k \in [0, \pi/2]$. For $\xi \in \mathbb{R}$ and for $\xi = is_0 \in \mathbb{C}$, we can write this function in terms of the hypergeometric function, which will be useful when searching for a bound on φ^J_ξ, while the resulting form will reveal that the function is monotonic in η_k with maximum at $\eta_k = 0$ and minimum at $\eta_k = \pi/2$,

$$\begin{aligned}\frac{\varphi^J_\xi(\eta_k)}{(\cos\eta_K)^{J+1}} =& 2^J J!\frac{(2J+2)_{\xi-J-1}}{(\xi - J - 1)!}\,{}_2F_1\left(-\xi+1+J, \xi+1+J; \frac{3}{2}+J; \frac{1-\sin\eta_k}{2}\right) = \\ =& 2^J J!\frac{\Gamma(J+1+\xi)}{\Gamma(2J+2)\Gamma(\xi-J)}\,{}_2F_1\left(-\xi+1+J, \xi+1+J; \frac{3}{2}+J; \frac{1-\sin\eta_k}{2}\right) = \\ =& 2^J J!\frac{(\xi-J)_{2J+1}}{\Gamma(2J+2)}\sum_{n=0}^{\infty}\frac{(-\xi+1+J)_n(\xi+1+J)_n}{\left(\frac{3}{2}+J\right)_n}\frac{\left(\frac{1-\sin\eta_k}{2}\right)^n}{n!} = \\ =& 2^J\frac{(\xi-J)_{2J+1}\,J!}{\Gamma(2J+2)}\frac{\Gamma\left(\frac{3}{2}+J\right)}{\Gamma\left(-\xi+J+1\right)\Gamma\left(\xi+J+1\right)}\times\end{aligned}$$

$$
\begin{aligned}
&\times \sum_{n=0}^{\infty} \frac{\Gamma(-\xi+J+1+n)\Gamma(\xi+J+1+n)}{\Gamma\left(\frac{3}{2}+J+n\right)} \frac{\left(\frac{1-\sin\eta_k}{2}\right)^n}{n!} = \\
&= \frac{\Gamma(3/2)}{2^J}(\xi-J)_{2J+1} \frac{1}{(1-\xi)_J \Gamma(1-\xi)(1+\xi)_J \Gamma(1+\xi)} \times \\
&\times \sum_{n=0}^{\infty} \frac{|\Gamma(\xi+J+1+n)|^2}{\Gamma\left(\frac{3}{2}+J+n\right)} \frac{\left(\frac{1-\sin\eta_k}{2}\right)^n}{n!} = \\
&= \frac{(-1)^J \Gamma(3/2)}{2^J} \frac{(\xi-J)_{2J+1}}{(\xi-J)_J (1+\xi)_J \xi} \frac{\sin\pi\xi}{\pi} \sum_{n=0}^{\infty} \frac{|\Gamma(\xi+J+1+n)|^2}{\Gamma\left(\frac{3}{2}+J+n\right)} \frac{\left(\frac{1-\sin\eta_k}{2}\right)^n}{n!} = \\
&= (-1)^J \frac{\Gamma(3/2)}{2^J} \frac{\sin\pi\xi}{\pi} \sum_{n=0}^{\infty} \frac{|\Gamma(\xi+J+1+n)|^2}{\Gamma\left(\frac{3}{2}+J+n\right)} \frac{\left(\frac{1-\sin\eta_k}{2}\right)^n}{n!} \ ,
\end{aligned} \tag{4.70}
$$

where we used the Gamma duplication formula for $z = J+1$, the formula for the negative Pochhamer symbol $(-a)_n = (-1)^n (a-n+1)_n$ for $a = \xi - 1$ and $n = J$, the Euler reflection formula for $z = \xi$, and the relation $\Gamma(\bar{z}) = \overline{\Gamma(z)}$ – true for $z = (J+1) + is_0$. In all further considerations, we will focus on the purely imaginary solution to the problem. Hence, we set $\xi = is_0$ for $s_0 \in \mathbb{R}$. It quickly becomes clear that the function φ_ξ^J becomes purely imaginary, because $\sin(\pi\xi) = i\sinh(\pi s_0)$. The only other factors dependent on ξ are $|\Gamma(\xi+J+1+n)|^2 > 0$. For J-even and $s_0 > 0$, the imaginary part of the function φ_ξ^J is positive and monotonic in η_k, hence its minimum and maximum is at $\eta_k = \pi/2$ and $\eta_k = 0$, respectively. For J-odd and $s_0 > 0$, the imaginary part of the function is negative. The function φ_ξ^J is anti-symmetric in s_0.

For $\xi = is_0$, the polynomial A_{J+1} in Eq. (4.68) is purely imaginary for J-even and $A_{J+1} \in \mathbb{R}$ for J-odd. In both cases the respective imaginary or real part of $A_{J+1}(s_0)$ simplifies to a polynomial

$$
\begin{aligned}
B_{J+1}(s_0) &= i(-1)^{J/2} s_0 \prod_{k=1}^{J/2} \left(s_0^2 + (2k)^2\right) \ , \quad \text{for } J\text{−even} \\
B_{J+1}(s_0) &= (-1)^{(J+1)/2} \prod_{k=1}^{(J+1)/2} \left(s_0^2 + (2k-1)^2\right) \ , \quad \text{for } J\text{−odd} \ .
\end{aligned} \tag{4.71}
$$

The term $\cos\left(\frac{\pi}{2}(J+is_0)\right)$ is equal to $(-1)^{J/2}\cosh\left(\frac{\pi}{2}s_0\right)$ for J-even and $i(-1)^{(J+1)/2}\sinh\left(\frac{\pi}{2}s_0\right)$ for J-odd. Hence, for $\xi = is_0$ the term $\dot{\varphi}_\xi^J(0)$ in Eq. (4.52) simplifies to

$$
\begin{aligned}
\dot{\varphi}_\xi^J(0) &= -\ is_0 \prod_{k=1}^{J/2} \left(s_0^2 + (2k)^2\right) \cosh\left(\frac{\pi}{2}s_0\right) \ , \quad \text{for } J\text{−even} \ , \\
\dot{\varphi}_\xi^J(0) &= i \prod_{k=1}^{(J+1)/2} \left(s_0^2 + (2k)^2\right) \sinh\left(\frac{\pi}{2}s_0\right) \ , \quad \text{for } J\text{−odd} \ ,
\end{aligned} \tag{4.72}
$$

where we include the global sign term $(-1)^{J+1}$. The function $\dot{\varphi}_\xi^J(0)$ is anti-symmetric in s_0.

Let us slightly rewrite the Bethe-Peierls boundary condition at unitarity in Eq. (4.52)

$$
0 = \frac{\sin(2\beta)}{4} \dot{\varphi}_\xi^J(0) + (-1)^J \varphi_\xi^J(\beta) =: iG^J(s_0) \ . \tag{4.73}
$$

Solving this equation in s_0 is equivalent to finding roots of the function $G^J(s_0)$. We multiply the defining equation for $G(s_0)$ by i because all terms are purely imaginary for $\xi = is_0$. Because both the terms $\dot{\varphi}^J_\xi(0)$ and $\varphi^J_\xi(\beta)$ are anti-symmetric in s_0, we can restrict our search for roots to $s_0 > 0$. We immediately notice that the corresponding roots for $s_0 < 0$ result in the same eigenvalue $\xi^2 = (-is_0)^2 = (is_0)^2 = -s_0^2$. In all further considerations, we assume $s_0 > 0$. For J-odd, the function $G^J(s_0)$ is positive for all $s_0 > 0$, because both the terms $\sim \dot{\varphi}^J_\xi(0)$ and $\sim \varphi^J_\xi(\beta)$ are positive, due to cancellation of the $(-1)^J$ coefficient. At $s_0 = 0$ the limit of $G^J(s_0)$ is zero, due to the terms $\sim \sinh$. Therefore, there are no roots for $G^J(s_0)$ for J odd.

For J-even, the two terms, one proportional to $\sim \dot{\varphi}^J_\xi(0) < 0$ and the second $\sim \varphi^J_\xi(\beta) > 0$, compete in various ranges of s_0 as long as the mass-dependent kinematic angle $\beta := \beta(m_i, m_j, m_k) \in [0, \pi/2]$ is finite. Let us begin by analyzing the behavior of $G^J(s_0)$ for $s_0 \to 0$. The behavior of $\dot{\varphi}^J_\xi(0)$ near $s_0 = 0$ is given by,

$$\begin{aligned}\dot{\varphi}^J_\xi(0) &= -\cos\left(\frac{\pi}{2}(is_0 + J)\right) B_{J+1}(s_0) = -(-1)^{J/2}\cosh\left(\frac{\pi s_0}{2}\right) i(-1)^{J/2} s_0 \prod_{k=1}^{J/2}(s_0^2 + (2k)^2) = \\ &= -i\cosh\left(\frac{\pi s_0}{2}\right) s_0 \prod_{k=1}^{J/2}(s_0^2 + (2k)^2) = -i\left[1 + \mathcal{O}(s_0^2)\right] s_0 \left[\prod_{k=1}^{J/2}(2k)^2 + \mathcal{O}(s_0^2)\right] .\end{aligned} \tag{4.74}$$

We should note that the linear term grows very rapidly with increasing J. In fact it is equal to $\prod_{k=1}^{J/2}(2k)^2 = 2^J((J/2)!)^2$, so the growth is dominated by a factorial. As we will see below, the behavior of $G^J(s_0)$ for large s_0 is dominated by the negative $\sim \varphi^J_\xi(\beta)$ term. Hence, it is only possible to find zeroes of the $G^J(s_0)$ function in a finite range of β for which the linear terms near $s_0 = 0$ are positive, thanks to the decreasing (both with J and s_0) term proportional to $\sim \varphi^J_\xi(\beta)$.

The third equality in Eq. (4.70) is a formula for $\varphi^J_\xi(\beta)$, which we will use for the study of behavior of $\varphi^J_\xi(\beta)$ near $s_0 = 0$,

$$\begin{aligned}\frac{\varphi^J_\xi(\beta)}{(\cos\beta)^{J+1}} &= 2^J J! \frac{(is_0 - J)_{2J+1}}{\Gamma(2J+2)} \underbrace{\sum_{n=0}^{\infty} \frac{(-is_0 + 1 + J)_n (is_0 + 1 + J)_n}{\left(\frac{3}{2} + J\right)_n} \frac{(1 - \sin\beta)^n}{2^n n!}}_{} = \\ &= \frac{2^J J!}{(2J+1)!} i(-1)^J s_0 \prod_{k=1}^{J}(s_0^2 + k^2) \left[\sum_{n=0}^{\infty} \frac{(1+J)_n (1+J)_n}{\left(\frac{3}{2} + J\right)_n} \frac{(1 - \sin\beta)^n}{2^n n!} + \mathcal{O}(s_0^2)\right] = \\ &= i\frac{2^J J!}{(2J+1)!}(-1)^J s_0 \left[\prod_{k=1}^{J} k^2 + \mathcal{O}(s_0^2)\right] \left[\sum_{n=0}^{\infty} \frac{((1+J)_n)^2 (1 - \sin\beta)^n}{n! \prod_{k=1}^{n}(1 + 2k + 2J)} + \mathcal{O}(s_0^2)\right] = \\ &= i\underline{\frac{2^J J!}{(2J+1)!}}(-1)^J s_0 \left[(J!)^2 + \mathcal{O}(s_0^2)\right] \underbrace{\left[\sum_{n=0}^{\infty} \frac{((1+J)_n)^2 (1 - \sin\beta)^n}{n! \prod_{k=1}^{n}(1 + 2k + 2J)} + \mathcal{O}(s_0^2)\right]}_{} ,\end{aligned} \tag{4.75}$$

where we use the fact that the underbracketed sum is symmetric in s_0. Therefore, its expansion around $s_0 = 0$ can not contain a linear term ($\sim s_0$). The convergence of the underbraced series for $(1 - \sin\beta)/2 \in [0, 1/2]$ is ensured by the convergence of the underbracketed sum defining the hypergeometric function – although a more detailed analysis of the convergence of these series goes beyond the scope of this thesis. Let us consider the behavior of the linear

term near $s_0 = 0$ for large, even J,

$$\begin{aligned}\frac{\varphi_\xi^J(\beta)}{is_0(\cos\beta)^{J+1}} &\approx \frac{2^J J!}{(2J+1)!}\left[(J!)^2+\mathcal{O}(s_0^2)\right]\left[\sum_{n=0}^{\infty}\frac{J^{2n}\,(1-\sin\beta)^n}{(2J)^n\,n!}+\mathcal{O}(s_0^2)\right]= \\ &= \frac{2^J J!}{(2J+1)!}\left[(J!)^2+\mathcal{O}(s_0^2)\right]\left[\sum_{n=0}^{\infty}\left(\frac{J}{2}\right)^n\frac{(1-\sin\beta)^n}{n!}+\mathcal{O}(s_0^2)\right]= \\ &= \frac{2^J J!}{(2J+1)!}\left[(J!)^2+\mathcal{O}(s_0^2)\right]\left[\exp\left(\frac{J}{2}(1-\sin\beta)\right)+\mathcal{O}(s_0^2)\right]\,.\end{aligned} \tag{4.76}$$

For finite β, and J-even the linear term of $\varphi_\xi^J(\beta)$ has slower growth in J than the linear term of $\dot\varphi_\xi^J(0)$, which can be seen by analyzing the quotient

$$\begin{aligned}\frac{\varphi_\xi^J(\beta)/(is_0)}{\dot\varphi_\xi^J(0)/(-is_0)} &\underset{\simeq}{s_0\to 0} \frac{2^J\frac{J!}{(2J+1)!}(J!)^2\exp\left(\frac{J}{2}(1-\sin\beta)\right)(\cos\beta)^{J+1}}{2^J\left(\left(\frac{J}{2}\right)!\right)^2}= \\ &= \frac{(J!)^3}{(2J+1)!\left(\left(\frac{J}{2}\right)!\right)^2}\exp\left(\frac{J}{2}(1-\sin\beta)\right)(\cos\beta)^{J+1}\simeq \\ &\simeq \frac{(2\pi J)^{\frac{3}{2}}\left(\frac{J}{e}\right)^{3J}}{(4\pi J)^{\frac{1}{2}}\left(\frac{2J}{e}\right)^{2J}(\pi J)\left(\frac{J}{2e}\right)^{J}}\exp\left(\frac{J}{2}(1-\sin\beta)\right)(\cos\beta)^{J+1}= \\ &= \sqrt{2}\,\frac{J^{3J}}{(2J)^{2J}J^J\left(\frac{1}{2}\right)^J}\exp\left(\frac{J}{2}(1-\sin\beta)\right)(\cos\beta)^{J+1}= \\ &= \sqrt{2}\,\frac{1}{2^J}(\cos\beta)^J\exp\left(\frac{J}{2}(1-\sin\beta)\right)\cos\beta \\ &= \sqrt{2}\cos\beta\underbrace{\left(\frac{\cos\beta}{2}e^{\frac{1-\sin\beta}{2}}\right)^J}\xrightarrow{J\to\infty}0\,,\end{aligned} \tag{4.77}$$

where we used the Stirling approximation. The underbracketed β-dependent term is smaller than one for $\beta\in[0,\pi/2]$, which is why the quotient tends to zero. One can also show that this quotient is monotonic in J. We should note that the approximation given in Eq. (4.76) approaches the exact value given in Eq. (4.75) either from below or above – depending on the exact value of β. It can be shown that one can always find a range for which the approximation is an upper bound on Eq. (4.75). We will restrict our considerations to $J=0$ and $J=2$. We will show that for $J=0$ the linear term of the expansion of $G^J(s_0)$ near $s_0=0$ is positive for all $\beta\in[0,\pi/2]$. Then, for $J=2$ – the range of β where the linear term is positive – decreases. This range becomes smaller for each consecutive J (even). Let us now analyze the behavior of $G^J(s_0)$ for $s_0\to\infty$. As we have already mentioned, the $\varphi_\xi^J(\beta)$ function has a maximum for $\beta=0$. We can compare the behavior of both components of $G^J(s_0)$ by analyzing the upper bound of the quotient for J-even

$$\begin{aligned}\frac{\varphi_\xi^J(\beta)/i}{\dot\varphi_\xi^J(0)/(-i)} &\le \frac{\varphi_\xi^J(0)/i}{\dot\varphi_\xi^J(0)/(-i)}=\frac{\sinh\left(\frac{\pi s_0}{2}\right)\prod_{k=1}^{J/2}(s_0^2+(2k-1)^2)}{\cosh\left(\frac{\pi s_0}{2}\right)s_0\prod_{k=1}^{J/2}(s_0^2+(2k)^2)}= \\ &= \tanh\left(\frac{\pi s_0}{2}\right)\frac{\prod_{k=1}^{J/2}(s_0^2+(2k-1)^2)}{s_0\prod_{k=1}^{J/2}(s_0^2+(2k)^2)}\xrightarrow{s_0\to\infty}1\cdot 0=0\,,\end{aligned} \tag{4.78}$$

where we used Eqs. (4.69) and (4.71) and a derivation similar to the third equality in Eq. (4.74). So, the $G^J(s_0)$ function is negative for $s_0\to\infty$ and J-even.

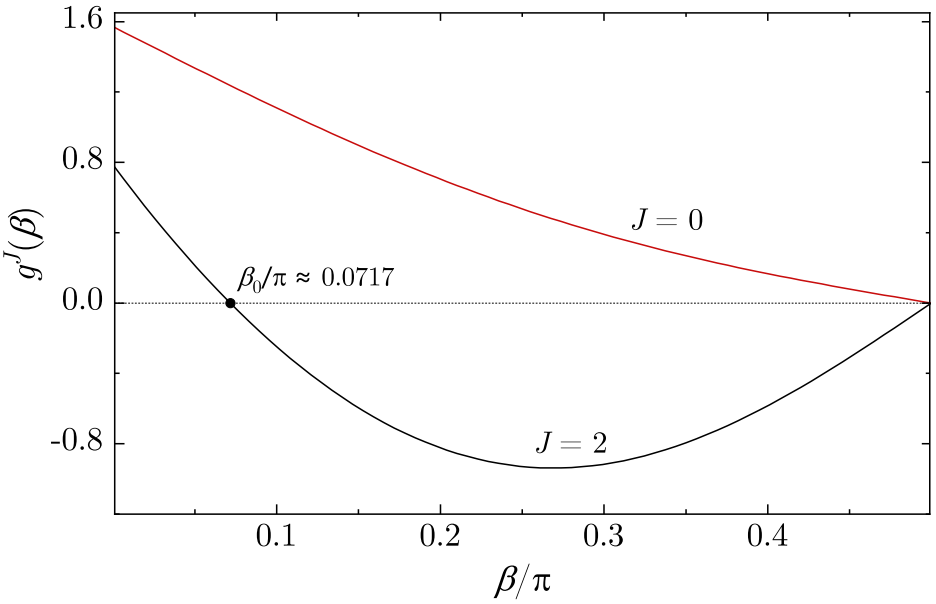

Figure 4.1: The $g^J(\beta)$ functions representing the behavior of the linear term of the expansion of the $G^J(s_0)$ near $s_0 = 0$. For $J > 2$, the range, where the linear term is positive, decreases further.

Using Eq. (4.74) and Eq. (4.75) let us now analyze the linear term of the function $G^J(s_0)$ near $s_0 = 0$ for $J = 0$ and $J = 2$

$$\begin{aligned} G^J(s_0) &= s_0 \left[-\frac{\sin(2\beta)}{4} + \cos\beta \sum_{n=0}^{\infty} \frac{((1)_n)^2 (1-\sin\beta)^n}{n! \prod_{k=1}^{n}(1+2k)} \right] + \mathcal{O}(s_0^3) \ , \quad J = 0 \ , \\ G^J(s_0) &= s_0 \left[-\sin(2\beta) + \frac{2}{15}(\cos\beta)^3 \sum_{n=0}^{\infty} \frac{((3)_n)^2 (1-\sin\beta)^n}{n! \prod_{k=1}^{n}(5+2k)} \right] + \mathcal{O}(s_0^3) \ , \quad J = 2 \ . \end{aligned} \tag{4.79}$$

Therefore, we aim to analyze the β-dependent functions.

$$\begin{aligned} g^0(\beta) &= -\frac{\sin(2\beta)}{4} + \cos\beta \sum_{n=0}^{\infty} \frac{((1)_n)^2 (1-\sin\beta)^n}{n! \prod_{k=1}^{n}(1+2k)} \ , \\ g^2(\beta) &= -\sin(2\beta) + \frac{2}{15}(\cos\beta)^3 \sum_{n=0}^{\infty} \frac{((3)_n)^2 (1-\sin\beta)^n}{n! \prod_{k=1}^{n}(5+2k)} \ . \end{aligned} \tag{4.80}$$

The functions $g^J(\beta)$ are presented in Figure 4.1. The function $g^0(\beta)$ is positive for all $\beta \in [0, \pi/2]$, meaning that in the first approximation (up to linear terms in s_0) we expect an imaginary solution to the Bethe-Peierls boundary condition given in Eq. (4.73) for three bosons with any masses. Equivalently, for $J = 0$, the function $G^J(s_0)$ is positive for small s_0 for any $\beta \in [0, \pi/2]$ but diverges to $-\infty$ for $s_0 \to \infty$.

For $J = 2$ and up to the first approximation, the solutions to Eq. (4.73) or the roots of $G^J(s_0)$ can only be found in the range $\beta \in [0, \beta_0]$, where $\beta_0/\pi \approx 0.0717$. Including more powers of s_0 in the expansion of the $G^J(s_0)$ near $s_0 = 0$ further decreases the range of β, where roots can be found. Figure 4.2 presents the $G^J(s_0)$ functions for $J = 0$ and their dependence on β and s_0. The effective potentials in Eq. (4.10) become attractive and scale simply as R^{-2} in the region where $r_0 \ll R \ll |a_{ij}|$, where r_0 is a characteristic length of

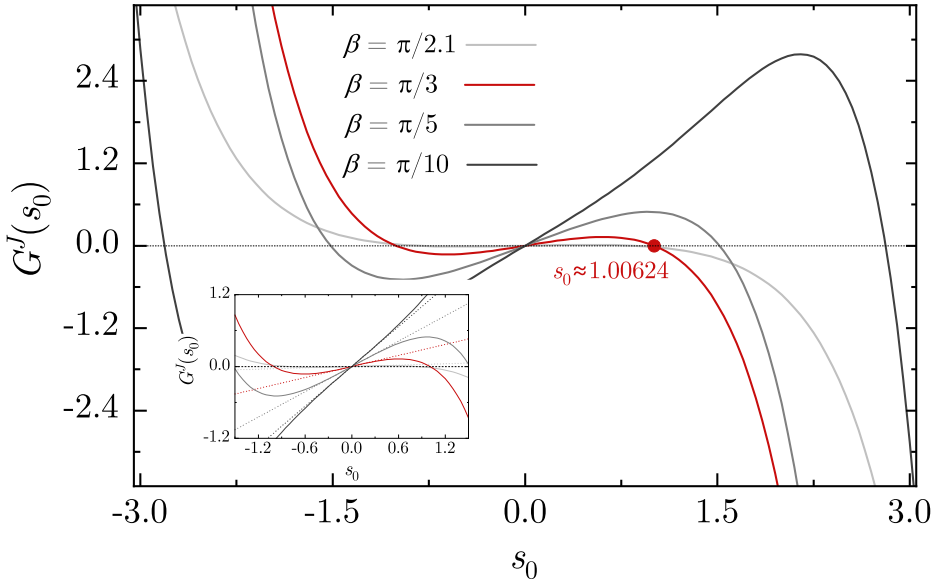

Figure 4.2: The $G^J(s_0)$ function, defined in Eq. (4.73), presented for $J = 0$ and 4 values of β. The function $G^J(s_0)$ is anti-symmetric in s_0. The roots of $G^J(s_0)$ define the purely imaginary parameter $\xi = is_0$ responsible for the Efimov effect as was shown in Eq. (4.10). The inset shows the linear terms $g^J(\beta)$ of the expansion of $G^J(s_0)$ near s_0 – defined in Eq. (4.80). The linear terms are positive for $s_0 > 0$ for all $\beta \in [0, \pi/2]$.

the underlying interaction, defining the behavior of the potentials at short-range. By solving Eq. (4.73) (or equivalently finding roots of $G^J(s_0)$ for various values of J, we found that the Efimov effect occurs for identical bosons only in the $J^\pi = 0^+$ state. In this case, it corresponds to the imaginary solution $\xi \approx 1.0062378i$ [151, 185, 186], obtained by substituting $\xi = is_0$ into Eq. (4.73) and solving for s_0. For all other cases where $J^\pi \neq 0$, Eq. (4.73) yields only real values of ξ, as was shown in Fig. 4.1 – implying that the resulting three-body potentials are repulsive. To visualize the dependence of the $G^J(s_0)$ function on J we present it for increasing J and $\beta = \pi/3$ in Figure 4.3. For $\beta \in [0, \beta_0]$ there are no roots of $G^J(s_0)$ at $J = 2$. The function diverges rapidly to $-\infty$ as J increases.

At unitarity, the non-adiabatic couplings $W_{\nu\nu'}$ in the hyperradial Schrödinger equation given in Eq. (3.118) vanish [119]. Using Eq. (4.10) and the purely imaginary results $\xi = is_0$ obtained in this Section, the hyperradial Schrödinger equation becomes

$$-\left[\frac{d^2}{dR^2} + \frac{s_0^2 + 1/4}{R^2} + k^2\right] F_\nu(R) = 0 \ . \tag{4.81}$$

The solutions to this equation for sufficiently small energy $2\mu|E|/\hbar^2 = |k^2| \ll |s_0|^2/r_0^2$ are of the form obtained by inserting the ansatz $F_\nu(R) = R^b$ into the zero-energy equation

$$\begin{aligned} 0 &= -\left[\frac{d^2}{dR^2} + \frac{s_0^2 + 1/4}{R^2}\right] R^b \ , \\ 0 &= \left[b(b-1) + s_0^2 + \frac{1}{4}\right] R^{b-2} \ , \end{aligned} \tag{4.82}$$

and solving for $b = 1/2 \pm is_0$. Thus, the form of the solutions is given by

$$F_\nu(R) = \sqrt{R}\left[a_\nu R^{is_0} + \beta_\nu R^{-is_0}\right] = \sqrt{R}\,\alpha_\nu\left(R^{is_0} + \frac{\beta_\nu}{\alpha_\nu} R^{-is_0}\right) \ , \tag{4.83}$$

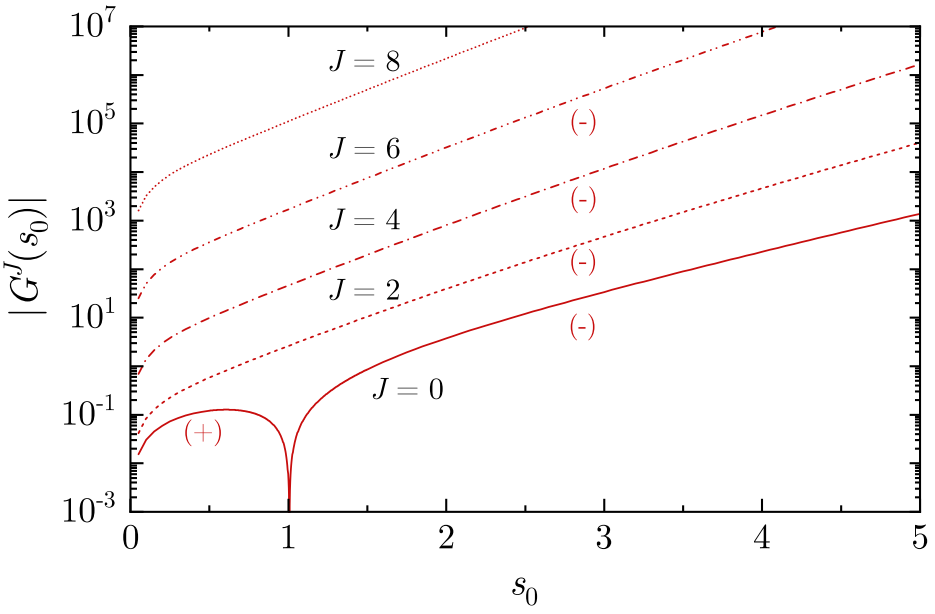

Figure 4.3: The absolute value of the $G^J(s_0)$ function, defined in Eq. (4.73), presented for $J = 0, \ldots, 8$ and $\beta = \pi/3$. The brackets denote the sign of the function in a given region. Only the $J = 0$ has got one root for $s_0 > 0$, due to the positive linear term of the expansion of $G^J(s_0)$ near $s_0 = 0$, given by Eqs. (4.74) and (4.75).

A short-range boundary condition results in a specific value of the ratio β_ν/α_ν. We should note that we consider now a simple boundary condition at small hyperradius R. In contrast, the Bethe-Peierls boundary condition was imposed on the two-body interactions dominated by the length scale defined through the interparticle scattering length a_{ij}. The aforementioned ratio has units of inverse length Λ to the power of $-2i|s_0|$ [214],

$$\begin{aligned} F_\nu(R) &= \sqrt{R}\left[\alpha_\nu \Lambda^{-is_0}\left(\Lambda^{is_0}R^{is_0} + \Lambda^{-is_0}R^{-is_0}\right)\right] , \\ F_\nu(R) &= \sqrt{R}\left[\alpha_\nu \Lambda^{-is_0}\left(e^{is_0\ln(\Lambda R)} + e^{-is_0\ln(\Lambda R)}\right)\right] , \\ F_\nu(R) &\overset{R\gg r_0}{\simeq} \sqrt{R}\cos\left(s_0\ln(\Lambda R)\right) . \end{aligned} \tag{4.84}$$

Thus, the three-body wavefunction shows log-periodic oscillations in R with the phase $\phi = s_0\ln(\Lambda/\Lambda_0)$ represented by a new inverse-length scale parameter Λ expressed in some predetermined unit Λ_0.

Crucially, due to the R^{-2} behavior of the Efimov potential, the Eq. (4.81) is scale-invariant. Although the short-range boundary condition does not allow for continuous scale-invariance, Eq. (4.81) is still invariant under *discrete* transformations $R \to \lambda_0^n R$, where $\lambda_0 = e^{\pi/|s_0|}$ and $n \in \mathbb{N}$. Thus, if the boundary condition allows for the Efimov channel to support a trimer at some (small) binding energy $2\mu E/\hbar^2 = k^2 = i^2\kappa^2 < 0$, the discrete scale-invariance ensures an infinity of solutions with energies $E/\lambda_0^{2n} < 0$. The value of the scaling factor is given by $\lambda_0 \approx 22.69 \approx \sqrt{515}$ for three identical bosons.

Remarkably, the results by V. Efimov predict that the discrete scale invariance holds also at large, but finite interparticle scattering lengths $a := a_{ij}$. This can be verified by multiplying a^{-1}, k and R in Eqs. (4.51) and (4.81). The solution given by Eq. (4.84) holds in the range $r_0 \ll R \ll |a|$ and the Efimov $\sim 1/R^2$ potential still governs this intermediate region. For $R > |a|$, the energy of the Efimov channel is given by the Feshbach dimer $\hbar^2/(2\mu_{2b}a^2)$, where

μ_{2b} is the two-body reduced mass. The Efimov states become unbound at the atom–dimer threshold, and their number becomes finite. While the exact derivation of the behavior of Efimov physics for finite $|a|$ lies beyond the scope of this thesis, an intuitive picture involves analyzing the accumulation phase of the three-body wavefunction for bound trimers. In this context, consider the Eq. (4.81) for $k^2 = i^2\kappa^2 < 0$ describing the Efimov bound states. Let us slightly rewrite the general form of the solutions given in Eq. (4.84)

$$F_\nu(R) = \sqrt{R}\left[Ae^{is_o \ln(\kappa R)} + Be^{-is_o \ln(\kappa R)}\right] . \tag{4.85}$$

In the short-range, $R \sim r_0$, the wavefunction can not be easily determined by semi-analytical methods. However, assuming that the two-body interaction supported no two-body bound states other than the Feshbach dimer, the probability of an incoming hyperradial wave must be totally reflected at short distances. Thus, the amplitudes of the incoming and outgoing hyperradial waves must be equal in magnitude, and the relation $A = -e^{2i\theta_*}B$ holds for some angle θ_*. The solutions given in Eq. (4.85) can therefore be written in the form [166, 224]

$$F_\nu(R) \approx \sqrt{\kappa R}\sin\left(s_0 \ln(c\,\kappa R) + \theta_*\right) , \tag{4.86}$$

where c is an arbitrary constant, and the angle θ_* is determined by the short-range boundary condition. Using this form of F_ν, the angle θ_* can be found by evaluating the logarithmic derivative at some point $R = R_0$ in the intermediate region

$$\begin{aligned} R_0\frac{F'_\nu(R_0)}{F_\nu(R_0)} &= \frac{1}{2} + s_0 \cot\left[\theta_* + s_0 \ln(c\kappa R)\right] , \\ \theta_* &= -\,s_0 \ln(c\,\kappa R) + \operatorname{arccot}\left[\frac{1}{s_0}\left(R_0\frac{F'_\nu(R_0)}{F_\nu(R_0)} - \frac{1}{2}\right)\right] . \end{aligned} \tag{4.87}$$

The term proportional to $\sim$ arccot is not dependent on the energy E or the wavenumber κ. It can therefore be included as an inverse-length scale unit Λ_0,

$$\theta_* = -s_0 \ln(c\,\kappa/\Lambda_0) . \tag{4.88}$$

The term Λ_0/c is a complicated function of R_0 and $R_0\frac{F'_\nu(R_0)}{F_\nu(R_0)}$. It can be shown that Λ_0 is a three-body parameter, defined through the binding energy of the first Efimov state $|E_1| = \hbar^2\Lambda_0^2/m$, where m is the mass of one of the identical bosons [166].

As we mentioned, the Schrödinger equation remains scale-invariant in the intermediate range $r_0 \ll R \ll |a|$. We can therefore parametrize the wavenumber κ and the inverse of the scattering length a^{-1} using a set of polar coordinates (h, ζ)

$$\begin{aligned} a^{-1} &= h\cos\zeta , \\ \kappa &= h\sin\zeta . \end{aligned} \tag{4.89}$$

At a fixed angle ζ, the spectrum of the Efimov states shows the same scale-invariance as was shown at unitarity. All three-body bound states are universal in the (a^{-1}, κ) plane. At the point where the intermediate- and long-range connect, i.e., at $R \sim |a|$, the outgoing hyperradial wave can either be reflected or transmitted to the long-range and become the three-atom or atom-dimer scattering state. The coefficients for reflection and transmission are described by a unitary matrix dependent on ζ only [224]. In a finite range of ζ, the amplitude of the scattering states at long range tends to zero. The probability is therefore

also reflected from the long-range, resulting in the relation $A = e^{-i\Delta(\zeta)}B$. Connecting the solutions in the intermediate- and long-range yields the relation

$$2\theta_* + \Delta(\zeta) = 0 \mod 2\pi \ . \tag{4.90}$$

The phase $\Delta(\zeta)/2$ arises from the Skorniakov–Ter-Martirosian (STM) integral equation for zero-range interactions, and represents the hyperradial wave that is reflected from the long-distance region [166]. Expressing Eq. (4.90) using Eq. (4.88) gives

$$2s_0 \ln(c\kappa/\Lambda_0) - \Delta(\zeta) = -2n\pi \ , \quad n \in \mathbb{N} \ . \tag{4.91}$$

Dividing this equation by $2s_0$ and taking the exponent yields

$$\begin{aligned} \frac{\kappa}{\Lambda_0} e^{\ln c} e^{-\Delta(\zeta)/(2s_0)} &= e^{-n\pi/s_0} \ , \\ |E_{(n)}| + \frac{\hbar^2}{ma^2} =: \frac{\hbar^2\kappa^2}{m} &= \frac{\hbar^2\Lambda_0^2}{m} e^{-2\pi n/s_0} e^{\Delta'(\zeta)/s_0} \ , \end{aligned} \tag{4.92}$$

where we introduce the notation $|E_{(n)}| = \hbar^2\kappa_n/m$ for the binding energy of the n-th Efimov trimer, and we included the c parameter in the modified phase function $\Delta'(\zeta)$. The wavenumber κ_n is in range $\Lambda_0 \ll \kappa_n \ll 1/|a|$. Thus, we can relate the scale of the first to the short-range interaction length scale $\Lambda_0 \sim 1/r_0$. Using this relation, we can evaluate the number of Efimov bound states for finite $|a|$. We consider that $|E_{(N)}| \approx 0$ for some maximum value $N \in \mathbb{N}$ in Eq. (4.92)

$$\begin{aligned} \frac{\hbar^2}{ma^2} &\approx \frac{\hbar^2\Lambda_0^2}{m} e^{-2\pi N/s_0} e^{\Delta'(\zeta)/s_0} \ , \\ \frac{1}{|a|} &\approx \frac{1}{r_0} e^{-\pi N/s_0} e^{\Delta'(\zeta)/s_0} \ , \\ \ln\left(\frac{|a|}{r_0}\right) &\approx \frac{\pi N}{s_0} + \frac{\Delta'(\zeta)}{s_0} \ , \\ N &\approx \frac{s_0}{\pi} \ln\left(\frac{|a|}{r_0}\right) \ . \end{aligned} \tag{4.93}$$

where we neglected the correction $\Delta'(s_0)$ as it negligible compared to N [166].

4.2. The three-body recombination

Three-body inelastic processes are widely recognized as the main effect limiting the dynamics of atomic collisions and the stability of atomic and molecular gases. In ultracold conditions and for pure atomic gases, the main inelastic loss process is the *three-body recombination* given by the schematic reaction equation

$$A + B + C \to AB + C \ , \tag{4.94}$$

where three free particles interact, with two of them combining to form a dimer and the third one carrying away part of the released kinetic energy. Other types of inelastic processes – relevant in atomic-molecular gas mixtures – include the *atom-molecule relaxation*

$$AB^* + C \to AB + C \ , \tag{4.95}$$

which is a collision-induced transition from a two-body bound state to a more deeply bound two-body bound state of a molecule AB. For high enough temperature or weak binding energy of the molecule, another important process is the *collision-induced dissociation*

$$AB^* + C \to A + B + C \ , \tag{4.96}$$

leading to a loss of weakly bound molecules. These processes – especially the three-body recombination (TBR) – can be described by scattering theory, which is the aim of this Section. The experimental relevance of inelastic processes was described in Chapter 1. A typical three-body collision can proceed along multiple possible pathways. Each of the pathways is associated with a given set of three-body quantum channels and the non-adiabatic couplings defined in Eqs. (3.117) and (3.119) [119]. We should note that other types of reactions are possible, specifically the chemical transitions between molecular states of various particles involved in a collision. These processes are governed by the short-range transitions at $R \sim r_0$, with r_0 being the characteristic length of interactions. They can generally only be described by numerical solutions to the hyperradial Schrödinger equation.

The three-body recombination rate is a key observable of three-body dynamics in ultracold gases. It provides direct insight into how interactions among three atoms lead to loss processes and the formation of bound states. Measuring this rate enables the experimental identification of Efimov resonances and other few-body phenomena, and helps determine the stability and lifetime of strongly interacting atomic and molecular systems. Dependence of the recombination rate on the scattering length or temperature reveals universal properties of three-body physics. We will provide a sketch of the derivation of this observable stemming from d-dimensional scattering theory described in Section 3.3 and in Ref. [225]. For large R, with the assumption that $V \to 0$, the solutions of the hyperradial Schrödinger equation given in Eqs. (3.112) and (3.114) take the asymptotic form [225],

$$\Psi^I(R, \Omega_d) = \sum_{\lambda\mu} A_{\lambda\mu} \mathcal{Y}_{\lambda\mu}(\Omega_d) \left[\cos\delta_\lambda \, j_\lambda^d(kR) - \sin\delta_\lambda \, n_\lambda^d(kR) \right] \ , \tag{4.97}$$

where $A_{\lambda\mu}$ are unknown coefficients of the expansion, δ_λ is the d-dimensional scattering phase shift, $j_\lambda^d(kR)$ and $n_\lambda^d(kR)$ are the hyperspherical Bessel and Neumann functions defined in Ref. [226], $\mathcal{Y}_{\lambda\mu}(\Omega_d)$ are the solutions to eigenvalue problem for the grand angular momentum operator $\mathbf{\Lambda}^2(\Omega_d)$ as described in Sections 3.2.2 and 3.2.3 – with eigenvalue λ, and where μ is an index describing the linearly independent homogeneous polynomials of degree λ restricted to the unit sphere in SO(d), i.e., the degeneracy of the hyperspherical harmonics, similarly to m describing the degeneracy of spherical harmonics of degree l for $d = 3$, i.e., two-body scattering. The exact definition of the hyperspherical Bessel functions is given by [226]

$$j_\lambda^d(x) = \frac{\Gamma(\alpha) 2^{\alpha-1} J_{\alpha+\lambda}(x)}{(d-4)!! x^\alpha} \ , \quad n_\lambda^d(x) = \frac{\Gamma(\alpha) 2^{\alpha-1} N_{\alpha+\lambda}(x)}{(d-4)!! x^\alpha} \ , \tag{4.98}$$

where $\alpha = \frac{d}{2} - 1$. On the other hand, the wavefunction at large R can be described by the sum of an incoming plane wave $e^{i\,\mathbf{k}\cdot\mathbf{R}}$ and an outgoing scattered spherical wave $e^{ikR}/R^{(d-1)/2}$

$$\Psi^{II}(R, \Omega_d) = e^{i\,\mathbf{k}\cdot\mathbf{R}} + f(\hat{\mathbf{k}}, \hat{\mathbf{k}}') \frac{e^{ikR}}{R^{(d-1)/2}} \ , \tag{4.99}$$

where $f(k, k')$ is the scattering amplitude, k is the wavenumber, and where $\mathbf{R}$ is a vector comprised of the hyperradius R and the hyperangles $\Omega_d := \Omega$ representing the direction of observation. Its orientation is equal to the orientation of the incoming wavenumber, i.e.,

$\hat{\mathbf{R}} = \hat{\mathbf{k}}'$. Combining Eqs. (4.97) and (4.99) allows us to find the scattering amplitude by analyzing the terms proportional to $\sim \frac{e^{ikR}}{R^{(d-1)/2}}$ in the expression $\Psi^I(R,\Omega) - e^{i\,\mathbf{k}\cdot\mathbf{R}}$. To this end, let us consider the asymptotic ($R \to \infty$) behavior of the hyperspherical Bessel and Neumann functions [226]

$$\begin{aligned} j_\lambda^d(kR) &\to \sqrt{\frac{2}{\pi}}\frac{\Gamma(\alpha)2^{\alpha-1}}{(d-4)!!(kR)^{(d-1)/2}}\cos\left(kR - \frac{\pi\lambda}{2} - \frac{\pi(d-1)}{4}\right) , \\ n_\lambda^d(kR) &\to \sqrt{\frac{2}{\pi}}\frac{\Gamma(\alpha)2^{\alpha-1}}{(d-4)!!(kR)^{(d-1)/2}}\sin\left(kR - \frac{\pi\lambda}{2} - \frac{\pi(d-1)}{4}\right) . \end{aligned} \tag{4.100}$$

Using these relations, we get in Eq. (4.97),

$$\begin{aligned} \cos\delta_\lambda\, j_\lambda^d(kR) - \sin\delta_\lambda\, n_\lambda^d(kR) &= \sqrt{\frac{2}{\pi}}\frac{\Gamma(\alpha)2^{\alpha-1}}{(d-4)!!(kR)^{(d-1)/2}}\cos\left(kR - \frac{\pi\lambda}{2} - \frac{\pi(d-1)}{4} + \delta_\lambda\right) , \\ \cos\delta_\lambda\, j_\lambda^d(kR) - \sin\delta_\lambda\, n_\lambda^d(kR) &= \sqrt{\frac{2}{\pi}}\frac{\Gamma(\alpha)2^{\alpha-1}}{(d-4)!!(kR)^{(d-1)/2}}\frac{1}{2}\left(e^{ikR}e^{-i\eta_\lambda}e^{i\delta_\lambda} + e^{-ikR}e^{i\eta_\lambda}e^{-i\delta_\lambda}\right) , \end{aligned} \tag{4.101}$$

where $\eta_\lambda = \frac{\pi}{2}\left(\lambda + \frac{d}{2}\right) - \frac{\pi}{4}$. Thus, the asymptotic solutions Ψ^I are given by

$$\Psi^I = \sqrt{\frac{2}{\pi}}\frac{\Gamma(\alpha)2^{\alpha-1}}{(d-4)!!(kR)^{(d-1)/2}}\sum_{\lambda=0}^{\infty}\frac{1}{2}e^{-i\delta_\lambda}\left(e^{ikR}e^{-i\eta_\lambda}e^{2i\delta_\lambda} + e^{-ikR}e^{i\eta_\lambda}\right)\sum_\mu A_{\lambda\mu}\mathcal{Y}_{\lambda\mu}(\hat{\mathbf{R}}) . \tag{4.102}$$

Let us consider the expansion of the plane wave $e^{i\,\mathbf{k}\cdot\mathbf{R}}$, given in Ref. [226]

$$e^{i\,\mathbf{k}\cdot\mathbf{R}} = (d-2)!!\frac{2\pi^{d/2}}{\Gamma(d/2)}\sum_{\lambda=0}^{\infty} i^\lambda j_\lambda^d(kR)\sum_\mu \mathcal{Y}^*_{\lambda\mu}(\hat{\mathbf{k}})\mathcal{Y}_{\lambda\mu}(\hat{\mathbf{R}}) . \tag{4.103}$$

Asymptotically, for $R \to \infty$ it is given by

$$\begin{aligned} e^{i\,\mathbf{k}\cdot\mathbf{R}} &= (d-2)!!\frac{2\pi^{d/2}}{\Gamma(d/2)}\sqrt{\frac{2}{\pi}}\frac{\Gamma(d/2-1)2^{d/2-2}}{(d-4)!!(kR)^{(d-1)/2}}\times \\ &\times\sum_{\lambda=0}^{\infty} i^\lambda\frac{1}{2}\left(e^{ikR}e^{-i\eta_\lambda} + e^{-ikR}e^{i\eta_\lambda}\right)\sum_\mu \mathcal{Y}^*_{\lambda\mu}(\hat{\mathbf{k}})\mathcal{Y}_{\lambda\mu}(\hat{\mathbf{R}}) \\ &= \sqrt{\frac{1}{2\pi}}\frac{(2\pi)^{\frac{d}{2}}}{(kR)^{(d-1)/2}}\sum_{\lambda=0}^{\infty} i^\lambda\left(e^{ikR}e^{-i\eta_\lambda} + e^{-ikR}e^{i\eta_\lambda}\right)\sum_\mu \mathcal{Y}^*_{\lambda\mu}(\hat{\mathbf{k}})\mathcal{Y}_{\lambda\mu}(\hat{\mathbf{R}}) . \end{aligned} \tag{4.104}$$

Matching the asymptotic solutions given in Eq. (4.102) for $\delta_\lambda = 0$ with the plane wave yields the equation for $A_{\lambda\mu}$,

$$A_{\lambda\mu} = (2\pi)^{\frac{d}{2}} i^\lambda\frac{(d-4)!!}{\Gamma(\alpha)2^{\alpha-1}}\mathcal{Y}^*_{\lambda\mu}(\hat{\mathbf{k}})\, e^{i\delta_\lambda} . \tag{4.105}$$

We can finally compare the solutions Ψ^I and Ψ^{II} to obtain the scattering amplitude. The outgoing-wave part (so only terms proportional to $\sim e^{ikR}$) of the expression $\Psi^I - e^{i\,\mathbf{k}\cdot\mathbf{R}}$ yields the scattering amplitude

$$\begin{aligned} f(\hat{\mathbf{k}},\hat{\mathbf{k}}') \overset{\sim e^{+ikR}}{=} \frac{e^{ikR}}{R^{(d-1)/2}}\left(\Psi^I - e^{i\,\mathbf{k}\cdot\mathbf{R}}\right) = \\ = \left(\frac{2\pi}{k}\right)^{(d-1)/2}\sum_{\lambda\mu} i^\lambda e^{-i\eta_\lambda}\left(e^{2i\delta_\lambda} - 1\right)\mathcal{Y}^*_{\lambda\mu}(\hat{\mathbf{k}})\mathcal{Y}_{\lambda\mu}(\hat{\mathbf{R}}) . \end{aligned} \tag{4.106}$$

This result immediately generalizes to the elastic scattering amplitude of an anisotropic short-range potential [225]

$$f(\hat{\mathbf{k}},\hat{\mathbf{k}}') = \left(\frac{2\pi}{k}\right)^{(d-1)/2} \sum_{\lambda\mu\lambda'\mu'} i^{\lambda} e^{-i\eta_\lambda} \mathcal{Y}^*_{\lambda\mu}(\hat{\mathbf{k}}) \mathcal{Y}_{\lambda'\mu'}(\hat{\mathbf{R}}) \left(S_{\lambda\mu\lambda'\mu'} - \delta_{\lambda\lambda'}\delta_{\mu\mu'}\right) \ , \tag{4.107}$$

where $S_{\lambda\mu\lambda'\mu'}$ is the S-matrix. Integrating the expression $|f(\hat{\mathbf{k}},\hat{\mathbf{k}}')|^2$ over all final hyperangles $\hat{\mathbf{k}}$ and *averaging* over all initial hyperangles $\hat{\mathbf{k}}'$, i.e., integrating and dividing by the surface area of the unit $(d-1)$-sphere $I_d = 2\pi^{d/2}/\Gamma(d/2)$, yields the integrated elastic scattering cross section

$$\sigma' = \left(\frac{2\pi}{k}\right)^{d-1} \frac{1}{I_d} \sum_{\lambda\mu\lambda'\mu'} \left|S_{\lambda\mu\lambda'\mu'} - \delta_{\lambda\lambda'}\delta_{\mu\mu'}\right|^2 \ . \tag{4.108}$$

The factors i^λ and $e^{-i\eta_\lambda}$ vanished in the sum due to the orthogonality of the hyperspherical function $\mathcal{Y}^*_{\lambda\mu}(\hat{\mathbf{k}})$ during integration. We interpret the result given in Eq. (4.108) as a generalized average cross section describing possible events of transitions between an initial and final quantum channel i, and f, defined by $i := \lambda\mu \to \lambda'\mu' =: f$. The unitarity of the S-matrix was ensured by its definition during the generalization of our result given in Eq. (4.106). Therefore, the expression for the cross-section also applies to inelastic collisions. We should note that we did not include all spin degeneracies in Eq. (4.108) nor did we average over the initial collision energies as would be more appropriate from an experimental standpoint. Identical particle symmetry is treated by summing all indistinguishable amplitudes before squaring. One then averages over initial directions and momenta at fixed energy, and integrates over distinguishable final states. The total cross section is then given by $\sigma = n_p\sigma'$, where n_p is the number of terms in the permutation symmetry projection operator, e.g., $n_p = N!$ for N identical particles. The cross section for the total angular momentum J and parity Π should include an additional $2J+1$ a degeneracy. Hence, the final expression for the total cross section of N colliding particles is given by

$$\sigma(J^\Pi) = n_p \left(\frac{2\pi}{k_i}\right)^{d-1} \frac{1}{I_d} \sum_{fi} (2J+1)|S^{J\Pi}_{fi} - \delta_{fi}|^2 \ . \tag{4.109}$$

The recombination rate is then given by

$$K_N^{J\Pi} = \frac{\hbar k_i}{\mu_N} \sigma(J^\Pi) \ , \tag{4.110}$$

where μ_N is the N-body reduced mass, and factor $\hbar k_i/\mu_N$ represents the N -body hyperradial *velocity*, which is a generalization of relative collision velocity to d-dimensions. For three interacting particles, we have $d = 6$, and the three-body recombination is given by

$$K_3^{J\Pi} = n_p \sum_{fi} 32\pi^2 \frac{\hbar(2J+1)}{\mu k_i^4} |S^{J\Pi}_{fi} - \delta_{fi}|^2 \ . \tag{4.111}$$

The k_i^{-4} scaling reflects the Wigner threshold law for three-body collisions, which indicates that low partial waves dominate the recombination rate at ultracold energies. The apparent universality of K_3 arises when a few parameters, such as the scattering length a or the three-body parameter κ_*, capture the microscopic details of the system and allow predictions of the rate of recombination in atomic systems without detailed knowledge of the short-range potential. The scaling $K_3 \sim a^4$ arises in ultracold conditions near a Feshbach resonance, while

the interference and resonant terms in K_3 stemming from Efimov physics show universal behavior [119, 166, 214]. Although the S-matrix depends implicitly on the short-range behavior of the potentials, the dependence becomes less relevant in the ultracold regime. The relative probabilities for recombination between channels often follow universal propensity rules [182]. The probabilities for the exact pathways for recombination are governed by the elements of the $|S_{fi}^{J\Pi} - \delta_{fi}|^2 \sim |T_{fi}|^2$ matrix. These elements can be determined by the WKB tunneling probability. A detailed discussion on the role of non-adiabatic couplings, as well as exact expressions capturing Efimov features in three-body recombination (TBR), is presented in Ref. [119].

4.3. The effective range theory

Parts of this Section are based on the 'End Matter' of the Ref. [227], to which the author of this thesis made leading and substantial contributions, both in research and computational analysis, as well as in writing. The author of this thesis performed all numerical calculations using Poland's high-performance computing infrastructure PLGrid (HPC center: ACK Cyfronet AGH), developed data analysis software for accurate interpretation of the results, made all plots, led the scientific discussion, implemented minor modifications to numerical codes developed by Jose D'Incao, and prepared the initial draft of the manuscript.

Effective-range theory is an important tool for analyzing low-energy scattering. It became an essential framework for the development of the universal theory of ultracold collisions. Effective-range theory provides the leading terms in the expansion of $k^{2l+1} \cot \delta_l$ as a function of the collision energy, where δ_l is the phase shift of the scattering wavefunction for angular momentum l and k is the collision wavenumber. For temperatures approaching the s-wave regime, we consider only $l = 0$.

The usual effective range theory assumes that potentials are *short-range* in the sense that they fall off faster than any power of $1/r$, where r is the interatomic distance. For such potentials and for angular momentum l, the well known result states that [215, 228–231]

$$k^{2l+1} \cot \delta_l = -\frac{1}{a_l} + \frac{1}{2} r_{\mathrm{eff,l}} k^2 + \mathcal{O}(k^4) \ . \tag{4.112}$$

Eq. (4.112) is modified for *long-range* potentials, i.e., ones that decay following the power law $V(r) \to -1/r^n$, for $r \to \infty$. If the potentials decay sufficiently rapidly at large r, only the higher-order terms are modified. Specifically, the van der Waals potentials give rise to a modified equation [232, 233]

$$k^{2l+1} \cot \delta_l = -\frac{1}{a_l} + \frac{1}{2} r_{\mathrm{eff,l}} k^2 + \mathcal{O}(k^4 \ln(k)) \ . \tag{4.113}$$

To understand the limits of applicability of the effective range expansion for more slowly decaying inverse power-law potentials than those with $n = 6$, we will need to gain some insight into solutions of the general radial Schrödinger equation

$$\left[\frac{d^2}{dr^2} + k^2 - \frac{l(l+1)}{r^2} - \frac{2\mu}{\hbar^2} V(r) \right] u(r) = 0 \ , \tag{4.114}$$

where μ is the two-body reduced mass, and $u(r)$ is the solution function related to the radial part $\mathcal{R}(r)$ of the total wavefunction by $u(r) = r\mathcal{R}(r)$. For short-range potentials $V(r)$ rapidly

approaches 0 for large r, and $u(r)$ approaches the linear combination of the free solutions without modifications

$$u(0) = 0,\ u(r) \to k^l \left[\cot\delta_l kr j_l(kr) - kr n_l(kr)\right],\ r \to \infty\ , \tag{4.115}$$

where $j_l(kr)$ and $n_l(kr)$ are the spherical Bessel functions.

If we define the scattering volumes a_l (scattering *length* for $l = 0$) as

$$\lim_{k\to 0} k^{2l+1} \cot\delta_l = -\frac{1}{a_l}\ , \tag{4.116}$$

we can analyze the behavior of the solutions in the limit $k \to 0$. Considering the asymptotic behavior of the spherical Bessel functions

$$j_l(z) = \frac{z^l}{(2l+1)!!}(1 + \mathcal{O}(z^2))\ , \tag{4.117}$$

$$n_l(z) = -\frac{(2l-1)!!}{z^{l+1}}(1 + \mathcal{O}(z^2))\ , \tag{4.118}$$

the first term in Eq. (4.115) behaves as

$$k^l \cot\delta_l\ kr j_l(kr) \approx k^l \left(-\frac{1}{a_l} k^{-(2l+1)}\right) \frac{(kr)^{l+1}}{(2l+1)!!} = \frac{-r^{l+1}}{(2l+1)!! a_l}\ , \tag{4.119}$$

Thus, the behavior $\tan\delta_l \approx \delta_l \sim k^{2l+1}$ given in Eq. (4.116) ensures that the term from Eq. (4.119) is regular for $k \to 0$. Let us consider the second term

$$-k^l\,(kr n_l(kr)) \approx -k^l \left[-(2l-1)!!(kr)^{-l}\right] = -(2l-1)!! r^{-l}\ . \tag{4.120}$$

The solutions to the free radial Schrödinger equation therefore approach the expression

$$u_0(r) \to (2l-1)!! r^{-l} - \frac{r^{l+1}}{(2l+1)!! a_l},\ r \to\ \infty, \tag{4.121}$$

where we use the subscript '0' to denote the behavior at $k \to 0$.

The first restriction for the effective range theory for long-range potentials is that $u_0(r)$ does not always have the asymptotic form shown in Eq. (4.121). There are additional terms, which fall off as powers of $1/r$ and which may interfere with the r^{-l} term. Their origin stems from the fact that the long-range potential cannot be completely neglected at $r \to \infty$. Let's consider a long-range potential

$$V(r) = -C_n/r^n\ , \tag{4.122}$$

where C_n is the interaction constant. With such interaction, the radial Schrödinger equation has the form

$$\left[\frac{d^2}{dr^2} + k^2 - \frac{l(l+1)}{r^2} + \frac{\beta_n^2}{r^n}\right] u(r) = 0\ , \tag{4.123}$$

where we introduce $\beta_n = \sqrt{2\mu C_n/\hbar^2}$ – the characteristic length of interaction. Upon the substitution

$$\rho = \frac{2\beta_n}{n-2} r^{-(n-2)/2}\ , u_0(r) = r^{\frac{1}{2}}\phi(\rho)\ , \tag{4.124}$$

the Eq. (4.123) at $k = 0$ transforms into

$$r^{-\frac{3}{2}} \frac{(n-2)^2}{2^2} \left[\rho^2\phi'' + \rho\phi' - \phi\frac{1}{(n-2)^2}\right] + r^{\frac{1}{2}}\phi\left(\frac{\beta_n^2}{r^n} - \frac{l(l+1)}{r^2}\right) = 0\ . \tag{4.125}$$

Further calculations reveal that this equation is a Bessel-type ordinary differential equation

$$\rho^2\phi'' + \rho\phi' + \phi\left[z^2 - \frac{(2l+1)^2}{(n-2)^2}\right] = 0 \ , \tag{4.126}$$

to which the solutions are two independent functions proportional to the cylindrical Bessel functions $J_\alpha(\rho)$ and $N_\alpha(\rho)$, with $\alpha = (2l+1)/(n-2)$. Hence, the two independent solutions to the radial Schrödinger equation at $k = 0$ with a long-range potential are

$$r^{\frac{1}{2}} J_{(2l+1)/(n-2)}(\rho) \text{ and } r^{\frac{1}{2}} N_{(2l+1)/(n-2)}(\rho) \ . \tag{4.127}$$

The asymptotic form of these solutions for $r \to \infty$ and thus $\rho \to 0$ (restricting $n > 2$) stems from the Frobenius series for the Bessel functions

$$J_\alpha(\rho) = \sum_{m=0}^{\infty} \frac{(-1)^m}{m!\Gamma(m+\alpha+1)} \left(\frac{\rho}{2}\right)^{2m+\alpha} \ , \tag{4.128}$$

and the relation between the Bessel functions of the first and second kind

$$N_\alpha(\rho) = \frac{J_\alpha \cos(\pi\alpha) - J_{-\alpha}(\rho)}{\sin(\pi\alpha)} \ . \tag{4.129}$$

Using the Eqs. (4.128) and (4.129), the definition of ρ in Eq. (4.124) and the Euler reflection formula $\Gamma(\alpha)\Gamma(1-\alpha) = \pi/\sin(\alpha\pi)$, we can finally arrive at the asymptotic form of the solutions for small ρ

$$r^{\frac{1}{2}} J_\alpha(\rho) = \frac{\beta_n^\alpha}{\Gamma(1+\alpha)(n-2)^\alpha} r^{-l} \left[1 - \frac{\beta_n^2}{(n-2)^2(1+\alpha)} r^{-(n-2)} + \mathcal{O}\left(r^{-2(n-2)}\right)\right] , \tag{4.130}$$

$$r^{\frac{1}{2}} N_\alpha(\rho) = -\frac{\Gamma(\alpha)}{\pi} \frac{(n-2)^\alpha}{\beta_n^\alpha} r^{l+1} \left[1 + \underbrace{\frac{\beta_n^2}{(n-2)^2(1-\alpha)} r^{-(n-2)}} + \mathcal{O}\left(r^{-2(n-2)}\right)\right] \ . \tag{4.131}$$

Generally, for $n > 2l+3$ – a condition called *the Wigner threshold law* – it follows that the leading terms in the asymptotic form of $u_0(r)$ are r^{l+1} and r^{-l} just as for the short-range potentials. The usual energy dependence $\delta_l \sim k^{2l+1}$ is then ensured for $k \to 0$. For $n < 2l+3$, the underbraced term in Eq. (4.131) becomes dominant over the r^{-l} term, and the two leading terms in the asymptotic form are r^{l+1} and r^{3+l-n}. Then, the behavior of the phase shift δ_l can no longer be modeled by $\sim k^{2l+1}$ for $k \to 0$ and the definition in Eq. (4.116) does not hold. For $n = 2l+3$, the leading terms in the asymptotic form of $u_0(r)$ are r^{l+1} and $r^{-l}\ln r$ and, again, Eq. (4.116) no longer represents the proper low-energy behavior of δ_l [234].

Let us now consider the case $l = 0$ and $n \geq 4$. We choose $n \geq 4 > 2 \cdot 0 + 3$ to ensure regular behavior, as defined in Eq. (4.116). Eqs. (4.115) and (4.121) become

$$\begin{aligned} u(0) &= 0 \ , \quad u(r) \to \cot\delta_0 \sin(kr) + \cos(kr) \ , \quad r \to \infty \ , \\ u_0(0) &= 0 \ , \quad u_0(r) \to 1 - \frac{r}{a} \ , \quad r \to \infty \ , \end{aligned} \tag{4.132}$$

where $a_0 := a$ is the scattering length. The solutions of the free Schrödinger equation ($V = 0$) for k finite $v(r)$, and $k = 0$ – $v_0(r)$, are given by

$$\begin{aligned} v(r) &= \cot\delta_0 \sin(kr) + \cos(kr) \ , \\ v_0(r) &= 1 - \frac{r}{a} \ . \end{aligned} \tag{4.133}$$

So, we have a set of equations

$$\begin{aligned} u'' + (k^2 - V)u = 0 \ , \quad u_0'' - Vu_0 = 0 \ , \\ v'' + k^2 u = 0 \ , \quad v_0'' = 0 \ . \end{aligned} \tag{4.134}$$

Let us compute the Wronskian

$$\begin{aligned} (uu_0' - u'u_0)' = uu_0'' + u'u_0' - u''u_0 - u'u_0' = uu_0'' - u''u_0 = \\ = u(Vu_0) - (V - k^2)uu_0 = k^2 uu_0 \ . \end{aligned} \tag{4.135}$$

Similarly, it can be shown that

$$(vv_0' - v'v_0)' = k^2 vv_0 \ . \tag{4.136}$$

Combining these two relations yields,

$$\left[(vv_0' - v'v_0) - (uu_0' - u'u_0)\right]_0^\infty = \int_0^\infty k^2(vv_0 - uu_0)\, dr \ . \tag{4.137}$$

The left-hand side of this equation is equal to zero for $r \to \infty$ because the solutions $u(r)$, $u_0(0)$ approach $v(r)$ and $v_0(r)$ as was shown in Eq. (4.132). At $r = 0$, we get

$$u(0)u_0'(0) - u'(0)u_0(0) = 0 \ , \tag{4.138}$$

because $u'(0)$ and $u_0'(0)$ do not diverge and due to boundary conditions shown in Eq. (4.132). Meanwhile the term proportional to v and v_0 is given by

$$v(0)v_0'(0) - v'(0)v_0(0) = 1 \cdot \left(-\frac{1}{a}\right) - (k \cot \delta_0) \cdot 1 = -\frac{1}{a} - k \cot \delta_0 \ . \tag{4.139}$$

Inserting these relations into Eq. (4.137), we get the integral equation showing the $\sim k^2$ behavior of the phase shift δ_0

$$k \cot \delta_0 = -\frac{1}{a} + \int_0^\infty k^2(vv_0 - uu_0)\, dr \ , \tag{4.140}$$

if $V(r)$ tends to zero for $r > r_0$, where r_0 is some finite length-scale. For $k \to 0$, the integral above is non-negligible only for $r \in [0, r_0]$. For $\hbar^2 k^2/(2\mu)$ sufficiently small compared to an average of the potential in the range $r \in [0, r_0]$, we could replace v and u by v_0 and u_0, respectively. We aim to analyze the cases for which such a *shape-independent* approximation can be applied to the exact formula given in Eq. (4.140), i.e., what conditions allow us to define the effective range

$$\frac{1}{2} r_{\text{eff}} = \int_0^\infty (v_0^2 - u_0^2)\, dr \ . \tag{4.141}$$

The shape-independent approximation fails for long-range potentials [234]. The asymptotic behavior of the solution u_0 given in Eq. (4.131) contains constant terms, terms $\sim r$, and terms $\sim r^{-(n-3)}$ (for $n \geq 4$), while v_0 contains only the constant and $\sim r$ terms. Thus, the function $v_0^2 - u_0^2$ will contain terms $\sim r^{-(n-4)}$ and so the shape-independent approximation results in a divergent integral for $n = 4$ (terms proportional to $\sim r^{4-n} \sim r^0$ result in linear divergence) and $n = 5$ (terms proportional to $\sim r^{4-5} \sim r^{-1}$ result in logarithmic divergence). Only sufficiently short-range potentials $n \geq 6$ support a convergent integral.

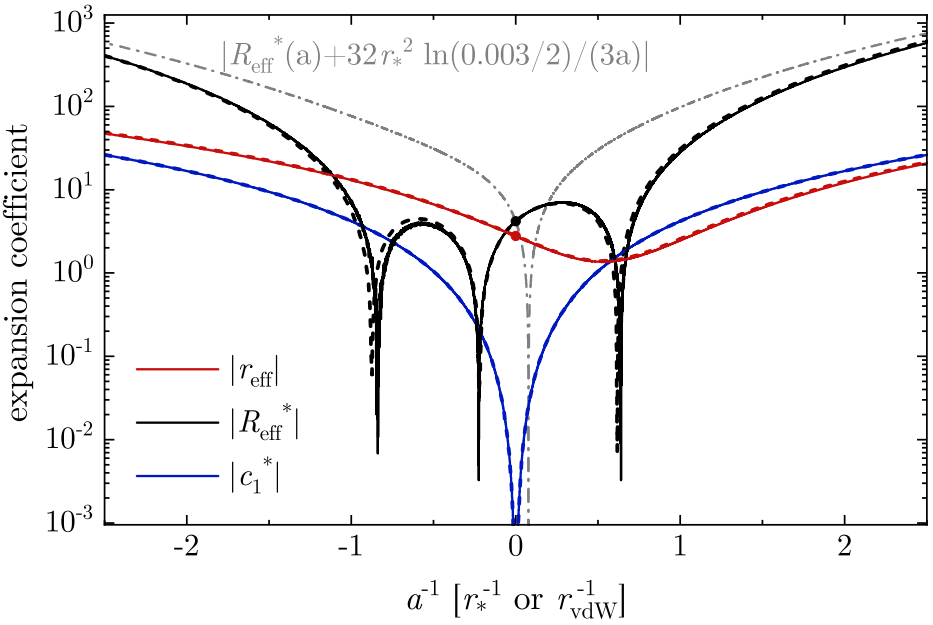

Figure 4.4: The (generalized) effective ranges for the ion-atom (black solid line) and neutral (red solid line) two-body interactions. The coefficient $\sim k$ obtained for the ionic expansion is marked as c_1^* (blue solid line). Dashed lines represent the analytical expressions given by Eq. (34) of Ref. [12] for the neutral interaction (red), the expression for $c_1^*(a)$ (blue), and the expression given by Eq. (4.143), in which we set $r_{\rm eff}^* = 0$ (black) – for the ion-atom interaction. The gray dot-dashed line shows the generalized ionic effective range plus the estimated logarithmic term at $k = 0.003\ r_*^{-1}$. The units $r_{\rm vdW} = (2\mu C_6/\hbar^2)^{1/4}/2$ and $r_* = (2\mu C_4/\hbar^2)^{1/2}/2$ are proportional to the characteristic lengths of interaction for the $n = 4$, and $n = 6$ potentials.

Long-range potentials, like the ones representing the ion-atom induction dominating interaction at $n = 4$, therefore require a more general approach to find the effective range expansion. Terms proportional to $\sim k$ and $\sim k^2 \ln k$ appear in the $k \cot \delta_0$ expansion [234, 235]

$$k \cot \delta_0 = -\frac{1}{a} + c_1^*(a)k + \frac{16 r_*^2}{3a} k^2 \ln\left(\frac{r_* k}{2}\right) + \frac{1}{2} R_{\rm eff}^*(a) k^2 + \mathcal{O}(k^3)\ , \tag{4.142}$$

where $c_1^*(a) = 4\pi r_*^2/(3a^2)$, and where

$$R_{\rm eff}^*(a) = r_{\rm eff}^* + \frac{4\pi r_*}{3} + \frac{160 r_*^2}{9a} - \frac{64\psi\left(\frac{3}{2}\right) r_*^2}{3a} - \frac{16\pi r_*^3}{3a^2} - \frac{32\pi^2 r_*^4}{9a^3}\ , \tag{4.143}$$

is the *generalized* effective range for the ion-atom interaction. In the above equation, we define $r_{\rm eff}^*$ to be the ion-atom effective range. We relate the modifications in the ionic $k \cot \delta_0$ expansion to corresponding changes in the universal theory of few-body collisions arising from long-range interactions.

We present the calculated results for the $k \cot \delta_0$ expansion in Figure 4.4. The coefficients of the effective range expansion are plotted against $1/a$ in units rescaled for both the neutral and charged interactions. These coefficients were obtained by fitting the relevant expression to 40 data points between $k = 0.003\ r_*^{-1}$ and $k = 0.01\ r_*^{-1}$. The results for the $\sim k^2$ coefficient in the case of a neutral interaction closely match the analytical expression reported in Ref. [12].

Likewise, the $\sim k$ coefficient reproduces the expected $\sim 1/a^2$ dependence accurately. For the ion–atom system, the $\sim k^2$ coefficient is obtained by subtracting the $\sim$ ln term from $k \cot \delta_0$ before fitting. Specifically, we evaluate the scattering length at $k = 0.003 r_*^{-1}$, where $k \cot \delta_0$ converges to $-1/a$. The numerical values are compared to Eq. (4.143) under the approximation $r_{\text{eff}} \approx 0$. Any deviations from this formula provide an estimate of the ion–atom effective range. Because the non-linear $\sim$ ln term reduces the numerical stability of the fit, we instead assess its influence by adding it to the $\sim k^2$ coefficient after the fitting procedure. This term has a significant impact on the $\sim k^2$ behavior of the $k \cot \delta_0$ function.

Chapter 5

Weakly bound three-body states in ion-atom-atom systems

This Chapter is based on Ref. [227], to which the author of this thesis made leading and substantial contributions. The author of this thesis performed all numerical calculations using Poland's high-performance computing infrastructure PLGrid (HPC center: ACK Cyfronet AGH), developed data analysis software for accurate interpretation of the results, made all plots, led the scientific discussion, implemented minor modifications to numerical codes developed by Jose D'Incao, and prepared the initial draft of the manuscript.

In this Chapter, we calculate the bound and scattering properties of a system of two neutral atoms and an ion near an ion-atom Feshbach resonance. Our results indicate that long-range ion-atom interactions lead to significant deviations from the universal behavior predicted by contact or van der Waals potentials. We find that ionic systems display an overall suppression of inelastic transitions, leading to recombination rates and lifetimes of the Efimov state that are orders of magnitude larger than those for neutral atoms. We further characterize the dense spectra of triatomic molecular ions with extended lifetimes. Our results provide deeper insight into the universality and structure of three-body ionic systems and establish them as a promising platform for exploring novel few- and many-body phenomena with long-range interactions.

Cold mixtures of laser-cooled ions and atoms provide exceptional opportunities for exploring and controlling quantum systems, enabling precise manipulation of both quantum states and collision dynamics [96, 236]. These hybrid systems have become a cornerstone of quantum science, with applications spanning quantum simulation [98, 99], quantum information processing [100, 237], cold controlled chemistry [102, 104, 105, 117], and few- and many-body quantum physics [106, 238–240]. Recently, ultracold ion-atom mixtures have been realized in the quantum regime [111, 118], enabled by the large mass imbalance between heavy ions and light neutral atoms, which suppresses micromotion-induced heating [116]. This achievement allows controllable interactions near ion-atom Feshbach resonances [109, 111, 241] through tunability of the s-wave scattering length [12], thereby opening new avenues for investigating complex quantum few- and many-body phenomena governed by long-range ion-atom interactions [107, 107, 108, 242–246]. In particular, the possibility of using Feshbach resonances to control the effective ion-atom interaction and to sympathetically cool ions using ion-atom confinement-induced resonances was investigated in Refs. [247, 248].

Building on this progress, it is important to recognize that ultracold gases are intrinsically shaped by few-body processes. Among these, three-body recombination – a fundamental chemical reaction in which three free atoms react to form a diatomic molecule carrying away

the excess energy – is the dominant mechanism driving atomic and molecular losses, thereby limiting both sample lifetimes and achievable densities [110] necessary for the observation of few- and many-body dynamics. Conversely, recombination is not only a loss mechanism but also a powerful diagnostic tool. Its rate and product distribution provide sensitive probes of fundamental quantum effects such as Efimov physics [119, 166, 205, 214], enable detailed studies of state-to-state ultracold chemistry [249–254], and serve as a key method for detecting Feshbach resonances in both neutral and ion-atom systems [12, 111]. This multifaceted role highlights the potential of recombination to reveal crucial aspects of few- and many-body quantum dynamics. The growing ability to control ion-atom systems at ultracold temperatures naturally motivates a closer look at how few-body processes and interactions unfold in the presence of the long-range ion-atom interactions.

Classical and semiclassical theories of ion-atom-atom systems have provided valuable insight into three-body recombination at temperatures well above the quantum regime [112–114, 255–257], establishing a solid foundation for understanding the basic dynamics. With ultracold experiments now pushing deep into the quantum domain, exciting new questions arise that naturally call for a fully quantum-mechanical, non-perturbative description. For instance, while the Efimov universality in heteronuclear, neutral systems – characterized by short-range interactions – is well understood [122, 258], the impact of the long-range ion-atom interaction remains largely unexplored, preventing a deeper insight into the structure and dynamics of strongly interacting ionic few-body systems [259]. Equally compelling are opportunities to map out the influence of the long-range interaction on other non-universal or chemical aspects like the state distribution of diatomic molecular ions produced by recombination [249–253], and the structure and stability of triatomic molecular ions, which can be potentially created in ion-atom systems.

We aim to investigate universal and non-universal aspects of ionic three-body quantum systems composed of two identical bosonic atoms, ^{7}Li, and a heavy ion, ^{138}Ba$^+$. Near an ion-atom Feshbach resonance, we find that the ionic system (LiLiBa$^+$) Efimov physics is also manifested in a universal way, but with the three-body recombination rate, L_3, being strongly suppressed compared to its neutral counterpart (LiLiBa) [122]. We also found that the Efimov states in LiLiBa$^+$ possess lifetimes up to 5 orders of magnitude longer than those of LiLiBa, making them more accessible to experimental observation and manipulation. These results confirm that systems with long-range ion-atom interactions belong to a new class of universality [259]. We also show that the product state distribution of recombination for both ionic and neutral systems follows the same $1/E_b$ propensity rule observed in homonuclear systems [249–253], with no significant preference for forming Li_2 or LiBa molecules. Finally, we characterize weakly bound triatomic molecular ions, confirming the high density of states characteristic of long-range ion-atom interactions. Together, these results provide deeper insight into the universality, stability, and structure of ion-atom systems and establish them as a promising platform for exploring novel few- and many-body phenomena with long-range interactions.

5.1. Ion-atom-atom dynamics

Our investigation of the universality of the ion-atom-atom dynamics begins with the adiabatic hyperspherical representation as described in Chapter 3 [119, 195, 202]. In the hyperspherical representation, the system's internal motion and rotations are described by a set of hyperangles Ω, while its overall size is described by the hyperradius R [119, 195, 202]. Bound and scattering properties of the system are obtained through solutions of the hyperradial

Schrödinger equation

$$\left[-\frac{\hbar^2}{2\mu}\frac{d^2}{dR^2} + U_\nu(R) - E\right] F_\nu(R) + \sum_{\nu'} W_{\nu\nu'}(R) F_{\nu'}(R) = 0 \ , \tag{5.1}$$

where $\mu = (m_B^2 m_X/M)^{1/2}$ is the three-body reduced mass of a system of two identical bosonic atoms, B, and a third dissimilar atom, X, of masses m_B and m_X, respectively, total mass $M = 2m_B + m_X$, and ν represents the set of quantum numbers characterizing each channel. The hyperradial Schrödinger equation (5.1) describes the hyperradial motion governed by the three-body effective potentials $W_\nu(R) = U_\nu(R) + W_{\nu\nu}(R)$ supporting bound and resonant states and non-adiabatic couplings $W_{\nu\neq\nu'}(R)$ driving the inelastic transitions between the different channels. Both U_ν and $W_{\nu\nu'}$ are determined via the solutions of the hyperangular Hamiltonian, containing all the interatomic interactions [119, 195, 202]. In Figure 5.1 we display the adiabatic potentials for the LiLiBa and LiLiBa$^+$ systems relevant to our present study.

Here, we assume the interactions in the three-body system to be a pairwise sum of the interatomic interactions between the identical bosons (in our case, ^{7}Li), v_{BB}, and that between the bosons and the third particle (Ba or Ba$^+$), v_{BX}. In our interaction model, the interaction between identical bosons is given by the Lennard-Jones potential $v_{BB}(r) = -C_6^B/r^6(1 - \lambda_B^6/r^6)$ while for the interspecies interaction it is given either by a Lennard-Jones potential $v_{BX}(r) = -C_6/r^6(1 - \lambda_X^6/r^6)$, in the case of the neutral Li-Ba pair, or by the regularized polarization potential $v_{BX}(r) = -C_4/r^4(1-\lambda_X^4/r^4)$, for the Li-Ba$^+$ pair. Here, C_4 and C_6 are long-range induction and dispersion coefficients [96, 260, 261], r is the interatomic distance, and λ_B and λ_X parameters are adjusted to produce the desired value of the s-wave scattering length as well as the number of bound states each interaction pair can support. For our studies, the interaction between Li atoms, v_{BB}, is set with $\lambda_B \approx 19.58\, a_0$, producing two s-wave Li_2 molecular states and the background scattering length of $-27.3\, a_0$ [262–264], where a_0 is the Bohr radius, while we vary λ_X for v_{BX} to simulate the changes of the interspecies scattering length, a_{BX}, near a Feshbach resonance.

Besides the distinct short- and long-range character of the v_{BX} interaction for neutral and ionic systems, another important distinction is the characteristic length and energy scales defining the onset of universality in the system. While for neutral systems, the relevant scales are determined by the van der Waals length and energy given respectively by $r_{\rm vdW} = (2\mu_{BX}C_6/\hbar^2)^{1/4}/2$ and $E_{\rm vdW} = \hbar^2/(2\mu_{BX}r_{\rm vdW}^2)$, where $\mu_{BX} = m_B m_X/(m_B + m_X)$, for the ionic system they are defined by the polarization length and energy, $r_* = (2\mu_{BX}C_4/\hbar^2)^{1/2}/2$ and $E_* = \hbar^2/(2\mu_{BX}r_*^2)$, respectively. In our system, they are equal to: $r_{\rm vdW} \approx 44.99\ a_0$, $E_{\rm vdW} \approx k_B \times 6409.39\ \mu$K (or $h \times 133.55$ MHz), $r_* \approx 707.03\ a_0$, and $E_* \approx k_B \times 25.95\ \mu$K (or $h \times 0.54075$ MHz), illustrating the disparate length and energy scales relevant for neutral and ionic systems caused by the strong polarization effects. To ensure the proper comparison between neutral and ionic systems, we will express the results for each system in terms of its characteristic length and energy scales wherever appropriate.

For our scattering calculations, we define the three-body recombination constant for a system of two identical bosons at collision energy E as [225],

$$L_3(E) = \sum_J \sum_{f,i} 32\pi^2\hbar \frac{(2J+1)}{\mu k^4} |S_{fi}^J|^2 = \sum_f L_{3f} \ , \tag{5.2}$$

with $k = (2\mu E/\hbar^2)^{1/2}$, f running over all final (atom-dimer) channels, i over the initial (three-body continuum) channels (see Fig. 5.1). Here, L_{3f} is the partial recombination rate into the

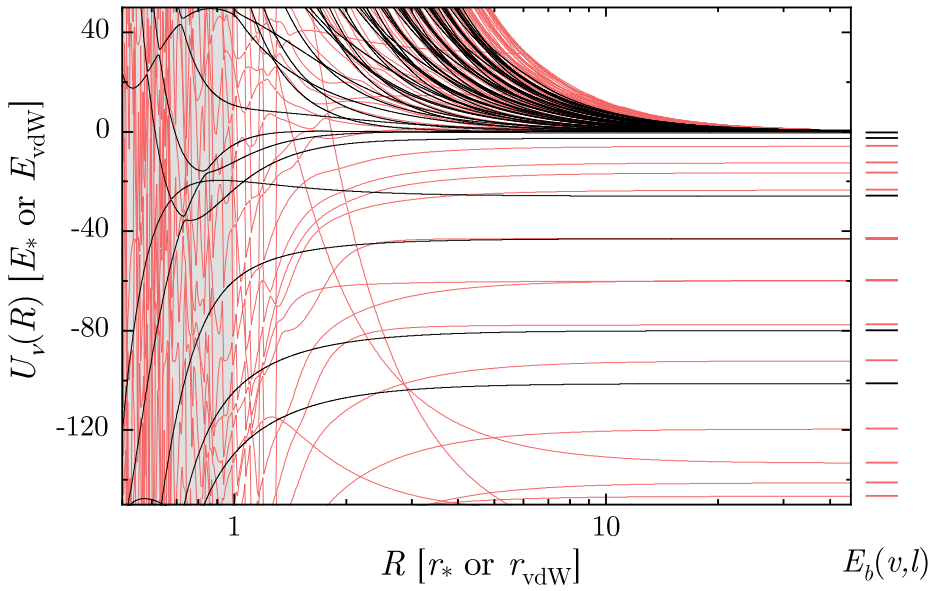

Figure 5.1: The three-body hyperspherical potentials $U_\nu(R)$ for the LiLiBa$^+$ (black) and LiLiBa (red) systems calculated at $a_{BX} = 0.1$ (r_* or $r_{\rm vdW}$) for our interaction model supporting six BX s-wave bound states and two BB s-wave bound states. For large R ($R/r_{\rm vdW} \gg 1$ or $R/r_* \gg 1$), potentials $U_\nu(R) > 0$ correspond to three-body continuum channels, describing collisions between three free atoms, while potentials $U_\nu(R) \simeq -E_b(v,l) < 0$ are atom-molecule channels describing collisions between an atom and a molecule. Here, $E_b(v,l)$ denotes the diatomic molecular binding energies of the rovibrational states of the BX and BB interactions. According to the number of the atom-dimer channels in the figure and considering values of $E_{\rm vdW}$ and E_* in absolute units, we estimate that the density of diatomic states for the ionic systems to be a 100 times larger than for the neutral counterpart.

final state f, and the corresponding S-matrix obtained from the solutions of Eq. (5.1) using the methodology developed in Ref. [202]. For the regime of ultracold collisions ($E \ll E_{\rm vdW}$ or E_*), we only consider the lowest total three-body angular momentum $J = 0$ as higher partial-waves contributions are suppressed in this regime [196, 266].

Figures 5.2(a) and 5.2(b) present the three-body recombination rate, L_3, for LiLiBa (red solid lines) and LiLiBa$^+$ (black solid lines) at collision energy $E/k_B = 0.01\mu$K as a function of the interspecies scattering lengths, a_{BX}. In the figure, we also show the rate $L_3^{\rm w}$ for recombination into the weakly bound Feshbach molecular state ($a_{BX} > 0$) as well as recombination into all other deeply bound states, $L_3^{\rm d} = L_3 - L_3^{\rm w}$. For the ionic system, we use a Li-Li interaction supporting 2 s-wave states while the Li-Ba$^+$ supports 6 s-wave states (for a total of $\sim$10 molecular states). For the neutral system, we use for both Li-Li and Li-Ba interactions that support 2 s-wave states (for a total of $\sim$40 states). For both ionic and neutral systems, we include 50 three-body continuum states in our calculations. We estimate our results to be converged to within 1-2%. In the attempt to gain a better understanding of how recombination proceeds for ionic systems, in the inset of Figs. 5.2(a) and 5.2(b) we show the product state distribution L_{3f}/L_3 in terms of the binding energy of the final molecular state, E_b, for both $a_{BX} > 0$ and $a_{BX} < 0$, respectively. Although for LiLiBa$^+$ there are two types of molecular final products (Li$_2$+Ba$^+$ or LiBa$^+$+Li), our results in the inset of Figs. 5.2(a) and 5.2(b) verifies the same $L_{3f}/L_3 \sim 1/E_b$ propensity rule found for neutral homonuclear ^{87}Rb and ^{85}Rb recombination [249–253], with no preference over Li$_2$ (open symbol) or LiBa$^+$ (closed symbol)

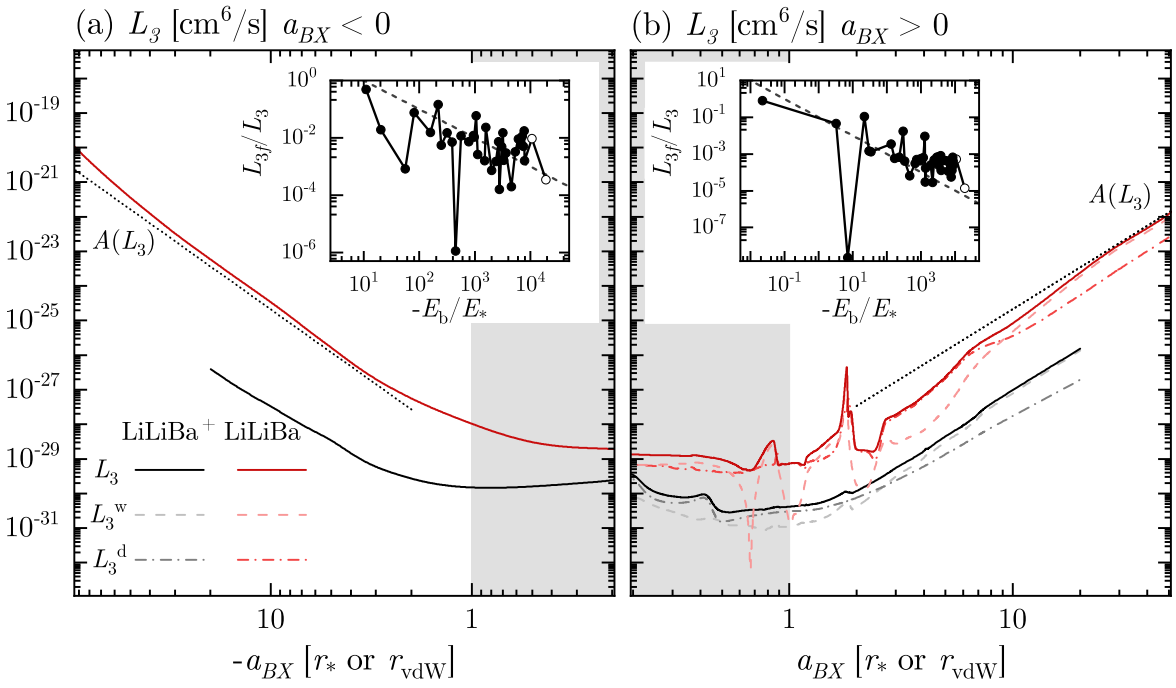

Figure 5.2: (a), (b): Three-body recombination rate L_3 and partial rates $L_3^{\rm w}$ and $L_3^{\rm d}$ for LiLiBa (red) and LiLiBa$^+$ (black). The results for LiLiBa$^+$ recombination are multiplied by $(r_{\rm vdW}/r_*)^4$ in order to properly compare that with recombination of LiLiBa systems. For small values of $|a_{BX}| \lesssim r_*$ (or $r_{\rm vdW}$), L_3 displays resonant effects associated with high-partial waves diatomic molecular states [265], some of which are not resolved in the figure. Dotted lines represent the amplitude for L_3, $A(L_3)$, from the universal theory [122]. The insets of panels (a) and (b) display the product state distribution of LiLiBa$^+$ recombination, L_{3f}/L_3 [see Eq. (5.2)], in terms of the molecular final state binding energy, E_b, displaying the $1/E_b$ propensity rule of Ref. [251].

molecular states. This indicates that the same physical processes found for neutral (homonuclear) systems apply to ionic (heteronuclear) systems despite the highly complex nature of the three-body interactions at short distances ($R \lesssim r_*$ or $R \lesssim r_{\rm vdW}$ in Fig. 5.1).

For large values of $|a_{BX}|$, $|a_{BX}| \gtrsim r_*$ or $r_{\rm vdW}$, Fig. 5.2 shows that L_3 follows the expected a_{BX}^4 scaling behavior [119]. Moreover, in this range of a_{BX}, interference and resonant behaviors are expected. They are associated to the n-th ($n = 0, 1, 2, \ldots$) Efimov state for $a_{BX} = a_+ e^{n\pi/s_0} > 0$ and $a_{BX} = a_- e^{n\pi/s_0} < 0$, respectively [119, 166, 205, 214], with s_0 being the Efimov universal coefficient controlling the strength of the Efimov interaction. As usual, the expected values of three-body parameters $|a_+|$ and $|a_-|$ are typically larger than the characteristic range of the interactions [198]. However, since LiLiBa$^+$ and LiLiBa are both unfavorable mass-imbalanced systems ($m_X/m_B \gg 1$), the Efimov coefficient is small, $s_0 \approx 0.03562$, and geometric scaling extremely large, $e^{\pi/s_0} \approx 2 \times 10^{38}$, in comparison to $s_0 \approx 1.00624$ and $e^{\pi/s_0} \approx 22.7$ for three identical bosons systems. As a result, it is unlikely that such systems will display interference and resonance phenomena for experimentally accessible values of a_{BX}. Nevertheless, universal behavior is still expected for the amplitude of L_3, $L_3^{\rm w}$, and $L_3^{\rm d}$ as shown in Ref. [122]. Such universal results for L_3 (see Section 4.3) depend on the mass ratio m_X/m_B, a_+, a_-, and η, the non-universal inelasticity parameter describing decay to deeply bound molecular states [119, 166]. For the LiLiBa neutral system, our nu-

merical calculations for L_3 agree with the universal results of Ref. [122]. The straight lines in Figs. 5.2(a) and 5.2(b) represent the amplitude of the universal L_3 without the interference and resonant terms (see Section 4.3) and are denoted by $A(L_3)$. From the comparison to the universal results we obtain $a_- \approx 200\, r_{\rm vdW}$, $\eta \approx 0.17$ for $a_{BX} < 0$ and $\eta \approx 0.027$ for $a_{BX} > 0$.

For LiLiBa$^+$, we could not identify any reasonable set of parameters a_+, a_-, and η within the framework of the universal theory [122] that reproduces the recombination amplitude shown in Fig. 5.2. Furthermore, by employing different interaction models for the Li-Ba$^+$ potential – each supporting a different number of bound states – we confirm that our results for the LiLiBa$^+$ system are themselves universal, yet suppressed by a factor of about 250 compared to the corresponding universal predictions of Ref. [122]. We attribute this suppression of inelastic transitions to the difference in how the LiLiBa$^+$ interactions change as R approaches short distances, as compared to the LiLiBa case. As shown in Fig. 5.1, the three-body potentials for LiLiBa$^+$ vary more slowly as approaching short distances than those for LiLiBa, leading to smaller non-adiabatic couplings $W_{\nu\nu'}$ in Eq. (5.1) and suppressing inelastic transitions. We have verified this reduction of non-adiabatic couplings numerically.

Evidently, these findings raise the question of what makes the universality for ionic systems different than that of neutral atoms. In fact, as shown in Ref. [259], systems interacting via $1/r^6$ and $1/r^4$ interactions (in our case, the LiLiBa and LiLiBa$^+$ systems, respectively) belong to different universality classes and are characterized by different values of the universal three-body parameters (e.g., a_-) [267]. Although the universal theory [122] – constructed within the framework of the effective-field theory (EFT) assuming contact, zero-range interactions – does not provide the values of the three-body parameters, they provide universal expressions for L_3 in terms of such three-body parameters, as well as various universal relationships between them. The validity of these expressions has been extensively verified for neutral atomic systems belonging to the $1/r^6$ universality class. Nevertheless, systems within the $1/r^4$ universality class have fundamentally different low-energy properties manifested, for instance, via the effective-range expansion [64, 234, 268, 269]. We provide a detailed analysis of the difference between the effective range expansion for both $1/r^6$ and $1/r^4$ interactions in Section 4.3. Such modifications of the low-energy behavior suggest that changes to the universal EFT are required in order to properly describe the universality of ionic three-body systems, similar to those in Refs. [270, 271], which demonstrate the importance of treating $1/r^6$ and $1/r^4$ interactions within the EFT framework. Our results on the changes observed in our L_3 calculations for neutral and ionic systems, along with the $1/r^4$ universality class studies of Ref. [259], indicate that the ionic nature of the two-body interaction affects not only the universality of the three-body parameter but also the universal collision rates and other universal relationships derived from the EFT framework [122].

5.2. Efimov physics in ion-atom-atom systems

Although both the LiLiBa and LiLiBa$^+$ systems are unfavorable for Efimov physics (due to the value of the Efimov coefficient, $s_0 \approx 0.03562$) our calculations in Fig. 5.3 show that for $a_{BX} > 0$ the Efimov ground state remains bound for values of $a_{BX}/r_{\rm vdW}$ and a_{BX}/r_* much smaller than $e^{\pi/s_0} \approx 2 \times 10^{38}$. This can be explained by the variational principle of Ref. [272], which states that the ground state binding energy of a triatomic molecule can not exceed three times that of the diatomic molecule, preventing the Efimov ground state from crossing the atom-dimer threshold and becoming unbound [273, 274]. In Figure 5.3, we show the diatomic molecular energies of the corresponding Feshbach states, $E^*_{\rm 2b}$ (solid lines), along with the energies $E_{\rm 3b}$ (dashed lines with symbols) and width $\Gamma_{\rm 3b}$ (error bars) of the triatomic

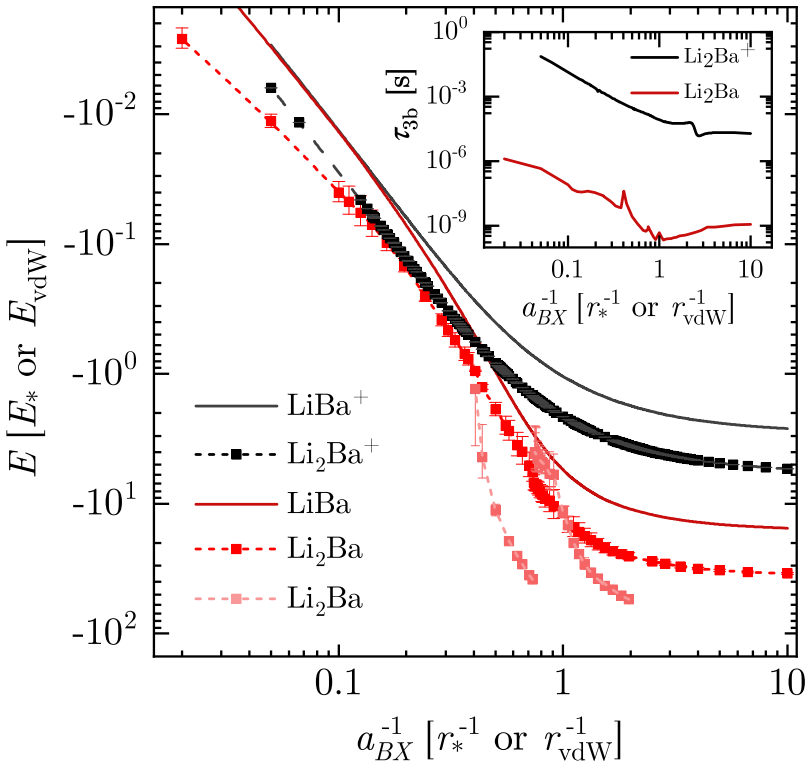

Figure 5.3: Energy of the lowest Efimov state for LiLiBa (red) and LiLiBa$^+$ (black) and the corresponding width Γ expressed as error bars. Two additional trimer states associated with two-body rotational states (pink) [265] are also presented, together with their energies and widths. The inset shows the lifetime $\tau = \hbar/\Gamma$ of the Efimov states for both LiLiBa and LiLiBa$^+$.

molecular states obtained via the time-delay calculations similar to that of Ref. [275]. While the energies of the Efimov ground state for the LiLiBa and LiLiBa$^+$ systems are similar (in relative units), their corresponding lifetime $\tau_{3b} = \hbar/\Gamma_{3b}$ are substantially different. The Efimov LiLiBa$^+$ ground state has a lifetime around 5 orders of magnitude longer than those of LiLiBa [see the inset of Fig. 5.3], with lifetimes as long as 100 ms for the range of a_{BX} shown in Fig. 5.3. The longer lifetimes for LiLiBa$^+$ states can be understood by the combination of their more weakly bound nature compared to the LiLiBa states – determined by the ratio of characteristic energies scales, $E_*/E_{\rm vdW} \approx 4.05 \times 10^{-3}$) – and the suppression by a factor of 250 of the inelastic transitions for LiLiBa$^+$ [see Figs. 5.2(a) and 5.2(b)] thus leading to an overall factor of $E_*/E_{\rm vdW}/250 \approx 1.62 \times 10^{-5}$. Long-lived ground Efimov states in neutral atoms have so far remained elusive, making ionic Efimov states likely to produce interesting regimes in the ultracold ion-atom gas mixture. While ionic Efimov states are extremely weakly bound ($|E_{3b}| \ll E_* \approx 25.95\ \mu$K for LiLiBa$^+$), and difficult to populate due to the yet limited temperature experiments can reach, their extreme large extent, $\langle R\rangle_{3b} \gg r_*$, can exceed the average interatomic distances (approximately 30 r_* for densities around 10^{12} cm^{-3}) potentially leading to novel physical regimes [97–99, 106, 107, 242–244, 276].

To further explore binding phenomena in ionic few-body states, and the differences to neutral atom systems, we also calculated the energy spectrum and the corresponding lifetimes of the triatomic molecular states beyond the energy range relevant for Efimov physics, i.e., $E > E_{\rm vdW} \approx h \times 133.55$ MHz for LiLiBa and $E > E_* \approx h \times 0.54075$ MHz for LiLiBa$^+$.

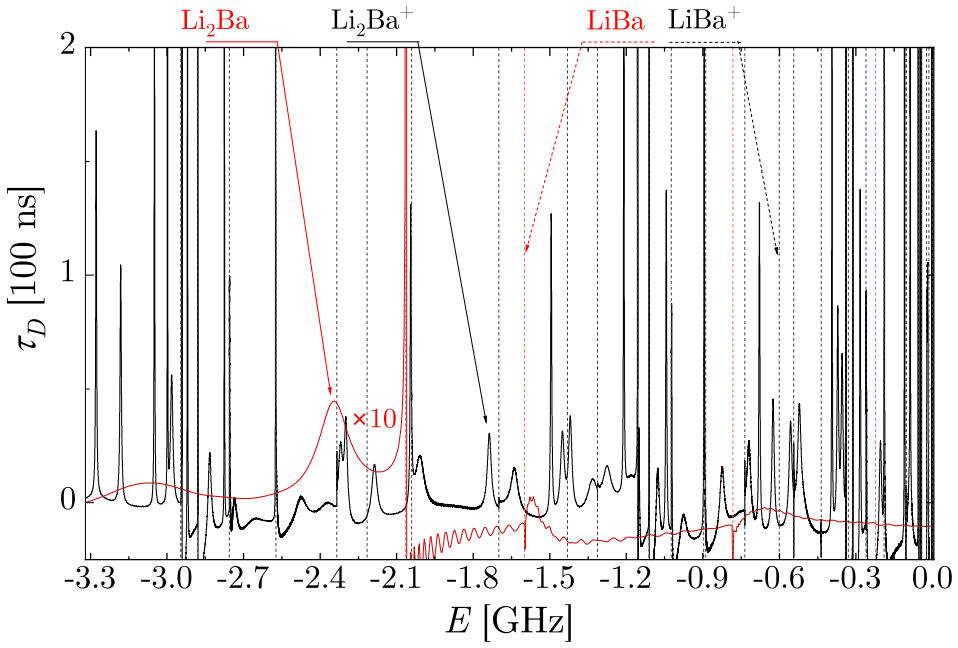

Figure 5.4: The time delay for ^{7}Li^{7}Li^{138}Ba (red) and ^{7}Li^{7}Li^{138}Ba$^+$ (black) calculated for $a_{BX} = 0.1$ (r_* or $r_{\rm vdW}$). The results for the neutral system have been multiplied by a factor of 10. The vertical dashed lines are the energies of two-body molecular states to which the effective potentials $W_\nu(R)$ converge at large values of R. The peaks and width of the time-delay parameter describe the energies and lifetimes of the three-body bound states supported by $W_\nu(R)$.

Figure 5.4 shows our calculations of the time delay $\tau_D(E)$ [275] for a broad range of energies (from 0 to $h \times 3.3$ GHz), with molecular energies E_r determined through the values of E in which $\tau_D(E)$ is maximal, i.e., $d\tau_D(E)/dE = 0$, and corresponding lifetimes given by $\tau_r = \tau_D(E_r)/4$. Figure 5.4 shows that, similar to the diatomic case (see caption of Fig. 5.1), the energy spectrum of triatomic molecular ions (black curve) is also much denser than that of the neutral system (red curve). [Note that in Fig. 5.4 the vertical dashed lines indicate the energy of the LiBa (red) and LiBa$^+$ (black) molecular states.]

Our calculations in Fig. 5.4 show that the Li$_2$Ba three-body molecular states have significantly shorter lifetimes than typical Li$_2$Ba$^+$ molecular states. Notably, certain states in the ionic system are unusually narrow. Such states are characterized by slightly increased lifetimes for lower binding energies, ranging from 1 to 10 μs.

5.3. The three-body recombination

Three-body recombination for $a_{BX} > 0$

The LiLiBa system has a large mass imbalance measured by $\delta = m_X/m_B$, where m_X is the mass of one dissimilar atom X, in our case the Barium atom, while the two Lithium atoms have masses m_B. We modify the implementation of the universal theory to the three-body problem for large scattering lengths to account for the heteronuclear properties of our system. Following Ref. [122], the rate $L_3^{\rm w}$ for recombination into the weakly bound Feshbach molecular

state ($a_{BX} > 0$) is given by

$$L_3^{\mathrm{w}} = 2C(\delta)\frac{D\left(\sin^2[s_0\ln(a_{BX}/a_+)] + \sinh^2(\eta)\right)}{\sinh^2(\pi s_0+\eta) + \cos^2[s_0\ln(a_{BX}/a_+)]}\frac{\hbar a_{BX}^4}{m_X}\ , \tag{5.3}$$

where $D = 128\pi^2(4\pi - 3\sqrt{3})$, a_+ is the three-body parameter ($a_+ > 0$), η is the inelasticity parameter, where $\eta \ll 1$ means low decay probability into deep dimers and $\eta \gg 1$ high decay probability, and the mass-dependent coefficient is denoted by $C(\delta)$. We present results for three-body recombination rates L_3 rather than the event rate constant $\alpha_{\mathrm{w}} = L_3/2$, which takes into account that two identical atoms are taking part in the collision. Ref. [122] provides the analytical formula for the mass coefficient

$$C(\delta) = \frac{(1+\delta)^2\arcsin[1/(1+\delta)] - \sqrt{\delta(2+\delta)}}{2(4\pi - 3\sqrt{3})}\ , \tag{5.4}$$

which is valid for $\delta > 2$. The universal rate for recombination into deep dimers is given by

$$L_3^{\mathrm{d}} = 2C(\delta)\frac{D\coth(\pi s_0)\cosh(\eta)\sinh(\eta)}{\sinh^2(\pi s_0+\eta) + \cos^2[s_0\ln(a_{BX}/a_+)]}\frac{\hbar a_{BX}^4}{m_X}\ . \tag{5.5}$$

For $a_{BX} > 0$, the Efimov state is expected to unbind into the Feshbach dimer at a_+, while successive Efimov levels cross the atom-dimer threshold at scattering lengths that are separated by the universal factor e^{π/s_0}. The interference between the decay pathways produces the characteristic log-periodic suppression of the three-body recombination rate, which is described by trigonometric factors $\sim\sin^2[s_0\ln(a_{BX}/a_+)]$ and $\sim\cos^2[s_0\ln(a_{BX}/a_+)]$. For our heteronuclear system, we obtain $s_0 \approx 0.03562$, corresponding to $e^{\pi/s_0} \approx 2\times 10^{38}$. Consequently, the log-period is very large, and the oscillations are inaccessible within any numerically feasible range of a_{BX}. Furthermore, the value of a_+ cannot be reliably determined in our range of L_3 calculations, because the Efimov trimer actually does not unbind into the atom-dimer threshold – as presented in Fig. 5.3. Thus, we treat the trigonometric factors as effectively constant. We propose that the interference terms $\sim\sin^2[s_0\ln(a_{BX}/a_+)]$ and $\sim\cos^2[s_0\ln(a_{BX}/a_+)]$ are set to 1 and 0, respectively. We emphasize that this approach represents a limiting-case approximation rather than a general prediction. In this way, however, we capture the universal scaling behavior of Efimov-related interferences by introducing a *maximum amplitude* for recombination into a weakly bound Feshbach molecular state, which is given by

$$A(L_3^{\mathrm{w}}) = 2C(\delta)\frac{D\left(1+\sinh^2\eta\right)}{\sinh^2(\pi s_0+\eta)}\frac{\hbar a_{BX}^4}{m_X}\ . \tag{5.6}$$

Similarly, the maximum amplitude for recombination into deep dimers is given by

$$A(L_3^{\mathrm{d}}) = 2C(\delta)\frac{D\coth(\pi s_0)\cosh(\eta)\sinh(\eta)}{\sinh^2(\pi s_0+\eta)}\frac{\hbar a_{BX}^4}{m_X}\ . \tag{5.7}$$

Naturally, the formula for the total recombination rate is therefore given by

$$A(L_3) = A(L_3^{\mathrm{w}}) + A(L_3^{\mathrm{d}})\ . \tag{5.8}$$

We fit the model presented in Eq. (5.8) to our numerical results and estimate the value $\eta \approx 0.027$.

Three-body recombination for $a_{BX} < 0$

For $a_{BX} < 0$, shallow, Feshbach dimers are absent. The atoms can only recombine into deep dimers. Following Ref. [122], the rate constant for the recombination into deep dimers is given by

$$L_3^{\mathrm{d}} = C(\delta)\frac{D\coth(\pi s_0)\sinh(2\eta)}{\sinh^2(\eta)+\sin^2[s_0\ln(a_{BX}/a_-)]}\frac{\hbar a_{BX}^4}{m_X}\ , \tag{5.9}$$

where a_- is the position of the Efimov resonance. Using limited data for the numerically calculated L_3 (obtained up to $|a_{BX}| < 100\ r_{\mathrm{vdW}}$) we give a very rough estimate that $a_- \approx -200\ r_{\mathrm{vdW}}$. Although $|a_-|$ is substantially smaller than a_+, the numerical limit of our calculations does not allow us to confidently include the term $\sin^2[s_0\ln(a_{BX}/a_-)]$ in our model for fitting. Instead, we follow the approach given for $a_{BX} > 0$ and compare our results to the maximum amplitude of the three-body recombination

$$A(L_3) = C(\delta)\frac{D\coth(\pi s_0)\sinh(2\eta)}{\sinh^2(\eta)}\frac{\hbar a_{BX}^4}{m_X}\ . \tag{5.10}$$

The fit of this model to numerical values allows us to approximate the value $\eta \approx 0.17$.

5.4. Mechanism of universality in ion-atom-atom systems

In our studies, we have explored the combination of various LiLi and $LiBa^+$ interaction models supporting different number of s-wave bound states. Although not strictly necessary for universality studies, we chose to display results obtained from the model where the Li-Li and Li-Ba^+ interactions support, respectively, 2 and 6 s-wave states because it more closely represents the real physics of the problem. Due to the largely different characteristic energy scales for the Li-Li and Li-Ba^+ interactions ($E_{\mathrm{vdW}}^{\mathrm{LiLi}}/E_* \approx 10^3$), it takes a Li-$Ba^+$ interaction supporting more states than the Li-Li to provide a similar strength at short distances. This ensures that Li-Li and Li-Ba^+ bound states overlap, leading to deeply bound three-body potentials associated with the $LiBa^+$ dimer channels comparable to those corresponding to the Li_2 dimers.

For universality studies near a Li-Ba^+ Feshbach resonance ($|a_{BX}|/r_* \gg 1$), it is crucial to compare results obtained from Li-Li and Li-Ba^+ model interactions, including different number of bound states, as they produce drastically different short-range physics. In order to further test universality, it is also important to explore Li-Li interaction models producing different scattering lengths, a_{BB}, to understand the impact of the interaction between neutral atoms in an ionic three-body problem.

In Figure 5.5 we provide evidence of $LiLiBa^+$ universality by comparing the energy of the lowest Efimov state obtained from $P_{n_s}P_{n_s^+}$ model interactions supporting different number of Li_2 and $LiBa^+$ s-wave bound states, n_s and n_s^+, respectively. The relative variations between the energies obtained from the two models remains within 2% for the range of scattering lengths shown in Fig. 5.5. We note that both models also present similarly long lifetimes for Efimov states, allowing us to point out the extended lifetimes in the ionic three-body systems as another universal property in the problem. Below, we will present our theoretical understanding of the physics leading to such universal properties while discussing the properties of the three-body effective potentials associated to the Efimov physics.

Similarly, we have investigated manifestations of universality in $LiLiBa^+$ recombination. However, we find that such signatures are considerably more subtle and difficult to realize to the same degree as those observed in the energy spectrum. In Fig. 5.6, we present our

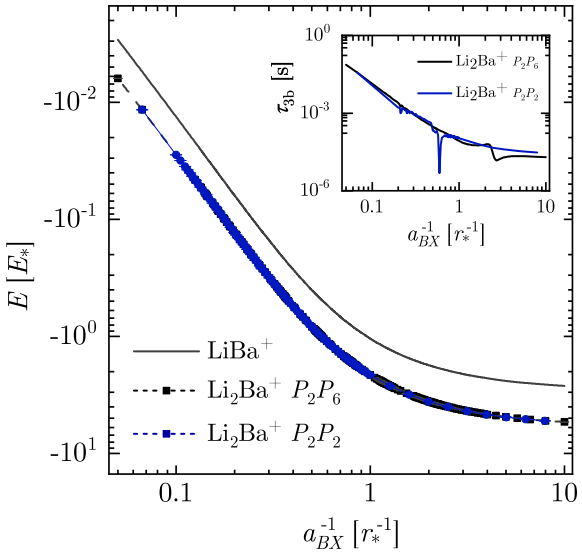

Figure 5.5: Energy of the lowest Efimov state and the corresponding width Γ expressed as error bars for LiLiBa$^+$ calculated for two interacting models supporting m BB s-wave bound states and n BX s-wave bound states – marked 'P_mP_n'. The inset shows the lifetime $\tau = \hbar/\Gamma$ of the Efimov states for LiLiBa$^+$ for both of the interaction models. The perturbation of the lifetime of the Efimov state at $a_{BX} \simeq 1$ is a result of the three-body state interference with a high-partial wave diatomic molecular state.

results for the three-body recombination rate $L_3(a_{BX} > 0)$ obtained from the P_2P_2 and P_2P_6 models, together with the corresponding partial contributions from recombination into the weakly bound LiBa$^+$ s-wave state, L_3^w, and into the remaining deeply bound channels, $L_3^d = L_3 - L_3^w$. While a degree of universality is indirectly reflected in L_3^d, the clearest signatures for $a_{BX} > 0$ emerge through L_3^w, particularly in the limit $\eta \to 0$, where $L_3^d \to 0$. In our calculations, however, $\eta \neq 0$, and although the behavior of L_3 may not appear at first sight as strong evidence of universality, we argue it remains fully consistent with it.

The main challenge in probing universality via L_3 in a system with an unfavorable mass ratio, $m_B/m_X \ll 1$, such as ours, stems from the extremely weak Efimov attraction characterized by $s_0 \approx 0.03562$. This leads to an extraordinarily large geometric scaling parameter, $e^{\pi/s_0} \approx 2 \times 10^{38}$, characterizing the log-periodic occurrence of Efimov features ($a_- < 0$ corresponding to resonances and $a_+ > 0$ to interference minima) in L_3. This has primarily two effects. First, within the framework in which the three-body parameters a_- and a_+ are universally set by the short-range length scale r_* – analogous to the familiar $|a_-| \approx 10\, r_{\rm vdW}$ relation for identical bosons for which $e^{\pi/s_0} \approx 22.7$ – the weakness of the Efimov interaction implies that both a_- and a_+ should likely be expected to occur at values much larger than $10\, r_*$. Second, the enormous scaling factor e^{π/s_0} indicates that the characteristic range in a_{BX} over which a given Efimov feature develops is itself vastly expanded compared to the identical-boson case. Consequently, resolving universal behavior would require variations of a_{BX} over many orders of magnitude.

The limited interval accessible in our calculations ($|a_{BX}| \leq 20 r_*$) is therefore insufficient to clearly reveal such universality. [Note that $|a_{BX}| = 20 r_*$ is by no means small in absolute terms, corresponding to $|a_{BX}| \approx 440\, r_{\rm vdW} \approx 1.4 \times 10^4\, a_0$ where $r_{\rm vdW}$ is the van der Waals length for the Li–Li interaction.] As a result, our calculations explore an extremely small fraction of a period of log-periodic behavior of L_3 and a modest variations of η, represent-

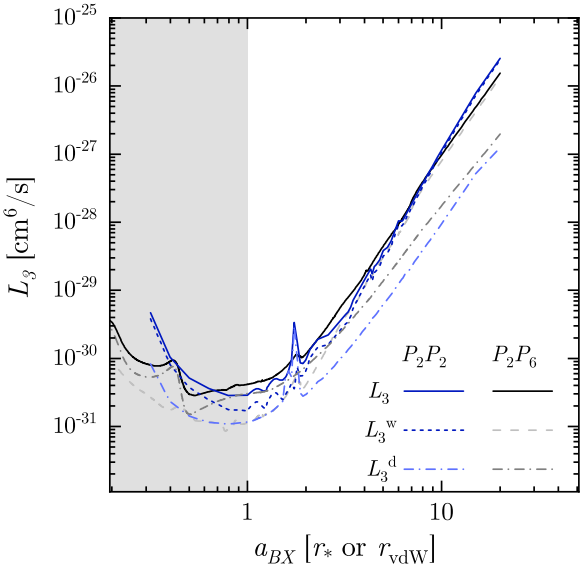

Figure 5.6: (a), (b) Three-body recombination rate L_3 and partial rates $L_3^{\rm w}$ and $L_3^{\rm d} = L_3 - L_3^w$ for LiLiBa$^+$ calculated for two interacting models: P_2P_2 and P_2P_6'. For small values of $|a_{BX}| \lesssim r_*$, L_3 display non-universal resonant effects associated with high-partial waves diatomic molecular states [265], some of which are not resolved in the figure.

ing differences from distinct model interactions, can produce substantial changes within this restricted range of a_{BX}. For instance, using Eq. (5.3) for L_3^w and setting $a_+ = 100r_*$, the values of L_3^w obtained using $\eta = 0.1$ and $\eta = 0.125$ can differ between 42%-76% for values of a_{BX} within the $[r_*,20r_*]$ range, i.e., away from $a_{BX} = a_+$. A much smaller variation in L_3^w is observed for values of $s_0 > 1.00624$ corresponding to the cases with three identical bosons and systems with a favorable mass ratio, $m_B/m_X \gg 1$, thus indicating a stronger sensitivity to η for systems with $m_B/m_X \ll 1$. In this context, we believe the level of variations observed for L_3 shown in Fig. 5.6 is still consistent with universal behavior, although not enough to make a claim nearly as strong as that found for the energies of the Efimov states in Fig. 5.5.

Similar to the universality with neutral atoms, we have found that the hallmark of universality in strongly interacting ionic three-body systems is also a repulsive barrier in the effective three-body potential describing Efimov physics, which prevents atoms from reaching short distances and probing non-universal effects. In Figure 5.7, we demonstrate this and compare the effective potentials $W_\nu(R) = U_\nu(R) + W_{\nu\nu}(R)$ for both LiLiBa (tones of red) and LiLiBa$^+$ (tones of gray) systems with $a_{BX} = \pm\infty$ and a_{BB} set to the Li-Li background value, $a_{BB} = -27.3a_0$. These results were obtained from different model potentials (P_1P_n and P_2P_n, with $n = 1$ to 4) and are presented in relative units. In both neutral and ionic cases there exist a repulsive barrier preventing atoms to approach short distances defined in each case by the corresponding characteristic range of the interactions–$R/r_{\rm vdW} \lesssim 2$ for neutral and $R/r_* \lesssim 2$ for ionic systems.

Although Fig. 5.7 indicates that both strongly interacting neutral and ionic three-body systems are universal, there are a few key differences that make ionic systems unique. It is clear from Fig. 5.7 that the strength of the effective interaction is deeper (in relative units) for neutral atoms than for ionic systems, near the corresponding equilibrium positions, $R \approx 2r_{\rm vdW}$ and $R \approx 2r_*$, respectively. More importantly, neutral potentials change faster than ionic potentials as R approaches short distances. In the adiabatic representation, fast changes

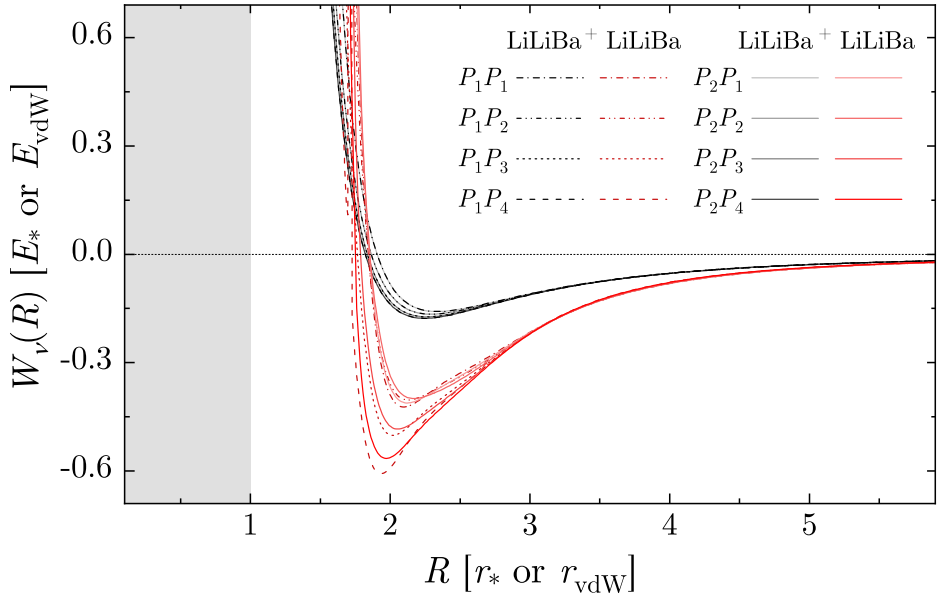

Figure 5.7: Three-body effective potential, $W_\nu(R) = U_\nu(R) + W_{\nu\nu}(R)$, for the Efimov channel at $a_{BX} \to \infty$, for the LiLiBa$^+$ (tones of gray) and LiLiBa (tones of red) systems presented in relative units. The potentials are calculated for P_2P_n interaction models ($n = 1$ to 4). The value of a_{BB} is set to the background scattering length for ^{7}Li atoms ($a_{BB} = -27.3a_0$).

in R are associated with the increase of non-adiabatic effects. In fact, in Fig. 5.8 we show the non-adiabatic effects in the effective potentials $W_\nu(R) = U_\nu(R) + W_{\nu\nu}(R)$ originated from the diagonal non-adiabatic coupling, $W_{\nu\nu}(R)$. This figure clearly shows that three-body interactions $U_\nu(R)$ varies much faster for neutral [Fig. 5.8(a)] than for ionic [Fig. 5.8(b)] systems, which leads to much larger diagonal non-adiabatic couplings $W_{\nu\nu}$.

In fact, since in hyperspherical representation inelastic transitions are driven exclusively from non-adiabatic couplings $W_{\nu\nu'}(R)$ [see: Eq. (3.119)], the suppression of non-adiabatic effects for ionic systems (relative to neutral systems) has a profound impact on various relevant observables. In our case, we are mostly interested in three-body observables for processes that involve the Efimov channel. In particular, the non-adiabatic couplings between this channel and deeply bound diatomic channels control the amplitude of recombination as well as the lifetime of Efimov states. As a result, characterizing such non-adiabatic effects can potentially elucidate important properties of the system. For each pair of channels ν and ν', the strength of the non-adiabatic coupling is characterized by

$$f_{\nu\nu'}(R) = \frac{\hbar^2}{2\mu} \frac{P^2_{\nu\nu'}(R)}{|U_\nu(R) - U_{\nu'}(R)|}, \tag{5.11}$$

where $P_{\nu\nu'}(R)$ is the first-order non-adiabatic coupling [see Eq. (3.120)]. However, for systems containing various bound states, the number of channels that contribute to the inelastic transitions can be quite large. In order to encapsulate the overall effect of all relevant transitions, we define the strength of the non-adiabatic couplings between the Efimov channel, ν, with the deeply bound diatomic channels, ν', by summing over all channels ν',

$$f^d_\nu(R) = \sum_{\nu'} f_{\nu\nu'}(R). \tag{5.12}$$

In Figure 5.9, we show the effective coupling strength, $f^d_\nu(R)$, for both LiLiBa and LiLiBa$^+$

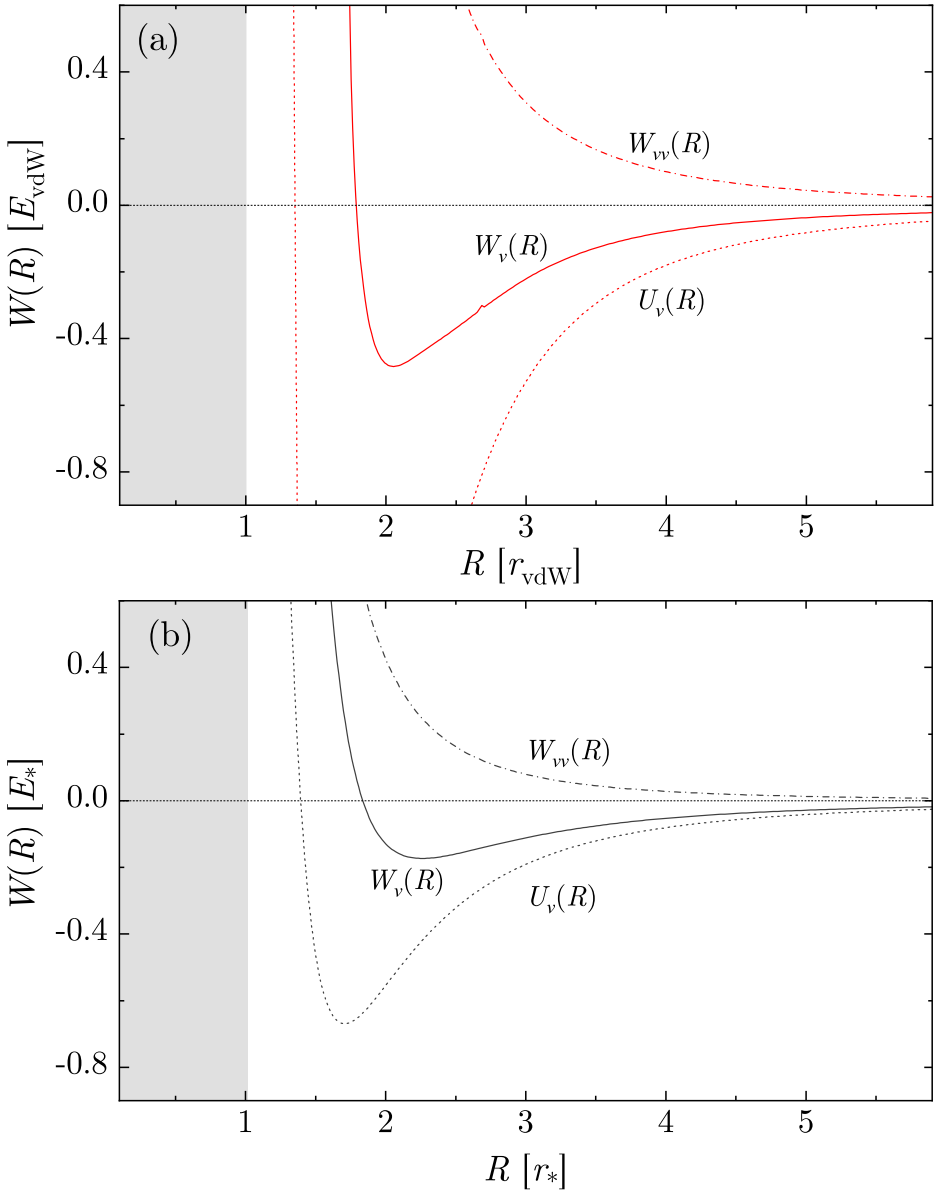

Figure 5.8: The three-body hyperspherical potentials $U_\nu(R)$ and the diagonal parts of the three body effective potential matrix $W_{\nu\nu}(r)$, as well as the three-body effective potentials $W_\nu(R) = U_\nu(R) + W_{\nu\nu}(R)$ for the Efimov channel at $a_{BX} = \pm\infty$, for the (a) LiLiBa and (b) LiLiBa^+ system calculated using the P_2P_3 interaction model.

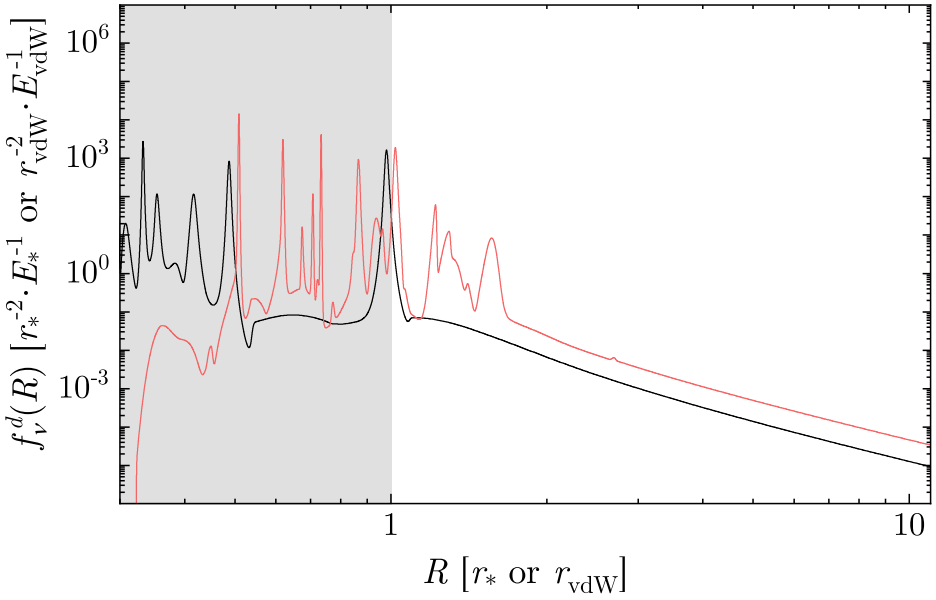

Figure 5.9: The sums of non-adiabatic couplings between the Efimov channel and all deeply bound states $f_\nu^d(R)$ for the LiLiBa (red) and LiLiBa$^+$ (black) systems calculated using the P_2P_3 interaction model.

systems, emphasizing the suppression of non-adiabatic effects for ionic systems. For large values of R, $f_\nu^d(R)$ falls off as $1/R^3$ [277] for both neutral and ionic systems, however, with an amplitude for ionic systems that is a factor 4 smaller than for neutrals. As R approaches short distances, $f_\nu^d(R)$ for neutral systems display various enhancements for $R/r_{\rm vdW} \lesssim 2$ associated to avoided-crossings characteristic of heteronuclear neutral atom systems [278], while $f_\nu^d(R)$ for ionic systems remains smooth, and with a significant smaller amplitude, until $R/r_* \lesssim 1$. While we associate this suppression of non-adiabatic transitions with the long lifetimes for ionic Efimov states, the suppression of the ionic recombination L_3 is likely a combination of changes in the long-range diagonal nonadiabatic coupling [see Figs. 5.8(a) and (b)] and off-diagonal non-adiabatic couplings represented in Fig. 5.9.

It is also crucial to emphasize the role of the intraspecies scattering length a_{BB} in the universal properties of a heteronuclear BBX system with large a_{BX} scattering length. The importance of a_{BB} in neutral atoms systems is a well known result [258, 279, 280] and evidently should play a similar role in our ionic three-body system, LiLiBa$^+$. For neutral atoms BBX systems with strong interspecies vdW interactions, $|a_{BX}| \gg r_{\rm vdW}^{BX}$, universality should in general be determined in terms of characteristic range on the interactions, $r_{\rm vdW}^{BX}$. However, whenever $|a_{BB}| \gtrsim r_{\rm vdW}^{BX}$, BBX universality is expected now to be determined in terms of a_{BB}. In the numerical studies of Ref. [258] [see Fig. 2 of this reference], for instance, noticeable changes on the Efimov states at $a_{BX} = \pm\infty$ are observed for values of $|a_{BB}| \gtrsim 0.26 r_{\rm vdW}^{BX}$, which is a small number (in absolute units).

However, there is a fundamental difference between what is found for neutral atoms and our studies. For ionic systems, universality is set in terms of the characteristic range of the atom-ion (BX) interaction, r_*, which is typically much larger than neutral atoms short-range length scales ($r_{\rm vdW}^{BB}$ or $r_{\rm vdW}^{BX}$). In this case, the expectation is that it would require a larger value for a_{BB} (in absolute units) for changes in universality to take place than what is found for neutral atoms systems. This effect can be seen in Fig. 5.10, where we show the effective potentials for LiLiBa$^+$ with $a_{BX} = \pm\infty$ and different values of a_{BB}, displayed in the figure

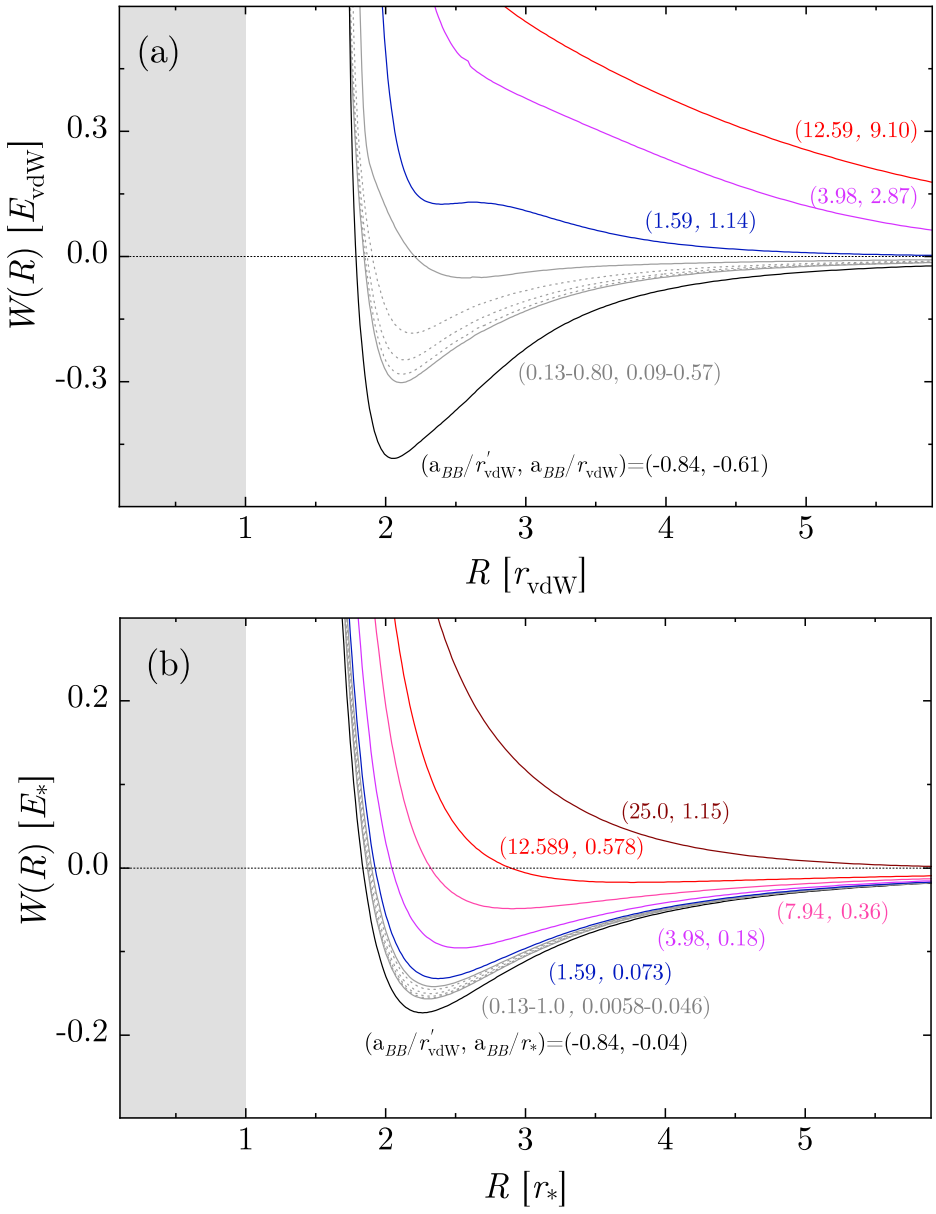

Figure 5.10: Three-body effective potential $W(R)$ for the Efimov channel at $a_{BX} = \pm\infty$, for the (a) LiLiBa and (b) LiLiBa$^+$ system, calculated using the P_2P_3 interaction model. The potentials are calculated for many values of a_{BB} ranging from $-0.84035 r'_{\rm vdW}$ $(-0.039 r_*)$ to $25 r'_{\rm vdW}$ $(1.149 r_*)$, where $r'_{\rm vdW}$ is the van der Waals length related to the BB interaction.

in units of $r_* \approx 707.03a_0$, for the $LiBa^+$ (BX) interaction, and $r_{vdW} \approx 32.8a_0$, for the LiLi (BB) interaction. Figure 5.10 shows that changes beyond 15% on the three-body interactions near its minimum are observed for $a_{BB} \gtrsim 3.981 r_{vdW} = 0.183 r_*$, a point where a_{BB} should become the dominant length scale characterizing universality in the problem. Since changes in the depth of the three-body potentials do not directly translate, for instance, into changes on the energies of the Efimov states [in Ref. [198] it was found that changes of about 30% on the minimum of the potential caused less than 10% variation of the energy of a Efimov state], a more quantitative analysis is required in order to quantify the effects of changes of a_{BB} in the universal properties of the system. Nevertheless, Fig. 5.10 qualitatively shows that a_{BB} also plays a role in the universality in ionic three-body systems, but in a less critical way than found for neutral atoms. While for ionic systems BBX universality is insensitive to the BB interaction for $|a_{BB}| \lesssim r_*$, therefore allowing for large values and variations of a_{BB}, for neutral systems BBX universality is substantially modified for much smaller values of $|a_{BB}| \gtrsim r_{vdW}^{BX}$.

5.5. Summary

In summary, we investigated universal and non-universal aspects of ionic three-body systems composed of two identical bosonic atoms, ^{7}Li, and a heavy ion, $^{138}Ba^+$. We found that near an ion-atom Feshbach resonance, the ionic system ($LiLiBa^+$) exhibits Efimov physics in close analogy to its neutral counterpart (LiLiBa), but with recombination rate, L_3, strongly suppressed compared to the neutral case [122], suggesting that the long-range ion-atom interaction defines a class of universality where both universal three-body parameters [259] and their universal relationships are distinct from universality for neutral atom systems [122]. We characterized the energy and lifetime of Efimov ground state in both $LiLiBa^+$ and LiLiBa systems and found that the lifetime of the ionic Efimov state is five orders of magnitude longer than its neutral counterpart, consistent with the difference of characteristic energy scales (E_{vdW} and E_*) and the suppression factor found for the ionic L_3. We also characterized weakly bound triatomic molecular ions, confirming the expected high density of states characteristic of long-range ion-atom interactions. The generally longer lifetimes of ion-atom-atom systems constitute a key advantage for future experiments, opening new avenues to explore few- and many-body effects in ultracold ion-atom systems.

Chapter 6

Universality near narrow Feshbach resonances

Strongly interacting systems present unique scattering properties reflecting universal weakly bound three-body states – the Efimov states. The existence of such states is a purely quantum phenomenon and has attracted significant theoretical and experimental research interest since its observation in the context of ultracold atomic gases [150]. The theoretical description of Efimov physics and the related few-body dynamics is generally greatly simplified in dilute, resonantly interacting samples. Physical observables such as the energy and lifetimes of the Efimov states exhibit universal behavior, i.e, the described properties are independent of the microscopic details of the system.

The Efimov effect occurs at $|a| \to \infty$, where a is the two-body scattering length. Exactly at unitarity, infinitely many Efimov bound states form as a result of a resonantly induced three-body interaction of the form $\sim -1/R^2$, where R is the hyperradius. Under such conditions, the energies of Efimov states present geometric scaling properties with energies related by the geometric factor $(e^{\pi/s_0})^2 \approx 22.7^2$. As a result, other scattering properties present similar log-periodic behavior to the most notorious case related to the values of $a < 0$ in which a Efimov state becomes bound, $a_-^{(n)}$, causing a resonance in three-body recombination. In this case, all consecutive resonances follow the universal pattern in which each resonance occur a factor 22.7 larger than the previous one, i.e., $a_-^{n+1}/a_-^n = e^{\pi/s_0} \approx 22.7$.

Conditions for Efimov related phenomena require $|a|$ to be much larger than all other length scales of the system, including the characteristic length of interaction, e.g., the van der Waals length r_{vdW} in the case of neutral atoms systems. Efimov states therefore naturally emerge in the vicinity of two-atom Feshbach resonances. Considerable scientific focus, both theoretical and experimental, has recently been placed on the limits of universality of Efimov physics controlled by the fundamental properties of the underlying Feshbach resonances [183, 184], namely, its strength (or width) as characterized by the dimensionless s_{res} parameter [14]. It stems from the van der Waals theory of interactions between two neutral atoms and classifies the basic properties of Feshbach resonances.

Earlier theoretical studies [119, 198, 205, 258, 259, 281–283] have shown that the position of the lowest Efimov resonance is itself universal, $a_-^0 = -9.7\, r_{\mathrm{vdW}}$, which is now known as Efimov-van der Waals (vdW) universality. Although such a universal result is expected only for broad Feschbach resonances ($s_{\mathrm{res}} \gg 1$), experimental measurements, including those for narrow resonances ($s_{\mathrm{res}} < 1$), fell within 20% of this value. As a result, a better understanding of the effects of the width of the Feshbach resonance on Efimov universality is still lacking. In the case of broad resonances, a universal repulsive wall appears in the effective three-body potentials

at $R \approx 2\,r_{\rm vdW}$, tying the universality to long-range behavior of the underlying interaction. However, recent experimental studies [158] have provided evidence that the long-range Efimov interactions indeed depend strongly on the width of the Feshbach resonances; specifically, they lose their universal character as $s_{\rm res}$ becomes smaller. Other experimental studies have also provided conclusive evidence of deviations from the universal value $-9.7\,r_{\rm vdW}$ near an intermediate-strength ($s_{\rm res} \gtrsim 1$) Feshbach resonance in ^{39}K at 33.5820(14) G [184, 284].

In this Chapter, we expand on research on three-body interactions presented in Ref. [158]. Investigating across a range of Feshbach resonance widths, we confirm deviations from vdW universality [183] for narrow ($s_{\rm res} < 1$) resonances by determining the energies of the Efimov trimer in the ground and excited states. Within our framework, these modifications emerge from the appearance of a repulsive interaction in the Efimov channel ($|a| = \infty$) beyond short distances, i.e., $R > 2r_{\rm vdW}$. Our studies are performed with parameters relevant for ^{7}Li atoms, which features a narrow Feshbach resonance at 894 G with $s_{\rm res} \approx 0.493$, but do not restrict them to a fixed value of $s_{\rm res}$.

6.1. The interaction model

We solve the three-body problem by employing the adiabatic hyperspherical representation [202]. Within this framework, the motion of the three-body system can be separated into the hyperradial and hyperangular parts as described in Chapter 3. The hyperradius R determines the overall scale of the system, while the remaining degrees of freedom are captured by a set of hyperangles Ω, which describe both the internal motion and the system's rotations.

Upon rescaling the total wavefunction using the appropriate asymptotics $\Psi = \psi/R^{5/2}$ and separating out the center-of-mass motion, the three-body Schödinger equation can be written in the following form

$$\left[-\frac{\hbar^2}{2\mu}\frac{\partial^2}{\partial R^2} + \hat{H}_{\rm ad}(R,\Omega)\right]\psi(R,\Omega) = E\psi(R,\Omega)\ , \tag{6.1}$$

where the adiabatic Hamiltonian, $\hat{H}_{\rm ad}$, is given by

$$\hat{H}_{\rm ad} = \frac{\Lambda^2(\Omega) + 15/4}{2\mu R^2} + \hat{V}_T(R,\Omega)\ . \tag{6.2}$$

The hyperangular part of the kinetic energy as represented by the grand-angular momentum operator, $\Lambda^2(\Omega)$, and $\hat{V}_T(R,\Omega)$ is the three-body interaction potential.

The adiabatic separability of the hyperradial and hyperangular motion of the three-body system allows us to impose the adiabatic expansion on the total wavefunction

$$\psi_\nu(R,\Omega) = \sum_\nu F_\nu(R)\Phi_\nu(R;\Omega)\ , \tag{6.3}$$

where $F_\nu(R)$ are the hyperradial wavefunctions, $\Phi_\nu(R;\Omega)$ are the channel functions, and ν represents the set of quantum numbers describing each channel. The channel functions form an orthonormal basis of the expansion and are the solutions of the adiabatic equation

$$\hat{H}_{\rm ad}\Phi_\nu(R;\Omega) = U_\nu(R)\Phi_\nu(R;\Omega)\ , \tag{6.4}$$

at fixed R, where $U_\nu(R)$ are the three-body hyperspherical potentials.

Using the adiabatic expansion, we obtain the hyperradial Schrödinger equation. It is a set of coupled differential equations, which allow us to find the hyperradial wavefunctions $F_\nu(R)$

$$\left[-\frac{\hbar^2}{2\mu}\frac{d^2}{dR^2} + U_\nu(R) - E\right] F_\nu(R) + \sum_{\nu'} W_{\nu\nu'}(R) F_{\nu'}(R) = 0 \ . \tag{6.5}$$

The hypperradial Schrödinger equation describes the motion of the three-body system governed by the three-body effective potential matrix $W_{\nu\nu'}(R)$ defined by

$$W_{\nu\nu'}(R) = 2P_{\nu\nu'}(R)\frac{d}{dR} + Q_{\nu\nu'}(R) \ . \tag{6.6}$$

The derivative, non-adiabatic, couplings $P_{\nu\nu'}(R)$ and $Q_{\nu\nu'}(R)$ are given by

$$\begin{aligned} P_{\nu\nu'}(R) &= -\frac{\hbar^2}{2\mu}\left\langle \Phi_\nu(R) \middle| \frac{\partial \Phi_{\nu'}(R)}{\partial R} \right\rangle \\ Q_{\nu\nu'}(R) &= -\frac{\hbar^2}{2\mu}\left\langle \Phi_\nu(R) \middle| \frac{\partial^2 \Phi_{\nu'}(R)}{\partial R^2} \right\rangle \end{aligned} \ , \tag{6.7}$$

where the brackets denote integrating over the hyperangles. The first derivative coupling is zero, $P_{\nu\nu}(R) = 0$, for $\nu' = \nu$ due to the orthonormality of the channel functions $\Phi_\nu(R)$. Thus, the diagonal part of the $W_{\nu\nu}(R)$ matrix is equal to the non-adiabatic coupling $Q_{\nu\nu}(R)$.

The potential operator is defined in terms of a pairwise sum

$$\hat{V}_T(R,\Omega) = \hat{V}(r_{12}) + \hat{V}(r_{23}) + \hat{V}(r_{31}) \ , \tag{6.8}$$

where r_{ij} is the interparticle distance for an atom pair ij, and $\hat{V}$ is the corresponding pairwise interaction. We introduce the interaction potential in a way that allows us to model the Feshbach resonance between two two-body spin channels. Therefore, we use a two-channel model of the interatomic interactions

$$\hat{V}(r) = \begin{pmatrix} v_{\mathrm{bg}}^{\mathrm{O}}(r) & v_{\mathrm{c}}(r) \\ v_{\mathrm{c}}(r) & v_{\mathrm{bg}}^{\mathrm{C}}(r) + \Delta E(B) \end{pmatrix} \ . \tag{6.9}$$

The background interaction potential $v_{\mathrm{bg}}^{\mathrm{O/C}}$ characterizing the open and closed channels is described by the Lennard-Jones potential, modeling van der Waals forces for the open – O and closed – C channels

$$v_{\mathrm{bg}}^{\mathrm{O/C}}(r) = -\frac{C_6}{r^6}\left(1 - \frac{\left(\lambda_{\mathrm{bg}}^{\mathrm{O/C}}\right)^6}{r^6}\right) \ . \tag{6.10}$$

The open and closed channels are coupled through a coupling function

$$v_{\mathrm{c}}(r) = \alpha \exp\left[-\frac{(r-\beta)^2}{2\gamma^2}\right] \ . \tag{6.11}$$

where α is the coupling's *amplitude* measured in van der Waals energy, β is the coupling position and γ – the width of the Gaussian function. We note that order to produce a sensible model in which s_{res} can be be properly tuned, a number of considerations have been taken into account. For instance, if γ is too small, the coupling is highly localized in r, reducing the effective overlap between channels and limiting the ability to tune the resonance through α; on

the other hand if γ is too large, the coupling becomes overly delocalized, leading to excessive open-close channel mixing and preventing an accurate description of the properties of narrow resonances. We have found that the value $\gamma = 0.05\, r_{\rm vdW}$ allows for the accurate reproduction of the resonance behavior in all ranges of the $s_{\rm res}$. We set β at the minimum of the closed-channel potential, where the bound-state wavefunction is largest, thereby maximizing the interchannel overlap and enhancing the resonance. The background interaction between ^{7}Li atoms is set with background scattering length of $-27.3\, a_0$ [262–264], where a_0 is the Bohr radius, while we use various values of $\lambda_{\rm bg}$ for either channel as described in more detail below. To simulate the changes of the scattering length, a, near a Feshbach resonance, we vary the B-field dependent energy difference between the open and closed channels given by

$$\Delta E(B) = \varepsilon + \delta u B \ , \tag{6.12}$$

where we use exemplary values $\varepsilon = 2\ E_{\rm vdW}$ and $\delta u = 8 \cdot 10^{-3} E_{\rm vdW}/{\rm G}$. We should note, however, that the physical properties of the Feshbach resonance are dependent only on the relative comparison between the energy shift ε, the Zeeman energy $\delta u B$, and the energy scales defining the coupling strength.

6.2. The tuning of the $s_{\rm res}$ parameter

The properties of a magnetically tuned Feshbach resonance are characterized by the background scattering length $a_{\rm bg}$, the resonance position B_0, the magnetic width Δ, and the differential magnetic moment $\delta\mu$, which together provide a complete description of the low-energy scattering behavior near the resonance [12, 52]. The background scattering length captures the open-channel physics in the absence of the resonance and is therefore determined solely by the underlying interatomic potential of the entrance channel. As we mentioned above, a crucial derived quantity is the dimensionless resonance strength parameter $s_{\rm res}$, which quantifies the relative importance of open- and closed-channel contributions and allows one to classify resonances as open-channel dominated ($s_{\rm res} \gg 1$) or closed-channel dominated ($s_{\rm res} \ll 1$) as defined by theory in Ref. [285].

To understand the non-universal behavior of the Efimov effect, we must tune the $s_{\rm res}$ parameter by changing the amplitude of the off-diagonal couplings defined in Eq. (6.11). For a given value of α, we solve the two-body Schrödinger equation and compute the scattering observables from the resulting wavefunctions, based on the interaction model given in Eq. (6.9). We then analyze the scattering length $a(B)$ near the resonance position B_0, where it is expected to follow the function

$$a(B) = a_{\rm bg}\left(1 - \frac{\Delta}{B - B_0}\right). \tag{6.13}$$

To extract the resonance parameters, we use the transformed quantities $x(B) = B - B_0$, $y(B) = a(B)(B - B_0)$ and perform a linear fit of y as a function of x. From the fitted slope $a_{\rm bg}^{\rm fit}$, where we use the superscript to distinguish this quantity from the initial background scattering length, and intercept $-a_{\rm bg}\Delta$, we determine the background scattering length and the $s_{\rm res}$ parameter using the relation [12]

$$s_{\rm res} = a_{\rm bg}\Delta\frac{\delta u}{\bar{a}\bar{E}} \ , \tag{6.14}$$

where $\bar{a} = 4\pi/\Gamma(1/4)^2\, r_{\rm vdW}$ is the *mean* scattering length, and $\bar{E} = \hbar^2/(2\mu\bar{a}^2)$ is the corresponding energy scale [12].

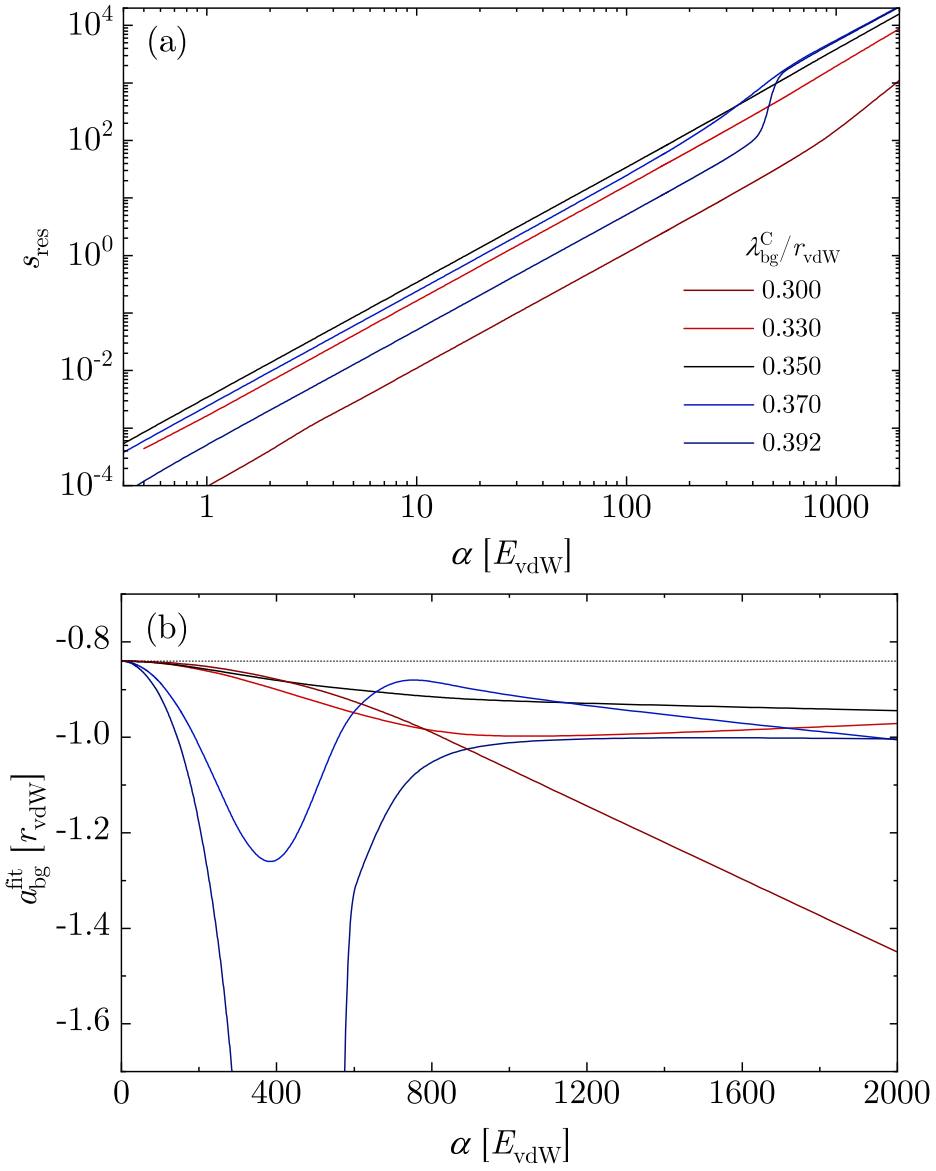

Figure 6.1: (a) The resonance strength parameter s_{res} and (b) the fitted background scattering length $a_{\mathrm{bg}}^{\mathrm{fit}}$ for a model supporting three s-wave bound states in the open channel, as defined by Eq. (6.10), with $\lambda_{\mathrm{bg}}^{\mathrm{O}} = 0.392805\, r_{\mathrm{vdW}}$. The closed channel supports $m \geq 3$ bound states. Results are shown for models with increasing values of $\lambda_{\mathrm{bg}}^{\mathrm{C}}$. The black dotted line indicates the initial background scattering length for ^{7}Li, $a_{\mathrm{bg}} = -0.84035\, r_{\mathrm{vdW}}$.

When constructing the interaction model at unitarity, the number of two-body s-wave bound states in both open and closed channels must be considered. In Efimov physics, the presence of deeply bound states can modify the short-range three-body phase and consequently influence the three-body parameter [184, 198]. Thus, we consider interaction models denoted '$P_nP_m(v)$' – supporting n and m s-wave bound states in the open and closed channels, respectively. The open and closed channels are defined such that, in the absence of coupling, they reproduce the background scattering length a_{bg}. The closed-channel bound states are labeled by v, with $v = -1$ denoting the least-bound state. In this work, we use $v = -2$

because the least-bound state ($v = -1$) can be strongly affected by threshold effects, while more deeply bound states are dominated by short-range physics. Figure 6.1 presents the s_{res} parameter and the $a_{\mathrm{bg}}^{\mathrm{fit}}$ as a function of the coupling amplitude α. The discrepancy between the fitted background scattering length $a_{\mathrm{bg}}^{\mathrm{fit}}$ and the initial value for ^{7}Li, $a_{\mathrm{bg}} = -0.84035\, r_{\mathrm{vdW}}$, results from *coupling-induced* resonances. These resonances emerge when the coupling $v_c(r)$ mixes open- and closed-channel components of the system's eigenstates, producing hybridized states that manifest as resonances in the scattering observables.

The coupling-induced states modify the background scattering properties. As the parameter α increases – both the resonance width Δ and the magnetic-field range B over which the main resonance ($v = -2$) dominates the scattering – also increase. This results in an overlap between features of the main resonance and those associated with the coupling-induced states. The resonance width is proportional to the square of the coupling matrix element, specifically the overlap integral between the coupling function and the scattering and bound-state wavefunctions [12]. Figure 6.1(a) demonstrates the relationship between coupling-induced perturbation and the approximate $\sim \alpha^2$ scaling of the parameter s_{res}. The most pronounced features occur for $\lambda_{\mathrm{bg}}^{\mathrm{C}} = 0.392\, r_{\mathrm{vdW}}$ at $\alpha \approx 400\, E_{\mathrm{vdw}}$. The behavior of $a_{\mathrm{bg}}^{\mathrm{fit}}$ presented in Fig. 6.1(b) does not show any monotonic dependence on $\lambda_{\mathrm{bg}}^{\mathrm{C}}$. Therefore, to provide a more accurate representation of the background physics, the $P_nP_m(v)$ interaction models are modified. The open channel, in the absence of coupling, still reproduces the background scattering length a_{bg}. Meanwhile, the short-range physics of the closed channel is tuned by decreasing $\lambda_{\mathrm{bg}}^{\mathrm{C}}$, which results in increasing the number of s-wave bound states in the closed channel. Consequently, what we called the $v = -2$ state beforehand, becomes a state characterized by a quantum number $v < -2$. Nevertheless, the same state is used to ensure unitarity at resonance for any value $\lambda_{\mathrm{bg}}^{\mathrm{C}}$. Eventually, the model is specified by a value of $\lambda_{\mathrm{bg}}^{\mathrm{C}}$ selected to ensure that $a_{\mathrm{bg}}^{\mathrm{fit}}$ deviates from a_{bg} by no more than 5% across the entire range of α. The corresponding parameter values $\lambda_{\mathrm{bg}}^{\mathrm{O/C}}$ are listed in Table 6.1. We denote the modified models as $P_nP'_m(v)$. In the absence of coupling, they support n s-wave bound states in the open-channel and m' s-wave bound states in the closed channel, where $m' \geq m$.

Table 6.1: The value of open and closed channel parameters $\lambda_{\mathrm{bg}}^{\mathrm{O}}$ and $\lambda_{\mathrm{bg}}^{\mathrm{C}}$ determining the short-range physics of the interaction potential defined in Eq. (6.10).

Model	$\lambda_{\mathrm{bg}}^{\mathrm{O}}/r_{\mathrm{vdw}}$	$\lambda_{\mathrm{bg}}^{\mathrm{C}}/r_{\mathrm{vdw}}$
$P_2P'_2(-2)$	0.465470	0.397
$P_3P'_2(-2)$	0.392804	0.350
$P_3P'_3(-2)$	0.392804	0.294
$P_4P'_2(-2)$	0.346119	0.300
$P_4P'_3(-2)$	0.346119	0.270
$P_4P'_4(-2)$	0.346119	0.250

6.3. The Efimov spectrum

To investigate the universality of Efimov physics at unitarity, we calculated the energy spectrum and corresponding lifetimes of Efimov states for homonuclear bosonic systems. These observables were obtained from the time delay $\tau_D(E)$ [275], evaluated over the energy range $E \in [-10\, E_{\mathrm{vdW}}, 0\, E_{\mathrm{vdW}}]$. Bound-state energies E_b were identified as the energies E, where $\tau_D(E)$ is maximal, i.e., where $d\tau_D(E)/dE = 0$. The lifetimes are equal to $\tau_r = \tau_D(E_b)/4$.

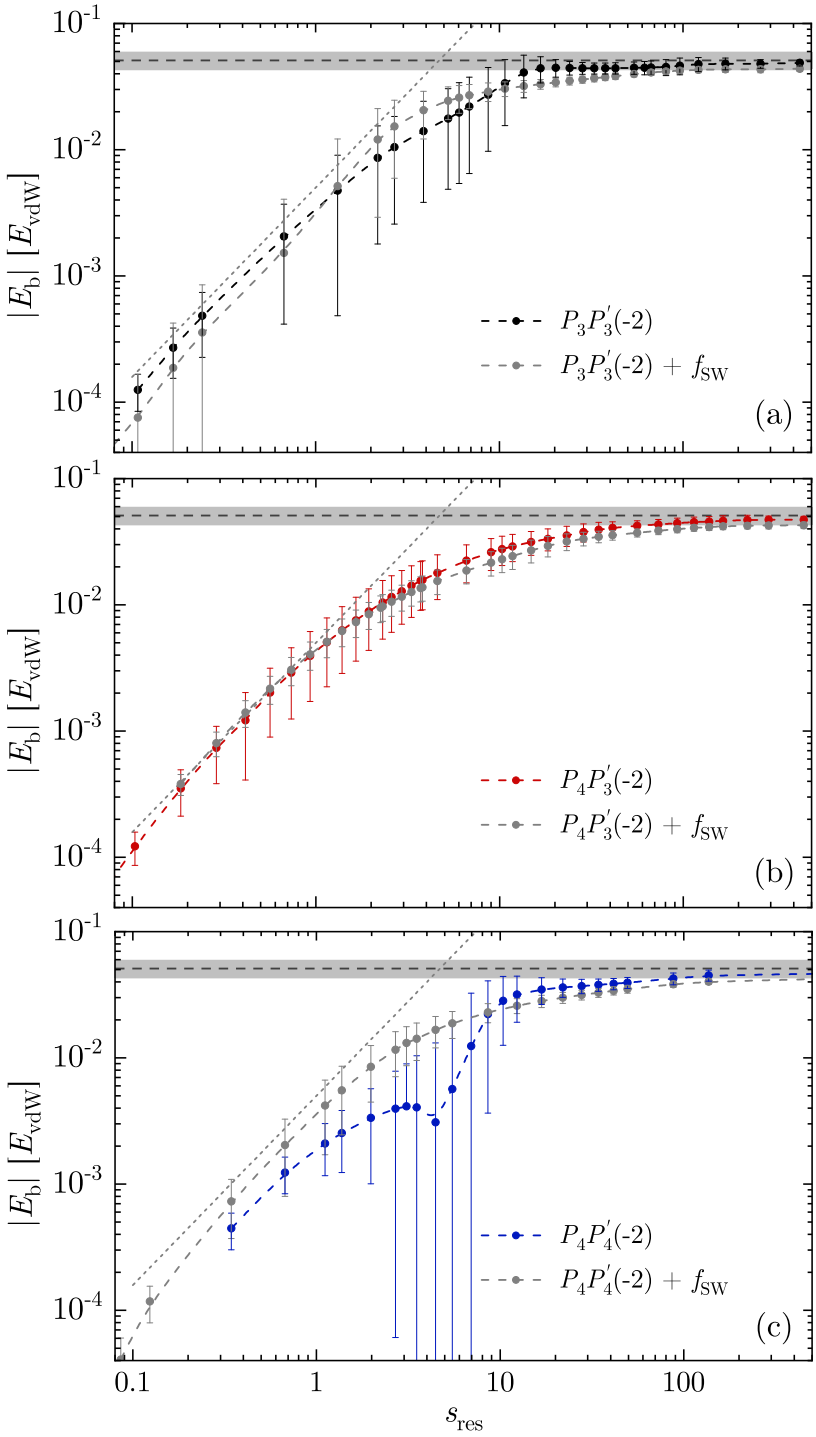

Figure 6.2: The binding energies of the ground Efimov states and their corresponding widths Γ expressed as error bars calculated using the (a) $P_3P_3'(-2)$, (b) $P_4P_3'(-2)$ and (c) $P_4P_4'(-2)$ models. Gray points and error bars show the Efimov states obtained using the corresponding model with the added soft-wall potential f_{SW}. The dark gray, dashed line shows the universal limit of the energy of the ground Efimov state [198], while the light gray shaded region indicates a $\pm 15\%$ range. The light gray, dashed line shows the power-law dependence $\sim s_{res}^{3/2}$, which matches the results obtained in Ref. [286]. Dashed lines between the points are guides to the eye.

.

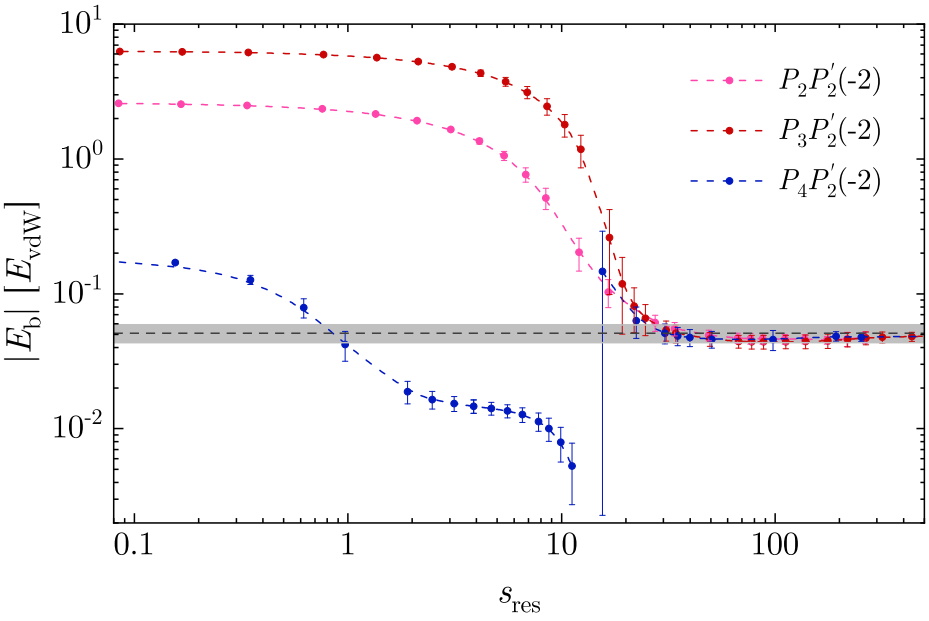

Figure 6.3: The binding energies of the ground Efimov states and their corresponding widths Γ expressed as error bars calculated using the $P_2P_2'(-2)$, $P_4P_2'(-2)$ and $P_4P_2'(-2)$ models.

Figure 6.2 illustrates that, for interaction models supporting a sufficiently large number of two-body s-wave bound states, the results agree with those obtained using the modified zero-range approach of Ref. [286]. As shown in Figs. 6.2(a)-(c), in the non-universal regime ($s_{res} \lesssim 1$) the Efimov states binding energy decreases and their lifetime is reduced. This behavior is associated with an effective repulsive contribution in the Efimov channel that emerges at hyperradii $R \gtrsim 4\, r_{vdW}$ for narrow resonances [158].

Figure 6.2(a) and 6.2(c) further show deviations from universal behavior for both narrow ($s_{res} \ll 1$) and intermediate ($s_{res} \sim 1$) Feshbach resonance widths. These deviations manifest as shifts in the Efimov binding energies and a reduction in lifetimes, which in some cases almost leads to the disappearance of the Efimov state. The mechanism behind the unbinding of the Efimov states is a strong coupling of the Efimov state with the continuum. The models display a non-monotonic dependence on the resonance strength. The strongest reduction in lifetimes are observed at $s_{res} \sim 1$ for the $P_3P_3'(-2)$ interaction model and at $s_{res} \sim 5$ for the $P_4P_2'(-2)$ interaction model.

To understand the origin of these non-universal effects, we introduce a probing scheme in which an additional repulsive three-body interaction is applied to all hyperspherical potentials $U_\nu(R)$. This interaction is implemented using a soft-wall potential of the form

$$f_{SW}(R) = E_{SW}\left[1 - \left(\tanh\left(\frac{R}{R_0}\right)\right)^{12}\right]^{12}. \tag{6.15}$$

The barrier position is set to $R_0 = 1.25\, r_{vdW}$ and the amplitude to $E_{SW} = 10\, E_{vdW}$. At $R \approx 2\, r_{vdW}$, where an effective repulsive potential arises due to deformation of the three-body configuration and which ensures the universality of Efimov physics [198], the soft-wall potential remains non-negligible, with $f_{SW}(R) \approx 0.035\, E_{vdW}$. As a result, a small shift in the Efimov binding energy is observed even in the universal regime ($s_{res} \gg 1$), as shown in Fig. 6.2.

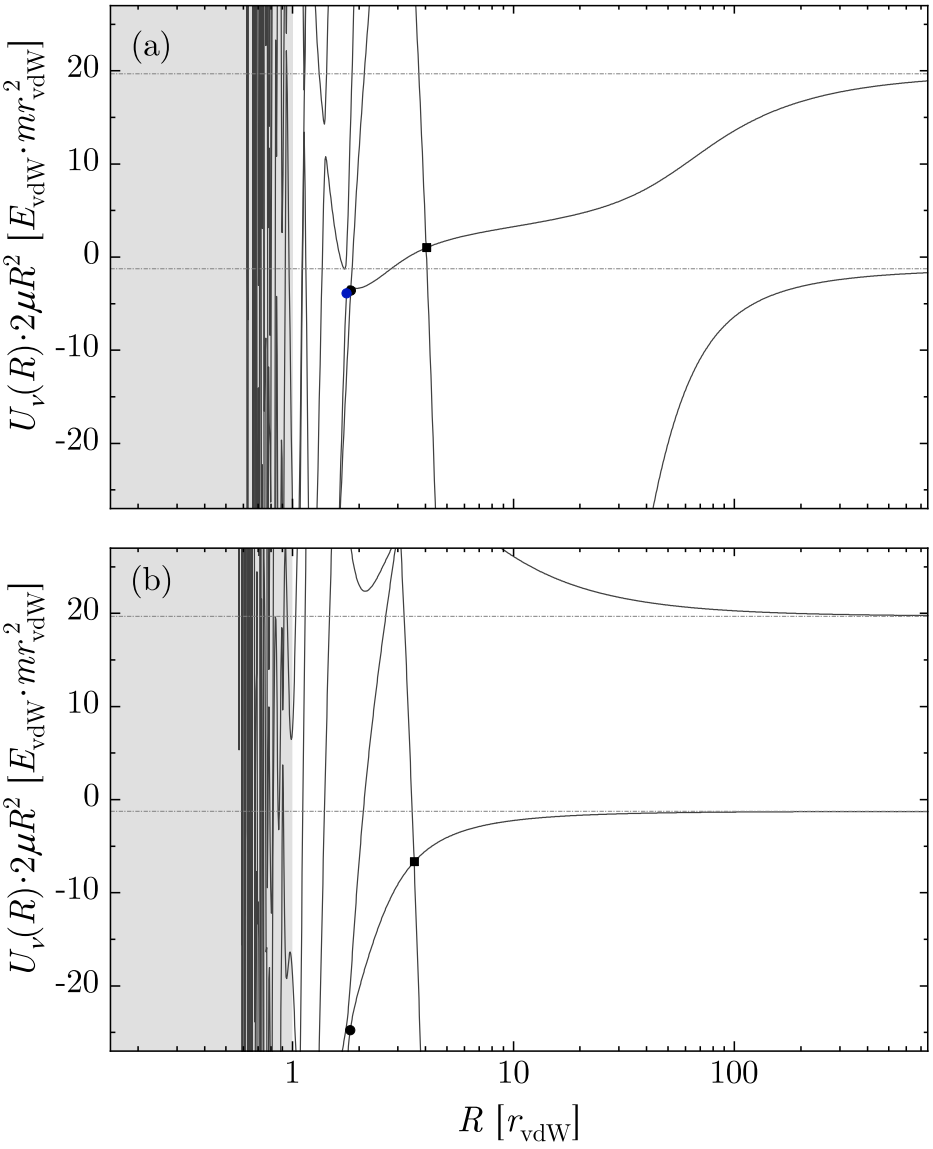

Figure 6.4: The three-body hyperspherical potentials $U_\nu(R)$ multiplied by the factor $2\mu R^2$ calculated for (a) $s_{\rm res} \approx 0.67$ and (b) $s_{\rm res} \approx 264.0$ for the $P_3P_3'(-2)$ interaction model. The symbols show the position of the avoided crossings between the atom-molecule channel describing the: $l = 2$ open-channel (■, black), $l = 4$ open-channel (•, black), $l = 2$ closed-channel (•, blue) molecular bound-state and the (a) first-continuum, (b) the Efimov channel. The gray, dot-dashed lines show the asymptotic quantum numbers characterizing the effective potentials at large R, namely $-(s_0^2+1/4) \approx -(1.0062378+1/4)$, and $(s_1^2+1/4) \approx (4.4652946+1/4)$ [119].

The soft-wall potential suppresses access of the Efimov state to the short-range, where non-adiabatic couplings appear due to multiple avoided crossings. The couplings enhance decay into deeply bound states and therefore reduce the lifetime of the Efimov states. Thus, we observe that soft-wall models display longer lifetimes by a factor of $1.5 - 2.5$. Furthermore, in Fig. 6.2 we show that for all investigated models, the non-universal effects are absent, indicating that they arise from short-range non-adiabatic effects.

Figure 6.3 shows that, in the non-universal regime, Efimov states can transition through a

classically forbidden region stemming from the repulsive interaction and continuously evolve into a short-range deeply bound trimer state. In all investigated models, $P_n P_2'(-2)$ for $n \in 2, 3, 4$, a Feshbach resonance arises from coupling between the scattering state in the open channel and the ground bound state of the closed channel. As a result, closed-channel contributions play a significant role in the three-body dynamics. The resonant, closed-channel bound-state is localized in the short-range, which further increases its coupling with the potentials there. The non-universal perturbations appear for the $P_4 P_2'(-2)$ interaction model. These models support only a small number of s-wave bound states, and thus their applicability to realistic physical systems is limited.

To further analyze the nonadiabatic effects that lead to deviations from van der Waals universality for narrow Feshbach resonances, we compute the relevant adiabatic hyperspherical potentials, shown in Fig. 6.4. For $s_{\text{res}} = 264.0$, which lies in the universal regime, the Efimov channel exhibits the characteristic attractive $\sim 1/R^2$ behavior supporting weakly bound Efimov trimers. In addition, it shows a narrow avoided crossing with the open-channel d-wave molecular state at $R \approx 3.8, r_{\text{vdW}}$. Another avoded crossing with the open-channel g-wave molecular state is present at $R \approx 1.8, r_{\text{vdW}}$, $E \approx -24\, E_{\text{vdW}}$. Both avoided crossings do not affect the universal Efimov physics, because they occur at energies well below the relevant energy range.

For $s_{\text{res}} \approx 0.67$, the structure of the adiabatic potentials changes qualitatively. The lowest continuum channel becomes classically accessible and exhibits crossings with multiple channels. In addition, a closed-channel state with $l = 2$ appears, which remains weakly coupled to the continuum. As a result, the closed-channel component contributes significantly to the metastable states in this regime. Non-adiabatic couplings in the non-universal regime drive the decay of the Efimov state into deeply bound molecular states and can lead to its disappearance, as shown in Fig. 6.2(a). A similar structure of adiabatic potentials is observed for all investigated interaction models.

In summary, we investigated universal and non-universal aspects of homonuclear bosonic systems at unitarity across a wide range of Feshbach resonance strengths. We found that for narrow resonances, the breakdown of van der Waals is partially consistent with results given in Ref. [286]. The non-universal behavior of the Efimov spectrum is further modified by non-adiabatic effects, resulting in decreased lifetimes of the Efimov states, which are coupled to the continuum and can become nearly unbound. We pinpoint these effects to inelastic decay driven by short-range non-adiabatic couplings. A complementary result indicates that in the non-universal regime, for interaction models involving a lower number of two-body s-wave bound states, the Efimov trimer can continuously transition into short-range deeply bound trimer states. An interesting pathway for future research involves the analysis of non-universal effects in systems of various species with varying background scattering lengths.

Chapter 7

Strategies for computational accuracy

The restrictions on numerical calculations of three-body observables can be attributed to two-body physics. The challenge in computations stems from the rapid increase in the size of the finite-dimensional or truncated subspace of the full Hilbert space used for numerical calculations, relative to the number of two-body bound states supported by the interaction model. As we have already established in Chapter 1 – most quantitative calculations in three-body physics involve the analysis of three-body recombination. Due to the limits in computational accuracy, numerical calculations of three-body recombination can generally be performed either in the universal regime or through modeling the decay into deeply bound states via a single inelastic parameter [166, 202]. In this Chapter, we aim to highlight a range of numerical issues that must be addressed to describe the dynamics of few-body interactions in ultracold systems properly. For systems with neutral interactions, like the LiLiBa system described in Chapter 5 or the universal system comprised of three homonuclear bosons described in Chapter 6, the collisions in the quantum regime have been extensively studied and described, e.g., in Refs. [251, 265]. Most of the computational challenge remains with the ion-atom-atom systems, like the $LiLiBa^+$ described in Chapter 5. The effects of long-range potentials in ion-atom-atom systems, as well as the drastically different energy and length scales compared to neutral systems, have not been widely studied numerically in strongly interacting ionic few-body systems.

Calculations of effective three-body potentials, three-body recombination rates, and three-body observables, such as the scattering phase shift and binding energies, require determining the S-matrix. In order to do that, we use a wide range of numerical methods to solve both the eigenvalue problem for the adiabatic Hamiltonian – Eq. (3.117), and the hyperradial Schrödinger equation (3.118). We implement the numerical methods described in Refs. [202, 287] using the LAPACK library in FORTRAN.

7.1. The eigenvalue problem for the adiabatic hamiltonian $\hat{H}_{\rm ad}$

The channel functions are the solutions to the eigenvalue problem for the adiabatic Hamiltonian. We expand them using the Wigner D matrices, analogously to the total wavefunction in Eq. (3.220)

$$\Phi_\nu := \Phi^{\lambda\Pi v}_{Jm'}(R;\Omega) = \sum_m \widetilde{\Phi}^{\lambda\Pi v}_{Jm'm}(R;\theta,\phi)\, D^J_{m'm}(\alpha,\beta,\gamma)\ , \tag{7.1}$$

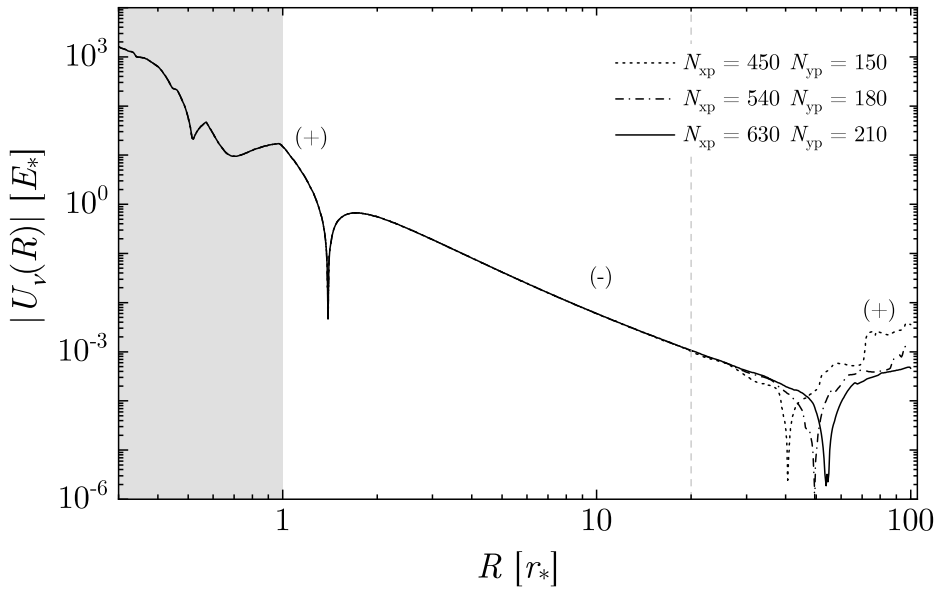

Figure 7.1: The absolute value of the three-body hyperspherical potentials $U_\nu(R)$ for the Efimov channel at $a_{BX} \to \infty$ calculated for the $LiLiBa^+$ system using a basis set of $N_{\rm xp}$, $N_{\rm yp}$ B-spline functions – as described in Eq. (7.2). The vertical line marks the practical limit $\sim 20\, r_*$ of numerical calculations.

We solve Eq. (3.117) by expanding the functions $\widetilde{\Phi}^{\lambda\Pi v}_{Jm'm}(R;\theta,\phi)$ onto a direct product of third-order basis splines

$$\widetilde{\Phi}_\nu(R;\theta,\phi) := \widetilde{\Phi}^{\lambda\Pi v}_{Jm'm}(R;\theta,\phi) = \sum_{i=1}^{N_{\rm xp}} \sum_{j=1}^{N_{\rm yp}} c_\nu^{ij}(R)\, B_i(\theta)\, B_j(\phi)\ . \tag{7.2}$$

Thus, the channel functions $\widetilde{\Phi}^{\lambda\Pi v}_{Jm'm}$ are approximated using a finite basis of spline functions $B_i(\theta)$, $B_j(\phi)$ – constructed as products of one-dimensional B-splines in each variable. The B-spline functions are localized, smooth, piecewise polynomials. As a result, the original differential equation is reduced to a finite-dimensional matrix eigenvalue problem.

Figure 7.1 illustrates the convergence of the three-body hyperspherical potentials $U_\nu(R)$ with an increasing number of basis functions. We find that $N_{\rm xp} = 630$ and $N_{\rm yp} = 210$ represent the practical limit for achieving reliable precision. Increasing the number of B-splines beyond these values does not lead to a further reduction of the computational error observed at $R \gtrsim R_{\rm n}$, where $R_{\rm n} = 20\, r_*$.

In the configuration space (θ, ϕ), the three-body potential $V(R,\Omega)$ exhibits rapidly varying attractive (approaching its minimum) and repulsive behavior for configurations in which the distance between any pair of particles becomes small. For large values of R, this region of configuration space shrinks rapidly. In ion-atom-atom systems, the characteristic length scale r_* is several orders of magnitude larger than $r_{\rm vdW}$. Consequently, for $R \gtrsim R_{\rm n}$, the subspace in which $V(R,\Omega)$ varies strongly with θ and ϕ becomes too small to be effectively resolved by increasing the number of B-splines, as its extent approaches the limits imposed by machine precision.

At large hyperradii, $R \sim 10^1 - 10^2\, r_*$, the energies of the three-body hyperspherical

adiabatic potentials are of the order of

$$\sim \frac{\hbar^2}{2\mu R^2} \sim 10^{-14}\text{–}10^{-15}\, E_h.$$

In contrast, the diagonal elements of the adiabatic Hamiltonian $\hat{H}_{\rm ad}$, which depend on the potential $V(R,\Omega)$ integrated over $d\Omega$, take values of the order of $10^0 - 10^2\, E_h$ within the region of configuration space where the potential varies strongly. As a result, the accurate description of $U_\nu(R)$ at large distances requires a relative precision of the order of $10^{-16} - 10^{-17}\, E_h$, which is comparable to the limits of standard double-precision arithmetic in FORTRAN – usually associated with the IEEE 754 64-bit floating point format.

While this limitation could, in principle, be overcome by using the quadruple-precision arithmetic, doing so would involve a significant increase in both the computational time and memory usage – by a factor of $10^1 - 10^2$. Finally, the upper bound on the number of basis functions in the ϕ coordinate is further constrained by the reduced configuration space arising from the BBX (Bose–Bose–X) symmetry of the LiLiBa$^+$ system.

7.2. The slow-variable discretization method

The computational methods used for solving the hyperradial Schrödinger equation (3.118) were described in detail in Refs. [202, 287] and involve the use of the *slow variable discretization* (SVD) method [201] based on the discrete variable representation (DVR) and used together with the R-matrix propagation method. Generally, the R-matrix propagation method is one of the most widely used and effective numerical techniques for calculating scattering observables [288]. The R-matrix – $\boldsymbol{\mathcal{R}}$ is defined by a generalization of the inverse logarithmic derivative $u(r)/u'(r)$ in one-channel scattering, where $u(r)$ is the solution to the radial Schrödinger equation

$$\boldsymbol{\mathcal{R}}(R) = \boldsymbol{\mathcal{F}}(R)\,[\overline{\boldsymbol{\mathcal{F}}}(R)]^{-1}\ , \tag{7.3}$$

where

$$\begin{aligned} \boldsymbol{\mathcal{F}}_{\nu\nu'}(R) &= \int d\Omega\, \Phi_\nu(R;\Omega)^* \psi_{\nu'}(R,\Omega)\ , \\ \overline{\boldsymbol{\mathcal{F}}}_{\nu\nu'}(R) &= \int d\Omega\, \Phi_\nu(R;\Omega)^* \frac{\partial}{\partial R} \psi_{\nu'}(R,\Omega)\ , \end{aligned} \tag{7.4}$$

and where the relation between the total three-body wavefunction $\psi_{\nu'}$ and the channel functions Φ_ν is given in Eq. (3.116). The $\boldsymbol{\mathcal{K}}$- and $\boldsymbol{\mathcal{S}}$-matrices are determined using the $\boldsymbol{\mathcal{R}}$-matrix

$$\begin{aligned} \boldsymbol{\mathcal{K}} &= (\boldsymbol{f} - \boldsymbol{f}'\boldsymbol{\mathcal{R}})(\boldsymbol{g} - \boldsymbol{g}'\boldsymbol{\mathcal{R}})^{-1}\ , \\ \boldsymbol{\mathcal{S}} &= (1 + i\boldsymbol{\mathcal{K}})(1 - i\boldsymbol{\mathcal{K}})^{-1}\ , \end{aligned} \tag{7.5}$$

where $\boldsymbol{f}$, $\boldsymbol{f}'$, $\boldsymbol{g}$, and $\boldsymbol{g}'$ are diagonal matrices defined by the asymptotic solutions f_ν, g_ν and their derivatives f'_ν, g'_ν expressed in terms of the spherical Bessel functions as described in Ref. [202].

We established in Chapter 4 that the non-adiabatic couplings $P_{\nu\nu'}(R)$, $Q_{\nu\nu'}(R)$ control the pathways for inelastic transitions and therefore the convergence of the scattering observables. They can be evaluated using the solutions $\Phi_\nu(R;\Omega)$ to the adiabatic equation (3.117) in accordance with definitions given in Eq. (3.120)

$$\begin{aligned} P_{\nu\nu'}(R) &= \int d\Omega\, \Phi_\nu(R;\Omega)^* \frac{\partial}{\partial R} \Phi_\nu(R;\Omega)\ , \\ Q_{\nu\nu'}(R) &= \int d\Omega\, \Phi_\nu(R;\Omega)^* \frac{\partial^2}{\partial R^2} \Phi_\nu(R;\Omega)\ . \end{aligned} \tag{7.6}$$

These matrices could be evaluated by a simple estimate of the differential

$$\frac{\partial}{\partial R}\Phi_\nu(R;\Omega) \approx \frac{\Phi_\nu(R+\Delta R;\Omega) - \Phi_\nu(R-\Delta R;\Omega)}{2\Delta R} \ , \tag{7.7}$$

and then used to solve the hyperradial Schrödinger equation in the form given by Eq. (3.118). However, this approach is only feasible when the non-adiabatic couplings do not change rapidly with R, which is true at large distances, say $R > R_{\rm SVD}$ – for some input value $R_{\rm SVD}$ – or when the decay into deeply bound states is suppressed for a model involving a low number of bound states. For the $LiLiBa^+$ system, we set $R_{\rm SVD} = 30\, r_*$, which also constitutes a practical, numerical limit resulting from finite computational and memory cost.

Hence, at short distances – $R \leq R_{\rm SVD}$ – the proper resolution of the non-adiabatic couplings is crucial for the physical description of inelastic processes in three-body systems. In this region, we solve the Eq. (3.117) and use the channel functions $\Phi_\nu(R;\Omega)$ as a starting point for the SVD approach. We solve the hyperradial Schrödinger equation in the form given by Eq. (3.114) by expanding the total wavefunction $\psi_\nu(R,\Omega)$ using the DVR basis functions $\pi_i(R)$ [202]

$$\psi_\nu(R,\Omega) = \sum_{i\nu'} c_{i\nu',\nu}\pi_i(R)\Phi_{\nu'}(R;\Omega) \ . \tag{7.8}$$

The DVR basis is defined using the Gauss-Legendre quadrature points x_i and weights w_i, which allows us to efficiently evaluate or approximate integrals of any function $g(x)$

$$\int_1^1 g(x)\, dx \cong \sum_{i=1}^{N} g(x_i) w_i \ , \tag{7.9}$$

where we use $N = 10$. The DVR basis functions $\pi_i(R)$ are proportional to the weight-normalized *Lagrange interpolating polynomials* [202]. These definitions allow us to efficiently evaluate the matrix elements of any function $H(R)$. Furthermore, the following relation holds for any $H(R)$

$$\int_{a1}^{a2} \pi_i(R) H(R) \pi_j(R)\, dR \cong H(R_i)\delta_{ij} \ , \tag{7.10}$$

where a_1, $a_2 \in \mathbb{R}$. The equation above is the main result of the DVR approach. Using DVR, the kinetic energy operator is treated as a coupling operator between each value of R defined on a finite grid and the interaction potential $\tilde{V}(R) := V(R;\Omega)$ in Eq. (3.114) becomes a set of coupled potential surfaces represented by a diagonal matrix at each R [289]. The slow-variable discretization method utilizes a slightly different channel basis, where we evaluate the channel functions Φ_ν at R_i instead of R

$$\psi_\nu(R,\Omega) = \sum_{i\nu'} c_{i\nu',\nu}\pi_i(R)\Phi_{\nu'}(R_i;\Omega) \ . \tag{7.11}$$

One can show that the expansion coefficients $c_{i\nu',\nu}$ are the same for the two expansions in Eqs. (7.8) and (7.11) as long as the DVR approximation given in Eq. (7.10) can be applied to $H(R) := \Phi_\nu(R;\Omega)$ [202]. Substituting the expanded wavefunction $\psi_\nu(R,\Omega)$ into the hyperradial Schrödinger equation (3.114) yields the equations for coefficients $c_{i\nu',\nu}$, which are then used to evaluate the R-matrix through definitions given in Eq. (7.4) [287]. The R-matrix, in turn, yields the scattering observables dependent on the S-matrix.

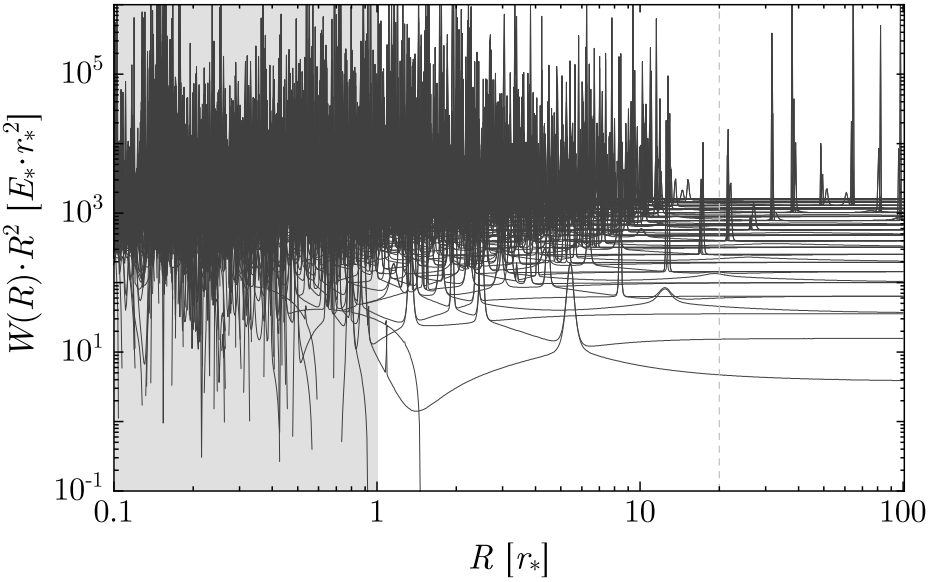

Figure 7.2: Three-body continuum effective potentials $W_\nu(R) = U_\nu(R) - \frac{\hbar^2}{2\mu}Q_{\nu\nu}(R)$ multiplied by R^2 to show their repulsive $\sim R^2$ behavior calculated for the LiLiBa$^+$ system at $a_{BX} = 1.30\, r_*$. For $R \to \infty$ the channels tend to their asymptotic behavior given by $\hbar^2\left[\lambda_i(\lambda_i+4)+15/4\right]/(2\mu R^2)$ for integer λ_i.

7.3. The convergence of the three-body recombination rate

As we discussed in the previous Section, an accurate calculation of the non-adiabatic couplings is essential for a proper physical description of the three-body collisions. Figure 7.2 shows the interplay between the non-adiabatic couplings and the repulsive $\sim R^2$ behavior of the diagonal part of the effective three-body potential matrix $W_\nu(R) = U_\nu(R) - \frac{\hbar^2}{2\mu}Q_{\nu\nu}(R)$. The channel structure is set by the $U_\nu(R)$ term, while the peaks in the effective potentials come from the diagonal non-adiabatic coupling terms $Q_{\nu\nu}(R)$. These peaks, similarly to peaks associated with the off-diagonal functions $P_{\nu\nu'}(R)$ and $Q_{\nu\nu'}(R)$, occur at avoided crossings, which arise from short-range interactions or shape resonances. The latter correspond to quasi-bound states in higher rotational channels that become embedded in the continuum. In ion–atom–atom systems, the long-range polarization tail of the interaction and the centrifugal barriers occurring at comparatively larger distances than in neutral systems cause the avoided crossings, and thus the associated peaks, to extend to large values of R, reaching positions beyond R_{SVD}. As we have shown in Fig. 7.2, using the crude method given by Eq. (7.7) for $R > R_{\mathrm{SVD}}$ could influence the description of the three-body collision only at collision energies well beyond the quantum regime, because the peaks $Q_{\nu\nu}(R)$ that need to be resolved in this range appear for high-energy continuum channels. Nevertheless, the theoretically relevant channels lying at energies such that $W_\nu(R)\cdot R^2 \sim (10^0 - 10^2)\, E_*\cdot r_*^2$ exhibit the features associated with $Q_{\nu\nu'}(R)$ before and in the vicinity of the numerical limit R_{n} described in Section 7.1.

In order to address the numerical challenge with the proper description of the non-adiabatic couplings as well as the numerical error most relevant in the most weakly bound channel, as described in Section 7.1, we have employed a regularization scheme, which models the behavior of channels at long-range. This model, which we call the *restricted* model, involves a transition

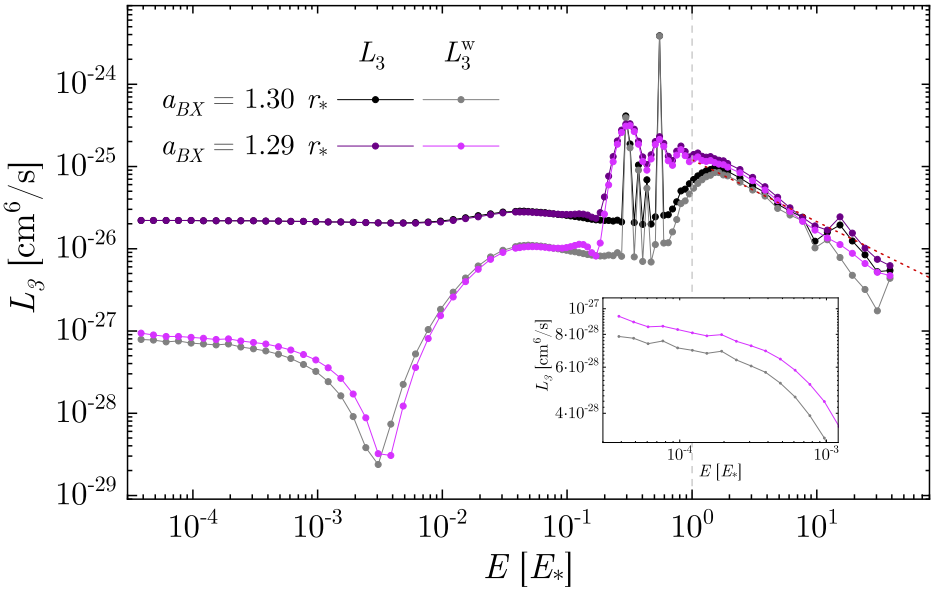

Figure 7.3: The three-body recombination rate L_3 and partial rate L_3^{w} for LiLiBa$^+$ calculated using the *restricted* model for $a_{BX} = 1.30\, r_*$ (black, gray) and $a_{BX} = 1.29\, r_*$ (purple, magenta). The inset shows the oscillatory behavior of L_3^w at low energies, which stems from finite-range boundary conditions at $R = R_f$. The dashed, red line shows the power law scaling $\sim E^{-3/4}$ stemming from thermal effects found for ion-atom-atom systems in Ref. [290].

to asymptotic behavior of $W_\nu(R)$ given by Eq. (3.122). The transition is given by

$$W_\nu(R) = W_\nu^n(R)\ (1 - O(R - R_{\mathrm{c}})) + \left[-E_b + \frac{\hbar^2 l(l+1)}{2\mu R^2}\right] O(R - R_{\mathrm{c}})\ , \tag{7.12}$$

for bound channels, where the $W_\nu^n(R)$ are the numerically obtained three-body effective potentials, $O(x)$ is the unit step function, the values of the relative angular momentum l and the binding energy E_b are found using a finite-range polynomial fit, where we set $R_{\mathrm{c}} = R_{\mathrm{n}}$. For the Efimov channel, we have $E_b = 0$ and $l = 0$. For continuum channels, we used a smooth cut-off function to define the transition to the asymptotic behavior of the potentials given by Eq. (3.123)

$$W_\nu(R) = W_\nu^n(R)\ (1 - C_{\mathrm{o}}(R, R_{\mathrm{c}}, n_c)) + \hbar^2 \frac{\lambda(\lambda+4) + 15/4}{2\mu R^2} C_{\mathrm{o}}(R, R_{\mathrm{c}}, n_c)\ , \tag{7.13}$$

where the cut-off function is defined by

$$C_{\mathrm{o}}(R, R_{\mathrm{c}}, n_c) = O(R - R_{\mathrm{c}}) + O(R_{\mathrm{c}} - R) \exp\left[-\left(\frac{R_{\mathrm{c}}}{R} - 1\right)^{n_c}\right]\ , \tag{7.14}$$

where we use $n_c = 8$. The $(1 - C_{\mathrm{o}})$ function decreases sharply from one to zero in the range $R \in [R_{\mathrm{c}}/2, R_{\mathrm{c}}]$. In addition, we turned off couplings to excited, theoretically irrelevant, high-energy continuum channels. Using a simple numbering scheme for ν, we consider channels with $\nu > 10$. On these channels, we enforced the vanishing of the non-adiabatic couplings

$$\begin{aligned} P_{\nu\nu'}(R) &= P_{\nu\nu'}^n(R)\,(1 - C_{\mathrm{o}}(R, R_{\mathrm{c}}, n_c))\ , \\ Q_{\nu\nu'}(R) &= Q_{\nu\nu'}^n(R)\,(1 - C_{\mathrm{o}}(R, R_{\mathrm{c}}, n_c))\ , \end{aligned} \tag{7.15}$$

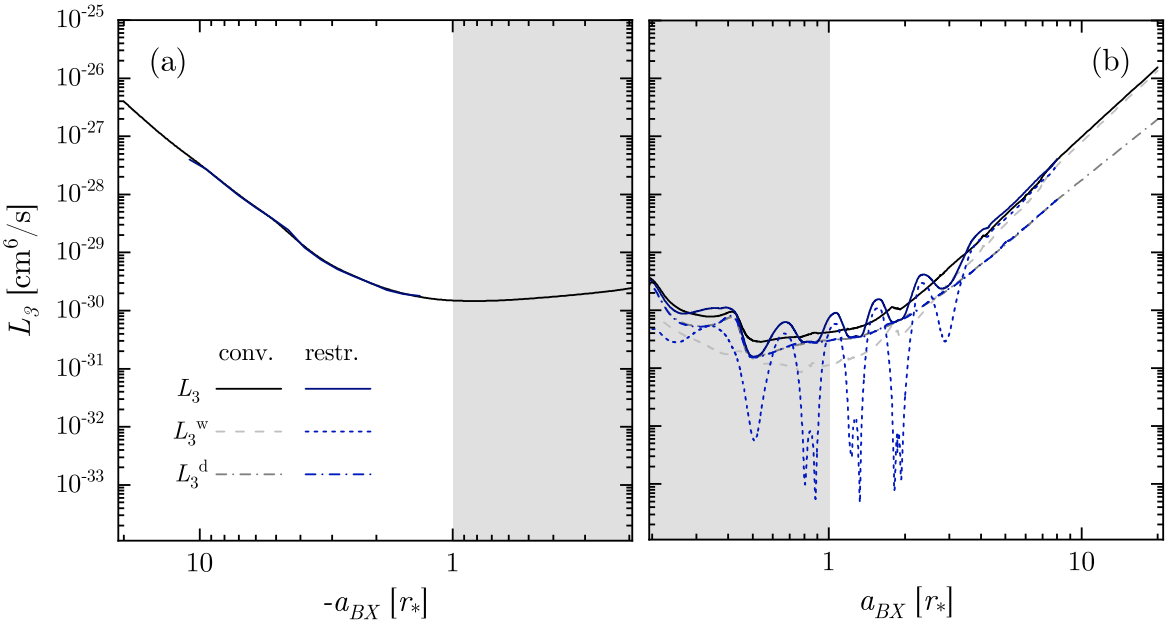

Figure 7.4: (a), (b): The three-body recombination rate L_3 and partial rates L_3^{w} and L_3^{d} for $LiLiBa^+$ calculated using the *converged* (black, *conv.*) and *restricted* (blue, *restr.*) models. The results for $LiLiBa^+$ recombination are multiplied by $(r_{\mathrm{vdW}}/r_*)^4$ to properly compare with results in Fig. 5.2.

where $P^n_{\nu\nu'}(R)$, $Q^n_{\nu\nu'}(R)$ are the $P_{\nu\nu'}(R)$ and $Q_{\nu\nu'}(R)$ matrices obtained numerically. For the excited continuum channels, the regularization condition in Eq. (7.13) was therefore slightly changed as it was imposed on $U_\nu(R)$ instead of $W_\nu(R)$.

Figure 7.3 shows the numerical instability of the total and partial recombination rates at collision energies E in the range $(10^{-1} - 10^0)\, E_*$. It is a result of numerical error associated with the resolution of non-adiabatic coupling for continuum channels $\nu \lesssim 10$. In the low-energy limit, the three-body recombination rate approaches a constant value, reflecting the dominance of quantum threshold behavior [195, 202]. For high collision energies $E > 1E_*$, the recombination rate exhibits a power-law decay $\sim E^{-3/4}$ characteristic of thermally dominated dynamics [290]. The finite value of R at which we impose the Dirichlet boundary condition on the hyperradial part of the total wavefunction R_f is also the ending point of the R-matrix propagation. Placing the boundary condition at R_f effectively introduces an artificial phase shift in the total wavefunction. An additional small error in the three-body recombination rate at low energy is visible in the inset of Figure 7.3.

The *restricted* model proves useful for stabilizing scattering observables at low collision energies, where quantum effects dominate the three-body dynamics. Nevertheless, this approach introduces a systematic error in the calculation of the three-body recombination rate in the limit $E \to 0$. Figure 7.4 shows that, in the non-universal regime $a_{BX} \in [0.1\, r_*, 5\, r_*]$, the partial rate L_3^w exhibits a suppression pattern. If physical, such behavior would indicate a novel interference mechanism not previously observed in theoretical or experimental studies of three-body recombination in ultracold systems.

To clarify its origin, we performed additional calculations and found that the suppression of the TBR rate arises from the vanishing scheme imposed on the non-adiabatic couplings [Eq. (7.15)]. We therefore carried out calculations within an alternative approach, referred to as the *converged* model, which keeps the regularization conditions given in Eqs. (7.12)

and (7.13), while omitting the constraint given by Eq. (7.15).

These results demonstrate that the pathways for recombination in the $LiLiBa^+$ system rely, at least in part, on long-range non-adiabatic couplings. The restricted model effectively imposes an artificial outer boundary, truncating phase accumulation of the total wavefunction and modifying the relative phases between recombination pathways. As a consequence, the observed suppression pattern is not physical but instead reflects a cutoff-induced interference. This behavior is found to be numerically stable; in particular, a similar suppression appears in the energy dependence of the partial rate $L_3^{\mathrm{w}}(E)$, as shown in Fig. 7.3 for $E \sim (10^{-3}{-}10^{-2})\, E_*$.

Chapter 8

Conclusion & Outlook

To summarize, this thesis explores several aspects of weakly bound quantum states in strongly interacting few-body systems. We computed bound and scattering properties of the ion-atom-atom system near an ion-atom Feshbach resonance, focusing on the $LiLiBa^+$ system and comparing it with the neutral LiLiBa system. We found that systems with long-range ion-atom interactions belong to a new class of universality. A manuscript presenting these results was accepted for publication in Physical Review Letters [227]:

- J. Gębala, M. Tomza, and J. P. D'Incao, *Universality in ionic three-body systems near an ion-atom Feshbach resonance*, accepted to Phys. Rev. Lett. (2026).

Furthermore, we analyzed Efimov spectra in homonuclear bosons near narrow Feshbach resonances and confirmed that the non-universal properties of Efimov states arise from atom-dimer repulsion. We also showed that the short-range behavior of the effective three-body potentials plays an important role in the description of Efimov states near narrow resonances. The results presented here are currently being consolidated into a manuscript intended for submission to Physical Review A or Physical Review Letters:

- J. Gębala, M. Tomza, and J. P. D'Incao, *Non-universality of Efimov physics near narrow Feshbach resonances*, in preparation.

Finally, we performed a detailed numerical study of three-body recombination in ion-atom-atom systems, identified key numerical and systematic errors, and outlined strategies to control them.

An important direction for future research is the investigation of universality in few-body systems characterized by increasingly complex long-range interactions. While this thesis primarily addressed isotropic ion-atom interactions and resonantly interacting atomic systems, recent advances now enable the study of strongly interacting quantum matter with tunable anisotropic interactions. In this context, a primary research direction is the study of microwave shielding in polar molecules [291–293]. This effect suppresses short-range collisional loss by generating a long-range repulsive barrier through microwave-dressed rotational states. Experimental studies have demonstrated an increased ratio of elastic to inelastic collisions and achieved the first stable, evaporatively cooled ultracold molecular gases. More recent work indicates that this effect is broadly universal across molecular species and can be employed not only for stabilization but also for tunable control of dipolar interactions, establishing microwave shielding as a key tool for engineering strongly interacting quantum dipolar matter [294]. A recent quantum treatment of microwave-shielded dipolar molecules [295] predicts that Efimov trimers can emerge even in the presence of long-range anisotropic interactions.

Shielding induces universal two- and three-body behavior, including Efimov scaling and a universal three-body parameter.

More broadly, the universality of few-body phenomena should be considered beyond conventional ultracold atomic gases, including systems in reduced dimensions. Recent research has examined the Efimov effect in low-dimensional quantum platforms [296]. It has been demonstrated that the Efimov effect can also appear in 1D long-range quantum spin chains. In this system, magnons (spin excitations in a spin chain) behave as interacting quantum particles. When the interactions are tuned to resonance, the system first develops continuous scale invariance and subsequently discrete scale invariance, providing evidence for the Efimov effect.

Returning to conventional ultracold gases, a somewhat less recent study investigated three-body physics in a typical system of ultracold atoms interacting via a van der Waals potential [274]. As we discussed in Chapter 5, the authors of Ref. [274] showed that the binding energy of a triatomic ground state is bounded above by three times the diatomic binding energy, which prevents the Efimov ground state from crossing the atom–dimer threshold and becoming unbound. Furthermore, the work also finds that higher partial waves, especially d-wave contributions, can noticeably shift the three-body parameter even in nominally s-wave-dominated regimes. Overall, this work refined our understanding of Efimov physics and suggests an interesting direction for future research: identifying the conditions and systems in which the three-body parameters associated with ground and excited Efimov states are constrained by the variational principle.

Furthermore, an important direction for future studies is the study of reactive few-body processes. Ref. [297] presents ultracold chemistry as a controllable platform for studying few-body quantum physics, where reactions are governed by quantum scattering rather than classical dynamics. The article highlights theoretical tools, including the multichannel quantum-defect theory and statistical models, that can describe these processes. In this context, the work identifies three-body recombination (TBR) as a particularly promising area for further research, since ultracold systems allow it to be studied with unprecedented control and insight into both universal behavior and its breakdown.

Our results and the proposed topics for future studies reinforce the view that ultracold few-body systems offer a uniquely controlled environment for investigating complex quantum dynamics. Recent advances in experimental control and numerical methods offer a promising pathway for a systematic description of the boundary between universal and non-universal behavior. Accordingly, this work clarifies specific aspects of ion-neutral and neutral three-body physics and contributes to the broader effort to understand emergent universality in quantum few-body systems.

Bibliography

[1] C. Adams and E. Riis, *Laser cooling and trapping of neutral atoms*, Prog. Quantum Electron. **21**, 1 (1997).

[2] N. Šantić, D. Buhin, D. Kovačić, I. Krešić, D. Aumiler, and T. Ban, *Cooling of atoms using an optical frequency comb*, Sci. Rep. **9**, 2510 (2019).

[3] W. Ketterle and N. Van Druten, *Evaporative cooling of trapped atoms*, in *Advances in atomic, molecular, and optical physics* (Academic Press, 1996) p. 181–236.

[4] W. Petrich, M. H. Anderson, J. R. Ensher, and E. A. Cornell, *Stable, tightly confining magnetic trap for evaporative cooling of neutral atoms*, Phys. Rev. Lett. **74**, 3352 (1995).

[5] S. Chu, *Nobel lecture: The manipulation of neutral particles*, Rev. Mod. Phys. **70**, 685–706 (1998).

[6] C. N. Cohen-Tannoudji, *Nobel lecture: Manipulating atoms with photons*, Rev. Mod. Phys. **70**, 707–719 (1998).

[7] W. D. Phillips, *Nobel lecture: Laser cooling and trapping of neutral atoms*, Rev. Mod. Phys. **70**, 721–741 (1998).

[8] E. A. Cornell and C. E. Wieman, *Nobel lecture: Bose-Einstein condensation in a dilute gas, the first 70 years and some recent experiments*, Rev. Mod. Phys. **74**, 875–893 (2002).

[9] W. Ketterle, *Nobel lecture: When atoms behave as waves: Bose-Einstein condensation and the atom laser*, Rev. Mod. Phys. **74**, 1131–1151 (2002).

[10] P. Courteille, R. S. Freeland, D. J. Heinzen, F. A. van Abeelen, and B. J. Verhaar, *Observation of a Feshbach resonance in cold atom scattering*, Phys. Rev. Lett. **81**, 69 (1998).

[11] S. Inouye, M. Andrews, J. Stenger, H. Miesner, D. Stamper-Kurn, and W. Ketterle, *Observation of Feshbach resonances in a Bose–Einstein condensate*, Nature **392**, 151 (1998).

[12] C. Chin, R. Grimm, P. Julienne, and E. Tiesinga, *Feshbach resonances in ultracold gases*, Rev. Mod. Phys. **82**, 1225 (2010).

[13] P.-I. Schneider, Y. V. Vanne, and A. Saenz, *Feshbach resonances of harmonically trapped atoms*, Phys. Rev. A **83**, 030701 (2011).

[14] P. S. Julienne and J. M. Hutson, *Contrasting the wide Feshbach resonances in* ^{6}Li *and* ^{7}Li, Phys. Rev. A **89**, 052715 (2014).

[15] A. Micheli, G. K. Brennen, and P. Zoller, *A toolbox for lattice-spin models with polar molecules*, Nat. Phys. **2**, 341–347 (2006).

[16] S. L. Cornish, N. R. Claussen, J. L. Roberts, E. A. Cornell, and C. E. Wieman, *Stable* ^{85}Rb *Bose-Einstein condensates with widely tunable interactions*, Phys. Rev. Lett. **85**, 1795 (2000).

[17] P. O. Fedichev, M. W. Reynolds, and G. V. Shlyapnikov, *Three-body recombination of ultracold atoms to a weakly bound s level*, Phys. Rev. Lett. **77**, 2921 (1996).

[18] M. Greiner, O. Mandel, T. Esslinger, T. W. Hänsch, and I. Bloch, *Quantum phase transition from a superfluid to a mott insulator in a gas of ultracold atoms*, Nature **415**, 39–44 (2002).

[19] T. Kinoshita, T. Wenger, and D. S. Weiss, *Observation of a one-dimensional tonks-girardeau gas*, Science **305**, 1125–1128 (2004).

[20] B. Paredes, A. Widera, V. Murg, O. Mandel, S. Fölling, I. Cirac, G. V. Shlyapnikov, T. W. Hänsch, and I. Bloch, *Tonks–girardeau gas of ultracold atoms in an optical lattice*, Nature **429**, 277–281 (2004).

[21] Z. Hadzibabic, P. Krüger, M. Cheneau, B. Battelier, and J. Dalibard, *Berezinskii–kosterlitz–thouless crossover in a trapped atomic gas*, Nature **441**, 1118–1121 (2006).

[22] A. Griesmaier, J. Werner, S. Hensler, J. Stuhler, and T. Pfau, *Bose-Einstein condensation of chromium*, Phys. Rev. Lett. **94**, 160401 (2005).

[23] J. Sánchez-Baena, G. Pascual, R. Bombín, F. Mazzanti, and J. Boronat, *Thermal behavior of Bose-Einstein condensates of polar molecules*, Phys. Rev. Res. **7**, 033080 (2025).

[24] K. M. O'Hara, S. L. Hemmer, M. E. Gehm, S. R. Granade, and J. E. Thomas, *Observation of a strongly interacting degenerate fermi gas of atoms*, Science **298**, 2179–2182 (2002).

[25] T. Bourdel, J. Cubizolles, L. Khaykovich, K. M. F. Magalhães, S. J. J. M. F. Kokkelmans, G. V. Shlyapnikov, and C. Salomon, *Measurement of the interaction energy near a Feshbach resonance in a* ^{6}Li *fermi gas*, Phys. Rev. Lett. **91**, 020402 (2003).

[26] T. Bourdel, L. Khaykovich, J. Cubizolles, J. Zhang, F. Chevy, M. Teichmann, L. Tarruell, S. J. J. M. F. Kokkelmans, and C. Salomon, *Experimental study of the bec-bcs crossover region in lithium 6*, Phys. Rev. Lett. **93**, 050401 (2004).

[27] M. Bartenstein, A. Altmeyer, S. Riedl, S. Jochim, C. Chin, J. H. Denschlag, and R. Grimm, *Collective excitations of a degenerate gas at the bec-bcs crossover*, Phys. Rev. Lett. **92**, 203201 (2004).

[28] M. W. Zwierlein, C. A. Stan, C. H. Schunck, S. M. F. Raupach, A. J. Kerman, and W. Ketterle, *Condensation of pairs of fermionic atoms near a Feshbach resonance*, Phys. Rev. Lett. **92**, 120403 (2004).

[29] C. Chin, M. Bartenstein, A. Altmeyer, S. Riedl, S. Jochim, J. H. Denschlag, and R. Grimm, *Observation of the pairing gap in a strongly interacting fermi gas*, Science **305**, 1128 (2004).

[30] X. Li, S. Wang, X. Luo, Y.-Y. Zhou, K. Xie, H.-C. Shen, Y.-Z. Nie, Q. Chen, H. Hu, Y.-A. Chen, X.-C. Yao, and J.-W. Pan, *Observation and quantification of the pseudogap in unitary fermi gases*, Nature **626**, 288 (2024).

[31] T. Hartke, B. Oreg, C. Turnbaugh, N. Jia, and M. Zwierlein, *Direct observation of nonlocal fermion pairing in an attractive fermi-hubbard gas*, Science **381**, 82 (2023).

[32] R. Yao, S. Chi, M. Wang, R. J. Fletcher, and M. Zwierlein, *Measuring pair correlations in bose and fermi gases via atom-resolved microscopy*, Phys. Rev. Lett. **134**, 183402 (2025).

[33] J. Argüello-Luengo, A. González-Tudela, and J. I. Cirac, *Optical lattice quantum simulator of dynamics beyond born-oppenheimer*, Phys. Rev. Lett. **135**, 133402 (2025).

[34] P. Díaz, D. Laroze, and B. A. Malomed, *The variational reduction for low-dimensional fermi gases and bose–fermi mixtures: A brief review*, Condens. Matter **4**, 10.3390/condmat4010022 (2019).

[35] A. G. Truscott, K. E. Strecker, W. I. McAlexander, G. B. Partridge, and R. G. Hulet, *Observation of fermi pressure in a gas of trapped atoms*, Science **291**, 2570 (2001).

[36] F. Schreck, L. Khaykovich, K. L. Corwin, G. Ferrari, T. Bourdel, J. Cubizolles, and C. Salomon, *Quasipure bose-einstein condensate immersed in a fermi sea*, Phys. Rev. Lett. **87**, 080403 (2001).

[37] D. M. Stamper-Kurn and M. Ueda, *Spinor bose gases: Symmetries, magnetism, and quantum dynamics*, Rev. Mod. Phys. **85**, 1191 (2013).

[38] I. Bloch, J. Dalibard, and S. Nascimbène, *Quantum simulations with ultracold quantum gases*, Nat. Phys. **8**, 267 (2012).

[39] T. Lahaye, C. Menotti, L. Santos, M. Lewenstein, and T. Pfau, *The physics of dipolar bosonic quantum gases*, Rep. Prog. Phys. **72**, 126401 (2009).

[40] G. Pupillo, A. Micheli, M. Boninsegni, I. Lesanovsky, and P. Zoller, *Strongly correlated gases of rydberg-dressed atoms: Quantum and classical dynamics*, Phys. Rev. Lett. **104**, 223002 (2010).

[41] M. Rigol, V. Dunjko, and M. Olshanii, *Thermalization and its mechanism for generic isolated quantum systems*, Nature **452**, 854 (2008).

[42] J. Dalibard, F. Gerbier, G. Juzeliūnas, and P. Öhberg, *Colloquium: Artificial gauge potentials for neutral atoms*, Rev. Mod. Phys. **83**, 1523 (2011).

[43] M. Z. Hasan and C. L. Kane, *Colloquium: Topological insulators*, Rev. Mod. Phys. **82**, 3045 (2010).

[44] W. S. Bakr, J. I. Gillen, A. Peng, S. Fölling, and M. Greiner, *A quantum gas microscope for detecting single atoms in a Hubbard-regime optical lattice*, Nature **462**, 74 (2009).

[45] D. Jaksch and P. Zoller, *The cold atom hubbard toolbox*, Ann. Phys. **315**, 52 (2004).

[46] H. Feshbach, *Unified theory of nuclear reactions*, Ann. Phys. **5**, 357 (1958).

[47] H. Feshbach, *A unified theory of nuclear reactions. ii*, Ann. Phys. **19**, 287 (1962).

[48] U. Fano, *Effects of configuration interaction on intensities and phase shifts*, Phys. Rev. **124**, 1866 (1961).

[49] U. Fano, G. Pupillo, A. Zannoni, and C. Clark, *On the absorption spectrum of noble gases at the arc spectrum limit*, J. Res. Natl. Inst. Stand. Technol. **110**, 583 (2005).

[50] H. C. Bryant, B. D. Dieterle, J. Donahue, H. Sharifian, H. Tootoonchi, D. M. Wolfe, P. A. M. Gram, and M. A. Yates-Williams, *Observation of Resonances near 11 eV in the Photodetachment Cross Section of the* H^- *Ion*, Phys. Rev. Lett. **38**, 228 (1977).

[51] W. C. Stwalley, *Stability of spin-aligned hydrogen at low temperatures and high magnetic fields: New field-dependent scattering resonances and predissociations*, Phys. Rev. Lett. **37**, 1628 (1976).

[52] E. Tiesinga, B. J. Verhaar, and H. T. C. Stoof, *Threshold and resonance phenomena in ultracold ground-state collisions*, Phys. Rev. A **47**, 4114 (1993).

[53] A. Mohammadi, A. Krükow, A. Mahdian, M. Deiß, J. Pérez-Ríos, H. da Silva, M. Raoult, O. Dulieu, and J. Hecker Denschlag, *Life and death of a cold* barb^+ *molecule inside an ultracold cloud of rb atoms*, Phys. Rev. Res. **3**, 013196 (2021).

[54] K.-k. Ni, S. Ospelkaus, M. H. G. De Miranda, A. Pe'er, B. Neyenhuis, J. J. Zirbel, S. Kotochigova, P. S. Julienne, D. S. Jin, and J. Ye, *A high phase-space-density gas of polar molecules*, Science **322**, 231 (2008).

[55] J. W. Park, S. A. Will, and M. W. Zwierlein, *Ultracold dipolar gas of fermionic* $^{23}\mathrm{Na}^{40}\mathrm{K}$ *molecules in their absolute ground state*, Phys. Rev. Lett. **114**, 205302 (2015).

[56] M. Morita, M. B. Kosicki, P. S. Żuchowski, P. Brumer, and T. V. Tscherbul, *Magnetic Feshbach resonances in ultracold atom-molecule collisions*, Phys. Rev. A **110**, L021301 (2024).

[57] M. L. González-Martínez and P. S. Żuchowski, *Magnetically tunable Feshbach resonances in* $\mathrm{Li} + \mathrm{Er}$, Phys. Rev. A **92**, 022708 (2015).

[58] T. L. Nicholson, S. Blatt, B. J. Bloom, J. R. Williams, J. W. Thomsen, J. Ye, and P. S. Julienne, *Optical Feshbach resonances: Field-dressed theory and comparison with experiments*, Phys. Rev. A **92**, 022709 (2015).

[59] Z. Li and R. V. Krems, *Electric-field-induced Feshbach resonances in ultracold alkali-metal mixtures*, Phys. Rev. A **75**, 032709 (2007).

[60] E. , M. J. Mark, R. Hart, J. G. Danzl, L. Reichsöllner, V. Melezhik, P. Schmelcher, and H.-C. Nägerl, *Confinement-induced resonances in low-dimensional quantum systems*, Phys. Rev. Lett. **104**, 153203 (2010).

[61] A. J. Moerdijk, B. J. Verhaar, and A. Axelsson, *Resonances in ultracold collisions of* $^6\mathrm{Li}$, $^7\mathrm{Li}$, *and* $^{23}\mathrm{Na}$, Phys. Rev. A **51**, 4852 (1995).

[62] B. Gao, *Solutions of the schrödinger equation for an attractive* $1/r^6$ *potential*, Phys. Rev. A **58**, 1728 (1998).

[63] B. Gao, *Binding energy and scattering length for diatomic systems*, J. Phys. B **37**, 4273 (2004).

[64] V. V. Flambaum, G. F. Gribakin, and C. Harabati, *Analytical calculation of cold-atom scattering*, Phys. Rev. A **59**, 1998 (1999).

[65] T. Haensch and A. Schawlow, *Cooling of gases by laser radiation.*, Opt. Commun. **13**, 68 (1975).

[66] D. J. Wineland, R. E. Drullinger, and F. L. Walls, *Radiation-pressure cooling of bound resonant absorbers*, Phys. Rev. Lett. **40**, 1639 (1978).

[67] A. L. Migdall, J. V. Prodan, W. D. Phillips, T. H. Bergeman, and H. J. Metcalf, *First observation of magnetically trapped neutral atoms*, Phys. Rev. Lett. **54**, 2596 (1985).

[68] S. Chu, J. E. Bjorkholm, A. Ashkin, and A. Cable, *Experimental observation of optically trapped atoms*, Phys. Rev. Lett. **57**, 314 (1986).

[69] E. L. Raab, M. Prentiss, A. Cable, S. Chu, and D. E. Pritchard, *Trapping of neutral sodium atoms with radiation pressure*, Phys. Rev. Lett. **59**, 2631–2634 (1987).

[70] C. Monroe, W. Swann, H. Robinson, and C. Wieman, *Very cold trapped atoms in a vapor cell*, Phys. Rev. Lett. **65**, 1571 (1990).

[71] J. E. Padilla-Castillo, J. Cai, P. Agarwal, P. Kukreja, R. Thomas, B. G. Sartakov, S. Truppe, G. Meijer, and S. C. Wright, *Magneto-optical trapping of aluminum monofluoride*, Phys. Rev. Lett. **135**, 243401 (2025).

[72] N. V. Vitanov, A. A. Rangelov, B. W. Shore, and K. Bergmann, *Stimulated Raman adiabatic passage in physics, chemistry, and beyond*, Rev. Mod. Phys. **89**, 015006 (2017).

[73] U. Gaubatz, P. Rudecki, S. Schiemann, and K. Bergmann, *Population transfer between molecular vibrational levels by stimulated raman scattering with partially overlapping laser fields. a new concept and experimental results*, J. Chem. Phys. **92**, 5363 (1990).

[74] K. Bergmann, H.-C. Nägerl, C. Panda, G. Gabrielse, E. Miloglyadov, M. Quack, G. Seyfang, G. Wichmann, S. Ospelkaus, A. Kuhn, and et al., *Roadmap on STIRAP applications*, J. Phys. B **52**, 202001 (2019).

[75] C. Monroe, D. M. Meekhof, B. E. King, S. R. Jefferts, W. M. Itano, D. J. Wineland, and P. Gould, *Resolved-sideband raman cooling of a bound atom to the 3d zero-point energy*, Phys. Rev. Lett. **75**, 4011 (1995).

[76] V. Vuletić, C. Chin, A. J. Kerman, and S. Chu, *Degenerate Raman sideband cooling of trapped cesium atoms at very high atomic densities*, Phys. Rev. Lett. **81**, 5768 (1998).

[77] E. Zohar, Y. Florshaim, O. Zilberman, A. Stern, and Y. Sagi, *Degenerate raman sideband cooling of* ^{40}K *atoms*, Phys. Rev. A **106**, 063111 (2022).

[78] S. E. Hamann, D. L. Haycock, G. Klose, P. H. Pax, I. H. Deutsch, and P. S. Jessen, *Resolved-sideband raman cooling to the ground state of an optical lattice*, Phys. Rev. Lett. **80**, 4149 (1998).

[79] A. M. Kaufman, B. J. Lester, and C. A. Regal, *Cooling a single atom in an optical tweezer to its quantum ground state*, Phys. Rev. X **2**, 041014 (2012).

[80] W. Paul, *Electromagnetic traps for charged and neutral particles*, Rev. Mod. Phys. **62**, 531–540 (1990).

[81] A. D. Ludlow, M. M. Boyd, J. Ye, E. Peik, and P. O. Schmidt, *Optical atomic clocks*, Rev. Mod. Phys. **87**, 637 (2015).

[82] H. Häffner, C. Roos, and R. Blatt, *Quantum computing with trapped ions*, Phys. Rep. **469**, 155 (2008).

[83] C. Monroe and J. Kim, *Scaling the ion trap quantum processor*, Science **339**, 1164 (2013).

[84] R. Blatt and C. F. Roos, *Quantum simulations with trapped ions*, Nat. Phys. **8**, 277–284 (2012).

[85] D. Leibfried, R. Blatt, C. Monroe, and D. Wineland, *Quantum dynamics of single trapped ions*, Rev. Mod. Phys. **75**, 281 (2003).

[86] C. Schneider, D. Porras, and T. Schaetz, *Experimental quantum simulations of many-body physics with trapped ions*, Rep. Prog. Phys. **75**, 024401 (2012).

[87] P. Zhang, A. Dalgarno, and R. Côté, *Scattering of* Yb *and* Yb^+, Phys. Rev. A **80**, 030703 (2009).

[88] S. Willitsch, *Coulomb-crystallised molecular ions in traps: Methods, applications, prospects*, Int. Rev. Phys. Chem. **31**, 175–199 (2012).

[89] M. S. Safronova, D. Budker, D. DeMille, D. F. J. Kimball, A. Derevianko, and C. W. Clark, *Search for new physics with atoms and molecules*, Rev. Mod. Phys. **90**, 025008 (2018).

[90] M. Fan, R. A. Ready, H. Li, S. Kofford, R. Kwapisz, C. A. Holliman, M. S. Ladabaum, A. N. Gaiser, J. R. Griswold, and A. M. Jayich, *Laser cooling and trapping of* $^{224}Ra^+$, Phys. Rev. Res. **5**, 043201 (2023).

[91] P. D. Lett, R. N. Watts, C. I. Westbrook, W. D. Phillips, P. L. Gould, and H. J. Metcalf, *Observation of atoms laser cooled below the doppler limit*, Phys. Rev. Lett. **61**, 169 (1988).

[92] J. Dalibard and C. Cohen-Tannoudji, *Laser cooling below the doppler limit by polarization gradients: simple theoretical models*, J. Opt. Soc. Am. B **6**, 2023 (1989).

[93] S. Ejtemaee and P. C. Haljan, *3d sisyphus cooling of trapped ions*, Phys. Rev. Lett. **119**, 043001 (2017).

[94] C.-C. Chen, J. L. Siegel, B. D. Hunt, T. Grogan, Y. S. Hassan, K. Beloy, K. Gibble, R. C. Brown, and A. D. Ludlow, *Clock-line-mediated sisyphus cooling*, Phys. Rev. Lett. **133**, 053401 (2024).

[95] L. E. Hillberry, D. Budker, S. M. Rochester, and M. G. Raizen, *Efficient cooling of high-angular-momentum atoms*, J. Phys. B **56**, 155301 (2023).

[96] M. Tomza, K. Jachymski, R. Gerritsma, A. Negretti, T. Calarco, Z. Idziaszek, and P. S. Julienne, *Cold hybrid ion-atom systems*, Rev. Mod. Phys. **91**, 035001 (2019).

[97] R. Gerritsma, A. Negretti, H. Doerk, Z. Idziaszek, T. Calarco, and F. Schmidt-Kaler, *Bosonic Josephson junction controlled by a single trapped ion*, Phys. Rev. Lett. **109**, 080402 (2012).

[98] U. Bissbort, D. Cocks, A. Negretti, Z. Idziaszek, T. Calarco, F. Schmidt-Kaler, W. Hofstetter, and R. Gerritsma, *Emulating solid-state physics with a hybrid system of ultracold ions and atoms*, Phys. Rev. Lett. **111**, 080501 (2013).

[99] K. Jachymski and A. Negretti, *Quantum simulation of extended polaron models using compound atom-ion systems*, Phys. Rev. Res. **2**, 033326 (2020).

[100] L. Ratschbacher, C. Sias, L. Carcagni, J. M. Silver, C. Zipkes, and M. Köhl, *Decoherence of a single-ion qubit immersed in a spin-polarized atomic bath*, Phys. Rev. Lett. **110**, 160402 (2013).

[101] T. V. Tscherbul, P. Brumer, and A. A. Buchachenko, *Spin-orbit interactions and quantum spin dynamics in cold ion-atom collisions*, Phys. Rev. Lett. **117**, 143201 (2016).

[102] L. Ratschbacher, C. Zipkes, C. Sias, and M. Köhl, *Controlling chemical reactions of a single particle*, Nat. Phys. **8**, 649 (2012).

[103] P. S. Julienne, *Cool ion chemistry*, Nat. Phys. **8**, 642 (2012).

[104] T. Sikorsky, Z. Meir, R. Ben-Shlomi, N. Akerman, and R. Ozeri, *Spin-controlled atom–ion chemistry*, Nat. Commun. **9**, 920 (2018).

[105] A. D. Dörfler, P. Eberle, D. Koner, M. Tomza, M. Meuwly, and S. Willitsch, *Long-range versus short-range effects in cold molecular ion-neutral collisions*, Nat. Commun. **10**, 5429 (2019).

[106] R. Côté, V. Kharchenko, and M. D. Lukin, *Mesoscopic molecular ions in Bose-Einstein condensates*, Phys. Rev. Lett. **89**, 093001 (2002).

[107] G. E. Astrakharchik, L. A. P. Ardila, R. Schmidt, K. Jachymski, and A. Negretti, *Ionic polaron in a Bose-Einstein condensate*, Commun. Phys. **4**, 94 (2021).

[108] S. Ding, M. Drewsen, J. J. Arlt, and G. M. Bruun, *Mediated interaction between ions in quantum degenerate gases*, Phys. Rev. Lett. **129**, 153401 (2022).

[109] F. Thielemann, J. Siemund, D. von Schoenfeld, W. Wu, P. Weckesser, K. Jachymski, T. Walker, and T. Schaetz, *Exploring atom-ion Feshbach resonances below the s-wave limit*, Phys. Rev. X **15**, 011051 (2025).

[110] T. Weber, J. Herbig, M. Mark, H.-C. Nägerl, and R. Grimm, *Three-body recombination at large scattering lengths in an ultracold atomic gas*, Phys. Rev. Lett. **91**, 123201 (2003).

[111] P. Weckesser, F. Thielemann, D. Wiater, A. Wojciechowska, L. Karpa, K. Jachymski, M. Tomza, T. Walker, and T. Schaetz, *Observation of Feshbach resonances between a single ion and ultracold atoms*, Nature **600**, 429–433 (2021).

[112] J. Pérez-Ríos and C. H. Greene, *Universal temperature dependence of the ion-neutral-neutral three-body recombination rate*, Phys. Rev. A **98**, 062707 (2018).

[113] J. Pérez-Ríos, S. Ragole, J. Wang, and C. H. Greene, *Comparison of classical and quantal calculations of helium three-body recombination*, J. Chem. Phys. **140**, 044307 (2014).

[114] J. Pérez-Ríos and C. H. Greene, *Communication: Classical threshold law for ion-neutral-neutral three-body recombination*, J. Chem. Phys. **143**, 041105 (2015).

[115] W. M. Itano, J. C. Bergquist, J. J. Bollinger, and D. J. Wineland, *Cooling methods in ion traps*, Phys. Scr. **T59**, 106 (1995).

[116] M. Cetina, A. T. Grier, and V. Vuletić, *Micromotion-induced limit to atom-ion sympathetic cooling in paul traps*, Phys. Rev. Lett. **109**, 253201 (2012).

[117] H. Hirzler, R. S. Lous, E. Trimby, J. Pérez-Ríos, A. Safavi-Naini, and R. Gerritsma, *Observation of chemical reactions between a trapped ion and ultracold Feshbach dimers*, Phys. Rev. Lett. **128**, 103401 (2022).

[118] T. Feldker, H. Fürst, H. Hirzler, N. Ewald, M. Mazzanti, D. Wiater, M. Tomza, and R. Gerritsma, *Buffer gas cooling of a trapped ion to the quantum regime*, Nat. Phys. **16**, 413 (2020).

[119] J. P. D'Incao, *Few-body physics in resonantly interacting ultracold quantum gases*, J. Phys. B **51**, 043001 (2018).

[120] J. P. D'Incao, H. Suno, and B. D. Esry, *Limits on universality in ultracold three-boson recombination*, Phys. Rev. Lett. **93**, 123201 (2004).

[121] H.-W. Hammer and L. Platter, *Efimov states in nuclear and particle physics*, Annu. Rev. Nucl. Part. Sci. **60**, 207 (2010).

[122] K. Helfrich, H.-W. Hammer, and D. S. Petrov, *Three-body problem in heteronuclear mixtures with resonant interspecies interaction*, Phys. Rev. A **81**, 042715 (2010).

[123] J. Voigtsberger, S. Zeller, J. Becht, N. Neumann, F. Sturm, H.-k. Kim, M. Waitz, F. Trinter, M. Kunitski, A. Kalinin, J. Wu, W. Schöllkopf, D. Bressanini, A. Czasch, J. B. Williams, K. Ullmann-Pfleger, L. P. H. Schmidt, M. S. Schöffler, R. E. Grisenti, T. Jahnke, and R. Dörner, *Imaging the structure of the trimer systems* $^4He_3$ *and* $^3He^4He_2$, Nat. Commun. **5**, 5765 (2014).

[124] A. Härter, A. Krükow, M. Deiß, B. Drews, E. Tiemann, and J. H. Denschlag, *Population distribution of product states following three-body recombination in an ultracold atomic gas*, Nat. Phys. **9**, 512 (2013).

[125] A. Simoni and J. m. Launay, *Ultracold atom-molecule collisions with hyperfine coupling*, Laser Phys. **16**, 707 (2006).

[126] J. H. Huckans, J. R. Williams, E. L. Hazlett, R. W. Stites, and K. M. O'Hara, *Three-body recombination in a three-state fermi gas with widely tunable interactions*, Phys. Rev. Lett. **102**, 165302 (2009).

[127] G. L. Schumacher, J. T. Mäkinen, Y. Ji, G. G. T. Assumpção, J. Chen, S. Huang, F. J. Vivanco, and N. Navon, *Observation of anomalous decay of a polarized three-component Fermi gas*, Nat. Commun. **17**, 174 (2026).

[128] S. Peng, H. Liu, J. Li, and L. Luo, *Collisional cooling of a Fermi gas with three-body recombination*, Commun. Phys. **7**, 101 (2024).

[129] Y. Ji, G. L. Schumacher, G. G. T. Assump ç ao, J. Chen, J. T. Mäkinen, F. J. Vivanco, and N. Navon, *Stability of the repulsive fermi gas with contact interactions*, Phys. Rev. Lett. **129**, 203402 (2022).

[130] C. A. Regal, C. Ticknor, J. L. Bohn, and D. S. Jin, *Tuning p-wave interactions in an ultracold fermi gas of atoms*, Phys. Rev. Lett. **90**, 053201 (2003).

[131] K. Welz, M. Gerken, B. Zhu, E. Lippi, M. Rautenberg, L. Chomaz, and M. Weidemüller, *Anomalous loss behavior in a single-component fermi gas close to a p-wave Feshbach resonance*, Phys. Rev. A **107**, 053310 (2023).

[132] M. Waseem, J. Yoshida, T. Saito, and T. Mukaiyama, *Quantitative analysis of p-wave three-body losses via a cascade process*, Phys. Rev. A **99**, 052704 (2019).

[133] X.-Y. Chen, M. Duda, A. Schindewolf, R. Bause, I. Bloch, and X.-Y. Luo, *Suppression of unitary three-body loss in a degenerate bose-fermi mixture*, Phys. Rev. Lett. **128**, 153401 (2022).

[134] H.-W. Hammer, A. Nogga, and A. Schwenk, *Colloquium: Three-body forces: From cold atoms to nuclei*, Rev. Mod. Phys. **85**, 197 (2013).

[135] N. Gross, Z. Shotan, S. Kokkelmans, and L. Khaykovich, *Nuclear-spin-independent short-range three-body physics in ultracold atoms*, Phys. Rev. Lett. **105**, 103203 (2010).

[136] B. L. Tolra, K. M. O'Hara, J. H. Huckans, W. D. Phillips, S. L. Rolston, and J. V. Porto, *Observation of reduced three-body recombination in a correlated 1d degenerate bose gas*, Phys. Rev. Lett. **92**, 190401 (2004).

[137] R. J. Fletcher, A. L. Gaunt, N. Navon, R. P. Smith, and Z. Hadzibabic, *Stability of a unitary bose gas*, Phys. Rev. Lett. **111**, 125303 (2013).

[138] B. S. Rem, A. T. Grier, I. Ferrier-Barbut, U. Eismann, T. Langen, N. Navon, L. Khaykovich, F. Werner, D. S. Petrov, F. Chevy, and et al., *Lifetime of the bose gas with resonant interactions*, Phys. Rev. Lett. **110**, 163202 (2013).

[139] P. Makotyn, C. E. Klauss, D. L. Goldberger, E. A. Cornell, and D. S. Jin, *Universal dynamics of a degenerate unitary Bose gas*, Nat. Phys. **10**, 116 (2014).

[140] U. Eismann, L. Khaykovich, S. Laurent, I. Ferrier-Barbut, B. S. Rem, A. T. Grier, M. Delehaye, F. Chevy, C. Salomon, L.-C. Ha, and C. Chin, *Universal loss dynamics in a unitary bose gas*, Phys. Rev. X **6**, 021025 (2016).

[141] R. J. Fletcher, R. Lopes, J. Man, N. Navon, R. P. Smith, M. W. Zwierlein, and Z. Hadzibabic, *Two- and three-body contacts in the unitary bose gas*, Science **355**, 377 (2017).

[142] A. G. Sykes, J. P. Corson, J. P. D'Incao, A. P. Koller, C. H. Greene, A. M. Rey, K. R. A. Hazzard, and J. L. Bohn, *Quenching to unitarity: Quantum dynamics in a three-dimensional Bose gas*, Phys. Rev. A **89**, 021601 (2014).

[143] S. Laurent, X. Leyronas, and F. Chevy, *Momentum Distribution of a Dilute Unitary Bose Gas with Three-Body Losses*, Phys. Rev. Lett. **113**, 220601 (2014).

[144] D. H. Smith, E. Braaten, D. Kang, and L. Platter, *Two-Body and Three-Body Contacts for Identical Bosons near Unitarity*, Phys. Rev. Lett. **112**, 110402 (2014).

[145] M. Barth and J. Hofmann, *Efimov correlations in strongly interacting Bose gases*, Phys. Rev. A **92**, 062716 (2015).

[146] J. P. Corson and J. L. Bohn, *Bound-state signatures in quenched Bose-Einstein condensates*, Phys. Rev. A **91**, 013616 (2015).

[147] S.-J. Jiang, J. Maki, and F. Zhou, *Long-lived universal resonant bose gases*, Phys. Rev. A **93**, 043605 (2016).

[148] F. Chevy and C. Salomon, *Strongly correlated Bose gases*, J. Phys. B **49**, 192001 (2016).

[149] V. E. Colussi, H. Kurkjian, M. Van Regemortel, S. Musolino, J. van de Kraats, M. Wouters, and S. J. J. M. F. Kokkelmans, *Cumulant theory of the unitary bose gas: Prethermal and Efimovian dynamics*, Phys. Rev. A **102**, 063314 (2020).

[150] T. Kraemer, M. Mark, P. Waldburger, J. Danzl, C. Chin, B. Engeser, K. Pilch, A. Jaakkola, H.-C. Nägerl, and R. Grimm, *Evidence for Efimov quantum states in an ultracold gas of caesium atoms*, Nature **440**, 315 (2006).

[151] V. Efimov, *Energy levels arising from resonant two-body forces in a three-body system*, Phys. Lett. B **33**, 563 (1970).

[152] F. Ferlaino, S. Knoop, M. Mark, M. Berninger, H. Schöbel, H.-C. Nägerl, and R. Grimm, *Collisions between tunable halo dimers: Exploring an elementary four-body process with identical bosons*, Phys. Rev. Lett. **101**, 023201 (2008).

[153] F. Ferlaino, S. Knoop, M. Berninger, W. Harm, J. P. D'Incao, H.-C. Nägerl, and R. Grimm, *Evidence for universal four-body states tied to an Efimov trimer*, Phys. Rev. Lett. **102**, 140401 (2009).

[154] F. Ferlaino, A. Zenesini, M. Berninger, B. Huang, H.-C. Nägerl, and R. Grimm, *Efimov resonances in ultracold quantum gases*, Few-Body Syst. **51**, 113 (2011).

[155] M. Zaccanti, B. Deissler, C. D'Errico, M. Fattori, M. Jona-Lasinio, S. Müller, G. Roati, M. Inguscio, and G. Modugno, *Observation of an Efimov spectrum in an atomic system*, Nat. Phys. **5**, 586 (2009).

[156] M. Berninger, A. Zenesini, B. Huang, W. Harm, H.-C. Nägerl, F. Ferlaino, R. Grimm, P. S. Julienne, and J. M. Hutson, *Universality of the three-body parameter for Efimov states in ultracold cesium*, Phys. Rev. Lett. **107**, 120401 (2011).

[157] M. Berninger, A. Zenesini, B. Huang, W. Harm, H.-C. Nägerl, F. Ferlaino, R. Grimm, P. S. Julienne, and J. M. Hutson, *Feshbach resonances, weakly bound molecular states, and coupled-channel potentials for cesium at high magnetic fields*, Phys. Rev. A **87**, 032517 (2013).

[158] Y. Yudkin, R. Elbaz, J. P. D'Incao, P. S. Julienne, and L. Khaykovich, *Reshaped three-body interactions and the observation of an Efimov state in the continuum*, Nat. Commun. **15**, 2127 (2024).

[159] G. Barontini, C. Weber, F. Rabatti, J. Catani, G. Thalhammer, M. Inguscio, and F. Minardi, *Observation of heteronuclear atomic Efimov resonances*, Phys. Rev. Lett. **103**, 043201 (2009).

[160] N. Gross, Z. Shotan, S. Kokkelmans, and L. Khaykovich, *Observation of universality in ultracold* ^{7}Li *three-body recombination*, Phys. Rev. Lett. **103**, 163202 (2009).

[161] N. Gross, Z. Shotan, O. Machtey, S. Kokkelmans, and L. Khaykovich, *Study of Efimov physics in two nuclear-spin sublevels of* ^{7}Li, C. R. Phys. **12**, 4 (2011).

[162] S. Knoop, F. Ferlaino, M. Mark, M. Berninger, H. Schöbel, H.-c. Nägerl, and R. Grimm, *Observation of an Efimov-like trimer resonance in ultracold atom–dimer scattering*, Nat. Phys. **5**, 227 (2009).

[163] S. Knoop, F. Ferlaino, M. Berninger, M. Mark, H.-C. Nägerl, R. Grimm, J. P. D'Incao, and B. D. Esry, *Magnetically controlled exchange process in an ultracold atom-dimer mixture*, Phys. Rev. Lett. **104**, 053201 (2010).

[164] O. Machtey, D. A. Kessler, and L. Khaykovich, *Universal dimer in a collisionally opaque medium: Experimental observables and Efimov resonances*, Phys. Rev. Lett. **108**, 130403 (2012).

[165] S. E. Pollack, D. Dries, and R. G. Hulet, *Universality in three- and four-body bound states of ultracold atoms*, Science **326**, 1683 (2009).

[166] E. Braaten and H.-W. Hammer, *Universality in few-body systems with large scattering length*, Phys. Rep. **428**, 259 (2006).

[167] A. N. Wenz, T. Lompe, T. B. Ottenstein, F. Serwane, G. Zürn, and S. Jochim, *Universal trimer in a three-component fermi gas*, Phys. Rev. A **80**, 040702 (2009).

[168] T. Lompe, T. B. Ottenstein, F. Serwane, K. Viering, A. N. Wenz, G. Zürn, and S. Jochim, *Atom-dimer scattering in a three-component fermi gas*, Phys. Rev. Lett. **105**, 103201 (2010).

[169] S. Nakajima, M. Horikoshi, T. Mukaiyama, P. Naidon, and M. Ueda, *Nonuniversal Efimov atom-dimer resonances in a three-component mixture of* ^{6}Li, Phys. Rev. Lett. **105**, 023201 (2010).

[170] S. Nakajima, M. Horikoshi, T. Mukaiyama, P. Naidon, and M. Ueda, *Measurement of an Efimov trimer binding energy in a three-component mixture of* ^{6}Li, Phys. Rev. Lett. **106**, 143201 (2011).

[171] R. J. Wild, P. Makotyn, J. M. Pino, E. A. Cornell, and D. S. Jin, *Measurements of tan's contact in an atomic Bose-Einstein condensate*, Phys. Rev. Lett. **108**, 145305 (2012).

[172] R. S. Bloom, M.-G. Hu, T. D. Cumby, and D. S. Jin, *Tests of universal three-body physics in an ultracold bose-fermi mixture*, Phys. Rev. Lett. **111**, 105301 (2013).

[173] M. Kunitski, S. Zeller, J. Voigtsberger, A. Kalinin, L. P. H. Schmidt, M. Schöffler, A. Czasch, W. Schöllkopf, R. E. Grisenti, T. Jahnke, D. Blume, and R. Dörner, *Observation of the Efimov state of the helium trimer*, Science **348**, 551 (2015).

[174] J. Johansen, B. J. DeSalvo, K. Patel, and C. Chin, *Testing universality of Efimov physics across broad and narrow Feshbach resonances*, Nat. Phys. **13**, 731 (2017).

[175] Y. Nishida, S. Moroz, and D. T. Son, *Super Efimov effect of resonantly interacting fermions in two dimensions*, Phys. Rev. Lett. **110**, 235301 (2013).

[176] D. K. Gridnev, *Three resonating fermions in flatland: proof of the super Efimov effect and the exact discrete spectrum asymptotics*, J. Phys. A **47**, 505204 (2014).

[177] S. Moroz and Y. Nishida, *Super Efimov effect for mass-imbalanced systems*, Phys. Rev. A **90**, 063631 (2014).

[178] L. P. H. de Goey, T. H. M. v. d. Berg, N. Mulders, H. T. C. Stoof, B. J. Verhaar, and W. Glöckle, *Three-body recombination in spin-polarized atomic hydrogen*, Phys. Rev. B **34**, 6183 (1986).

[179] A. J. Moerdijk, H. M. J. M. Boesten, and B. J. Verhaar, *Decay of trapped ultracold alkali atoms by recombination*, Phys. Rev. A **53**, 916 (1996).

[180] A. J. Moerdijk and B. J. Verhaar, *Collisional two- and three-body decay rates of dilute quantum gases at ultralow temperatures*, Phys. Rev. A **53**, R19 (1996).

[181] E. Nielsen and J. H. Macek, *Low-energy recombination of identical bosons by three-body collisions*, Phys. Rev. Lett. **83**, 1566 (1999).

[182] B. D. Esry, C. H. Greene, and J. P. Burke, *Recombination of three atoms in the ultracold limit*, Phys. Rev. Lett. **83**, 1751 (1999).

[183] R. Schmidt, S. P. Rath, and W. Zwerger, *Efimov physics beyond universality*, Eur. Phys. J. B **85**, 386 (2012).

[184] R. Chapurin, X. Xie, M. J. Van de Graaff, J. S. Popowski, J. P. D'Incao, P. S. Julienne, J. Ye, and E. A. Cornell, *Precision test of the limits to universality in few-body physics*, Phys. Rev. Lett. **123**, 233402 (2019).

[185] V. N. Efimov, *Weakly-bound states of 3 resonantly-interacting particles*, Sov. J. Nucl. Phys. **12**, 589 (1971).

[186] V. Efimov, *Energy levels of three resonantly interacting particles*, Nucl. Phys. A **210**, 157 (1973).

[187] B. R. Johnson, *On hyperspherical coordinates and mapping the internal configurations of a three body system*, J. Chem. Phys. **73**, 5051 (1980).

[188] J. Macek and K. A. Jerjian, *Adiabatic hyperspherical treatment of* HD^+, Phys. Rev. A **33**, 233 (1986).

[189] J. Macek, *Loosely bound states of three particles*, Z. Phys. D **3**, 31 (1986).

[190] E. Nielsen, D. Fedorov, A. Jensen, and E. Garrido, *The three-body problem with short-range interactions*, Phys. Rep. **347**, 373 (2001).

[191] O. I. Kartavtsev and J. H. Macek, *Low-Energy Three-Body recombination near a Feshbach resonance*, Few-Body Syst. **31**, 249 (2002).

[192] J. H. Macek, S. Ovchinnikov, and G. Gasaneo, *Solution for boson-diboson elastic scattering at zero energy in the shape-independent model*, Phys. Rev. A **72**, 032709 (2005).

[193] N. P. Mehta, S. T. Rittenhouse, J. P. D'Incao, and C. H. Greene, *Efimov states embedded in the three-body continuum*, Phys. Rev. A **78**, 020701 (2008).

[194] B. D. Esry, C. H. Greene, Y. Zhou, and C. D. Lin, *Role of the scattering length in three-boson dynamics and Bose - Einstein condensation*, J. Phys. B **29**, L51 (1996).

[195] H. Suno, B. D. Esry, C. H. Greene, and J. P. Burke, *Three-body recombination of cold helium atoms*, Phys. Rev. A **65**, 042725 (2002).

[196] J. P. D'Incao and B. D. Esry, *Scattering length scaling laws for ultracold three-body collisions*, Phys. Rev. Lett. **94**, 213201 (2005).

[197] B. D. Esry and C. H. Greene, *A ménage à trois laid bare*, Nature **440**, 289 (2006).

[198] J. Wang, J. P. D'Incao, B. D. Esry, and C. H. Greene, *Origin of the three-body parameter universality in Efimov physics*, Phys. Rev. Lett. **108**, 263001 (2012).

[199] Y. Wang, J. P. D'Incao, and B. D. Esry, *Cold three-body collisions in hydrogen–hydrogen–alkali-metal atomic systems*, Phys. Rev. A **83**, 032703 (2011).

[200] J. Macek, *Properties of autoionizing states of he*, J. Phys. B **1**, 831 (1968).

[201] O. I. Tolstikhin, S. Watanabe, and M. Matsuzawa, *'Slow' variable discretization: a novel approach for Hamiltonians allowing adiabatic separation of variables*, J. Phys. B **29**, L389 (1996).

[202] J. Wang, J. P. D'Incao, and C. H. Greene, *Numerical study of three-body recombination for systems with many bound states*, Phys. Rev. A **84**, 052721 (2011).

[203] D. L. Knirk, *Approach to the description of atoms using hyperspherical coordinates*, J. Chem. Phys. **60**, 66 (1974).

[204] S. Vinogradov, P. D. Smith, and E. Vinogradova, *Canonical Problems in Scattering and Potential Theory Part 1* (2001).

[205] C. H. Greene, P. Giannakeas, and J. Pérez-Ríos, *Universal few-body physics and cluster formation*, Rev. Mod. Phys. **89**, 035006 (2017).

[206] B. R. Johnson, *The classical dynamics of three particles in hyperspherical coordinates*, J. Chem. Phys **79**, 1906 (1983).

[207] B. R. Johnson, *The quantum dynamics of three particles in hyperspherical coordinates*, J. Chem. Phys **79**, 1916 (1983).

[208] F. T. Smith, *Lifetime matrix in collision theory*, Phys. Rev. **118**, 349 (1960).

[209] F. T. Smith, *A symmetric representation for Three-Body problems. i. Motion in a plane*, J. Math. Phys. **3**, 735 (1962).

[210] R. C. Whitten and F. T. Smith, *Symmetric Representation for Three-Body Problems. II. Motion in space*, J. Math. Phys. **9**, 1103 (1968).

[211] L. Wolniewicz, *A new numerical procedure for the construction of orthonormal hyperspherical functions*, J. Chem. Phys. **90**, 371 (1989).

[212] A. J. Dragt, *Classification of three-particle states according to SU_3*, J. Math. Phys. **6**, 533 (1965).

[213] Y. A. Simonov, *The Three-Body Problem. Complete Systen of Angular Functions*, Sov. J. Nucl. Phys. **3**, 461 (1966).

[214] P. Naidon and S. Endo, *Efimov physics: a review*, Rep. Prog. Phys. **80**, 056001 (2017).

[215] K. Huang and C. N. Yang, *Quantum-mechanical many-body problem with hard-sphere interaction*, Phys. Rev. **105**, 767 (1957).

[216] H. Bethe and R. Peierls, *Quantum theory of the diplon*, Proc. R. Soc. A **148**, 146 (1935).

[217] B. M. Axilrod and E. Teller, *Interaction of the van der waals type between three atoms*, J.Chem. Phys. **11**, 299 (1943).

[218] L. V. Faddeev, *Scattering theory for a three particle system*, Sov. Phys.-JETP **12**, 1014 (1961).

[219] D. V. Fedorov and A. S. Jensen, *Efimov effect in coordinate space faddeev equations*, Phys. Rev. Lett. **71**, 4103 (1993).

[220] G. Szegö, *Orthogonal Polynomials*, American Mathematical Society colloquium publications No. t. 23 (American Mathematical Society, 1959).

[221] B. M. Project, H. Bateman, A. Erdélyi, and U. S. O. of Naval Research, *Higher Transcendental Functions*, Higher Transcendental Functions No. t. 2 (McGraw-Hill, 1953).

[222] W. Bailey, *Generalized Hypergeometric Series*, Cambridge tracts in mathematics and mathematical physics (Stechert-Hafner Service Agency, 1964).

[223] E. Goursat, *Sur l'équation différentielle linéaire, qui admet pour intégrale la série hypergéométrique*, Ann. Sci. Éc. Norm. Supér. **10**, 3 (1881).

[224] E. Braaten, H.-W. Hammer, and M. Kusunoki, *Universal equation for Efimov states*, Phys. Rev. A **67**, 022505 (2003).

[225] N. P. Mehta, S. T. Rittenhouse, J. P. D'Incao, J. von Stecher, and C. H. Greene, *General Theoretical Description of N-Body Recombination*, Phys. Rev. Lett. **103**, 153201 (2009).

[226] J. Avery, *Hyperspherical Harmonics: Applications in Quantum Theory* (1989).

[227] J. Gębala, M. Tomza, and J. P. D'Incao, *Universality in ionic three-body systems near an ion-atom Feshbach resonance*, Phys. Rev. Lett. (2026).

[228] H. A. Bethe, *Theory of the effective range in nuclear scattering*, Phys. Rev. **76**, 38 (1949).

[229] R. Bishop, *Ground-state energy of a dilute fermi gas*, Ann. Physics **77**, 106 (1973).

[230] L. B. Madsen, *Effective range theory*, Am. J. Phys. **70**, 811 (2002).

[231] J. Pera and J. Boronat, *Low-energy scattering parameters: A theoretical derivation of the effective range and scattering length for arbitrary angular momentum*, Am. J. Phys. **91**, 90 (2023).

[232] A. Calle Cordón and E. Ruiz Arriola, *Low-energy universality and scaling of van der waals forces*, Phys. Rev. A **81**, 044701 (2010).

[233] B. R. Levy and J. B. Keller, *Low-energy expansion of scattering phase shifts for long-range potentials*, J. Math. Phys. **4**, 54 (1963).

[234] T. F. O'Malley, L. Rosenberg, and L. Spruch, *Low-energy scattering of a charged particle by a neutral polarizable system*, Phys. Rev. **125**, 1300 (1962).

[235] L. Spruch, T. F. O'Malley, and L. Rosenberg, *Modification of effective-range theory in the presence of a long-range potential*, Phys. Rev. Lett. **5**, 375 (1960).

[236] M. Deiß, S. Willitsch, and J. Hecker Denschlag, *Cold trapped molecular ions and hybrid platforms for ions and neutral particles*, Nat. Phys **20**, 713 (2024).

[237] H. Doerk, Z. Idziaszek, and T. Calarco, *Atom-ion quantum gate*, Phys. Rev. A **81**, 012708 (2010).

[238] A. Härter, A. Krükow, A. Brunner, W. Schnitzler, S. Schmid, and J. H. Denschlag, *Single ion as a three-body reaction center in an ultracold atomic gas*, Phys. Rev. Lett. **109**, 123201 (2012).

[239] J. M. Schurer, A. Negretti, and P. Schmelcher, *Unraveling the structure of ultracold mesoscopic collinear molecular ions*, Phys. Rev. Lett. , 063001 (2017).

[240] K. S. Kleinbach, F. Engel, T. Dieterle, R. Löw, T. Pfau, and F. Meinert, *Ionic impurity in a Bose-Einstein condensate at submicrokelvin temperatures*, Phys. Rev. Lett. **120**, 193401 (2018).

[241] M. Morita, J. Siemund, W. Wu, D. von Schoenfeld, J. Grieshaber, A. Wojciechowska, K. Jachymski, T. Walker, F. Thielemann, T. Schaetz, and M. Tomza, *Magnetic Feshbach resonances in* $Ba^+ + Li$ *collisions due to strong spin-orbit coupling*, arXiv:2507.12936 (2025), arXiv:2507.12936 .

[242] W. Casteels, J. Tempere, and J. T. Devreese, *Polaronic properties of an ion in a Bose-Einstein condensate in the strong-coupling limit*, J. Low Temp. Phys. **162**, 266 (2011).

[243] H. Hirzler, E. Trimby, R. S. Lous, G. C. Groenenboom, R. Gerritsma, and J. Pérez-Ríos, *Controlling the nature of a charged impurity in a bath of Feshbach dimers*, Phys. Rev. Res. **2**, 033232 (2020).

[244] E. R. Christensen, A. Camacho-Guardian, and G. M. Bruun, *Charged polarons and molecules in a Bose-Einstein condensate*, Phys. Rev. Lett. **126**, 243001 (2021).

[245] G. E. Astrakharchik, L. A. P. Ardila, K. Jachymski, and A. Negretti, *Many-body bound states and induced interactions of charged impurities in a bosonic bath*, Nat. Commun. **14**, 1647 (2023).

[246] R. Pessoa, S. A. Vitiello, and L. A. P. n. Ardila, *Fermi polaron in atom-ion hybrid systems*, Phys. Rev. Lett. **133**, 233002 (2024).

[247] V. S. Melezhik, Z. Idziaszek, and A. Negretti, *Impact of ion motion on atom-ion confinement-induced resonances in hybrid traps*, Phys. Rev. A **100**, 063406 (2019).

[248] V. S. Melezhik, *Improving efficiency of sympathetic cooling in atom-ion and atom-atom confined collisions*, Phys. Rev. A **103**, 053109 (2021).

[249] J. Wolf, M. Deiß, A. Krükow, E. Tiemann, B. P. Ruzic, Y. Wang, J. P. D'Incao, P. S. Julienne, and J. Hecker Denschlag, *State-to-state chemistry for three-body recombination in an ultracold rubidium gas*, Science **358**, 921 (2017).

[250] S. Haze, J. P. D'Incao, D. Dorer, M. Deiß, E. Tiemann, P. S. Julienne, and J. Hecker Denschlag, *Spin-Conservation Propensity Rule for Three-Body Recombination of Ultracold Rb Atoms*, Phys. Rev. Lett. **128**, 133401 (2022).

[251] S. Haze, J. P. D'Incao, D. Dorer, J. Li, M. Deiß, E. Tiemann, P. S. Julienne, and J. Hecker Denschlag, *Energy scaling of the product state distribution for three-body recombination of ultracold atoms*, Phys. Rev. Res. **5**, 013161 (2023).

[252] S. Haze, J.-L. Li, D. Dorer, J. D'Incao, P. S. Julienne, E. Tiemann, M. Deiß, and J. Hecker Denschlag, *Controlling few-body reaction pathways using a Feshbach resonance*, Nat. Phys. **21**, 228 (2025).

[253] J.-L. Li, P. S. Julienne, J. Hecker Denschlag, and J. P. D'Incao, *Spin hierarchy in van der waals molecule formation via ultracold three-body recombination*, Phys. Rev. A **111**, 013308 (2025).

[254] D. Dorer, S. Haze, J.-L. Li, J. P. D'Incao, E. Tiemann, P. S. Julienne, M. Deiß, and J. H. Denschlag, *Steering reaction flux by coupling product channels*, arXiv:2504.21727 (2025), arXiv:2504.21727 .

[255] J. Pérez-Ríos, *Cold chemistry: a few-body perspective on impurity physics of a single ion in an ultracold bath*, Molecular Physics **119**, e1881637 (2021).

[256] M. Mirahmadi and J. Pérez-Ríos, *Three-body recombination in physical chemistry*, Int. Rev. Phys. Chem. **41**, 233 (2022).

[257] M. Londoño, J. Madroñero, and J. Pérez-Ríos, *Cold atom-ion systems in radio-frequency multipole traps: Event-driven molecular dynamics and stochastic simulations*, Phys. Rev. A **108**, 053324 (2023).

[258] Y. Wang, J. Wang, J. P. D'Incao, and C. H. Greene, *Universal three-body parameter in heteronuclear atomic systems*, Phys. Rev. Lett. **109**, 243201 (2012).

[259] P. Naidon, S. Endo, and M. Ueda, *Microscopic origin and universality classes of the Efimov three-body parameter*, Phys. Rev. Lett. **112**, 105301 (2014).

[260] A. Derevianko, W. R. Johnson, M. S. Safronova, and J. F. Babb, *High-precision calculations of dispersion coefficients, static dipole polarizabilities, and atom-wall interaction constants for alkali-metal atoms*, Phys. Rev. Lett. **82**, 3589 (1999).

[261] B. Jeziorski, R. Moszynski, and K. Szalewicz, *Perturbation theory approach to intermolecular potential energy surfaces of van der waals complexes*, Chem. Rev. **94**, 1887 (1994).

[262] A. J. Moerdijk, W. C. Stwalley, R. G. Hulet, and B. J. Verhaar, *Negative scattering length of ultracold* ^{7}Li *gas*, Phys. Rev. Lett. **72**, 40 (1994).

[263] E. R. I. Abraham, W. I. McAlexander, C. A. Sackett, and R. G. Hulet, *Spectroscopic determination of the s-wave scattering length of lithium*, Phys. Rev. Lett. **74**, 1315 (1995).

[264] S. E. Pollack, D. Dries, M. Junker, Y. P. Chen, T. A. Corcovilos, and R. G. Hulet, *Extreme tunability of interactions in a* ^{7}Li *Bose-Einstein condensate*, Phys. Rev. Lett. **102**, 090402 (2009).

[265] J. Wang, J. P. D'Incao, Y. Wang, and C. H. Greene, *Universal three-body recombination via resonant d-wave interactions*, Phys. Rev. A **86**, 062511 (2012).

[266] B. D. Esry, C. H. Greene, and H. Suno, *Threshold laws for three-body recombination*, Phys. Rev. A **65**, 010705 (2001).

[267] From this perspective, our results for LiLiBa and $LiLiBa^+$ systems partially confirm university classes classification of [259] since we found that L_3 for LiLiBa is expected to display an Efimov resonance at $a_{BX} = a_- \approx -200 r_{\mathrm{vdW}}$ while $LiLiBa^+$ does not [see Fig. 5.2(a)].

[268] H. R. Sadeghpour, J. L. Bohn, M. J. Cavagnero, B. D. Esry, I. I. Fabrikant, J. H. Macek, and A. R. P. Rau, *Collisions near threshold in atomic and molecular physics*, J. Phys. B **33**, R93 (2000).

[269] S. J. Buckman and J. Mitroy, *Analysis of low-energy electron scattering cross sections via effective-range theory*, J. Phys. B **22**, 1365 (1989).

[270] D. Odell, A. Deltuva, and L. Platter, *Van der waals interaction as the starting point for an effective field theory*, Phys. Rev. A **104**, 023306 (2021).

[271] D. Odell, D. R. Phillips, and U. van Kolck, *Effective field theory for the bound states and scattering of a heavy charged particle and a neutral atom*, Phys. Rev. A **108**, 062817 (2023).

[272] L. W. Bruch and K. Sawada, *Inequality relating the ground-state energies of two and three bosons*, Phys. Rev. Lett. **30**, 25 (1973).

[273] M. D. Lee, T. Köhler, and P. S. Julienne, *Excited Thomas-Efimov levels in ultracold gases*, Phys. Rev. A **76**, 012720 (2007).

[274] P. M. A. Mestrom, J. Wang, C. H. Greene, and J. P. D'Incao, *Efimov–van der Waals universality for ultracold atoms with positive scattering lengths*, Phys. Rev. A **95**, 032707 (2017).

[275] E. Nielsen, H. Suno, and B. D. Esry, *Efimov resonances in atom-diatom scattering*, Phys. Rev. A **66**, 012705 (2002).

[276] H. Doerk, Z. Idziaszek, and T. Calarco, *Atom-ion quantum gate*, Phys. Rev. A **81**, 012708 (2010).

[277] J. P. D'Incao and B. D. Esry, *Manifestations of the Efimov effect for three identical bosons*, Phys. Rev. A **72**, 032710 (2005).

[278] Y. Wang, J. P. D'Incao, and B. D. Esry, *Cold three-body collisions in hydrogen–hydrogen–alkali-metal atomic systems*, Phys. Rev. A **83**, 032703 (2011).

[279] S. Häfner, J. Ulmanis, E. D. Kuhnle, Y. Wang, C. H. Greene, and M. Weidemüller, *Role of the intraspecies scattering length in the Efimov scenario with large mass difference*, Phys. Rev. A **95**, 062708 (2017).

[280] K. Oi, P. Naidon, and S. Endo, *Universality of Efimov states in highly mass-imbalanced cold-atom mixtures with van der waals and dipole interactions*, Phys. Rev. A **110**, 033305 (2024).

[281] P. Naidon and S. Endo, *Efimov physics: a review*, Rep. Prog. Phys. **80**, 056001 (2017).

[282] P. Naidon, S. Endo, and M. Ueda, *Physical origin of the universal three-body parameter in atomic Efimov physics*, Phys. Rev. A **90**, 022106 (2014).

[283] C. Chin, *Universal scaling of Efimov resonance positions in cold atom systems* (2011), arXiv:1111.1484 .

[284] X. Xie, M. J. Van de Graaff, R. Chapurin, M. D. Frye, J. M. Hutson, J. P. D'Incao, P. S. Julienne, J. Ye, and E. A. Cornell, *Observation of Efimov Universality across a Nonuniversal Feshbach Resonance in* ^{39}K, Phys. Rev. Lett. **125**, 243401 (2020).

[285] P. Naidon, *Closed-channel parameters of Feshbach resonances*, SciPost Phys. **18**, 036 (2025).

[286] C. Langmack, R. Schmidt, and W. Zwerger, *Efimov states near a Feshbach resonance and the limits of van der waals universality at finite background scattering length*, Phys. Rev. A **97**, 033623 (2018).

[287] K. Baluja, P. Burke, and L. Morgan, *R-matrix propagation program for solving coupled second-order differential equations*, Comput. Phys. Commun. **27**, 299 (1982).

[288] J. Tennyson, *Electron–molecule collision calculations using the r-matrix method*, Phys. Rep. **491**, 29 (2010).

[289] E. Tiesinga, C. J. Williams, and P. S. Julienne, *Photoassociative spectroscopy of highly excited vibrational levels of alkali-metal dimers: Green-function approach for eigenvalue solvers*, Phys. Rev. A **57**, 4257 (1998).

[290] A. Krükow, A. Mohammadi, A. Härter, J. H. Denschlag, J. Pérez-Ríos, and C. H. Greene, *Energy scaling of cold atom-atom-ion three-body recombination*, Phys. Rev. Lett. **116**, 193201 (2016).

[291] T. Karman and J. M. Hutson, *Microwave shielding of ultracold polar molecules*, Phys. Rev. Lett. **121**, 163401 (2018).

[292] L. Anderegg, S. Burchesky, Y. Bao, S. S. Yu, T. Karman, E. Chae, K.-K. Ni, W. Ketterle, and J. M. Doyle, *Observation of microwave shielding of ultracold molecules*, Science **373**, 779 (2021).

[293] A. Schindewolf, R. Bause, X.-Y. Chen, M. Duda, T. Karman, I. Bloch, and X.-Y. Luo, *Evaporation of microwave-shielded polar molecules to quantum degeneracy*, Nature **607**, 677 (2022).

[294] J. Dutta, B. Mukherjee, and J. M. Hutson, *Universality in the microwave shielding of ultracold polar molecules*, Phys. Rev. Res. **7**, 023164 (2025).

[295] S. Singh and C. H. Greene, *Efimov effect in ultracold microwave-shielded polar molecules* (2026), arXiv:2602.21433 .

[296] N. Sun, L. Feng, and P. Zhang, *Efimov effect in long-range quantum spin chains*, Commun. Phys. , 146 (2026).

[297] T. Karman, M. Tomza, and J. Pérez-Ríos, *Ultracold chemistry as a testbed for few-body physics*, Nat. Phys. **20**, 722 (2024)